

Role of PDE2A in cAMP/PKA signaling compartmentalization

Thesis Submitted for the Degree of Doctor of Philosophy

Hilary Term, 2018

Miguel Gonçalo de Oliveira Jones Ferrão Lobo

St John's College

Department of Physiology, Anatomy and Genetics

University of Oxford

Supervisor:

Professor Manuela Zaccolo

Role of PDE2A in cAMP/PKA signaling compartmentalization

Miguel Gonçalo de Oliveira Jones Ferrão Lobo, St John's College, University of Oxford

Thesis submitted for the degree of Doctor of Philosophy, Hilary 2018

Abstract

Background and Aims : cAMP/PKA signaling is compartmentalized within the cell, with tight spatial and temporal control of signal propagation underpinning specificity of response. The cAMP-degrading enzymes, phosphodiesterases (PDEs), are key regulators of this process. They are situated in specific subcellular domains within which they control local cAMP levels. Several components of the cAMP/PKA cascade have been identified in different mitochondrial compartments, including isoform 2 of PDE2A and multiple A-kinase anchoring proteins, suggesting the presence of multiple cAMP/PKA signaling domains within the organelle. The aims of this project were to examine the role of PDE2A in cAMP/PKA signaling compartmentalization and its biological function, with a particular focus on its role at the mitochondria.

Methods : Real-time PCR and fluorescence imaging were used to assess PDE2A expression and localization in different cell lines and tissues. Co-immunoprecipitation (Co-IP) was used to validate PDE2A2 interactors. Co-IP, electron microscopy and live-cell imaging were used to explore the role of PDE2A2 at the mitochondria. Fluorescence Resonance Energy Transfer (FRET) was used to investigate the involvement of PDE2A on endoplasmic reticulum (ER) Ca^{2+} handling and local cAMP/PKA dynamics.

Results : PDE2A2 localizes to the outer mitochondria membrane and intermembrane space and it interacts with several mitochondria and ER proteins, including components of the MINOS (mitochondrial inner membrane organizing system) complex and Caveolins. Functionally, PDE2A2 is involved in mitochondria degradation by mitophagy while PDE2A1 seems to be involved in the regulation of Ca^{2+} release from the ER. Phosphatases are responsible for the differential PKA dynamics between cytosol and ER.

Conclusions : PDE2A isoforms localize to different compartments and are involved in distinct cellular functions. The data presented in this thesis demonstrate that PDE2A2 activity at the mitochondria controls mitochondria clearance by mitophagy. This mechanism is dysregulated in multiple pathological conditions, making PDE2A2 a potential therapeutic target.

Declaration of own work and attribution

The work presented in this thesis was undertaken at the Department of Physiology, Anatomy and Genetics, University of Oxford, in the laboratory of Professor Manuela Zaccolo. All work presented is my own with the following exceptions where work was carried out in close collaboration: 1) The data gathered from Mass Spectrometry experiments in Chapter 4 were performed by Dr. Duangnapa Kovanich, previous member of the Zaccolo group, University of Oxford. 2) Preparation of the samples for electron microscopy in Chapter 5 were carried out as a service by Dr. Errin Johnson, Electron Microscopy Facility, University of Oxford. 3) Primary cultured neonatal rat ventricular myocytes (NRVM) and mouse embryonic fibroblasts (MEF) isolation was performed by Dr. Stefania Monterisi, previous member of the Zaccolo group, University of Oxford. This work has not been submitted for any other degree at this University or any other institution.

Miguel Lobo

March 2018

This thesis contains approximately 49,000 words.

Acknowledgements

The work presented in this thesis could not have been completed without the help of many others. First and foremost, I am grateful to my supervisor, Prof Manuela Zaccolo, for her support, help and access to an outstanding research environment. Her insightful comments and guidance have been invaluable in pursuing this work. I really enjoyed to work with her and my time in the lab in Oxford.

I am also grateful to the Medical Research Council and St. John's College for the funding provided as part of the DPhil in Physiology, Anatomy and Genetics at the University of Oxford, as well as the additional funding provided by St. John's College Special grant, Medical Research Council supplementary funding, Santander travel award, DPAG travel grant and British Heart Foundation Centre Research Excellence pump priming project grant.

I would like to express my appreciation to every member of the Zaccolo group for helping to make my time here one that I will never forget. I would like to thank Dr. Stefania Monterisi and Dr. Andreas Koschinski in particular for their important input regarding general lab rules and help with the primary cell isolation and microscope, as well as continuous supply of cakes and Italian chocolate candies. Special thanks to Dr. Katharina Schleicher for insightful discussions regarding PDE2A2 interactome and lipidomics and Dr. Nicoletta Surdo for guidance with the designing of RT-PCR primers. I would also like to thank my fellow PhD students Marcella Brescia and Nshunge Musheshe for their support and great spirit throughout the years.

Outside Zaccolo group, I would also like to extend my thanks to Dr. Inna Uliyakina for helping me with protein fractionation and cell proliferation assays. A really special thanks to Dr. Konstantinos Lefkimmiatis for his help at the beginning of my DPhil, weekly coffees and for convincing me to come to Oxford. I am grateful to Prof. Rainer Pepperkok and Dr. Marko Lampe for technical support and assistance on STED imaging carried out at the Advanced Light Microscopy Facility at the European Molecular Biology Laboratories, Heidelberg. I also thank Dr. Alzbeta Hulikova for being always very supportive and friendly.

Finally, I would like to thank Inna, for always brightening up my day and making me smile. Thank you for everything you have done over the last three years, and particularly for doing everything possible to support me and keep me happy! Para a minha família, muito obrigado por todo o apoio e pelo fornecimento contínuo de comida de qualidade que por aqui não abunda.

Acronyms and abbreviations

AC	Adenylyl cyclase
AhR	Aryl Hydrocarbon Receptor
AKAP	A-Kinase Anchoring Protein
AKAR	A-Kinase Activity Reporter
ANOVA	Analysis of Variance
ANP	Atrial Natriuretic Peptide
ATP	Adenosine Triphosphate
BN	Blue Native
BRET	Bioluminescence Resonance Energy Transfer
C	Catalytic Subunit of the PKA holoenzyme
CalA	Calyculin A
CaM	Calmodulin
CaMKII	Ca^{2+}/calmodulin-dependent protein kinase II
cAMP	Cyclic adenosine monophosphate
CAP	Catabolite Activator Proteins
CCCP	Carbonyl Cyanide m-Chlorophenylhydrazone
CFP	Cyan Fluorescent Protein
cGMP	Cyclic guanosine monophosphate
CK1	Casein Kinase 1
CNB	Cyclic Nucleotide-Binding domain
CNG	Cyclic Nucleotide-Gated channel
COP	Coat Protein
CREB	cAMP Response Element Binding protein
GRK	G protein coupled Receptors Kinases
CRP	cAMP Receptor Proteins
CsA	Cyclosporine A
DMSO	Dimethyl Sulphoxide
DNA	Deoxyribonucleic Acid
ECC	Excitation-Contraction Coupling
EDTA	Ethylene-diamine-tetra-acetic acid
eNOS	endothelial Nitric Oxide Synthase
EPAC	Exchange protein directly activated by cAMP

ER	Endoplasmic Reticulum
ERAD	ER-Associated Degradation
ERK	Extracellular signal-Regulated Kinases
FRAP	Fluorescence Recovery After Photobleaching
FRET	Fluorescence Resonance Energy Transfer
Fsk	Forskolin
G Protein	Guanosine-binding Protein
GAP	GTPase-Activating Protein
GAPDH	Glyceraldehyde 3-phosphate dehydrogenase
GDP	Guanosine Diphosphate
GEF	Guanine nucleotide Exchange Factor
GFP	Green Fluorescent protein
GPCR	G Protein-Coupled Receptor
GSK	Glycogen Synthase Kinase
GSKIP	GSK3β Interaction Protein
HEK	Human Embryonic Kidney cell line
Hsp20	Heat-shock protein 20
I-1	Phosphatase Inhibitor-1
IBMX	3-Isobutyl-1-Methylxanthine
IκB	NF-κB inhibitor protein (IκB)
IMM	Inner Mitochondrial Membrane
IMS	InterMembrane Space
IP	Immunoprecipitation
IP3	Inositol Trisphosphate
IP3R	Inositol Trisphosphate (IP3) Receptor
IS	Inhibitor Site
ISO	Isoproterenol
KO	Knockout
LAPD	Light-Activated Phosphodiesterase
LC3	Light Chain 3 protein
MAM	Mitochondria-Associated Membrane
MEF	Mouse Embryonic Fibroblasts
Mfn	Mitofusin
MINOS	Mitochondrial Inner membrane Organizing System

MRB	Mitochondria Resuspending Buffer
mRFP	Mitochondrial-targeted RFP
mtDNA	Mitochondrial DNA
MyoCF	Cardiac Fibroblast to Myofibroblast conversion
NFAT	Nuclear Factor of Activated T cells
NF-κB	Nuclear Factor κB
NRVM	Neonatal Rat Ventricular Myocytes
OMM	Outer Mitochondrial Membrane
PAGE	Polyacrylamide Gel Electrophoresis
PBS	Phosphate Buffered Saline
PCR	Polymerase Chain Reaction
PD	Parkinson's Disease
PDE	Phosphodiesterase
PEI	Polyetherimide
PGE	Prostaglandin E
PINK1	PTEN-Induced Putative Kinase 1
PK	Proteinase K
PKA	Protein Kinase A
PKG	Protein Kinase G
PKI	Protein Kinase A Inhibitor
PLN	Phospholamban
PM	Plasma Membrane
POPDC	Popeye Domain Containing
PP	Protein Phosphatase
PPP	Phosphoprotein Phosphatases
R	Regulatory Subunit of the PKA holoenzyme
RA	Retinoic Acid
RFP	Red Fluorescent protein
RIAD	RI Anchoring Disruptor
RSK1	Ribosomal S6 Kinase 1
RT	Room Temperature
RT-PCR	Reverse Transcription-PCR
RyR	Ryanodine Receptor
sAC	Soluble AC

SHR	Spontaneously Hypertensive Rats
S.E.M.	Standard Error of the Mean
SERCA	Sarcoplasmic Reticulum Ca^{2+}-ATPase
SKIP	Sphingosine Kinase Interacting Protein
SR	Sarcoplasmic Reticulum
STED	Stimulated Emission Depletion
TEM	Transmission Electron Microscopy
TBS	TRIS-buffered saline
TG	Thapsigargin
TGF-β	Transforming Growth Factor-beta
TmAC	Transmembrane AC
TnI	Inhibitory Troponin subunit
TRH	Thyrotropin-Releasing Hormone
UPS	Ubiquitin Proteasome System
VIP	Vasoactive Intestinal Peptide
YFP	Yellow Fluorescent Protein
WCL	Whole Cell Lysate
WLL	White Light Laser

Table of Contents

Abstract ..... **i**
Declaration of own work and attribution ..... **ii**
Acknowledgements ..... **iii**
Acronyms and abbreviations ..... **v**

Chapter 1 - Introduction **1**

1.1 Historical Background **2**
1.2 Components of the cAMP signaling pathway **5**
1.2.1 G-protein coupled receptors 6
1.2.2 Adenylyl Cyclases 8
1.2.3 Protein Kinase A and A-kinase anchoring proteins 10
1.2.4 Exchange Protein directly Activated by cAMP 16
1.2.5 Other cAMP effectors - cyclic nucleotide-gated channels and Popeye domain containing proteins 18
1.2.6 Phosphodiesterases 20
1.2.6.1 PDE2A 27
1.2.6.2 Biochemistry and Structure 28
1.2.6.3 Function and Regulation 30
1.2.6.4 Isoforms and Subcellular localization 34
1.2.6.5 Pharmacology and Perspectives 35
1.2.7 Phosphatases 38
1.3 cAMP subcellular compartments **41**
1.3.1 Mitochondria 41
1.3.2 Endoplasmic Reticulum 49
1.4 Aims of the project **53**

Chapter 2 - Materials and Methods **55**

2.1 Reagents and Molecular Biology **56**
2.1.1 Reagents and antibodies 56
2.1.2 Generation of constructs and ER-targeted FRET-based sensors 59
2.1.3 Real-Time PCR 62
2.2 Cell culture **64**

2.2.1 NRVMs culture and transfection 64
2.2.2 Isolation of Mouse Embryonic Fibroblasts 64
2.2.3 Cell lines 65
2.3 Biochemistry 65
2.3.1 Immunoprecipitation and western blot 65
2.3.2 Blue-Native gel 67
2.3.3 Mitochondria fractionation 67
2.3.4 Mitoplast preparation and protease protection assay 68
2.3.5 ER and MAM fractionation 68
2.3.6 Protein elution from FLAG beads and Protein-Lipid Overlay Assay 70
2.4 Imaging 71
2.4.1 Fluorescence Resonance Energy Transfer (FRET) Imaging 71
2.4.2 Live cell confocal imaging 72
2.4.3 Image Analysis of Parkin recruitment to Mitochondria and Mitophagy 72
2.4.4 Immunofluorescence 73
2.4.5 Stimulated emission depletion (STED) imaging 73
2.4.6 Cell Proliferation and Differentiation assays 74
2.4.7 Electron microscopy 74
2.5 Statistical Analysis 75

Chapter 3 - Expression and sub-cellular localization of PDE2A isoforms 76

3.1 Background 77
3.2 Expression of PDE2A isoforms in different cell types 79
3.3 Sub-mitochondrial localization of PDE2A2 84
3.4 PDE2A2 domains responsible for its targeting to the mitochondria 89
3.5 Conclusion 94

Chapter 4 - PDE2A2 interactors 96

4.1 Background 97
4.2 β-Taxilin 99
4.3 Caveolins 106
4.4 Other Endoplasmic Reticulum hits 111
4.5 MINOS complex 113
4.6 Other Mitochondrial hits 117
4.7 Conclusion 120

Chapter 5 - PDE2A2 regulates PKA-mediated phosphorylation of Mitofilin and Parkin-dependent mitophagy 123

5.1 Background 124
5.2 PDE2A regulates Mitofilin phosphorylation status 127
5.3 PDE2A2 interacts with Mitofilin through GAF-B domain 132
5.4 PDE2A2 regulates Parkin-dependent Mitophagy 136
5.5 Activation of PKG promotes Parkin recruitment to damaged mitochondria independently of PDE2A 141
5.6 CCCP promotes transient Mitofilin phosphorylation 143
5.7 Conclusion 146

Chapter 6 - PDE2A localizes to mitochondria-associated membranes (MAM) and regulates IP3-dependent Ca^{2+} release 149

6.1 Background 150
6.2 PDE2A2 interacts with Caveolins through its N-terminus 151
6.3 PDE2A2 interacts with Caveolin 1 at the MAM 155
6.4 PDE2A regulates IP3-dependent Ca^{2+} release from ER 158
6.5 Conclusion 166

Chapter 7 – Cytosol and ER are distinct cAMP/PKA signaling domains as a consequence of compartmentalized Phosphatase activity 168

7.1 Background 169
7.2 PKA signaling is not promptly terminated at the ER compared to cytosol 171
7.3 Phosphatases limit PKA activity in the cytosol 178
7.4 Conclusion 182

Chapter 8 - Discussion 183

8.1 Summary of Results and Discussion 185
8.1.1 Expression and sub-cellular localization of PDE2A 185
8.1.2 PDE2A2 interactors 188
8.1.3 PDE2A2 interaction with MINOS complex: role in the regulation of mitochondrial autophagy 189
8.1.4 PDE2A localization at the ER: regulation of Ca^{2+} handling 192
8.1.5 Phosphatases play a role in cAMP/PKA signaling compartmentalization 193

8.2 Concluding remarks 196

Chapter 9 - Appendices 197

9.1 Timing and Venue of Research 198

9.2 Research Funding 198

9.3 Publications arising from this work 199

Chapter 10 - References 200

Chapter 1 - Introduction

1.1 Historical Background

Half a century ago, the cyclic nucleotide adenosine 3', 5'-monophosphate (cAMP) was identified as a key intracellular second messenger that mediates the effects of hormones, neurotransmitters and other extracellular cues (Beavo and Brunton, 2002). It was first observed that cAMP is mainly produced at the cell membrane by adenylyl cyclase (AC) following G protein-coupled receptor (GPCR) activation, triggering several functional and at times opposing cellular processes, including cell proliferation and differentiation (Stork and Schmitt, 2002), gene expression (Yamamoto et al., 1988), apoptosis (Suen et al., 2008; Weissinger et al., 1997) and several metabolic processes, such as insulin secretion (Brisson et al., 1972), glycogen synthesis (Rous, 1970) or lipogenesis (Geelen and Vaartjes, 1977). cAMP activates several effector proteins, including Protein Kinase A (PKA), the Exchange Protein directly Activated by cAMP (EPAC) and Cyclic Nucleotide-Gated (CNG) ion channels. Phosphodiesterases (PDEs) are able to degrade cAMP while phosphatases counteract PKA-mediated phosphorylation, leading to the termination of the cAMP signal (Lefkimmiatis and Zaccolo, 2014). Since the observation of Mayer and colleagues in 1980 that a number of GPCR agonists could raise cellular cAMP to similar levels but resulted in distinct cellular effects (Hayes et al., 1980), it became clear that the original idea, that receptors and substrate availability is what specifies the cellular response to hormones, was too simplistic. Those early studies showed that although treatment with either prostaglandin E1 (PGE1) or the β-adrenergic receptor agonist isoproterenol (ISO) increased cAMP levels in the heart, only ISO increased strength of contraction (positive inotropy) whereas PGE1 had no effect on contractility. This was unexpected since both stimuli produced similar amounts of cAMP and comparable levels of PKA activation and clearly a 'linear cascade' model linking hormone binding to its receptor with generation of cAMP, activation of PKA and substrate phosphorylation was too simplistic to explain these observations. Instead, it was proposed that

the components of the cAMP signaling pathway are organized in such a way that cAMP is generated into distinct intracellular compartments. Direct evidence for the existence of cAMP domains and its functional role was found nearly 20 years later (Zaccolo and Pozzan, 2002; Nikolaev et al., 2006). The development of molecular tools for monitoring cAMP changes in real time in living cells provided a key methodological breakthrough (Nikolaev et al., 2004; Ponsioen et al., 2004; Zaccolo et al., 2000). The new techniques exploited Fluorescence Resonance Energy Transfer (FRET)-based sensors and fluorescence optical imaging of intact cells, thus allowing for the first time the detection of cAMP dynamics as they happen in the complex intracellular environment in real-time. The genetically encoded sensors take advantage of the cAMP binding domains (CBD) present in EPAC (Nikolaev et al., 2004; Ponsioen et al., 2004) or PKA (Zaccolo and Pozzan, 2002; Zaccolo et al., 2000) and sandwiched between two spectral variants of the green fluorescent protein (GFP). The conformational change that occurs on cAMP binding to the CBD changes the distance between the two fluorophores resulting in a change in FRET that can be detected when imaging the cells with a conventional optical microscope, making the methodology easy to apply. The subcellular resolution afforded by these sensors and the possibility to monitor changes in real time provided information on cAMP dynamics with unprecedented level of detail. In a recent advancement of this methodology, the cAMP sensors have been genetically modified and targeted to different intracellular compartments in order to detect cAMP events at specific subcellular sites thus further enhancing the spatial resolution of this approach and providing a more detailed map of the network organization and of the contribution of its regulatory elements (Allen and Zhang, 2006; DiPilato et al., 2004; Lefkimmiatis et al., 2013; Liu et al., 2011; Pendin et al., 2017; Surdo et al., 2017). These tools have not only provided additional strong evidence for compartmentalized cAMP signaling, but also uncovered the complexity and interconnectivity of the mechanisms that regulate cAMP subcellular domains and are starting to reveal the functional relevance of cAMP compartmentalization. Compartmentalization of

cAMP offers the possibility to target individual cAMP pools, rather than global intracellular cAMP levels, for therapeutic purposes in order to achieve greater efficacy and to reduce side effects (Maurice et al., 2014a). However, to achieve this, a detailed understanding of the subcellular organization and regulation of cAMP compartments and of their functional role is required. In this introduction, I will first describe the components of the cAMP signaling pathway, focusing on Phosphodiesterase 2A (PDE2A). Next, I will illustrate our current understanding of the topographical map of cAMP subcellular compartments, highlighting in particular the mitochondria and endoplasmic reticulum (ER) domains. The emphasis will be on those studies that link local regulation of cAMP with cellular function.

1.2 Components of the cAMP signaling pathway

The subcellular localization of microdomains is determined by several components of the cAMP signaling cascade:

- Signal generators: G-protein coupled receptors (GPCRs) and Adenylyl Cyclases (AC);
- Signal effectors: Protein Kinase A (PKA), Exchange Protein directly Activated by cAMP (EPAC), cyclic nucleotide-gated ion channels (CNG) and Popeye domain containing (POPDC) proteins;
- Signal terminators: Phosphodiesterases (PDEs) and Phosphatases;
- Clustering of signaling components: A-kinase anchoring proteins (AKAPs).

1.2.1 G-protein coupled receptors

Cells are able to capture and decode extracellular cues by the action of membrane receptors. Of these, GPCRs constitute the largest group in the human genome and are often studied as drug targets (Lagerström and Schiöth, 2008). GPCRs play a key role in signal transduction by detecting a vast array of 'first messengers' at the plasma membrane. Upon ligand binding, GPCRs undergo a conformational change resulting in activation of adaptor proteins - heterotrimeric guanosine-binding proteins (G-proteins). After activation, G-proteins release the Gα subunit which becomes free to associate and modulate the activity of ACs. Depending on the type of GPCR and which Gα subunit it is associated with, GPCRs can either activate or inhibit local cAMP production at the plasma membrane through Gαs or Gαi, respectively. The message from a huge number of extracellular cues is detected by GPCRs at the plasma membrane and the specific information content of each extracellular stimulus is retained despite all these signals converge into changes of cAMP levels. Distinct expression profiles of different GPCRs confer the first layer of diversity and specificity to cAMP signaling. Additionally, within the same cell, different lateral segregation of GPCRs at the plasma membrane may contribute to different responses to the same stimuli, further demonstrating the role of signaling compartmentalization. The long-accepted paradigm is that, upon activation, receptors are feedback phosphorylated by kinases such as G protein coupled receptors kinases (GRKs) or PKA resulting in rapid desensitization due to G protein uncoupling – short uncloping. G protein uncoupling is further enhanced by receptor internalization as part of the GPCR long-term desensitization process, mediated by binding of β-arrestin followed by GPCR endocytosis (Baillie and Houslay, 2005; Irannejad and von Zastrow, 2014; Kamal et al., 2012; Perry et al., 2002). Receptor internalization and subsequent degradation in the lysosome provides a mechanism that protects the cell against chronic stimulation while receptor recycling back to the plasma membrane induces resensitization and protects cells against prolonged hormone

resistance (Ferguson, 2001; Zhang and Eggert, 2013). However, recent studies have challenged the dogma that internalized GPCRs are inactive by showing that internalized GPCRs not only remain active but also exhibit sustained cAMP signaling (Calebiro et al., 2010; Ferrandon et al., 2009; Pavlos and Friedman, 2017). This was achieved by using FRET-based sensors that allow real-time observations of cAMP signaling and trafficking events in live cells (Calebiro et al., 2010; Irannejad et al., 2013) combined with enhanced bioluminescence resonance energy transfer (BRET) methods that measure GPCR activation and trafficking (Lan et al., 2012; Namkung et al., 2016; Stoddart et al., 2015). Thus, in addition to differential expression and localization of GPCRs at the plasma membrane, the ability of at least some GPCRs to trigger cAMP production after internalization provides a new and exciting feature to the model of cAMP signaling compartmentalization (Calebiro et al., 2009; Ferrandon et al., 2009; Irannejad et al., 2013).

1.2.2 Adenylyl Cyclases

Two classes of ACs, nine transmembrane AC (AC1 to AC9) and a soluble adenylyl cyclase (AC10; sAC), generate cAMP from adenosine triphosphate (ATP). All transmembrane ACs share the same general architecture yet they vary considerably outside their catalytic and transmembrane domains and are differentially regulated (Sunahara et al., 1996). AC1-9 are regulated by G proteins (stimulated or inhibited by Gαs or Gαi, respectively) upon GPCR stimulation. Additionally, they can be indirectly regulated by other signaling pathways. For example, AC1 and AC8 are Ca^{2+}-activated, whereas AC5 and AC6 are inhibited by Ca^{2+} (Halls and Cooper, 2017; Wachten et al., 2010). Other regulators of AC activity are forskolin or PKA-mediated phosphorylation, among others. A number of transmembrane ACs have been found to be part of multiprotein complexes organized by AKAPs (Bauman et al., 2006; Dessauer, 2009; Li et al., 2012) and including GPCRs/G proteins, PDEs and phosphatases (Carlisle Michel et al., 2004; Crossthwaite et al., 2006; Dupré et al., 2007), providing a structural basis for a non-homogeneous source of cAMP production. In contrast to AC1-9, sAC is not regulated by G proteins but, rather, is activated by bicarbonate (Bitterman et al., 2013; Chen et al., 2000) and ATP (Zippin et al., 2013) and can be stimulated by Mn^{2+} and Ca^{2+} (Braun, 1975; Braun and Dods, 1975). Although originally identified as a soluble enzyme, sAC has been subsequently identified to be present at specific subcellular sites, including mitochondria, nucleus, centrioles, mitotic spindles and mid-bodies (Valsecchi et al., 2014; Zippin et al., 2003). The specific regulation and subcellular localization of different ACs provides an important mechanism for compartmentalization of cAMP signaling. A study by Wachten et al. illustrates this mechanism well. The authors used targeted FRET-based sensors to detect cAMP in different subcellular domains in GH3B6 cells, a pituitary cell line that secretes prolactin in response to thyrotropin-releasing hormone (TRH) and vasoactive intestinal peptide (VIP). These two hypothalamic hormones act via different signaling pathways: TRH activates a G_q-coupled receptor and

therefore signals via IP_3-dependent Ca^{2+} release from the ER, whereas VIP activates a G_s coupled receptor that signals via cAMP. The authors found that in response to VIP a significant increase in cAMP was measured both in the cytosol and at the plasma membrane when compared to the level of cAMP detected by the AC8-targeted sensor, suggesting a coupling of the VIP receptor with ACs other than AC8 (and likely AC5/6). In contrast, when the same cells were stimulated with TRH, a dramatic increase in cAMP was registered by a AC8-targeted sensor while the cAMP response in the cytosol or at regions of the plasma membrane away from AC8 was reduced (Wachten et al., 2010). The different local cAMP response was due to Ca^{2+}-dependent activation of AC8 and to Ca^{2+}-dependent inhibition of AC5 and AC6 (as well as to concomitant stimulation of PDE1 by Ca^{2+}) (Wachten et al., 2010). These findings indicate that different stimuli can generate locally disparate cAMP responses via selective engagement of their specific receptors with individual ACs which react according to their contingent regulatory status (Wachten et al., 2010). Not only Ca^{2+} but also phosphorylation by the calcium-binding calmodulin (CaM) kinase, protein kinase C and PKA are involved in the regulation of certain ACs isoforms (Cooper and Crossthwaite, 2006; Halls and Cooper, 2017) .

1.2.3 Protein Kinase A and A-kinase anchoring proteins

PKA is the best characterized cAMP effector. In its inactive form, PKA is a heterotetramer of two regulatory (R) and two catalytic (C) subunits. Four types of R subunits (RIα, RIβ, RIIα and RIIβ) and three C subunits (Cα, Cβ and Cγ) have been described, which are responsible for the enzymatic actions of PKA and phosphorylate targets containing a [R/K][R/K/X]X[pS/pT] motif (Giansanti et al., 2013; Taylor et al., 1990). A dimer of R subunits binds and suppresses the activity of two C subunits in the absence of cAMP. Binding of cAMP to the R subunits causes a conformational change that relieves the inhibitory effect on the C subunits allowing phosphorylation of PKA targets (Taylor et al., 2005, 2013). The most significant difference between RI and RII isoforms is the auto-phosphorylation potential of the inhibitor site (IS) in RII subunits, which affects the interaction between RII and C subunits and consequently signal amplification (Torres-Quesada et al., 2017). Additionally, PKA tetramers containing RI-type subunits are activated at lower concentrations of cAMP compared to those including RII (Dostmann et al., 1990).

Apart from the inhibition of the C subunits, the R counterparts are also responsible for binding of the PKA holoenzyme to specific A kinase-anchoring proteins (AKAPs). AKAPs serve as key players in cAMP compartmentalization by constraining PKA to a specific subcellular location in physical proximity to PKA targets, increasing the specificity and efficiency of PKA signalosomes (Hulme et al., 2003; Lygren et al., 2007). An example of the importance of AKAPs was reported by Gorshkov et al., who observed that the cAMP gradients in developing hippocampal neurons, with higher cAMP levels in more distal regions of the axon compared to other regions of the cell, depend on proper anchoring of PKA by AKAPs. Disruption of PKA anchoring to AKAPs increased the cAMP gradient and led to enhanced axon elongation, suggesting delocalization of PKA tethered with regulatory proteins such as PDEs (Gorshkov et al., 2017).

Originally, it had been proposed that RII subunits have higher affinity for type II AKAP proteins than RI subunits for type I selective ones (Kritzer et al., 2012). Thus, the more cAMP-sensitive RI subunits would be found predominantly in the soluble fractions of the cells, whereas the RII-based enzymes, which require higher cAMP levels for activation, would be found in the particulate fractions (Taylor et al., 2012). However, several studies have recently identified several type I selective AKAPs with high affinity for RI subunits – SKIP, smAKAPs and Gpr161 (Bachmann et al., 2016; Burgers et al., 2012, 2016; Kovanich et al., 2010; Means et al., 2011). These new observations challenge the idea that more sensitive R subunits are found predominantly in the cytosol. Although most AKAPs display high affinities for RII PKA holoenzymes, dual specific AKAPs (e.g. D-AKAP1/2, Ezrin, Merlin, and AKAP220) interact with RI dimers as well, but typically with lower affinity (Herberg et al., 2000; Pawson and Scott, 2010;).

All AKAPs identified so far (> 30) share a short characteristic motif for R subunit interaction. The interaction between AKAPs and PKA occurs via binding of the dimerization-docking domain (D/D) located at the N-terminus of the R subunit and an amphipathic α-helix, generally encompassing 14-18 residues, that is conserved among the AKAP family. All four R subunit isoforms contain the conserved D/D domain (Banky et al., 1998; Gold et al., 2006). AKAPs include additional interaction sites that are responsible for their subcellular targeting as well as anchoring of other components of the cAMP pathway including receptors (Malbon, 2007; Malbon et al., 2004), ACs (Dessauer, 2009; Piggott et al., 2008), phosphatases (Dodge-Kafka et al., 2010) and PDEs (Scott et al., 2013). The diverse targeting domains present in the AKAPs recruit kinase activities to specific cell compartments, such as the plasma membrane, nucleus, mitochondria, endo/sarcoplasmic reticulum, the primary cilium and other cellular organelles, greatly contributing to the specificity and regulation of cAMP signaling (Langeberg and Scott, 2015). Thus, each AKAP has the capability of binding and compartmentalize different

combinations of kinase substrates, cAMP effectors and other regulator enzymes, ensuring a large diversity of PKA-focused signaling complexes (Greenwald and Saucerman, 2011).
One example of cAMP compartmentalization within the cytosol is given by the AKAP glycogen synthase kinase 3β (GSK3β) interaction protein (GSKIP), a cytosolic scaffolding protein that binds both PKA and GSK3β, that is involved in the regulation of β-catenin and Wnt signaling. The regulation of β-catenin by GSKIP is specific for this AKAP as the cytosolic AKAP220 (Reinton et al., 2000), which also binds PKA and GSK3β, does not affect Wnt signaling, highlighting PKA and GSK3β cytosolic compartmentalization by GSKIP (Dema et al., 2016).

Several diseases have been associated with AKAPs and their interacting partners, including heart failure, cancer and immunological, psychiatric and neurological disorders, making AKAP complexes potential drug targets. Direct evidence for the involvement of distinct AKAPs in cardiac diseases comes from genetic polymorphisms and knockout studies. For example, a single nucleotide polymorphism in the PKA-binding domain of D-AKAP2 can cause elevated resting heart rate and diminished heart rate variability. In agreement with this, mutant mice lacking the last 51 amino acids of the D-AKAP2 gene display cardiac arrhythmia and die prematurely (Tröger et al., 2012). Several disruptor peptides and small molecules have been developed and used to displace PKA from its anchor sites on AKAPs and to study the functional role of this interaction (Carr et al., 1992; Christian et al., 2011). Peptides that can selectively disrupt the interaction between AKAPs and either RI or RII have been developed. For instance, the peptide named SuperAKAP-IS is 10000-fold more selective for blocking AKAP interaction with RII compared to with RI (Gold et al., 2006) while RIAD (RI anchoring disruptor) shows 1000-fold higher affinity for RI blockade over RII blockade (Carlson et al., 2006). Disruptor peptides that displace PKA specifically from individuals AKAPs have been more difficult to generate since AKAPs share a characteristic motif for R subunit interaction. However, some progress has been achieved recently using a screening approach based on high-resolution

structural information. In this study a number of engineered RII subunit fragments that show some preference in disrupting interaction of RII with specific AKAPs were isolated. These peptides, named R_{Select}, were shown to have some selectivity for targeting the cognate AKAP in living cells, although their affinity of binding remains lower than endogenous full length RII subunits, limiting for the moment their applicability (Gold et al., 2013).

One good example of the importance of PKA anchoring to AKAPs in cAMP signaling compartmentalization was given by Di Benedetto and colleagues. Here, the authors targeted cAMP FRET-based sensors to RI- or RII-binding AKAPs to demonstrate that PKA type I and type II define distinct intracellular signaling compartments in cardiac myocytes. Specifically, ISO stimulation generated a cAMP response that was selectively confined to AKAP-anchored PKA type II. This cAMP pool led to Phospholamban (PLN) and troponin I phosphorylation and was sensitive to rolipram (PDE4 selective inhibitor), suggesting the presence of PDE4 in the same complexes. On the other hand, PGE1 and glucagon stimulation generated a cAMP response that was selectively confined to AKAP-anchored PKA type I. This pool of cAMP was sensitive to the PDE2A inhibitor EHNA but did not result in PLN or troponin I phosphorylation. Furthermore, by employing Fluorescence Recovery After Photobleaching (FRAP), the authors also showed that RI, similarly to RII, is predominantly anchored in cardiomyocytes by binding to specific endogenous AKAPs. These data contradict the accepted paradigm that type II PKA is associated with particulate subcellular fractions via binding to AKAPs, whereas type I PKA is primarily cytoplasmic (Di Benedetto et al., 2008). To further increase the complexity of cAMP/PKA signaling, it has been reported that the location of some AKAPs can shift in response to cellular conditions, translocating an entire signalosome across the cell (Smith et al., 2006).

Smith et al. have shown by using cryo-electron microscopy that intrinsically disordered domains within RII subunit of PKA anchored to AKAP18γ allow a remarkable level of conformational plasticity within the AKAP-PKA complex (Smith et al., 2013). This molecular plasticity would not only provide a ~16 nanometer radius of motion to the associated C subunits but also would modulate its enzymatic efficiency by orienting the anchored C subunit optimally towards substrates. Although this would generate a highly compartmentalized signal, the relevance of these structural fluctuations to cAMP/PKA signaling remains to be established. This observation contracdicts the original model in support of a model for C subunit regulation where PKA C subunits remain tethered to regulatory subunits during cAMP elevation. In other words, catalytically active PKA holoenzymes remain intact upon cAMP stimulation, either in the cytosol or anchored to organelles (Smith et al., 2017). The authors propose that the range of anchored PKA action is restricted to substrates within the immediate vicinity of the signalosome. This concept of "signaling island" would radically change our view of how AKAP complexes operate and indicates that protein phosphorylation is even more regionally confined than previously appreciated. This theory was partially supported by experiments showing no effect of β-AR stimulation on C-subunit co-immunoprecipitation with anchored RII subunits (Smith et al., 2017). However, this experiment does not exclude the possibility that R and C subunits re-associate during co-immunoprecipitation after cell lysis. Walker-Gray et al. developed a light-activated cross-linking approach to monitor PKA subunit interactions with temporal precision in living cells. They observed that, upon β-AR stimulation using ISO, C-RII association was reduced and this effect was abolished if cross-linking was performed after, but not before, cell lysis. The data obtained contradict the previous proposed theory that PKA catalytic subunits remain tethered to regulatory subunits during cAMP elevation. Additionally, they revealed that the regulatory subunits are always in large molar excess of catalytic subunits (average ~17-fold) in all cells and tissues tested. These observations support the original model where binding of cAMP to the R subunits causes a conformational change and release of the C

subunit, allowing phosphorylation of PKA targets. The authors therefore propose a more complete model whereby, after activation of an R and C subunits complex by cAMP, the range over which the released C subunit can phosphorylate substrates will depend on its rate of diffusion and the rate of recapture by R subunits (Walker-Gray et al., 2017). Future experiments will be required to resolve this open and controversial question.

1.2.4 Exchange Protein directly Activated by cAMP

A database screen conducted in 1998 to explain the insensitivity of cAMP-induced activation of the small GTPase Rap1 to inhibitors of PKA led to the identification of EPAC, an exchange protein directly activated by cAMP (also known as cAMP-GEF or RAPGEF3)(de Rooij et al., 1998). This approach identified independently two proteins containing a cyclic nucleotide-binding (CNB) domain: EPAC1 and EPAC2 (or RAPGEF3 and 4, respectively). EPAC1 and EPAC2 are multidomain proteins that consist of an N-terminal regulatory region and a C-terminal catalytic region. The regulatory region contains one (EPAC1) or two (EPAC2) CNB domains and has an auto-inhibitory function that is relieved by binding of cAMP due to conformational changes (Rehmann et al., 2006, 2008; de Rooij et al., 2000).

EPAC proteins function as guanine nucleotide exchange factors (GEFs) for both Rap1 and Rap2 (de Rooij et al., 2000). Rap is a small Ras-like GTPase that was first identified as a protein that could suppress the Ras-mediated oncogenic transformation of cells. It belongs to the Ras superfamily of small G proteins, specifically to the Rap subfamily, which cycle between an inactive guanosine diphosphate (GDP)-bound state and an active guanosine triphosphate (GTP)-bound state. Rap, whose activation by cAMP occurs independently of PKA, is activated by several extracellular stimuli and is involved in a large variety of cellular processes, including cell proliferation and adhesion, actin cytoskeleton dynamics, cell polarity, exocytosis, membrane protein recycling and cell differentiation (Bos, 2006). Several studies have showed the involvement of EPAC in cell migration and proliferation of several types of cancer, making EPAC a potential therapeutic target for cancer treatments (Kumar et al., 2018; Wang et al., 2017).

Similarly to PKA, EPAC proteins are spatially regulated by different anchoring mechanisms. In response to cAMP, EPAC1 is targeted to the plasma membrane, where it tethers to phosphatidic acid or to phosphorylated cytoskeleton proteins to induce its downstream effectors (Consonni et al., 2012; Gloerich and Bos, 2010; Gloerich et al., 2010; Ponsioen et al., 2009). Radixin has also been reported to bind EPAC1 and PKA simultaneously, bringing these two cAMP effectors together and creating a functional cAMP-sensing sub-plasma membrane compartment for efficient signal transduction (Hochbaum et al., 2011). EPAC2 is targeted to the plasma membrane after binding to activated Ras proteins, independently of its cAMP-induced conformational state (Li et al., 2006a). EPAC1 and EPAC2 show distinct activation pattern in response to cAMP raising stimuli, indicating that, similarly to PKA, differently localised EPAC isoforms are under the control of distinct pools of cAMP. In cardiac myocytes, for example, EPAC1 has been shown to be present at the plasmalemma, sarcoplasm and nuclear/perinuclear region (Cazorla et al., 2009; Pereira et al., 2015). Stimulation of β1-AR, but not β2-AR, induces the recruitment of a β-arrestin–EPAC1 signaling complex at the plasma membrane, whereby it activates a pro-hypertrophic signalling cascade involving the small GTPases Rap2 and Ras, and Ca^{2+}/calmodulin-dependent protein kinase II (CaMKII), triggering histone deacetylase nuclear export and initiation of a pro-hypertrophic gene programme (Berthouze-Duquesnes et al., 2013). In detail, under adrenergic stimulation, EPAC1–β-arrestin complex is recruited at the β1-AR, activating a pro-hypertrophic signaling pathway via CaMKII-dependent phosphorylation of ryanodine receptors (RyR), leading to Ca^{2+} leak from the sarcoplasmic reticulum (SR) and subsequent Calcineurin (CaN) activation. CaN will then activate nuclear transcription factor of activated T cells (NFAT) which promotes the expression of several hypertrophic genes (Métrich et al., 2010; Pereira et al., 2012; Ruiz-Hurtado et al., 2013). By contrast, EPAC2 localises at the T tubules (Pereira et al., 2015) and its activation by cAMP in response to β1-AR stimulation leads to CaMKII-dependent diastolic SR Ca^{2+} release and arrhythmias via a pathway that involves EPAC-PI3K-Akt-NOS1 (Pereira et al., 2013, 2017).

1.2.5 Other cAMP effectors - cyclic nucleotide-gated channels and Popeye domain containing proteins

Cyclic nucleotide-gated (CNG) channels are ion channels which are activated by the binding of cyclic nucleotides, including cAMP. CNG channels were first discovered in rod photoreceptors in 1985 (Fesenko et al., 1985; Yau and Nakatani, 1985). The channels are important cellular switches which translate changes in intracellular concentrations of cyclic nucleotides into changes in cations concentrations, such as Ca^{2+}, and membrane potential. CNG channels play a central role in the signal transduction pathways of vision and olfaction as well as in spontaneous depolarization of sinoatrial node cells for generation of cardiac pacemaker activity (Biel and Michalakis, 2009; Brown et al., 2006). Less interest has been demonstrated in the possible roles of CNG channels in other research areas, although several reports have suggested that they are widely distributed and particularly abundant within the central nervous system (Podda and Grassi, 2014).

While trying to identify novel genes involved in heart development, two groups independently identified the first member of the Popeye domain containing (POPDC) gene family (Andrée et al., 2000; Reese et al., 1999). POPDC is a transmembrane protein at the plasma membrane with three transmembrane domains and one Popeye domain facing the cytosolic side (Brand and Schindler, 2017). POPDC proteins have also been identified in the nucleoplasm in satellite cells. Its nuclear localization seems to be dependent on the differentiation status of the cell and is lost after myotube formation (Brand and Schindler, 2017). Other subcellular localizations have also been observed in striated muscle cells, including the intercalated discs (Soni et al., 2016), T-tubules and caveolae (Alcalay et al., 2013). The Popeye domain is 150 amino acid long and displays a strong structural similarity to the cAMP binding domain of the R subunit of PKA but low sequence similarity to either PKA or EPAC (Froese et al., 2012). Interestingly, although the Popeye domain is uniquely found in POPDC proteins, the catabolite activator

proteins (CAPs), which have the highest sequence similarity to POPDC, are cAMP receptor proteins (CRPs) that act as transcription factors and are found exclusively in bacteria (Brand and Schindler, 2017; Körner et al., 2003). Additionally, using a radioligand binding assay and FRET analysis, Froese at al. demonstrated that the cAMP affinity of POPDC proteins is around 10 fold higher than that of EPAC1 and similar to that of PKA (Froese et al., 2012). Evidence suggests that binding of cAMP leads to a conformational change in the Popeye domain, which may result in the exposure of a binding site for POPDC interacting proteins that are not able to interact with POPDC proteins when cAMP is not bound (Schindler and Brand, 2016). However, the role of POPDC proteins in cellular function and any role in cAMP signaling compartmentalization still remains to be elucidated.

1.2.6 Phosphodiesterases

Several studies have shown that the basal concentration of cAMP in a variety of cell types is around 1 μM (Beavo et al., 1974; Börner et al., 2011; Koschinski and Zaccolo, 2017). The diffusion coefficient of cAMP has been experimentally calculated to be around 40μm/s, only one order of magnitude lower than in water (Nikolaev et al., 2004; Richards et al., 2016). cAMP fast diffusion in the cell appears to contradict the notion of cAMP microdomains since one would expect it to result in fast equilibration and homogeneous distribution of cAMP across the cell (Kokkonen and Kass, 2017; Lefkimmiatis and Zaccolo, 2014; Terrin et al., 2006). However, other factors come into play inside a living cell to slow down cAMP diffusion at specific subcellular locations, including cAMP buffering by cAMP binding proteins, such as PKA R subunits (Chen et al., 1999; Lefkimmiatis et al., 2009), cytosol viscosity (Feinstein et al., 2012), physical barriers (Richards et al., 2016) and cAMP degradation mediated by PDEs (Houslay, 2010). PDEs probably are the most well characterized mediators of cAMP compartmentalization since they provide the only mechanism responsible for termination of the cAMP signal (Houslay, 2010). PDEs are members of a superfamily of enzymes that hydrolyze cyclic nucleotides (cAMP or cGMP - cyclic guanosine monophosphate), providing a fine tuned control of cAMP availability to regulate a specific molecular process at a specific nanodomain. The PDE superfamily comprises 8 different families of cAMP-degrading PDEs (PDE1, 2, 3, 4, 7, 8, 10, 11), transcribed from multiple genes that in turn generate many different isoforms (*Fig. 1.1*). Other families of PDEs exclusivelly degrade cGMP, namely PDE5, PDE6 and PDE9 (Bender and Beavo, 2006; Maurice et al., 2014a). Each member shares a similar structure but is functionally unique. Indeed, the catalytic domain located at the C-terminal region of each PDE gene is highly conserved (Conti and Beavo, 2007). Apart from the extensive number of isoforms that arise from multiple transcription starting points and alternative splicing, different PDE isoforms have different tissue distribution and each individual cell can express several

isoforms. Most cells express more than one PDE family and although PDEs exhibit a broad tissue distribution (*Table 1.1*), some cells are relatively enriched in specific PDEs; for example, the photoreceptor PDE6 is almost exclusively expressed in retinal rods and cones (Maurice et al., 2014a). The N-terminus of these proteins is quite diverse and confers unique regulatory properties and targeting sequences that result in tethering of each PDE to specific subcellular locations (Bender and Beavo, 2006; Shepherd et al., 2003). In addition, the N-terminal region can vary in posttranslational modifications (such as phosphorylation sites) that may modulate PDE activity and its ability to form complexes with other proteins in signalosomes while some PDEs can be allosterically regulated by cyclic nucleotides. For example, phosphorylation of PDE3, PDE4 and PDE10 modulates their enzymatic activity and the ability of these enzymes to form complexes with other proteins while PDE2 and PDE3 can be stimulated or inhibited, respectively, by cGMP (Kokkonen and Kass, 2017; MacKenzie et al., 2002). This diversity provides uniquely regulated signaling compartments within the cell, both in terms of magnitude and duration of cAMP-dependent events (Houslay and Milligan, 1997; Zaccolo et al., 2006).

The vast majority of all PDE inhibitors that have been developed target the catalytic site of the enzyme. Broad-spectrum inhibitors were discovered first followed by more selective and potent inhibitors for each PDE family. These have contributed significantly to our understanding of PDE dynamics in cAMP signaling (Francis et al., 2011; Kokkonen and Kass, 2017). Indeed, the involvement of PDEs in cAMP compartmentalization was first described in 1991. Hohl and Li showed that approximately 45 % of the cAMP generated upon ISO treatment of cardiac myocytes is found in the particulate fraction. In addition, ISO stimulation combined with inhibition of PDEs resulted in a total cAMP increase 3.4-fold greater, but the proportion of total cAMP residing in the particulate fraction declined to less than 20%. The authors concluded that this was a result of compartmentalized cAMP in the particulate fractions due to high PDE activity in the cytosol (Hohl and Li, 1991).

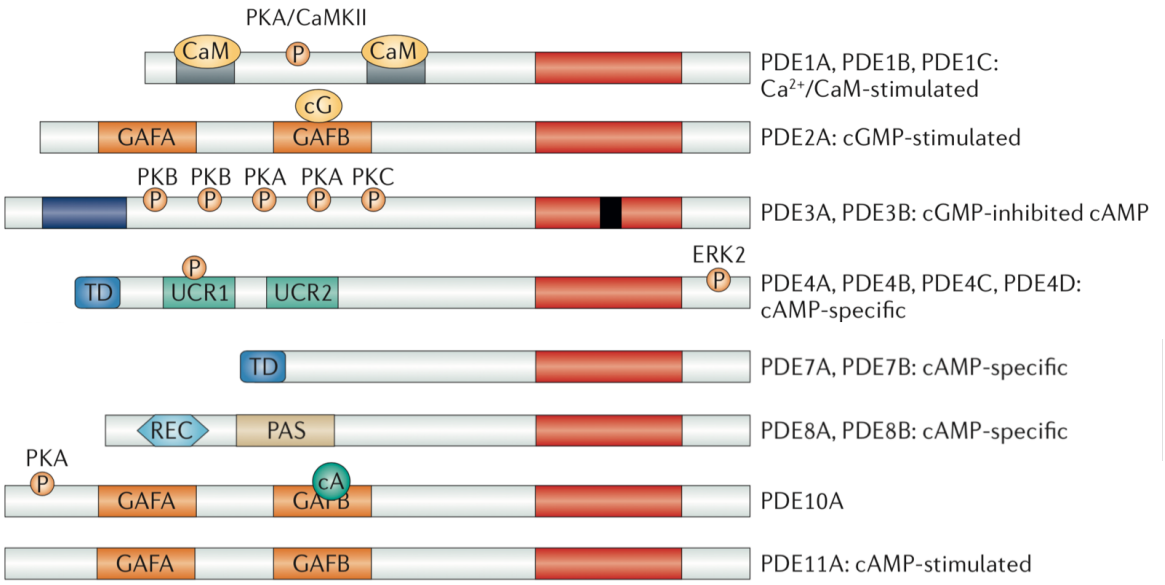


Figure 1.1 | **Structure and domain organization of 8 cAMP-degrading PDEs.**
The conserved catalytic domain (shown in red) is located in the carboxy-terminal portion of the PDEs. The catalytic domain of PDE3 contains a unique 44-amino-acid insert (shown in black). Many of the PDE families contain amino-terminal subdomains (such as GAF domains, transmembrane domains, targeting domains, upstream conserved regions (UCRs), PAS domains and REC domains) and N-terminal hydrophobic regions that are important in subcellular localization, in the incorporation of PDEs into compartmentalized signalosomes, in interactions with signalling molecules and molecular scaffolds, and in the regulation of PDE activity. GAF domains regulate the allosteric binding of cGMP (to PDE2 and PDE11), the allosteric binding of cAMP (to PDE10) and the regulation of catalytic activity (in PDE2). Phosphorylation sites are labelled on the figure. CaMKII, calcium/calmodulin-dependent protein kinase II; ERK2, extracellular signal-regulated kinase 2; PKA, protein kinase A; Pat7, 7-residue nuclear localization signal. Adapted from (Maurice et al., 2014a).

The development of cAMP-sensitive FRET-based sensors allowed for the first time direct visualization of the cAMP gradients and confirmation of the role of PDEs in shaping these intracellular cAMP microdomains, as shown by Zaccolo and Pozzan in rat neonatal cardiomyocyte (Zaccolo and Pozzan, 2002). These observations were followed by subsequent studies using isoform-specific PDE inhibitors. For example, inhibition of PDE4 in cardiac myocytes promotes cAMP generation and propagation of the signal in response to β-agonists, while PDE3 inhibition fails to produce similar effects, demonstrating the importance of distinctly localized PDEs in different signaling cascades (Mongillo et al., 2004).

Table 1.1 | **PDE tissue expression and impact of knockout in mice.**
E17, embryonic day 17; LPA, lysophosphatidic acid; TNF, tumour necrosis factor. Adapted from (Maurice et al., 2014a).

PDE family or gene	Tissue expression	Knockout mouse phenotypes
PDE1: PDE1A (nine variants) PDE1B (two variants) PDE1C (five variants)	Broad; significant in cardiac and vascular myocytes, central and peripheral neurons, lymphoid (T and B cells) and myeloid cells (macrophages have higher expression levels than monocytes) as well as in testes and sperm	PDE1B: increased exploratory behaviour, learning deficits, hyperactivity PDE1C: regulation of olfaction
PDE2: PDE2A (four variants)	Broad; significant in the brain, heart (myocytes), liver, adrenal cortex, endothelium and platelets	PDE2A: embryonic death (E17)
PDE3: PDE3A (three variants) PDE3B (one variant)	Broad; significant in cardiac and vascular myocytes, brain, liver, adipose tissues, pancreatic β-cells, endothelium, epithelium, oocytes and platelets	PDE3A: female infertility owing to oocyte meiosis arrest; dysregulated vascular myocyte proliferation PDE3B: white adipose tissue acquires brown adipose tissue characteristics
PDE4: PDE4A (seven variants) PDE4B (four variants) PDE4C (seven variants) PDE4D (nine variants)	Broad; significant in cells of the cardiovascular, neural, immune and inflammatory systems	PDE4A: no phenotype PDE4B: reduced TNF response to LPA PDE4C: none published PDE4D: delayed growth, impaired ovulation, reduced postnatal viability and refractory to muscarinic cholinergic stimulation
PDE7: PDE7A (three variants) PDE7B (four variants)	Broad in tissues including spleen, brain, lung and kidney as well as in lymphoid and myeloid cells	PDE7A: normal T cell activation; elevated antibody response to a T cell-dependent antigen PDE7B: none published
PDE8: PDE8A (five variants) PDE8B (six variants)	Broad; significant in testes (PDE8A) and thyroid (PDE8B)	PDE8A: increased Leydig testosterone release; increased sensitivity to luteinizing hormone; regulation of excitation–contraction coupling and calcium transients in cardiomyocytes PDE8B: enhanced memory and age-related decline in motor performance
PDE10: PDE10A (six variants)	Expression limited to brain and testes	PDE10A: decreased exploratory behaviour, hypoactivity, delayed acquisition of conditioned avoidance behaviour; female PDE10A-null mice are smaller
PDE11 (four variants)	Expression limited to prostate, testes and salivary and pituitary gland	PDE11A: enlarged lateral ventricles; abnormal behaviour

Terrin et al. further demonstrated that spatial displacement of specific PDEs by exogenously expressing its catalytically inactive mutant version (for instance, PDE4B and PDE4D) selectively affects the concentration of cAMP in individual subcellular compartments in HEK293 cells stimulated with PGE1 (Terrin et al., 2006). Indeed, selective displacement of endogenous PDEs by employing a dominant negative approach has been shown to effectively disrupt local cAMP domains (Baillie et al., 2003; Lynch et al., 2005; McCahill et al., 2005; Zoccarato et al., 2015).

PDEs are also markedly present in the cytosol, with PDE3 and PDE4 representing the major cAMP degrading activities in rat cardiomyocytes. However, PDE4 inhibition by only 10% accounts for a dramatic increase in cAMP, while complete PDE3 inhibition had only a marginal effect on cAMP response to β-AR stimulation. This reinforces the idea that not only PDEs expression levels but also their localization account for modulation of cAMP signaling (Mongillo et al., 2004). In another study, overexpression of catalytically inactive mutants of PDE2A2, PDE3A2, and PDE4D3 in neonatal rat cardiac myocytes showed that displacement of endogenous PDE4D3 and PDE3A2 results in cardiac myocyte hypertrophy, whereas the displacement of PDE2A2 counteracts the hypertrophic growth induced by chronic β-adrenergic stimulation (Zoccarato et al., 2015). This opposing effect is due to the different sub-cellular localization of these PDEs at different compartments, highlighting the importance of PDEs tethering to specific subcompartments in the modulation of local pools of cAMP.

Appart from the cytosol, PDE activity has been extensively studied in other organelles, such as mitochondria, ER/SR, plasma membrane and nucleus. The role of PDE2A in the regulation of mitochondrial dynamics, as well as PDE8, will be further described in section 1.3.1. Additionally, the role of PDE3A and PDE4D in the regulation of different cAMP pools at the SR and their biological relevance will be further detailed in section 1.3.2.

Using FRET sensors targeted to the plasma membrane and dominant negative versions of PDE4D3 and PDE4D7, Henderson *et al*. demonstrated that also PDE4D7 specifically localizes to the sub-plasma membrane where it regulates a local pool of cAMP involved in cell proliferation (Henderson et al., 2014). On the other hand, AKAP9 organises a macromolecular complex containing AC9, PKA, PP1, PDE4D3 and the PKA-regulated potassium channel I(Ks) sensitising PKA-dependent phosphorylation of the channel in response to β-adrenergic stimulation (Li et al., 2012).

Another scaffolding protein, β-arrestin (described in section 1.2.1 and 1.2.4.), has been shown to interact with EPAC1 and PDE4D5. Moreover, EPAC1 competes with PDE4D5 for interaction with β-arrestin following β_2AR activation. Dissociation of the PDE4D5-β-arrestin complex allowed the recruitment of EPAC1 to β_2AR and induced a switch from β_2AR non-hypertrophic signalling to a β_1AR-like pro-hypertrophic signalling cascade. β_1AR, but not β_2AR, induced EPAC1 translocation from the cytosol to the plasma membrane via a β-arrestin-dependent mechanism, resulting in activation of H-Ras through Rap2B, which induces hypertrophic signalling. On the other hand, both β_1AR and β_2AR stimulation induced activation of Rap1, which induces non-hypertrophic signalling (Berthouze-Duquesnes et al., 2013; Fujita et al., 2017). Thus, inhibition of the PDE4D5-β-arrestin interaction within the β_2AR signalosome destroyed the defined cAMP compartmentalization, demonstrating that in such a compartmentalized system, any change to the composition or location of the signalosomes can have dramatic effects (Berthouze-Duquesnes et al., 2013; Ellisdon and Halls, 2016).

Another well characterized signalling domain at the plasma membrane are caveolae, omega-shaped invaginations rich in cholesterol and sphingolipids (Han et al., 2016). Several ACs have been reported to interact with Caveolin, a key structural component of caveolae, such as AC3, AC4, AC5 and AC6 (Bogard et al., 2011; Schwencke et al., 1999; Swaney et al., 2006). The μ-opioid receptor (MOR) interacts with several components of the cAMP pathway, including $G_s\alpha$, PP2A and AC, that are brought together by Caveolin in caveolae. (Chakrabarti et al., 2016).

Although both AC5 and AC6 have been reported to localize to caveolae, other studies demonstrate that these AC isoforms exhibit distinct subcellular localization. The AC6 isoform is localized in the plasma membrane outside the t-tubular region and is responsible for β_1AR signalling-mediated enhancement of the L-type $Ca(^{2+})$ current (ICa,L) in ventricular myocytes. In contrast, the AC5 isoform is localized mainly in the t-tubular region where its influence on ICa,L, upon β_1AR or β_2AR stimulation, is restricted by PDE4D that are brought to close proximity by Caveolins, creating a local cAMP compartment (Timofeyev et al., 2013). The importance of caveolae to spatially regulated cAMP was confirmed by others, where disruption of caveolae in myocytes converted the sarcolemmal-confined cAMP signal associated with β_2AR stimulation to a global signal that targets proteins of the sarcoplasmic reticulum and myofilaments, with functional relevance in cardiovascular disease namely positive lusitropy (Calaghan et al., 2008).

AKAP95 (or AKAP8) is the only member of the large family of AKAPs which anchors PKA in the nuclear matrix in a cell-cycle dependent manner (Coghlan et al., 1994; Eide et al., 1998). Several different functions have been attributed to AKAP95, including DNA replication via interaction with minichromosome maintenance (MCM)2 protein and most likely independently from PKA (Eide et al., 2003), chromatin condensation through association with the RII subunit of PKA (Bomar et al., 2002; Collas et al., 1999), recruitment of Histone Deacetylase (HDAC) to mitotic chromosomes (Li et al., 2006b) and regulation of histone methylation and gene expression (Hu et al., 2016; Jiang et al., 2013). Additionally, AKAP95 has been shown to bind PDE4A (Asirvatham et al., 2004) and is involved in the PKA-mediated phosphorylation of the cAMP-responsive element binding protein (CREB) (Lu et al., 2017). Tyrosine phosphorylation of AKAP95 promotes its dissociation from chromatin and the nuclear matrix, although the impact on local cAMP signalling remains unclear (Kubota et al., 2015).

1.2.6.1 PDE2A

Among the PDE super family, phosphodiesterase 2 (PDE2A) is a cyclic GMP-stimulated phosphodiesterase that hydrolyzes both cAMP and cGMP. The unique feature of this PDE family is that its cAMP hydrolyzing activity can be either stimulated or inhibited by low or high concentrations of cGMP, respectively, allowing cross-talk between cGMP- and cAMP-mediated signaling (Erneux et al., 1980). PDE2A is likely to be involved in the regulation of a wide variety of processes since it is expressed in several different tissues, including brain, heart, liver and adrenal gland (Lobo and Zaccolo, 2018; Stephenson et al., 2009).

1.2.6.2 Biochemistry and Structure

The PDE2A holoenzyme is a homodimer of two 105 kDa subunits, each containing a N-terminal domain, a tandem of GAF domains (GAF A and GAF B; cGMP-stimulated PDE – *Anabaena* Adenylyl cyclase – *E. coli* FhlA transcription factor domain) and a C-terminal catalytic domain (*Fig. 1.2A*) (Martins et al., 1982). The GAF domains, which exist in a parallel dimeric structure as suggested by the crystal structure of PDE2A (*Fig. 1.2B*), are responsible for the dimerization of PDE2A holoenzyme. In particular, the connecting helices between GAF-A and B, and between GAF-B and the catalytic domain function as dimerization interfaces in PDE2A holoenzyme (Bender and Beavo, 2006).

All PDEs, including PDE2A, share a compact helical structure within the catalytic domain. Interestingly, a conserved glutamine residue (Gln859 in human PDE2A) in the catalytic domain functions as the key determinant for nucleotide specificity of PDEs in general. The surrounding residues anchor the glutamine residue in different orientations: in cAMP-specific PDEs, the glutamine residue orientation promotes the formation of hydrogen bonds with the adenine base; in cGMP-specific PDEs, this residue adopts a conformation that allows hydrogen bonding to the guanine base; in PDE2A, this residue can toggle between these two orientations conferring dual-specificity to the enzyme (Zhang et al., 2004). Other residues in the catalytic site, apart from Gln859, may play an additional role in determining substrate specificity.

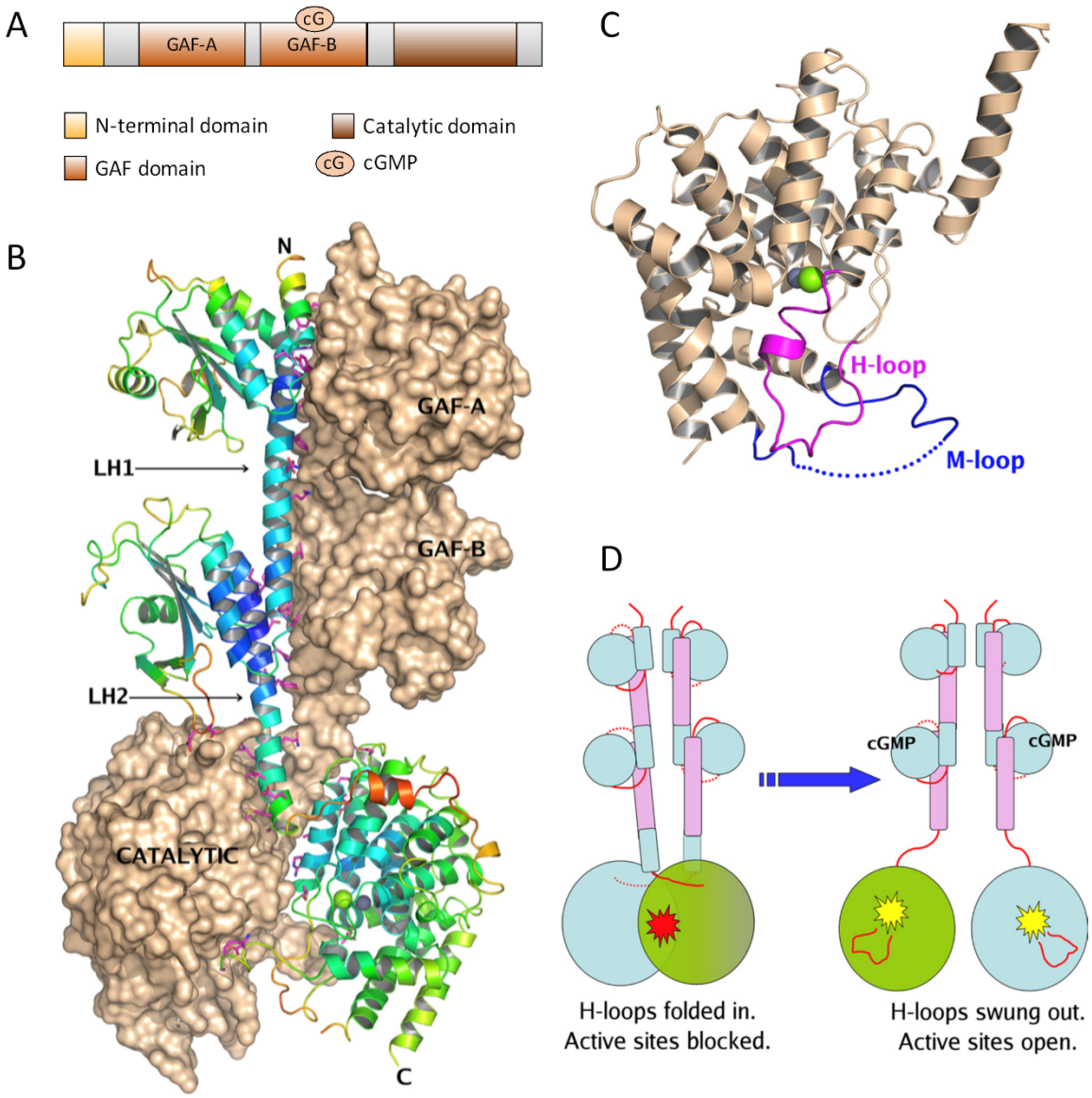


Figure 1.2 | **Domain organization and structure of PDE2.**
(A) PDE2A has a N-terminal domain, unique to each isoform, two GAF domains and one catalytic domain. cGMP binds with high affinity to the GAF-B domain causing activation of the PDE2A catalytic domain.
(B) Structure of human PDE2A (215-900) homodimer. The three domains are labeled in the figure, as well as the linker helices LH1 and LH2 that connect them. Molecule B is shown in surface representation, and molecule A is shown in a ribbons representation. The dimer interface extends over the surface of the entire molecule. The two catalytic sites in the vicinity of the Zn^{+2} and Mg^{+2} ions (shown as gray and green spheres) mutually occlude each other at the dimer interface.
(C) The active site, whose location can be inferred from the position of the Zn^{+2} and Mg^{+2} ions is partially occupied by residues from the H-loop.
(D) Proposed mechanism of activation. The H-loop, which was held in a position to occlude the substrate binding site in the catalytic domain, swings out, after cGMP binding to the GAF-B domain, making the substrate binding site accessible. Taken with permission from (Lobo and Zaccolo, 2018; Pandit et al., 2009).

1.2.6.3 Function and Regulation

PDE2A is a dual substrate enzyme able to hydrolyze both cAMP and cGMP with approximately equal affinity (K_m of 30 and 10 μM, respectively) and efficacy (V_{max} of 120 and 123 μmol min^{-1} mg^{-1}). This reaction produces either 5'-AMP or 5'-GMP, both inactive as a second messenger in cyclic nucleotides pathways (Francis et al., 2009). A special feature of PDE2A is that it displays positive cooperativity for both cyclic nucleotides, *i.e.*, both cAMP and cGMP regulate PDE2A enzymatic activity. Binding of nucleotides to the GAF-B domain (allosteric site) induces a conformational change in the protein and increases the catalytic activity of PDE2A (Martins et al., 1982). Although the affinity of GAF-B for cGMP is 10 times greater than for cAMP, usually cAMP levels within cells are much higher than cGMP. Indeed, low concentrations of cGMP stimulate cAMP hydrolysis through binding to GAF-B, since GAF-A does not bind cGMP. This allosteric stimulation of cAMP hydrolysis by cGMP is biologically more important than inhibition of cAMP hydrolysis via competitive binding to the catalytic site, although cAMP hydrolysis can be inhibited *in vitro* by high concentrations of cGMP. On the other hand, cAMP is able to stimulate cGMP hydrolysis but only at low concentrations of cGMP. Thus, allosteric interaction with both cyclic nucleotides can enhance the catalytic activity of PDE2A allowing cross-talk between cAMP and cGMP signaling pathways (Francis et al., 2009). The crystal structure of a dimerized PDE2A without cyclic nucleotides suggests that in this state the catalytic domain predominantly adopts a closed conformation in which the H- and M-loops (residues 702-723 and 830-856 of human PDE2A, respectively) are folded in at the dimer interface, preventing substrate access to the catalytic site. cGMP binding to GAF-B induces a conformational change between GAF-B and catalytic domain causing the catalytic domain to move apart and adopting an open conformation. This structural change allows the H-loop to swing open, allowing substrate access to the catalytic site (*Fig. 1.2C and D*) (Pandit et al., 2009).

AIP, a component of the aryl hydrocarbon receptor (AhR) complex, was shown to interact with PDE2A. Binding of PDE2A to AIP controls AhR mobility since their interaction inhibits the nuclear translocation of AhR in hepatocytes (de Oliveira and Smolenski, 2009). No further PDE2A binding partners had been identified for this enzyme at the time I started my project. So far there is no evidence of post-translational modifications that regulate PDE2A activity (Azevedo et al., 2014). There is also little knowledge regarding regulation of PDE2A gene expression or its turnover in cells, although it has been reported that PDE2A expression increases after treatment with vascular endothelial growth factor or tumor necrosis factor-α in human umbilical vein endothelial cells, as well as in heart failure, both in rodent models and in humans (Mehel et al., 2013; Seybold et al., 2005). However, the underlined mechanism remains unknown (Lobo and Zaccolo, 2018).

Cross-talk between cyclic nucleotides through PDE2A has important physiological functions, such as atrial natriuretic peptide (ANP)-dependent vasodilation and control of blood pressure. Stimulation of the glomerulosa cells in the adrenal cortex by ANP induces cGMP synthesis, followed by PDE2A activation and a consequent decrease of cAMP levels followed by reduction in aldosterone secretion and vasodilation (Zaccolo and Movsesian, 2007). Another example of cross-talk between cAMP and cGMP mediated by PDE2A is β-adrenergic signaling in the heart. Due to its specific subcellular localization, PDE2A has a significant impact in the regulation of β-adrenergic-induced cardiac inotropy, although it only accounts for approximately 3% of total PDE activity in neonatal rat cardiomyocytes. PDE2A is essentially ineffective in blocking intracellular cAMP increase in response to forskolin, a non-selective activator of adenylyl cyclases, although it blocks the rise of cAMP levels induced by β-adrenergic receptor agonists, namely norepinephrine. Enhancement of cAMP-degrading activity of PDE2A occurs, at least in part, through activation of β3-adrenergic receptors and a consequent activation of endothelial nitric oxide synthase (eNOS). Activated eNOS generates NO, which in turn activates soluble

guanylate cyclase to produce cGMP, promoting allosteric activation of PDE2A and cAMP hydrolysis, leading to reduced heart contractility (*Fig. 1.3*). The selective effect of PDE2A on cAMP generated by β-agonists suggests that PDE2A is tightly coupled to the β-adrenergic receptor system. This implies that PDE2A activity is highly compartmentalized and modulates a restricted pool of cAMP within the cell (Azevedo et al., 2014).

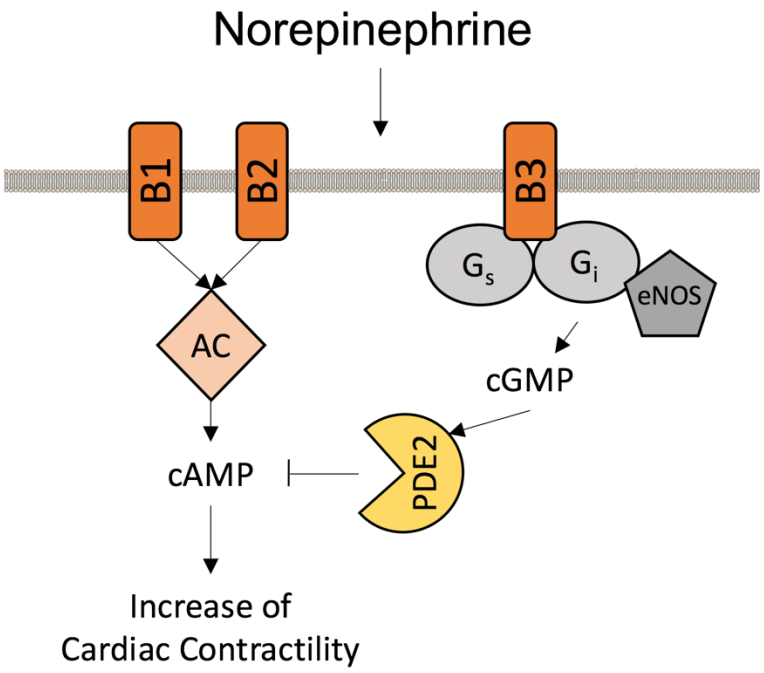


Figure 1.3 | **Role of PDE2A on cardiac contractility.**
PDE2A modulates the rise of cAMP levels induced by norepinephrine due to its coupling with the β-adrenergic receptor. Taken with permission from (Lobo and Zaccolo, 2018).

The ability of PDE2A to hydrolyze a confined pool of cAMP is supported by a number of studies. For example, while a rise in cAMP due to PDE3 and PDE4 inhibition results in hypertrophy, increasing cAMP levels via PDE2A inhibition counteracts hypertrophy. PDE2A inhibition involves the generation of a local pool of cAMP and activation of PKA type II subset, leading to

phosphorylation of the NFAT (Zoccarato et al., 2015). In line with this finding, increased expression of PDE2A has been reported to be associated with heart failure in several animal models as well as in humans (Aye et al., 2012), where excessive hydrolysis of a local pool of cAMP may result in reduced phosphorylation of NFAT and consequent activation of pro-hypertrophic genes, possibly contributing to the myocardial remodeling associated with heart failure.

PDE2A is expressed in a wide variety of human tissues, such as brain, neurons, heart, liver, kidney, lung, adrenal gland, platelets, endothelial cells or macrophages. Its biological functions include memory improvement, thrombin-induced activation of human platelets, excitation/contraction coupling, monocytes to macrophages differentiation and endothelial barrier function (Azevedo et al., 2014; Zaccolo and Movsesian, 2007). As suggested by several studies, the functional outcome downstream of PDE2A is unlikely to rely exclusively on the activity of this enzyme, as cyclic nucleotides levels are regulated by a complex network where multiple PDEs contribute simultaneously to regulate a specific pool of second messenger (Zaccolo and Movsesian, 2007). Additionally, other enzymes such as cAMP/cGMP-dependent kinases, phosphatases and cyclases, together with PDEs, form a complex signaling system that allows compartmentalization of cyclic nucleotides signaling in order to generate specific intracellular responses to different stimuli.

1.2.6.4 Isoforms and Subcellular localization

A single PDE2A gene (chromosome 11q13.4) gives rise to multiple PDE2A variants due to alternative splicing and use of alternative initiation codons: the soluble PDE2A1 and the membrane-associated PDE2A2 and PDE2A3 (Russwurm et al., 2009); in addition, the sequence for a PDE2A4 variant has been deposited (NCBI Reference Sequence: NM_001146209.2), however no further characterization of this isoform is available. All PDE2A isoforms share the same C-terminal sequence (including GAF-A, GAF-B and catalytic domains) but each isoform has a unique N-terminal region (Azevedo et al., 2014). These isoforms have been cloned from different tissues/organisms: bovine adrenal gland (PDE2A1), rat brain (PDE2A2) and human brain (PDE2A3). However, it still remains unclear which PDE2A isoform is expressed as a protein in a given tissue or species, due to the lack of reliable isoform-specific antibodies (Russwurm et al., 2009). Nevertheless, there are no known differences in kinetics behavior among the PDE2A isoforms.

The N-terminal region of each PDE2A isoforms differs in its hydrophobicity, making it likely to determine the subcellular localization of the different isoforms. The PDE2A1 variant, which has the most hydrophilic N-terminus, was originally isolated from the soluble fraction of bovine adrenal gland. N-terminal PDE2A fragments fused to a fluorescent protein were shown to be sufficient to mediate subcellular targeting (Acin-Perez et al., 2011a). According to this study, PDE2A1, PDE2A2 and PDE2A3 localize in the cytosol, mitochondria and plasma membrane, respectively. Indeed, the N-terminus of PDE2A3 features a motif for N-myristoylation of a Glycine residue at position 2, that determines its plasma membrane targeting (Russwurm et al., 2009).

1.2.6.5 Pharmacology and Perspectives

In the early years, Sutherland and colleagues determined that caffeine competes with cAMP or cGMP for access to the catalytic sites of PDEs, due to the fact that caffeine contains a purine similar to the adenine and guanine of cAMP or cGMP, respectively (*Fig. 1.4A*). Since PDEs act as terminators of cyclic nucleotide-dependent signals, this property has been exploited to develop several pharmacological compounds for therapeutic effect. In the 70s, a synthetic inhibitor (3-isobutyl-1-methylxanthine; IBMX) with a similar structure to caffeine was developed and, since then, it has been widely used to block PDE activity (*Fig. 1.4A*) (Francis et al., 2009).

PDE2A specific inhibitors provide a powerful tool for investigating cyclic nucleotides signaling and, more specifically, for dissecting the role played by this dual substrate phosphodiesterase in the complex cyclic nucleotide signaling pathway. For many years, the only PDE2A inhibitor available has been EHNA (erythro-9-(2-hydroxy-3-nonyl)adenine); however it lacks the high selectivity and potency for conclusive pharmacological evaluation since it also acts as a potent adenosine deaminase inhibitor (*Fig. 1.4A*) (Gomez and Breitenbucher, 2013). More recently, BAY-60-7550 (hereafter named BAY-60), a more potent and selective PDE2A inhibitor, has been developed (*Fig. 1.4A*) (Boess et al., 2004). BAY-60 inhibits the hydrolytic activity of purified PDE2A (IC50 = 0.002 μM) and is selective with respect to other PDE isoforms (50 fold versus PDE1C, >100 fold selectivity over other PDE isoforms). Animal studies have suggested promising effects of these compounds, especially BAY-60, in improving learning ability, although none of the inhibitors has been tested in humans (Boess et al., 2004). BAY-60 produced anti-depressant-like effects in stressed mice, supporting a potential role for PDE2A in cognitive impairment related to stress. Although the poor pharmacokinetic properties of BAY-60 probably preclude its use in clinical studies, the compound has been an essential tool to study the role of PDE2A in cyclic nucleotides signaling and to test the potential therapeutic use

of PDE2A inhibition (Gomez and Breitenbucher, 2013).

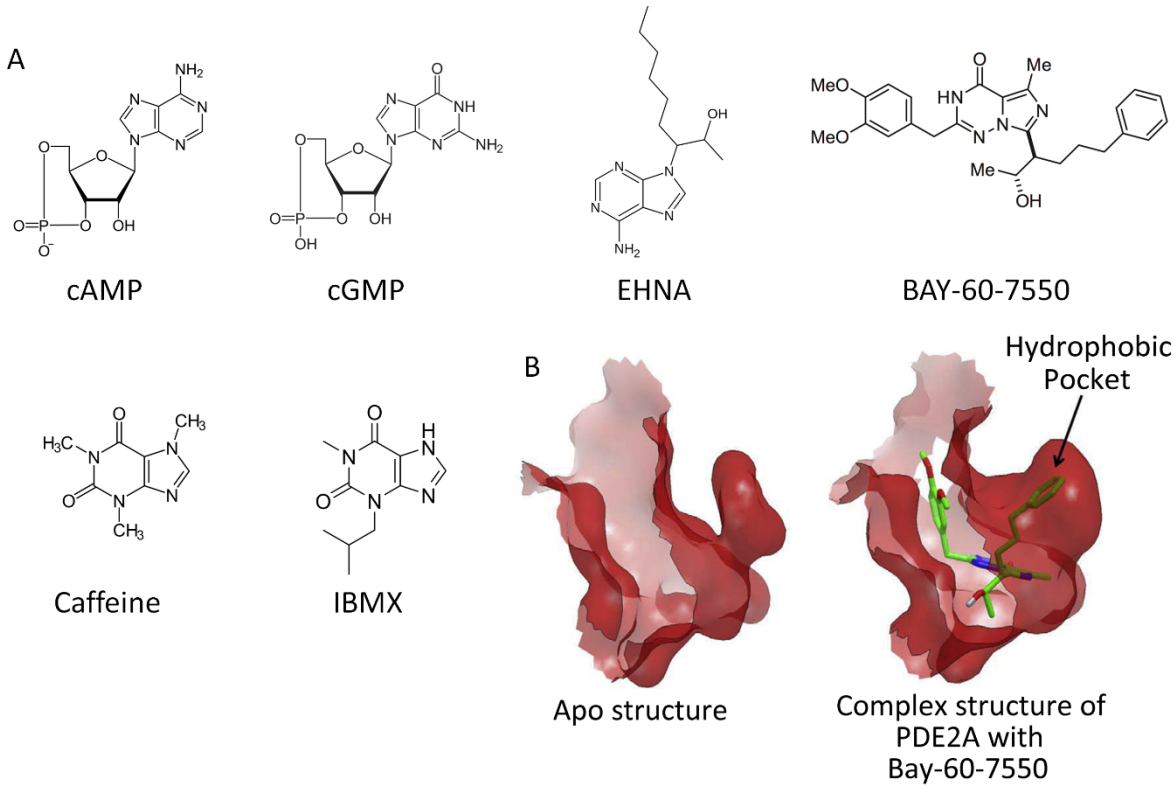


Figure 1.4 | **Overview of the chemical structure of cyclic nucleotides and PDE2A inhibitors.**
(A) Similarities between cyclic nucleotides and PDE2A inhibitors.
(B) Fitting of BAY-60 on the hydrophobic pocket of the catalytic domain. Taken with permission from (Gomez and Breitenbucher, 2013; Lobo and Zaccolo, 2018).

The crystal structure of PDE2A bound to BAY-60 showed that BAY-60 binds to the catalytic site of the enzyme and interacts with the conserved glutamate residue Gln589 (*Fig. 1.4B*). When compared with the Apo structure, it appears that binding of BAY-60 induces a conformational change of the enzyme that exposes a hydrophobic pocket which can accommodate the propylphenyl group of the compound. This may contribute to the high selectivity of BAY-60 for PDE2A over other members of the PDE family since this hydrophobic pocket has not been found in any other published PDE-inhibitor complex (Zhu et al., 2013). So far, there is only one PDE2A inhibitor under clinical study (phase I), developed by *Pfizer*, suggested for migraine (Maurice et al., 2014b).

More recently, PDE2A was characterized in human malignant melanoma pseudomyxoma peritonei cells which have mutations in PDE2A2. These PDE2A mutations were associated with down-regulation of cyclin A and induction of G_2/M arrest, thus raising the possibility that PDE2A2 might be a future target in treating malignant melanoma (Morita et al., 2013). Although no known diseases have been firmly associated with PDE2A mutations so far, PDE2A knockout mice have been reported to be embryonically lethal at E17-E18 (Stephenson et al., 2009). Additionally, a loss-of-function homozygous point mutation in the GAF-B domain of PDE2A has been recently associated with early-onset chorea, a neurological disorder characterized by abnormal involuntary movement , although the molecular mechanism remains to be studied (Salpietro et al., 2018).

1.2.7 Phosphatases

The phosphorylation state of a PKA target depends on the dynamic balance between PKA activity and phosphatase activity available in a specific cell compartment (Virshup and Shenolikar, 2009). Thus, phosphatases are the last checkpoint control for termination of the cAMP/PKA signaling cascade (Heijman et al., 2013).

The three most abundant and extensively studied serine/threonine phosphatases are members of the protein phosphatase type 1 (PP1) and type 2 (PP2) family, including PP2A and PP2B (also known as Calcineurin), designated PPPs (phosphoprotein phosphatases) (Virshup and Shenolikar, 2009). Indeed, PP1, PP2A and Calcineurin account for >90% of phosphatase activity in cardiac myocytes (Heijman et al., 2013). A key defining feature of all PPP proteins is that they are multimeric enzymes where the catalytic subunit is associated with numerous PPP regulatory subunits. These regulators are key determinants of PPP subcellular localization, substrate specificity and regulation of enzymatic activity, conferring high complexity to serine/threonine phosphatase system. Additionally, an increasing number of PPP inhibitory proteins that also control the dephosphorylation capacity of a specific phosphatase complex have been identified (Virshup and Shenolikar, 2009). Physical association of substrates with phosphatases (both the regulatory and catalytic subunits) is a common feature, narrowing down the substrate specificity of PPP. Unlike PKA, a well-defined consensus sequence in the substrates of protein phosphatases has not been found, confirming the importance of a specific substrate-binding surface for recognition of phosphoprotein substrates (Virshup and Shenolikar, 2009).

PP1 is ubiquitously expressed in most cell types. It includes three types of catalytic subunits that are expressed by different genes (PP1α, PP1γ, and PP1δ also known as PP1β) (Herzig and Neumann, 2000). Each PP1α and PP1γ isoform has two splice variants (PP1α1 and

PP1α2; PP1γ1 and PP1γ2) and different isoforms localize to distinct cellular regions. More specifically, in the heart, the myofibrillar fraction contains mainly PP1α (Herzig and Neumann, 2000), while PP1β predominantly localizes to the longitudinal SR and PP1γ is enriched in the junctional SR (Aoyama et al., 2011). PP1 catalytic subunits dimerize with more than 200 regulatory subunits (Heroes et al., 2013).

PP2A can form a dimer containing a catalytic (PP2A-C) and structural scaffold (PP2A-A) subunits, or a trimer consisting of scaffolding, catalytic and regulatory subunits. The scaffolding and catalytic subunits consist of two isoforms each (PP2A-Aα and PP2A-Aβ; PP2A- Cα and PP2A-Cβ) while the regulatory PP2A subunits are organized in four families (PP2A-B, PP2A-B′, PP2A-B″, and PP2A-B‴), most of which contain multiple isoforms with different splice variants (DeGrande et al., 2013; Heijman et al., 2013; Shi, 2009). The diversity of PP2A derives from the fact that cells can assemble more than 200 distinct protein complexes containing different combinations of PP2A-A, PP2A-B, PP2A-C, and other proteins (Virshup and Shenolikar, 2009). To further increase this diversity, different regulatory subunits can be expressed in different tissues at different times, leading to the presence of a variety of tissue-specific and age-specific PP2A complexes (Virshup and Shenolikar, 2009). Although regulatory subunit alpha and beta are mainly cytosolic, the gamma subunit is enriched in the cytoskeletal fraction, conferring different subcellular localizations to the PP2A holoenzyme (Strack et al., 1998).

Other studies have shown that the cytosol is enriched in phosphatase activity, mainly PP1 and PP2A (Haj Slimane et al., 2014), and/or lower PKA activity when compared to the outer mitochondrial membrane (OMM) (Lefkimmiatis et al., 2013). Phosphorylation of the inhibitory troponin subunit (TnI) predominantly determines Ca^{2+}-sensitivity of the myofilaments and cardiomyocytes contraction. PP1 and PP2A are the major phosphatases controlling dephosphorylation of myofilament proteins and β-AR stimulation contributes to PP2A

dissociation from the myofilament complex (Heijman et al., 2013; Yin et al., 2010), pointing at a dynamic regulation of phosphatase activity at this site. As mentioned before, the more sensitive RI subunits are found predominantly in the soluble fractions of the cell, meaning that lower cAMP levels can trigger PKA activity in the cytosol. The excess of phosphatases in the cytosol may limit PKA activity when compared to other organelles and functionally define distinct cAMP/PKA signaling microdomains (see Chapter 7).

Additionally, similarly to PP1, the regulatory subunits of PP2A contribute to substrate specificity, regulating the dephosphorylation of different phosphorylated residues on the same protein. For instance, the PP2A heterotrimer containing a B subunit (PPP2R2) dephosphorylates threonine 124 of SV40 large T antigen, while the same PP2A heterotrimer containing PPP2R3 dephosphorylates serines 120 and 123 (Cegielska et al., 1994; Virshup and Shenolikar, 2009).

Calcineurin is a Ca^{2+}-dependent phosphatase consisting of one catalytic (CNA) and one regulatory (CNB) subunit, linking Ca^{2+}- and cAMP/PKA signaling pathways. CNA is expressed by three genes (CNAα, CNAβ, and CNAγ) while CNB is expressed by two genes (CNBα and CNBβ) (Shi, 2009). Similarly to other phosphatases, there are several additional interacting proteins that modulate Calcineurin phosphatase activity, such as AKAP79 (Heijman et al., 2013).

1.3 cAMP subcellular compartments

The next two sections will illustrate our current understanding of organization and function of two cAMP signaling subcellular compartments, namely the mitochondria and the endoplasmic reticulum (ER).

1.3.1 Mitochondria

Mitochondria have been increasingly recognized over the past few years as organelles with tightly regulated cAMP signaling. Indeed, every mitochondrial compartment, including the outer mitochondrial membrane (OMM), the intermembrane space (IMS) and the mitochondrial matrix, potentially harbour a spatially and functionally distinct cAMP signalosome. Several components of the cAMP signaling pathway, including source of cAMP, effectors and terminators of the response, have been identified within different suborganelle compartments (Monterisi and Zaccolo, 2017).

The idea that cytosolic cAMP cannot reach the mitochondrial matrix was first purposed by Acin-Perez et al. who demonstrated that, unlike the OMM, the IMM is not permeable to cytosolic cAMP and suggested that the second messenger is generated within mitochondria by the carbon dioxide/bicarbonate-regulated soluble adenylyl cyclase (sAC) in response to metabolically generated carbon dioxide (*Fig. 1.5*) (Acin-Perez et al., 2009a). These findings were later confirmed using FRET-based sensors, showing that the IMM acts as a barrier to cAMP diffusion. Therefore, OMM and IMS are physically separated from the mitochondrial matrix which forms an independent cAMP domain separated from the cytosol. Evidence has been published in support of a mechanism whereby an increase of Ca^{2+} in the mitochondrial matrix stimulate a local cAMP increase that promotes mitochondria ATP synthesis (Di Benedetto et al., 2013; Lefkimmiatis et al., 2013; Wang et al., 2016). These findings suggest

that the mitochondrial matrix may host a cAMP signaling pathway that responds to metabolic changes and is independent of cytosolic cAMP signals (Lefkimmiatis and Zaccolo, 2014). The fact that PKA subunits lack any obvious mitochondrial targeting sequence challenges the idea of their presence in the matrix (Valsecchi et al., 2014). Indeed, cAMP signaling in the matrix remains controversial since experiments using FRET-based sensors targeted to the matrix failed to detect endogenous PKA activity in this compartment (Lefkimmiatis et al., 2013). Other studies suggest that alterations in mitochondrial cAMP and PKA activity, induced by cAMP analogues or PKA inhibitors, do not significantly affect Ca^{2+} stimulation of oxidative phosphorylation (Covian et al., 2014).

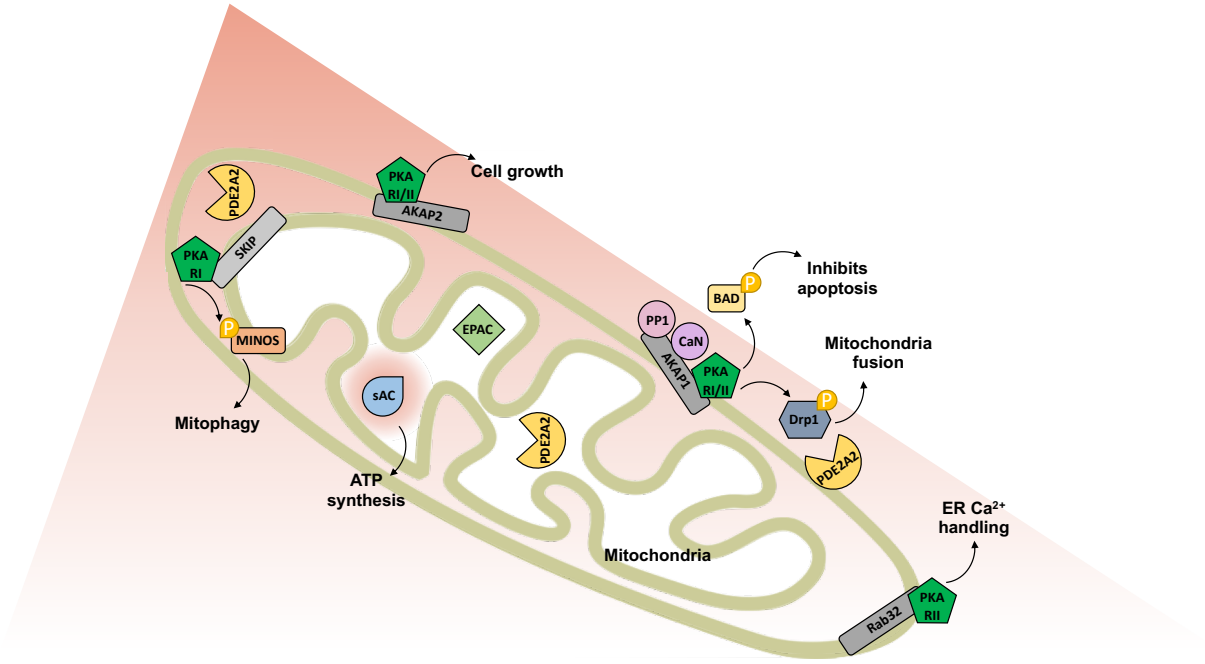


Figure 1.5 | **Overview of mitochondrial cAMP/PKA compartments.**
At the outer mitochondrial membrane there are three different AKAPs – AKAP1, AKAP2 and Rab32. AKAP 1 and 2 can form complexes with PKA type I and II while Rab32 only binds to PKA type II. AKAP1-bound PKA is involved in the phosphorylation of both pro-apoptotic protein BAD and fission regulator Drp1, two effectors that are involved in regulation of cell survival. The intermembrane space harbours SKIP, an AKAP specific for PKA type I. PKA in the intermembrane space can phosphorylate ChChD3, a component of the MINOS complex. Additionally, sAC has been identified as a cAMP source in the mitochondrial matrix. Red gradients represent cAMP generated either at the plasma membrane or mitochondrial matrix. CaN - Calcineurin.

Apart from different sources of cAMP, both cAMP effectors EPAC and PKA have been identified in mitochondria. EPAC1 was originally reported to localize to the mitochondria in a cell cycle-dependent manner, although its precise submitochondrial localization and function were still unclear (Qiao et al., 2002). Treatment of isolated mitochondria with EPAC-specific activators had no effect on oxygen consumption and oxidative phosphorylation activity (Acin-Perez et al., 2009a). However, another recent study suggests the existence of EPAC, both isoform 1 and 2, as cAMP effectors inside the mitochondrial matrix (Wang et al., 2016). The authors conclude that in rat cardiac myocytes, cAMP generated by sAC is responsible for the activation of EPAC1, which protects mitochondria from Ca^{2+} overload, dissipation of mitochondrial membrane potential and, eventually, cell death. On the other hand, it has been reported that during ischemia or acidosis, sAC translocates to the mitochondria, activating a local pool of PKA which phosphorylates and enhances the activity of the pro-apoptotic BAX protein (Appukuttan et al., 2012; Kumar et al., 2009). Contrary to the previous observations, these results suggest that sAC regulates and promotes mitochondria-dependent pathway of apoptosis, raising the question whether distinct mitochondrial pools of cAMP may have opposing effects. Additional research is needed to further clarify these opposing observations regarding the presence and effect of both sAC and EPAC on mitochondria biology and cell survival.

PKA R and C subunits were firstly isolated from purified mitochondria almost 30 years ago (Papa et al., 1999; Schwoch et al., 1990) and, in contrast to EPAC, PKA has been described in all mitochondrial compartments. An analysis of mitochondrial phosphoproteome by mass spectrometry identified over 100 potential PKA targets among proteins that localize to the mitochondria (Grimsrud et al., 2012). Most of these phosphorylation sites have not been investigated yet, suggesting that potentially there are still several mitochondrial signalosomes to be identified and characterized (Monterisi and Zaccolo, 2017). The targeting of PKA to the OMM and IMS is achieved via binding to a number of different AKAPs. At least three different

AKAPs have been found to associate with the OMM: AKAP1 (or its isoforms AKAP121, AKAP149 and S-AKAP84, depending on the species) (Affaitati et al., 2003; Ma and Taylor, 2002), AKAP2 (Wang et al., 2001) and Rab32 (Alto et al., 2002) (*Fig. 1.5*). The presence of several AKAPs at the OMM suggests that this site contains several cAMP signalosomes important for different cellular functions. PKA anchored at the OMM is activated by cytosolic cAMP and is involved in several functions, such as control of mitochondrial morphology (Merrill et al., 2011) or cell death (Affaitati et al., 2003). This suggests that depending on which cAMP/PKA hub is activated, different cellular outcomes may be triggered.

AKAP1 has two N-terminal splice variants, with the shorter form being targeted to the mitochondria trough a functional tubulin-binding motif on its N-terminus essential for mitochondrial localization. Another feature of this AKAP is the ability to bind both types of PKA holoenzymes, the type I and type II (Ma and Taylor, 2002; Torres-Quesada et al., 2017). AKAP1 induction stimulates PKA-dependent phosphorylation of the pro-apoptotic protein BAD, inhibits release of cytochrome c from mitochondria, and protects cells from apoptosis. However, point mutations that disrupt the binding of AKAP1 to PKA lead to increased apoptotic cell death (Affaitati et al., 2003; Harada et al., 1999). Other studies have reported that, in cardiac myocytes, downregulation or displacement of AKAP1 resulted in mitochondrial dysfunction and cell death, confirming the pro-survival actions of AKAP1-tethered PKA (Livigni et al., 2006; Perrino et al., 2010). Equally, it has been shown that the overexpression of AKAP1 promotes recruitment of PKA to the OMM and increased Dynamin-1-like protein (Drp1; GTPase involved in regulating mitochondrial fusion-fission balance) phosphorylation at Serine 637, inhibiting mitochondrial fission and promoting cell survival (Merrill et al., 2011). Collectively, AKAP1-tethered PKA seems to induce pro-survival mechanisms such as mitochondrial elongation and inhibition of apoptosis. Other components of the cAMP cascade have also been reported to interact with AKAP1, including Calcineurin (Abrenica et al., 2009), PP1 (Bridges et

al., 2006; Rogne et al., 2009) and PDE4A (Asirvatham et al., 2004), creating a macromolecular complex critical for mitochondrial function (Merrill and Strack, 2014).

Apart from BAD, other apoptosis-related proteins are substrates of PKA, namely BAX and BIM. However, PKA phosphorylation of these proteins has completely opposite effects: PKA phosphorylation of BAD at the OMM inhibits its apoptotic activity as mentioned before. In contrast, PKA-mediated phosphorylation of BAX promotes its translocation to mitochondria and triggers cytochrome c release and apoptosis, while phosphorylation of BIM increases its stability against proteasome-dependent degradation and promotes its apoptotic effect (Zhang et al., 2016). The fact that cAMP can elicit opposing responses through different effectors at the OMM implies that these must be regulated by different and independent mitochondrial signalosomes. Indeed, AKAP1-tethered PKA has been linked to regulation of BAD. However, it still remains to be studied to which signaling complexes BAX and BIM regulation are associated with and its independency from AKAP1-PKA complex.

AKAP2 is another AKAP that localizes to the mitochondria and anchors both RII and RI subunits of PKA (Wang et al., 2001). However, other studies reported absence of AKAP2 in the mitochondria at the neuromuscular junction (Perkins et al., 2001), which may suggest that this localization may be cell type-dependent (Monterisi and Zaccolo, 2017). AKAP2 can also interact with components of the cytoskeleton via its C-terminus (Sarma et al., 2015) and its overexpression promotes cell growth and is required for calcitonin-mediated migration of cancer cells (Li et al., 2017; Thakkar et al., 2016).

Rab32, a member of the Ras superfamily of small molecular weight G-proteins, was initially described as an AKAP for PKA RII involved in mitochondrial dynamics (Alto et al., 2002). More recent studies have shown that Rab32 localizes to mitochondria-associated membranes

(MAM), a specialized subdomain at the interface between mitochondria and ER that acts as an intracellular signaling hub (Bui et al., 2010; van Vliet et al., 2014). At the MAM, Rab32 is involved in the modulation of ER Ca^{2+} handling, in the regulation of the chaperon calnexin protein levels at the MAM and in the regulation of the phosphorylation status of both Bad and Drp1 via PKA, affecting mitochondrial dynamics and cell death (Bui et al., 2010).

Another AKAP, called sphingosine kinase interacting protein (SKIP), has been described in the IMS. SKIP was shown to specifically interact with PKA RI subunits, a feature of particular interest since RI subunits have higher affinity for cAMP compared to RII subunits and most AKAPs bind avidly to PKA-RII (Kovanich et al., 2010; Means et al., 2011). This raises the possibility that the population of PKA in the IMS might be responsive to levels of cAMP that are not sufficient to activate the OMM-tethered pool of PKA (Lefkimmiatis and Zaccolo, 2014). Indeed, PKA has been shown to phosphorylate ChChd3 and Mitofilin (Akabane et al., 2016; Darshi et al., 2011; Schauble et al., 2007a), components of the mitochondrial inner membrane organizing system (MINOS), a multiprotein complex that plays crucial roles in mitochondrial membrane architecture and formation of cristae junctions and contact sites between the outer and inner membranes (Pfanner et al., 2014). Since the MINOS complex is located at the IMM, this suggests that PKA located in the IMS, and possibly anchored through SKIP, may mediate ChChD3 and Mitofilin phosphorylation, although this remains to be confirmed. A mitochondrial kinase, PTEN-induced putative kinase 1 (PINK1), selectively recruits the ubiquitin ligase Parkin to damaged mitochondria, which modifies mitochondria by polyubiquitination, leading to mitochondrial autophagy (mitophagy). Mutations in these proteins are linked to Parkinson's disease (Pickrell and Youle, 2015). Akabane et al. showed that PKA-mediated phosphorylation of Mitofilin and ChChD3 reduces PINK1 levels at the OMM and, consequently, negatively regulates mitochondrial clearance by mitophagy (Akabane et al., 2016). This suggests that the cAMP in the IMS regulates mitophagy via MINOS complex while the OMM cAMP pool is

involved in mitochondria fission-fusion dynamics through Drp1. These data provide strong evidence that, although the OMM is permeable to cAMP, OMM and IMS are two separate cAMP domains involved in different functions. On the other hand, PINK1 has been shown to promote the binding of the RIIβ subunit to AKAP1, increasing PKA activity at this site and mitochondrial trafficking through Miro2 (mitochondrial Rho GTPase) in dendrites of cortical neurons (Das Banerjee et al., 2017). This would suggest a link between OMM and IMS and a possible cross-talk between cAMP signaling at these two sites.

The first report of PDEs at mitochondria dates back to 1982, when Cercek and Houslay, using cell fractionation experiments and PDE activity assays, found two different mitochondrial PDEs, associated with the OMM and the IMM, respectively (Cercek and Houslay, 1982). Among all PDE isoforms, only PDE2A and PDE8 have been linked to this organelle (Acin-Perez et al., 2011a; Shimizu-Albergine et al., 2012). However, consistent with the idea of a cAMP pool confined to the mitochondrial matrix, Acin-Perez et al. reported the existence of an isoform of PDE2A (PDE2A2) that localizes to the matrix of mitochondria isolated from liver and brain lysates (Acin-Perez et al., 2011a). This study showed that targeting of PDE2A2 to the matrix is mediated by its N-terminus and selective inhibition of PDE2A enhanced oxidative phosphorylation and ATP synthesis. However, recently, it has been shown that PDE2A2 localizes to OMM and IMS, rather than mitochondrial matrix, by performing protein fractionation, electron microscopy and super-resolution imaging (Monterisi et al., 2017). PDE2A2 regulates local cAMP levels at the OMM and PKA-dependent phosphorylation of Drp1, affecting mitochondria morphology and apoptotic cell death. These studies were unable to reveal any detectable PDE2A activity in the mitochondrial matrix using FRET imaging. In addition, they demonstrated using sAC knockout cells that the effect of PDE2A on mitochondria morphology and cell death are independent of any cAMP generated in the matrix.

Apart from isoform 2 of PDE2A, isoform A of PDE8 was also shown to co-localize with mitochondrial markers, unlike PDE8B which is distributed in the cytosol. However, both PDE8 isoforms were found to be involved in the regulation of testosterone production in testicular Leydig cells (Shimizu-Albergine et al., 2012; Tsai et al., 2011).

1.3.2 Endoplasmic Reticulum

A classic example of cAMP compartmentalization occurs in the cardiovascular system upon adrenergic stimulation which increases the rate and force of contraction of the heart as well as its relaxation. A critical event regulated by cAMP/PKA signaling is the diastolic Ca^{2+} reuptake via the sarcoplasmic reticulum (SR) Ca^{2+}-ATPase (SERCA2). The pump is part of a signalosome that includes the PKA RII subunit, AKAP18δ and the SERCA2-associated protein PLN (*Fig. 1.6*). In unstimulated myocytes, SERCA2 is inhibited by unphosphorylated PLN. Upon catecholamine-mediated stimulation of β-ARs, PKA-mediated phosphorylation of PLN removes its inhibitory effect on SERCA2, promoting Ca^{2+} refilling of the SR and decreasing of cytosolic Ca^{2+} (Götz et al., 2016; Henn et al., 2004; Rigatti et al., 2015). AKAP18δ acts as a scaffold that coordinates PKA phosphorylation of PLN and inhibition of this cAMP compartment. Disruption of this macromolecular complex was shown to interfere with phosphorylation of PLN and to prevent subsequent release of PLN from SERCA2, thereby affecting the SR Ca^{2+} re-uptake (Lygren et al., 2007). The cAMP pool that controls SERCA2 activity is also modulated by PDE3A and PDE4D (Kerfant et al., 2007). Indeed, PDE4D and PDE3A, but not PDE3B, have been shown to interact with SERCA2 and to regulate basal cAMP levels in SR microdomains containing SERCA2A-PLN and cardiac contractility (Beca et al., 2011, 2013; Schwoerer et al., 2008). Furthermore, phosphorylation of PDE3A1 at a PKA site in its unique N-terminal extension promotes its incorporation into SERCA2/AKAP18δ signalosomes, where it regulates a discrete cAMP pool that controls contractility by modulating phosphorylation-dependent protein-protein interactions (i.e., PDE3A1-SERCA2 and PDE3A1-AKAP18δ interactions), PLB phosphorylation, and SERCA2 activity (Ahmad et al., 2015).

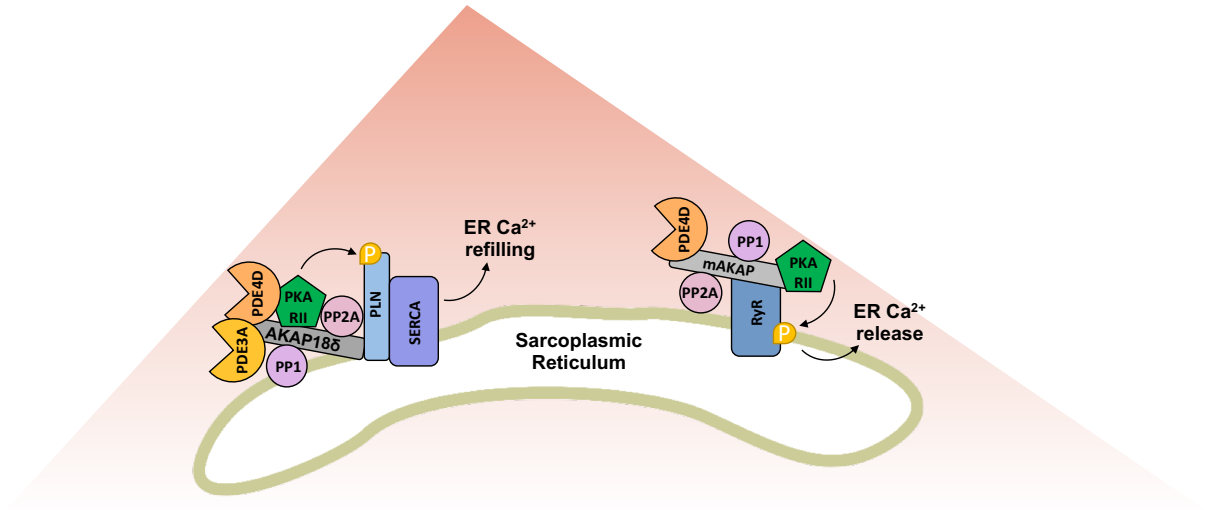


Figure 1.6 | **Overview of Sarcoplasmic Reticulum cAMP/PKA compartments in cardiac myocytes.** AKAP18δ tethers PKA type II near the complex SERCA/PLN. Under basal conditions, both PDE3A and PDE4D maintain cAMP levels low and PKA inactive. Upon catecholamine-mediated stimulation of β-ARs, PKA is activated and phosphorylates PLN. Phosphorylated PLN cannot efficiently inhibit SERCA function, allowing more efficient Ca^{2+} refilling of the ER. The local signal is terminated by the coordinated action of PDEs and phosphatases 1 and 2A. Similarly, mAKAP tethers PKA type II, PDE4D3, PP1 and PP2A in proximity of the ryanodine receptor Ca^{2+} channel (RyR). Red gradient represents a cAMP generated at the plasma membrane.

PP1β is the most significant PP1 isoform involved in regulating SR Ca^{2+} levels (Aoyama et al., 2011). Phosphatase inhibitor-1 (I-1) regulates phosphatase activity and has also been shown to be part of the signaling complex organized by AKAP18δ at the SR. PKA-mediated phosphorylation of I-1 induces potent inhibition of PP1, providing an additional level of regulation of SERCA2 activity (Nicolaou et al., 2009; Singh et al., 2011). Heat-shock protein 20 (Hsp20) has also been identified as an inhibitor of PP1, enhancing PLB phosphorylation and augmenting SR Ca^{2+} levels (Qian et al., 2011), indicating the existence of several pathways that regulate phosphatase activity in response to different stress signals (Heijman et al., 2013). AKAP18δ is the longest isoform of the AKAP18 family which consists of four splice variants (α, β, γ, and δ) with different size and tissue expression patterns. Several of these isoforms show distinct associations with Ca^{2+} signaling, as mentioned above (Torres-Quesada et al., 2017).

Unexpectedly, a knockout mouse model for AKAP18 did not show altered regulation of Ca^{2+} handling in cardiomyocytes (Jones et al., 2012). The authors suggest that the established model where AKAP18 is responsible for anchoring PKA near PLN has to be revised since other AKAPs may be responsible for this. Additionally, differences in AKAP18 expression between species is also a question raised by the authors that should be addressed in the future. The involvement of AKAP18 in synaptic plasticity and contextual memory formation was also recently unveiled (Jones et al., 2016).

Another well characterized cAMP signaling domain at the SR involves mAKAP (muscle specific AKAP), PP1, PP2A, PKA type II and the Ca^{2+} release channels ryanodine receptors (RyR) (*Fig. 1.6*). In failing human hearts, RyR receptors hyperphosphorylated by PKA at Ser-2808 results in defective channel function due to increased sensitivity to Ca^{2+}-induced activation. (Marx et al., 2000). This is associated with reduced association of PDE4D3 with RyR-containing signaling complex in human failing hearts (Lehnart et al., 2005). This is a very controversial topic since other studies have shown that RyR phosphorylation at Ser-2030 is not significantly altered in heart failure but, instead, retains PKA-dependence of phosphorylation (Xiao et al., 2006). Parallel studies showed that Ser-2808 phosphorylation is relatively insensitive to either PKA activation or inhibition (Bers, 2006). Although these studies indicate that Ser-2030, but not Ser-2808, is the major PKA phosphorylation site in RyR responding to PKA activation upon β-adrenergic stimulation, the authors also suggest that phosphorylation of RyR at Ser-2030 may be associated with altered Ca^{2+} handling and cardiac arrhythmia that is commonly observed in heart failure upon β-Adrenergic stimulation (Xiao et al., 2006). Additionally, other studies suggest that mAKAP is localized to the nuclear envelope, and not SR, where it interacts with local RyRs, both in neurons and striated cardiac and skeletal myocytes, three cell types where mAKAP is clearly expressed (Kapiloff et al., 1999; Passariello et al., 2015). These discrepancies may be due to lack of antibody specificity and thus further studies would help to

clarify this question. Phosphatases are key players at the SR, with cardiomyocyte specific deletion of PP2A causing cardiac hypertrophy by disrupting Ca^{2+} transients (Lei et al., 2015; Li et al., 2016).

1.4 Aims of the project

A plethora of cellular processes, including apoptosis and cell survival, depend on regulated changes of the key second messenger cAMP and its effector PKA. cAMP signaling is compartmentalized within the cell, with tight spatial and temporal control of signal propagation underpinning specificity of response. PDEs are a superfamily of cAMP degrading enzymes presenting unique regulation and subcellular localization. PDEs play a key role in the spatial regulation of cAMP propagation and modulate cAMP levels within individual subcellular compartments. By locally degrading cAMP, PDEs dictate which PKA subsets are activated and therefore the downstream targets that are phosphorylated. Compartmentalization of cAMP prompts the idea that with a detailed understanding of the organization, regulation and function of individual cAMP compartments it may be possible to target individual cAMP pools, rather than global intracellular cAMP levels, in order to achieve greater therapeutic efficacy and specificity (Maurice et al., 2014a).

PDE2A is a cGMP-activated phosphodiesterase that degrades both cAMP and cGMP and is expressed in a number of tissues, including brain and heart. A single PDE2A gene gives rise to multiple PDE2A variants due to alternative splicing and each isoform has a different subcellular localization. Genetic ablation of PDE2A results in high embryonic lethality past E17.5–E18.5 dpc, indicating that this enzyme is involved in vital biological functions (Stephenson et al., 2009). Previous evidence suggests localization of PDE2A2 to the mitochondrial matrix where it regulates ATP production via modulation of cAMP generated locally by sAC, although the mechanism is still unknown.

This thesis aims to characterize the role of PDE2A in cAMP/PKA signaling compartmentalization and its biological function, with a particular focus on its role at the mitochondria and ER. The specific aims of this work are:

Aim 1 – To characterize the cellular distribution of different PDE2A isoforms across different cell lines and tissues and their subcellular localization (Chapter 3);

Aim 2 – To validate PDE2A2 interactors (Chapter 4);

Aim 3 – To evaluate the role of PDE2A in mitochondrial biology (Chapter 5);

Aim 4 – To investigate the role of PDE2A on ER Ca^{2+} handling and cAMP dynamics (Chapter 6 and 7);

Chapter 2 - Materials and Methods

2.1 Reagents and Molecular Biology

2.1.1 Reagents and antibodies

BAY-60-7550 was from Cambridge Bioscience. Staurosporin was from Calbiochem. Collagenase was from Roche. Laminin (mouse) from BD Biosciences. Transfection reagents Transfectin and FuGeneHD were from BioRAD and Promega, respectively. Phosphate-Buffered Saline (PBS), DMEM, DMEM/F12, DMEM High Glucose, MEM199, Horse Serum, New born Calf Serum, Penicilline/Streptomycine, Trypsin 0.05 %, Glutamine and Lipofectamine 2000 were from Invitrogen. Suppliers of other materials, media and substances are mentioned in the respective section. Unless otherwise noted, all other reagents were obtained from Sigma-Aldrich. The antibodies used in this study are shown on Table 2.1.

Table 2.1 | **List of antibodies used in this thesis.**

Target	Species	Brand, Code	Dilution
ACSL4	mouse	SCBT, sc365230	1:1000
Anti-mouse Alexa Fluor 647	goat	Thermo, A-21235	1:250
Anti-mouse IgG-Peroxidase	goat	SCBT, sc2005	1:3000
Anti-mouse STAR 580	goat	Abberior, 2-0002-005-1	1:250
Anti-rabbit Alexa Fluor 532	goat	Thermo, A-11009	1:250
Anti-rabbit IgG-Peroxidase	goat	SCBT, sc2030	1:3000
Anti-rabbit STAR RED	goat	Abberior, 2-0012-011-9	1:250
Calcineurin	rabbit	Abcam, ab109412	1:1000

Calreticulin	rabbit	Cell Signaling, 2891	1:1000
Caveolin 3	rabbit	SCBT, sc5310	1:1000
Caveolin 1	rabbit	Abcam, 2910	1:1000
Caveolin 2	rabbit	Abcam, ab133484	1:1000
Cox1	mouse	SCBT, 166573	1:1000
Cytochrome C	mouse	Abcam, ab110325	1:1000
Dysbindin	rabbit	Abcam, ab124967	1:1000
Erlin2	rabbit	Abcam, ab129207	1:1000
FLAG	mouse	Cell Signaling, 8146	1:1000
FLAG	rabbit	Cell Signaling, 2368	1:1000
Full range Marker	-	GE, RPN800E	-
GAPDH	mouse	SCBT, sc166574	1:1000
GAPDH	rabbit	Proteintech, 60004-1-Ig	1:1000
GFP	mouse	SCBT, sc9996	1:1000
GFP	rabbit	Abcam, ab6556	1:1000
GRP75	mouse	SCBT, sc133137	1:1000
IP3R	mouse	BD Biosciences, 610313	1:1000
Mitofilin	mouse	Abcam, ab110329	1:500
Mitofusin 1	mouse	Abcam, ab56889	1:1000
Mitofusin 2	mouse	Abcam, ab56889	1:1000
Myc	rabbit	SCBT, sc789	1:1000
OXPHOS	mouse	Abcam, ab110411	1:3000

P-IP3R (S1756)	rabbit	Cell Signaling, 3760	1:1000
Parkin	mouse	Cell Signaling, 4211	1:500
PDE2A	rabbit	Abcam, ab14604	1:1000
PDE2A	rabbit	Proteintech, 55306-1-AP	1:1000
phospho-(Ser/Thr) PKA substrate	rabbit	Cell Signaling, 2964	1:1000
PINK1	rabbit	Cell Signaling, 6946	1:500
PKA Cγ	rabbit	Abcam, ab108385	1:1000
PKA RIIβ	mouse	SCBT, sc376778	1:1000
PKA RIIα	rabbit	SCBT, sc908	1:1000
PKA RIβ	mouse	SCBT, sc100414	1:1000
PKA RIα	mouse	Abcam, ab60064	1:1000
PKA Rβ	rabbit	Abcam, ab94612	1:1000
PP1	mouse	SCBT, sc7482	1:1000
PP2A	rabbit	Abcam, ab32141	1:1000
RFP	mouse	Chromotek, 6G6	1:1000
RFP	rabbit	Abcam, ab62341	1:1000
SAMM50	mouse	Atlas Antibodies, HPA042935	1:1000
SERCA2	goat	SCBT, sc8094	1:1000
TIM23	mouse	SCBT, sc514463	1:1000
TOM20	mouse	SCBT, sc11415	1:1000
TOM20	rabbit	SCBT, sc11415	1:1000
α-Tubulin	rabbit	Abcam, ab18251	1:5000

2.1.2 Generation of constructs and ER-targeted FRET-based sensors

A list of all constructs generated for this study can be found in Table 2.2. All constructs were generated by PCR amplification using the respective primers, followed by enzymatic digestion and then subcloned in-frame into the respective vector. All generated constructs were verified by sequencing.

Table 2.2 | **List of all plasmids used in this thesis.**
Plasmids are organized according to the fluorescent tag. Plasmids in bold correspond to plasmids that have been generated by myself for this study. No species was attributed to human engineered proteins. No company was assigned to plasmids that were already available in the laboratory or that were generated for this thesis.

Fluorescent Tag	Name	Species	Vector	Bacterial Resistance	Company
RFP/mCherry tag	mCherry-Parkin	Human	mCherry-C1	Kan	Addgene 23956
	Caveolin2b-RFP	Human	pEYFP-C1	Kan	-
	RFP	-	pEYFP-C1	Kan	-
	dnPDE2A2-RFP	mouse	pEYFP-C1	Kan	-
	PDE2A2-RFP	mouse	pEYFP-C1	Kan	-
	mRFP	-	pcDNA3	Amp	-
	N-terminal-RFP	**mouse**	**pEYFP-C1**	**Kan**	**-**
	N-terminal-GAF-A-RFP	**mouse**	**pEYFP-C1**	**Kan**	**-**
	GAF-A-RFP	**mouse**	**pEYFP-C1**	**Kan**	**-**
	GAF-A-GAF-B-RFP	**mouse**	**pEYFP-C1**	**Kan**	**-**
	GAF-B-RFP	**mouse**	**pEYFP-C1**	**Kan**	**-**
	GAF-B-C-terminal-RFP	**mouse**	**pEYFP-C1**	**Kan**	**-**
	C-terminal-RFP	**mouse**	**pEYFP-C1**	**Kan**	**-**
	ΔN-terminal-RFP	**mouse**	**pEYFP-C1**	**Kan**	**-**
	ΔC-terminal-RFP	**mouse**	**pEYFP-C1**	**Kan**	**-**
GFP tag	PDE2A2-GFP	Mouse	pEYFP-C1	Kan	-
	Caveolin3-GFP	Human	pEYFP-C1	Kan	-
	PDE2A1-GFP	Human	pCMV6-AC-GFP	Amp	Origene
	PDE2A2-GFP	Human	pCMV6-AC-GFP	Amp	Origene
	PDE2A3-GFP	Human	pCMV6-AC-GFP	Amp	Origene

GFP tag	**PDE2A4-GFP**	**Human**	**pCMV6-AC-GFP**	**Amp**	**-**
	Taxilinβ-GFP	Human	pCMV6-AC-GFP	Amp	Origene
	GFP	-	pEYFP-C1	Kan	-
	PDE2A1-GFP	**Human**	**pEYFP-C1**	**Kan**	**-**
	PDE2A2-GFP	**Human**	**pEYFP-C1**	**Kan**	**-**
	PDE2A3-GFP	**Human**	**pEYFP-C1**	**Kan**	**-**
	PDE2A4-GFP	**Human**	**pEYFP-C1**	**Kan**	**-**
	PDE2A1-GFP 1-27	**Human**	**pEYFP-C1**	**Kan**	**-**
	PDE2A2-GFP 1-41	**Human**	**pEYFP-C1**	**Kan**	**-**
	PDE2A2-GFP 1-17	**Human**	**pEYFP-C1**	**Kan**	**-**
	PDE2A2-GFP 1-137	**Human**	**pEYFP-C1**	**Kan**	**-**
	PDE2A2-GFP 17-934	**Human**	**pEYFP-C1**	**Kan**	**-**
	PDE2A3-GFP 1-48	**Human**	**pEYFP-C1**	**Kan**	**-**
	PDE2A3-GFP 1-24	**Human**	**pEYFP-C1**	**Kan**	**-**
	PDE2A4-GFP 1-39	**Human**	**pEYFP-C1**	**Kan**	**-**
	PDE2A4-GFP 1-15	**Human**	**pEYFP-C1**	**Kan**	**-**
	Caveolin 1 WT-GFP	**Human**	**pEYFP-C1**	**Kan**	**-**
	Caveolin 1 1-140-GFP	**Human**	**pEYFP-C1**	**Kan**	**-**
	Caveolin 1 94-178-GFP	**Human**	**pEYFP-C1**	**Kan**	**-**
	Caveolin 1 Δ61-100-GFP	**Human**	**pEYFP-C1**	**Kan**	**-**
	Caveolin 1 60-178-GFP	**Human**	**pEYFP-C1**	**Kan**	**-**
	Caveolin 1 77-178-GFP	**Human**	**pEYFP-C1**	**Kan**	**-**
	Caveolin 1 1-100-GFP	**Human**	**pEYFP-C1**	**Kan**	**-**
	Caveolin 1 1-80-GFP	**Human**	**pEYFP-C1**	**Kan**	**-**
	Caveolin 1 60-140-GFP	**Human**	**pEYFP-C1**	**Kan**	**-**
	Caveolin 1 77-178-GFP	**Human**	**pEYFP-C1**	**Kan**	**-**
	Mitofilin WT	**Human**	**pShuttle-IRES-GFP**	**Kan**	**-**
	Mitofilin S528A	**Human**	**pShuttle-IRES-GFP**	**Kan**	**-**
	Mitofilin S528D	**Human**	**pShuttle-IRES-GFP**	**Kan**	**-**
	Mitofilin S528E	**Human**	**pShuttle-IRES-GFP**	**Kan**	**-**
	pEGFP-LC3	Human	pEGFP-C2	Kan	Addgene 24920
FLAG/Myc tag	ChChD6	Human	pCMV6-Entry	Kan	Origene
	ChChD3	Human	pCMV6-Entry	Kan	Origene
	Metaxin2	Human	pCMV6-Entry	Kan	Origene
	Erlin2	Human	pCMV6-Entry	Kan	Origene
	DNAJC1	Human	pCMV6-Entry	Kan	Origene
	Mitofilin/Immt	Human	pCMV6-Entry	Kan	Origene

FLAG/Myc tag	TRIC-A	Human	pCMV6-Entry	Kan	Origene
	ALDH3A2	Human	pCMV6-Entry	Kan	Origene
	OPA1	Human	pCMV6-Entry	Kan	Origene
	VDAC1	Human	pCMV6-Entry	Kan	Origene
	VDAC2	Human	pCMV6-Entry	Kan	Origene
	VDAC3	Human	pCMV6-Entry	Kan	Origene
	Mitofusin2	Human	pCMV6-Entry	Kan	Origene
	SAMM50	Human	pCMV6-Entry	Kan	Origene
	Caveolin1	Human	pCMV6-Entry	Kan	Origene
	Mitofusin2-Myc	Human	pcDNA3.1(-)/Myc-His	Amp	Addgene 23213
	Mitofusin1-Myc	Human	pcDNA3.1(-)/Myc-His	Amp	Addgene 23212
	PDE2A1-FLAG	**Human**	**pCMV6-Entry**	**Kan**	**-**
	PDE2A2-FLAG	**Human**	**pCMV6-Entry**	**Kan**	**-**
	PDE2A3-FLAG	**Human**	**pCMV6-Entry**	**Kan**	**-**
	PDE2A4-FLAG	**Human**	**pCMV6-Entry**	**Kan**	**-**
	Taxilinβ	**Human**	**pCMV6-Entry**	**Kan**	**Origene**
FRET sensors	H90	-	pcDNA3	Amp	-
	ER-cyto-H90	**-**	**pcDNA3**	**Amp**	**-**
	ER-lumen-H90	**-**	**pcDNA3**	**Amp**	**-**
	AKAR4	-	pcDNA3	Amp	-
	ER-cyto-AKAR4	-	pcDNA3	Amp	Addgene 64733
	ER-lumen-AKAR4	**-**	**pcDNA3**	**Amp**	**-**
	d3cpv mito	-	pcDNA3	Amp	-
	d3cpv cytosolic	-	pcDNA3	Amp	-
	D1ER	-	pcDNA3	Amp	-

2.1.3 Real-Time PCR

Total RNA was extracted using the RNeasy Mini Kit (Qiagen) as instructed by the manufacturer. Total RNA was quantified and 1 µg from each sample was used for the reverse transcription reaction using random primers from the High Capacity cDNA Reverse Transcription Kit (Applied Biosystems). Obtained cDNA was amplified by PCR using primers specific for each PDE2A isoform (*Table 2.3*) followed by separation on agarose gel. All reverse transcription-PCR (RT-PCR) products were verified by sequencing.

Table 2.3 | **List of primers used for RT-PCR analysis of PDE2A isoforms mRNA.**
Primers are organized according to orientation, annealing site, isoform, species and sequence.

Orientation	Annealing site	Isoform	Species	Sequence
Forward	Exon 1	PDE2A1	Human	5’ ATGCGCCGACAGCCTG
Reverse	Exon 4/5			5’ ATAGCCTCCCGGACTTTCCC
Forward	Exon 1	PDE2A2		5’ ATGGTCCTGGTGCTGCACC
Reverse	Exon 4/5			5’ ATAGCCTCCCGGACTTTCCC
Forward	Exon 1	PDE2A3		5’ ATGGGGCAGGCATGCG
Reverse	Exon 4/5			5’ ATAGCCTCCCGGACTTTCCC
Forward	Exon 1	PDE2A4		5’ ATGAAGAAACAGAGGATCCAGGAG
Reverse	Exon 4/5			5’ ATAGCCTCCCGGACTTTCCC
Forward	Exon 3/4	PDE2A		5’ TCCCCCGAGTGGAAACTGTC
Reverse	Exon 5/6			5’ GCATGACCAGCACTTGGGTATC

Forward	Exon 1	PDE2A1	Mouse	5’ ATGCGCCGACAGCCTG
Reverse	Exon 4/5			5’ GATCACAGCTTCTCGAATTTTTCC
Forward	Exon 1	PDE2A2		5’ ATGGTCCTGGTGTTGCACCA
Reverse	Exon 4/5			5’ GATCACAGCTTCTCGAATTTTTCC
Forward	Exon 1	PDE2A3		5’ ATGGGGCAGGCATGCG
Reverse	Exon 4/5			5’ GATCACAGCTTCTCGAATTTTTCC
Forward	Exon 1	PDE2Ax		5’ ATGGCCCTGGGGCTTG
Reverse	Exon 4/5			5’ GATCACAGCTTCTCGAATTTTTCC
Forward	Exon 3/4	PDE2A		5’ GCTCCCCAAAGTGGAGACTGTC
Reverse	Exon 5/6			5’ TGACCAGCACTTGCATGTCA
Forward	Exon 1	PDE2A1	Rat	5’ ATGCGCCGACAGCCTG
Reverse	Exon 4/5			5’ CACAGCCTCTCGAATTTTTCCT
Forward	Exon 1	PDE2A2		5’ ATGGTCCTGGTGTTGCACCA
Reverse	Exon 4/5			5’ CACAGCCTCTCGAATTTTTCCT
Forward	Exon 1	PDE2A3		5’ ATGGGGCAGGCATGCG
Reverse	Exon 4/5			5’ CACAGCCTCTCGAATTTTTCCT
Forward	Exon 3/4	PDE2A		5’ GCTCCCCAAAGTGGAGACTGTC
Reverse	Exon 5/6			5’ ATGACCAGCACTTGCGTGTC

2.2 Cell culture

2.2.1 NRVMs culture and transfection

Primary cultured NRVM (Neonatal Rat Ventricular Myocytes) were isolated from 1- to 2-day old Sprague Dawley rats (Charles River) as described (Zaccolo and Pozzan, 2002). Myocytes were plated onto laminin coated coverslips or dishes and transfected with Transfectin following the supplier's instructions. Imaging experiments were performed 24–48 h after transfection.

2.2.2 Isolation of Mouse Embryonic Fibroblasts

Pregnant females obtained from crossing of heterozygous PDE2A KO (knockout) mice (line B6;129P2-Pde2atm1Dgen/H, provided by EMMA, UK), were sacrificed after 13 days of gestation (E.13 dpc) and the embryos collected, then placed into separate dishes containing phosphate buffered saline (PBS; Life Technologies). A segment of the tail was used for genotyping, whereas the head and the internal organs were removed. The remaining tissue was washed with PBS and incubated in trypsin at 37 °C for 5-10 min. The solution was pipetted until the tissue was completely homogenized and the isolated cells (Mouse Embryonic Fibroblasts – MEFs) were plated onto T75 flasks. For transfection, the cells were plated onto sterile 24 mm diameter coverslips in 6-well plates and maintained at 37 °C for 24 h.

2.2.3 Cell lines

HeLa, HEK293T and MEF cells were grown in DMEM + 10 % FBS. SH-SY5Y were grown in DMEM/F12 + 10 % FBS. All cell lines were maintained in a humidified CO_2 (5 %) incubator at 37 °C and were split every 2-3 days after reaching 80-90 % confluency. Cells were tested every other month for mycoplasma contamination by PCR. All plasmids were transfected into HeLa cells using FuGENE HD, into HEK293T cells using polyetherimide (PEI) or Lipofectamine 2000 and into MEFs or SH-SY5Y cells using jetPRIME (Polyplus transfection), according to manufacturer's instructions.

To trigger starvation, cells were washed four times and then incubated in Hanks balanced salt solution (HBSS) supplemented with 10 mM HEPES at pH 7.4, at 37 ºC for the indicated time (Gomes et al., 2011).

2.3 Biochemistry

2.3.1 Immunoprecipitation and western blot

Cells were washed twice with PBS and lysed for 5 min with RIPA buffer containing complete EDTA-free protease inhibitor cocktail tablets (Roche) and PhosSTOP phosphatase inhibitor cocktail (Roche). Lysates were clarified by centrifugation at 10000 rpm for 10 min at 4 °C and the supernatant and incubated at 4 °C for 2 h with 25 µL of anti-RFP/GFP/Myc antibody-linked beads (Chromotek) or anti-FLAG M2 beads (Sigma), respectively, or untagged beads (Chromotek), as a control. For immunoprecipitation of endogenous proteins, the supernatant was pre-cleared through incubation with Protein-G agarose beads (Invitrogen). The supernatant was then incubated for 2 h with the appropriate antibody at 4 °C and overnight incubation with Protein-G agarose beads, as previously described (Lobo et al., 2016). The

beads were pelleted by centrifugation for 1 min at 5000 g, washed 3-5x with wash buffer (Tris-HCl 0.1 M, NaCl 0.3 M, Triton X-100 1 % (v/v), pH 7.5) followed by elution with 1x sample buffer and spin-down. Whenever appropriate, a 5 min incubation at 90 °C was performed during elution. The immunoprecipitate was loaded and separated on SDS-PAGE gels and subsequently transferred to PVDF membranes (Millipore). After transfer, PVDF membranes were blocked for 1 h at room temperature in 5 % skimmed milk TBS-T (Alfa Aesar). Next, the membranes were incubated overnight at 4 °C with primary antibody diluted in 5 % skimmed milk TBS-T. The day after, the membranes were washed 3 times with TBS-T and incubated at room temperature for 1 h with a peroxidase-conjugated secondary antibody. After 3 washes with TBS-T, chemiluminescent detection was performed using ECL western blot Substrate (Thermo Scientific) or Clarity ECL (BioRAD) and Amersham Hyperfilm ECL photographic films (GE-Healthcare). Films were developed with a Xograph Compact X4 Automatic film Processor (Xograph). Signals were evaluated and analyzed using ImageJ (NIH) and Excel (Microsoft) software.

Note: many of the co-immunoprecipitation experiments described in Chapter 4 were performed using constructs that code for a FLAG tag since this is a very short tag that minimizes unspecific binding and has lower probability of disrupting the sub-cellular localization of the protein being expressed. On the other hand, PDE2A constructs code for a fluorescent tag, such as GFP or RFP, since these constructs had been previously generated in the lab and I have shown on Chapter 3 that this fluorescent tag does not affect PDE2A subcellular localization when compared with FLAG tag. Additionally, the original mass spectrometry experiment was performed using a PDE2A2 construct with a fluorescent tag.

2.3.2 Blue-Native gel

Blue-Native (BN)-PAGE was performed with the NativePAGE Bis-Tris Gel System (Thermo Fisher Scientific) as described previously (Schägger, 2001). In brief, the cell preparations were mixed with a 2/5 volume of 4x NativePAGE sample buffer and a 1/5 volume of NativePAGE 5 % G-250 sample additive and were separated by electrophoresis at 4 °C at 200−250 V on a 4−16 % Bis-Tris protein gel. Unstained Protein Standard (Thermo Fisher Scientific), consisting of IgM hexamer (1236 kDa), IgM pentamer (1048 kDa), apoferritin (720 and 480 kDa), B-phycoerythrin (242 kDa), lactate dehydrogenase (146 kDa), bovine serum albumin (66 kDa), and soybean trypsin inhibitor (20 kDa), was used as molecular weight marker. Western blot was performed immediately after running the BN-PAGE gel.

2.3.3 Mitochondria fractionation

Cytosolic and mitochondrial fractions from HeLa cells were generated using the Qproteome Mitochondria Isolation Kit (Qiagen), following the manufacturer's instructions. Treatment with 10 µM Proteinase K was performed on the mitochondrial fraction for 25 min at 25°C. Mitochondria were then lysed in RIPA buffer containing protease inhibitor provided by the kit. The same volume (15 µl) of cytosol and mitochondria treated and not treated with Proteinase K were loaded onto gels and blotted for cytosol and mitochondrial markers.

2.3.4 Mitoplast preparation and protease protection assay

After performing mitochondria fractionation, mitoplasts were prepared as described previously (Acin-Perez et al., 2011a). Mitochondria were resuspended in 200 µL MS-EGTA (225 mM mannitol, 75 mM sucrose, 5 mM HEPES, 1 mM EGTA, pH 7.4). Water (1/10 vol) and 0.1 mg digitonin were added, and the mixture was incubated on ice for 45 min. Then, KCl (150 mM) was added, followed by incubation for 2 min on ice and centrifugation at 18,000 g for 20 min at 4 °C. The pellet containing the mitoplast fraction was re-suspended in 65 µL of 300 mM Tris-HCl, 10 mM $CaCl_2$, pH 7.4. The supernatant containing the post-mitoplast fraction was precipitated with 12 % TCA and centrifuged at 18,000 g for 15 min at 4 °C. The pellet was resuspended in 200 µL acetone and centrifuged at 18,000 g for 15 min at 4 °C. Finally, the pellet was re-suspended in 20 µL of 300 mM Tris-HCl, 10 mM $CaCl_2$, pH 7.4

For the protease protection assays, mitoplasts were divided into three tubes: no treatment; proteinase K (PK); PK +1 % Triton X-100. Prior to PK treatment, one aliquot of mitoplasts was solubilized with 1 % Triton X-100 for 15 min on ice. 10 µM PK treatment was for 20 min at room temperature (RT), followed by PK inactivation with protease inhibitor.

2.3.5 ER and MAM fractionation

Subcellular fractionation was performed as described previously (Wieckowski et al., 2009). Briefly, cells were washed with PBS, detached by scraping and centrifuged at 600 g for 5 min at 4 °C. Cells were homogenized in intracellular buffer (225 mM mannitol, 75 mM sucrose, 0.1 mM EGTA and 30mM Tris-HCl, pH 7.4) using Teflon pestle. Cell debris were removed by centrifugation 600 g 5 min at 4 °C. After a second centrifugation of the supernatant at 7,000 g 10 min at 4 °C, the pellet containing mitochondria was collected and supernatant containing the non-mitochondrial fractions was centrifuged at 20,000 g 30 min at 4 °C. Further

centrifugation of the obtained supernatant at 100,000 g for 1 h at 4 °C resulted in the isolation of endoplasmic reticulum (ER; pellet) and cytosolic fraction (supernatant). Purification of the mitochondrial fraction was performed by differential centrifugation in Percoll (GE-Healthcare) medium (225 mM mannitol, 25 mM HEPES, 1 mM EGTA and 30 % Percoll (vol/vol), pH 7.4) at 95,000 g for 30 min at 4 °C. MAM (mitochondria-associated membranes) band was further centrifuged at 100,000 g for 1 h at 4 °C and the resulting pellet was resuspended in mitochondria resuspending buffer (MRB; 250 mM mannitol, 5 mM HEPES and 0.5 mM EGTA, pH 7.4). Pure mitochondria band was further centrifuged at 6,300 g for 10 min at 4 °C and the resulting pellet was resuspended in MRB.

PDE2A2 immunoprecipitation from each fraction (mitochondria, ER, MAM) was performed, if specified, after protein fractionation.

2.3.6 Protein elution from FLAG beads and Protein-Lipid Overlay Assay

Protein elution from anti-FLAG M2 beads (Sigma) was performed according to manufacturer's instructions using FLAG peptide (Sigma). Briefly, 100 µL FLAG peptide solution in TBS (100 ng/µL) was added to each sample and control resin followed by 30 min incubation at 4 °C. Samples were centrifuged at 5,000 g 30 sec at 4 °C and supernatant containing eluted protein was collected.

To assess direct lipid binding of PDE2A isoforms, a protein-lipid overlay assay was performed using Membrane Lipid Strips (P-6002; Echelon Biosciences) according to the manufacturer's recommendations. Briefly, membranes were blocked in PBS 1 % skimmed milk for 1 h at room temperature followed by incubation for 1 h with protein of interest (1 µg/mL) in PBS 1 % skimmed milk. After washing the membranes three times over a 30 min period in PBS, they were incubated for 1 h with anti-FLAG antibody in PBS 1 % skimmed milk at RT. Membranes were then washed as before and then incubated 1 h with anti-rabbit HRP conjugate (1/3000). After 3 washes with PBS, chemiluminescent detection was performed using ECL western blot Substrate (Thermo Scientific) or Clarity ECL (BioRAD) and Amersham Hyperfilm ECL photographic films (GE-Healthcare). Films were developed with a Xograph Compact X4 Automatic film Processor (Xograph). Signals were evaluated and analyzed using ImageJ (NIH) and Excel (Microsoft) software.

2.4 Imaging

2.4.1 Fluorescence Resonance Energy Transfer (FRET) Imaging

FRET imaging experiments were performed 24 h after transfection. Cells were maintained at room temperature in a modified Ringer solution (NaCl 125 mM, KCl 5 mM, Na_3PO_4 1 mM, $MgSO_4$ 1 mM, HEPES 20 mM, Glucose 5.5 mM, $CaCl_2$ 1 mM, pH 7.4), and imaged on an inverted microscope (Olympus IX71) using a PlanApoN, 60X, NA 1.42 oil immersion objective (Olympus, UK). The microscope was equipped with a CoolSNAP HQ^2 CCD camera (Photometrics) and a DV2 beam-splitter (MAG Biosystems, Photometrics) for simultaneous imaging of CFP and YFP emissions. The FRET filters used were: CFP excitation filter ET436/20x, dichroic mirror 455DCLP (all from Chroma Technology) in the microscope filter cube; dichroic mirror 505dcxr, YFP emission filter 535/30 nm, CFP emission filter 480/30 nm (Chroma Technology) in the beam splitter. Images were acquired using Metafluor software. FRET changes were measured as changes in the background-subtracted 545/480 nm fluorescence emission ratio (AKAR4-derived sensors) or the 480/545 nm fluorescence emission ratio (H90-derived sensors) upon excitation at 430 nm and expressed as R/R0, where R is the ratio at any given time t and R0 is the initial ratio at time = 0 s. FRET time courses were normalized to R0 since it is widely accepted in the scientific community (Di Benedetto et al., 2013; Monterisi et al., 2017) because it allows an easy comparison between different FRET curves. Nevertheless, quantification of these curves was performed by normalizing to final (Fsk/IBMX) FRET value and shown as a % of saturation.

2.4.2 Live cell confocal imaging

Fluorescence imaging was performed 24 h after cell transfection. Cells were kept at RT in Dulbecco's PBS (DPBS; Life Technologies) and imaged on a Fluoview FV1000 microscope, which is an inverted IX81 confocal system (Olympus, Tokyo, Japan), using a 60X, NA 1.35 oil immersion UPlanSApo objective (Olympus). The microscope was equipped with a Becker and Hickl FLIM system and with fluorescence filters suitable for UV and green or red dyes. Images were acquired using FluoView viewer software (FV10-ASW software, Olympus) and processed using ImageJ. Alternatively, fluorescence imaging was performed with a Zeiss LSM 700 on an inverted confocal microscope (Zeiss Axiovert, Germany).

2.4.3 Image Analysis of Parkin recruitment to Mitochondria and Mitophagy

mCherry-Parkin-expressing HEK293T or MEF cells were treated with the indicated reagents, followed by carbonyl cyanide m-chlorophenylhydrazone (CCCP) incubation (10 mM, 3 h) except when indicated. Intracellular localization of mCherry-Parkin was detected by fluorescence microscopy and analyzed using MetaFluor software, as described previously (Akabane et al., 2016). The extent of overlap between LC3-GFP and mRFP (mitochondrial marker) was quantified using Mander's co-localization coefficient (MCC; ImageJ, Coloc 2 plugin) by providing measures of the fraction of total probe fluorescence that co-localizes with the fluorescence of a second probe (i.e. fraction of LC3-GFP puncta that co-localizes with mRFP). This method was chosen since it is widely accepted and used in the field to measure the overlap between LC3 punctae and mitochondria as a measurement of mitophagy (Gómez-Sánchez et al., 2014; Khalil et al., 2015). Since this method can be quite sensitive to background subtraction, LC3 puncta analysis was performed by auto-thresholding images (ImageJ) to minimize human interference. Other methods are also commonly used to evaluate

co-localization between two signals, such as Pearson's correlation coefficient (PCC). Although this method is less sensitive to thresholding, it measures co-localization as a function of signal/intensity proportionality between two channels, which is not relevant for this particular scenario (Aaron et al., 2018). Therefore, MCC was used since it strictly measures co-localization independently of signal proportionality.

2.4.4 Immunofluorescence

Cells were fixed with 4 % (w/v) paraformaldehyde (8% when fixing mitochondrial structures) in TBS (Tris-buffered saline) for 10 min, washed in TBS, permeabilized with 0.5 % (v/v) Triton X-100 (TX) in TBS for 5 min and washed in TBS. Non-specific labelling was blocked with a 10 min incubation of 1 % normal goat serum (NGS; v/v) in Antibody Diluting Solution (AbDil; TBS 0.1 % TX, 2 % BSA and 0.1 % Azide) and all antibodies were diluted in AbDil 1 % NGS. Primary antibodies were incubated for 60 min. After 3 x 5 min washes, cells were treated with fluorescent-conjugated species-specific immunoglobulins (1:250 in AbDil 1 % NGS) for 60 min. After 3 x 5 min TBS washes, coverslips were mounted in Ibidi mounting media and sealed with nail varnish.

2.4.5 Stimulated emission depletion (STED) imaging

Confocal and STED images were obtained using a Leica TCS SP8 3x inverted microscope with a time-gated stimulated emission depletion (STED) module (Leica Microsystems GmbH, Germany), equipped with a white light laser (WLL) and an HC PL APO CS2 100x/1.40 oil objective. Excitation wavelength was 561 and 633 nm and depletion was achieved with a 775 nm laser. The pinhole was set to 0.5 airy units and the pixel size was 25 nm. Images of 1024

x 1024 pixels were acquired at a scan speed of 600 Hz with the number of line averages equal to 16 and frame accumulation of 2. Signal was detected with a hybrid detection system (Leica HyD). For confocal imaging the STED depletion beam was turned off and WLL intensity was decreased.

2.4.6 Cell Proliferation and Differentiation assays

SH-SY5Y cells can be differentiated to a neuronal-like phenotype with the combination of lowering the FBS content of the culture medium and Retinoic Acid (RA) treatment (Lopes et al., 2010). IncuCyte ZOOM Live-Cell Imaging system (Sartorius) was used to monitor the proliferation and differentiation activity of SH-SY5Y cells in 24-well plates. Cells were cultured in DMEM/F12 with 10 % FBS or with 1 % FBS in the presence of 1 µM BAY-60, 10 µM RA or 1 µM BAY-60 plus 10 µM RA. Media was replaced at 0 h, 48 h and 120 h. The plate was scanned and phase-contrast images were acquired in real time every 2 h from 0 to 218 h post treatment. Cell confluency (%) per well at each time point and quantified time-lapse curves were generated by IncuCyte ZOOM software.

2.4.7 Electron microscopy

Fixed samples were prepared for transmission electron microscopy (TEM). TEM samples were prepared and imaged as previously described (Peters and Hunziker, 2001). Briefly, pellet of cells were fixed with 4 % (w/v) paraformaldehyde and 0.05 % (w/v) glutaraldehyde (both EM grade) for 10 min, and then post-fixed for 30 min with 4 % paraformaldehyde alone, at RT. After washing with PBS, the cells were covered with 1 % gelatin in PBS for 10 min at 37 °C and then scraped, pelleted and incubated overnight in sucrose 2.3 M at 4 °C and prepared for sectioning (70 nm). Images were acquired on a FEI Tecnai T12 TEM system.

2.5 Statistical Analysis

Data are presented as means ± standard error of the mean (s.e.m.). Number of replicates is shown on figure legends. Differences between multiple groups were compared by analysis of variance (ANOVA) followed by a Tukey's or Sidak's multiple comparisons tests. Two-group analysis was performed by Student's t-test. Number of replicates is indicated in the figure legends. * = $P<0.05$; ** = $P<0.01$; *** = $P<0.005$; ns = not significant. All statistical analysis was performed using Prism 7 (GraphPad Prism) or Excel (Microsoft).

Chapter 3 - Expression and sub-cellular localization of PDE2A isoforms

3.1 Background

A single PDE2A gene gives rise to three PDE2A variants due to alternative splicing and use of alternative initiation codons: the soluble PDE2A1 and the membrane-associated PDE2A2 and PDE2A3 (Mika et al., 2012; Sonnenburg et al., 1991). In addition, the sequence for a PDE2A4 variant has been deposited (NCBI Reference Sequence: NM_001146209.2), however no further characterization of this isoform has been reported to date. The tissue and cell type expression pattern of PDE2A isoforms remains largely to be established; similarly, there is very limited information available on whether the different isoforms coexist in one species/tissue (Russwurm et al., 2009). Due to its different subcellular localization and depending on which isoforms are expressed in a given cell type, inhibition of PDE2A in different tissues/cells will most likely lead to multiple different functional effects. This reinforces the importance of characterizing the expression pattern of PDE2A isoforms across different tissues/cell types but also the subcellular localization of each isoform. The focus of this thesis is PDE2A2 and its role in mitochondria biology and function while other isoforms are explored to compare and contrast with PDE2A2. Therefore, to interpret results where PDE2A gene is knocked-out or a pharmacological inhibitor of PDE2A is used, it is very important to establish if the cell types under study express PDE2A2 or any other PDE2A isoforms. To gain information on the cellular distribution of different PDE2A isoforms, reverse transcription-PCR (RT-PCR) analysis was performed to assess isoform-specific mRNA levels in different cell types.

Recently, the existence of an independent intra-mitochondrial cAMP signaling pool was reported. This cascade consists of a matrix-localized cAMP source, the bicarbonate-activated soluble adenylyl cyclase (sAC) (Wuttke et al., 2001; Zippin et al., 2003), PKA holoenzyme (Acin-Perez et al., 2009b, 2011b; Sardanelli et al., 2006), and the cAMP-degrading enzyme PDE2A (Acin-Perez et al., 2011a). Matrix-confined PDE2A2, in hepatocytes and neurons, was

proposed to regulate the activity of the respiratory chain and ATP production via modulation of a local pool of cAMP generated by sAC (Acin-Perez et al., 2011a; Di Benedetto et al., 2013). It has been reported that IMM is impermeable to cAMP and that mitochondria harbour at least two distinct cAMP microdomains (matrix and OMM) with unique signaling characteristics that separate them functionally from non-mitochondrial cAMP pathways (Lefkimmiatis et al., 2013). Therefore, it is critical to establish to which mitochondrial compartment PDE2A2 localizes to, since this will likely reflect on its functional effects. To address this, PDE2A2 localization was characterized in NRVM (Neonatal Rat Ventricular Myocytes) and HeLa cells by performing super-resolution imaging and protein fractionation followed by western blot analysis.

Lastly, in order to target/disrupt PDE2A2 selectively at the mitochondria, without perturbing other isoforms, it is important to establish how PDE2A2 is targeted to this organelle. To address this, several PDE2A deletion mutants were generated by PCR amplification and their subcellular localization was assessed by either fluorescent imaging or protein fractionation followed by western blot analysis.

3.2 Expression of PDE2A isoforms in different cell types

RT-PCR was used to assess the presence of mRNA for the different isoforms in different cell types. A panel of different cell lines and tissues (both from healthy animals or disease models and at different ages) were analyzed for expression of PDE2A isoforms (*Fig. 3.1*). Forward primers specific for the N-terminal region of each isoform were designed, corresponding to exon 1 (first 16 up to 24 bp; *Table 2.3*). The reverse primer was common for all isoforms and anneals with exon 4 and 5 (primer 20 to 22 bp in length, depending on the species; *Fig. 3.1B*). To assess total PDE2A expression, primers were designed to recognize a region shared by all isoforms – forward primer anneals with exon 3 and 4 (primer 20 to 22 bp in length, depending on the species) while reverse primer binds to exon 5 and 6 (primer 20 to 22 bp in length, depending on the species). PCR products were run on an agarose gel and bands were excised and sent for sequencing, to confirm the identity of each PCR product.

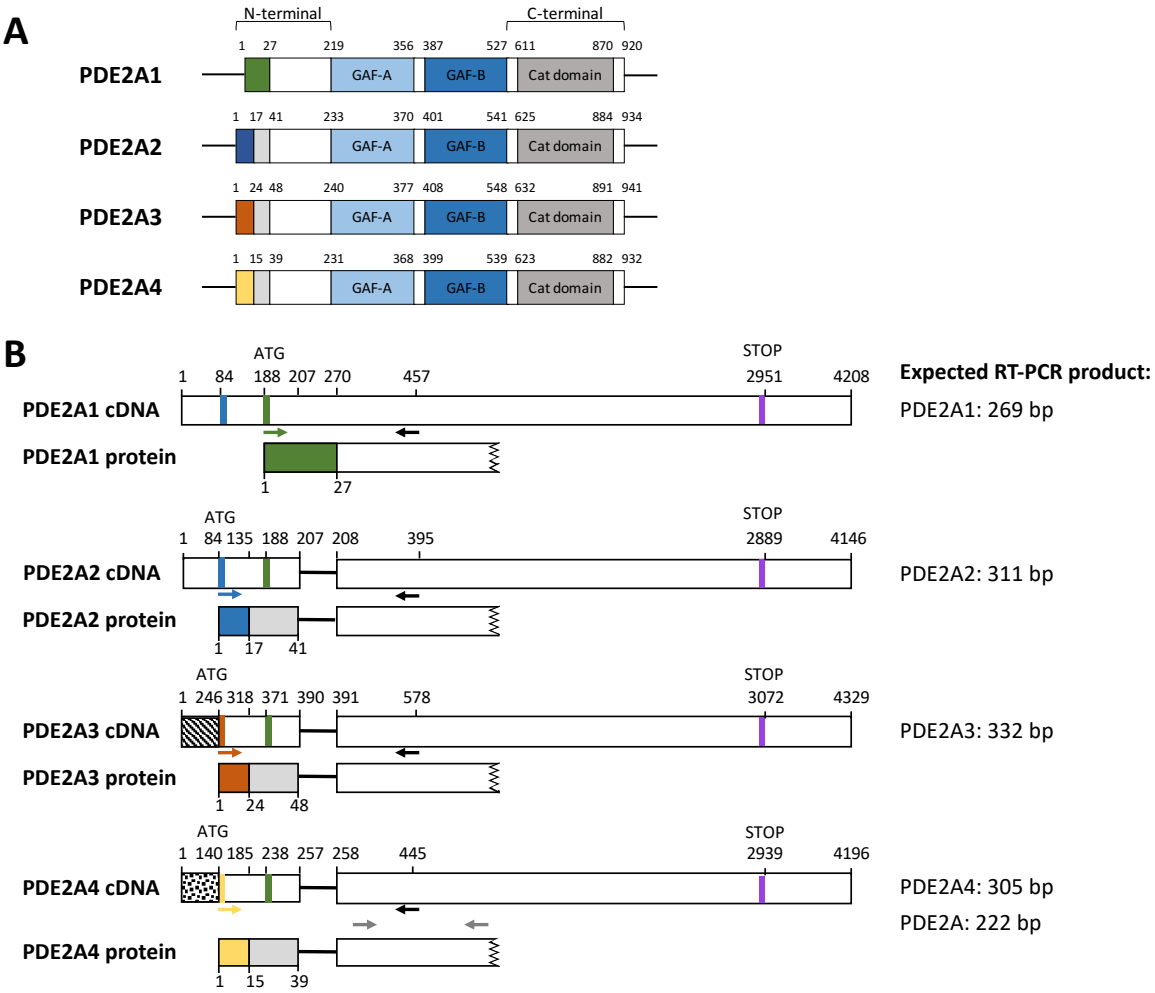
As seen in Figure 3.1B, the start codon for PDE2A1 is also present in the cDNA of the other isoforms while the start codon for PDE2A2 is also present in PDE2A1 cDNA. Therefore, when primers for PDE2A1 are used, all the other isoforms will also yield a PCR product, explaining the multiple bands pattern observed for PDE2A1. However, since PDE2A1 cDNA includes a unique sequence (207-270bp), the PCR product obtained for PDE2A1 is longer than for the other isoforms. In the same way, when a PCR is performed for PDE2A2, PDE2A1 will also be recognized, but this time the PCR product expected for PDE2A2 is shorter than for PDE2A1. In terms of protein sequence, all isoforms have a unique N-terminal sequence. PDE2A1 has a unique N-terminal protein sequence because the start codon for PDE2A1 is out of frame when compared with the start codon for the other isoforms. Additionally, if PDE2A2 ATG is used to start translation on PDE2A1 mRNA or PDE2A1 ATG is used instead of the respective isoform ATG, this will originate an early-stop codon and a short protein fragment.

Several different cells and tissues were analyzed. Regarding cell lines, MEFs, HEK293T and HeLa cells were tested for PDE2A isoforms expression (*Fig. 3.1C*). It was found that in all these cell lines PDE2A1 and PDE2A2 are the predominant isoforms. HEK293T cells also express PDE2A3, although the PCR amplification for this isoform gives consistently a very low yield. A positive control PCR reaction was performed to assess the quality of the reaction – for this reaction, plasmids encoding for each isoform were used in place of cDNA originated from cellular mRNA. As seen in Figure 3.1C, all reactions give similar bands in intensity when starting with the same amount of DNA, suggesting that differences in band pattern represent different expression pattern of PDE2A isoforms. In the amplifications from cDNA, a two-band pattern was observed for PDE2A1 and PDE2A2 across all cell lines, as explained above. After sequencing these PCR products, bands identified with * were confirmed to correspond to the expected PCR product while the other band is either another isoform or a shorter fragment arising from a premature stop codon (*Fig. 3.1I)*. The same pattern was observed in SH-SY5Y cells, a neuronal cell line, where the PDE2A3 band appears to be of similar intensity as the other two isoforms (*Fig. 3.1D)*. Primary stellate ganglia neurons from rat were also analyzed. In these cells, PDE2A2 is the major isoform, while PDE2A3 is expressed in wt but not in neurons obtained from spontaneously hypertensive rats (SHR) (*Fig. 3.1E)*.

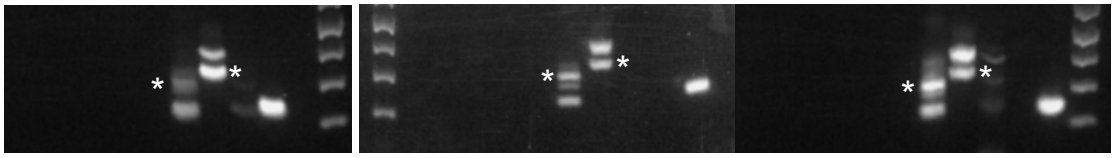
Neonatal myocytes from rat and wt or MDX (X-linked muscular dystrophy, model of Duchenne muscular dystrophy) mice were tested (*Fig. 3.1F)*, as well as heart tissues from adult rat and human, from control, dilated cardiomyopathy (DCM) and ischemic cardiomyopathy (ICM) patients (*Fig. 3.1G and H)*. The pattern found for all isolated cardiomyocytes or heart tissues was the same – PDE2A1 and PDE2A2 are the only PDE2A isoforms expressed in the heart.

Unfortunately, due to lack of commercially available antibodies specific for each isoform, it was not possible to confirm the mRNA data by measuring protein expression.

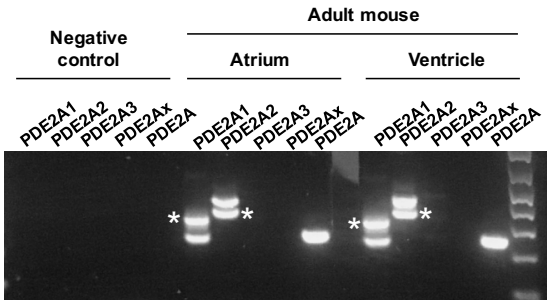
In conclusion, the above data show that isoforms 1 and 2 are more ubiquitously expressed compared to PDE2A3, at least among the cell lines and tissues tested in this study (*Fig. 3.1I*).


A
N-terminal
C-terminal
PDE2A1
PDE2A2
PDE2A3
PDE2A4
GAF-A
GAF-B
Cat domain
B
ATG
STOP
PDE2A1 cDNA
PDE2A1 protein
PDE2A2 cDNA
PDE2A2 protein
PDE2A3 cDNA
PDE2A3 protein
PDE2A4 cDNA
PDE2A4 protein
Expected RT-PCR product:
PDE2A1: 269 bp
PDE2A2: 311 bp
PDE2A3: 332 bp
PDE2A4: 305 bp
PDE2A: 222 bp
C
Negative control
MEF WT
Negative control
HEK293T
HeLa
Positive control
D
Sh-Sy5y
E
Negative control
Stellate Ganglia Neurons
WT
SHR

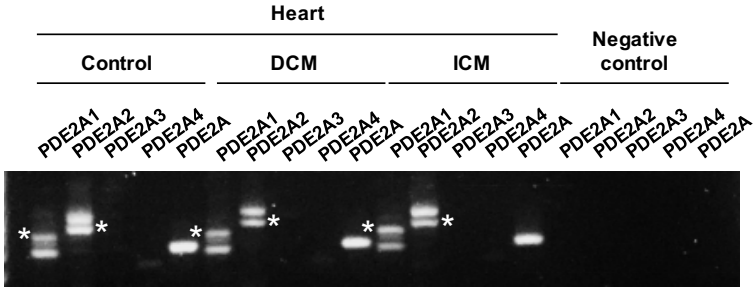
F



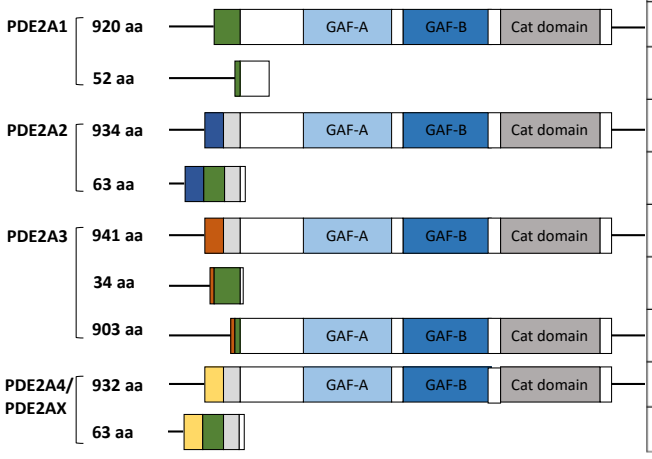
G



H



I



MEFs	HEK293T	HeLa	Sh-Sy5y	Stellate Ganglia WT	Stellate Ganglia SHR	Neonatal Rat	Neonatal mouse	Neonatal MDX mouse	Atrium adult mouse	Ventricle adult mouse	Human Heart WT	Human Heart DCM	Human Heart ICM
✓	✓	✓	✓	✓	x	✓	✓	✓	✓	✓	✓	✓	✓
✓	✓	✓	✓	✓	✓	✓	✓	✓	✓	✓	✓	✓	✓
✓	✓	✓	✓	✓	✓	✓	✓	✓	✓	✓	✓	✓	✓
✓	✓	✓	✓	x	x	✓	✓	✓	✓	✓	✓	✓	✓
x	✓	x	✓	✓	x	x	x	x	x	x	x	x	x
x	x	x	x	x	x	✓	x	✓	x	✓	x	x	x
x	x	✓	x	x	x	✓	x	✓	x	✓	x	x	x
x	x	x	x	ND	ND	ND	x	x	x	x	x	x	x
x	x	x	✓	ND	ND	ND	x	x	x	x	x	x	x

Figure 3.1 | **PDE2A1 and PDE2A2 are the most expressed PDE2A isoforms among different cells/tissues.**
(A) Schematic of PDE2A protein domains and differences among each isoform. Different color at the N-terminal region represents a different amino acid sequence.
(B) Schematic of PDE2A cDNA and differences among each isoform and respective protein sequence. Start codon is indicated for each cDNA, matching the color of the unique N-terminal region for each isoform. Note that start codon for PDE2A1 is also present in the cDNA of the other isoforms while start codon for PDE2A2 is also present on PDE2A1 cDNA. Primers used for PCR amplification are indicated by arrows. For each isoform, the size of the expected PCR product in base pairs (bp) is listed on the far right.
(C) PCR amplification of PDE2A isoforms cDNA obtained from MEFs, HEK293T and HeLa cells. PDE2Ax corresponds to another isoform in mouse that has been deposited - NCBI Reference Sequence: NM_001243758.1.
(D) PCR amplification of PDE2A isoforms cDNA obtained from SH-SY5Y cells.
(E) PCR amplification of PDE2A isoforms cDNA obtained from Stellate Ganglia Neurons from wt or spontaneously hypertensive rats (SHR).
(F) PCR amplification of PDE2A isoforms cDNA obtained from neonatal rat and wt or MDX neonatal mouse.
(G) PCR amplification of PDE2A isoforms cDNA obtained from adult mouse tissue. PDE2Ax corresponds to another isoform in mouse that has been deposited - NCBI Reference Sequence: NM_001243758.1.
(H) PCR amplification of PDE2A isoforms cDNA obtained from human heart tissue. DCM, Dilated Cardiomyopathy; ICM, Ischemic Cardiomyopathy.
(I) Schematic representation of all PDE2A isoforms detected on each cell type. Green/blue/orange/yellow represents PDE2A1/2/3/4 or X N-terminus, respectively.
For C to H, each PCR reaction was performed at least two times. * identifies the band corresponding to the expected size for PDE2A1, PDE2A2 or PDE2A3 PCR products.

3.3 Sub-mitochondrial localization of PDE2A2

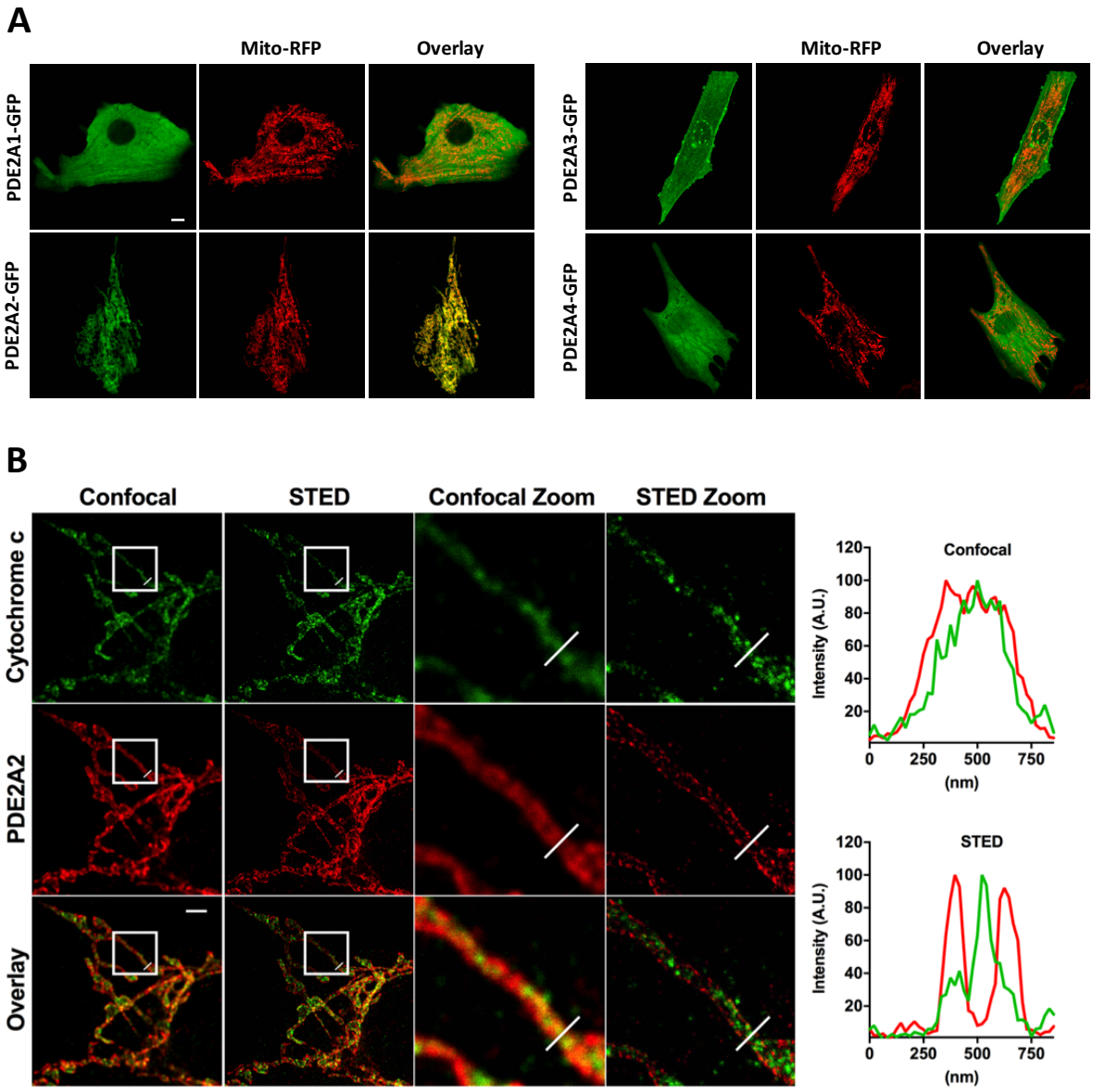
Expression of PDE2A2-GFP (C-terminally linked GFP) in primary NRVM showed a distinct localization to the mitochondria, unlike PDE2A1-GFP and PDE2A4-GFP, which are cytosolic, and PDE2A3-GFP, which localizes predominantly to the plasma membrane (*Fig. 3.2A*). Overexpression of a protein coupled to a relatively large tag, such as GFP, might lead to mistargeting or lack of anchoring of a substantial population. Nevertheless, expression of PDE2A isoforms tagged with FLAG, a peptide with 8 aminoacids, yield the same observations as GFP-tagged PDE2A (*results not shown*).

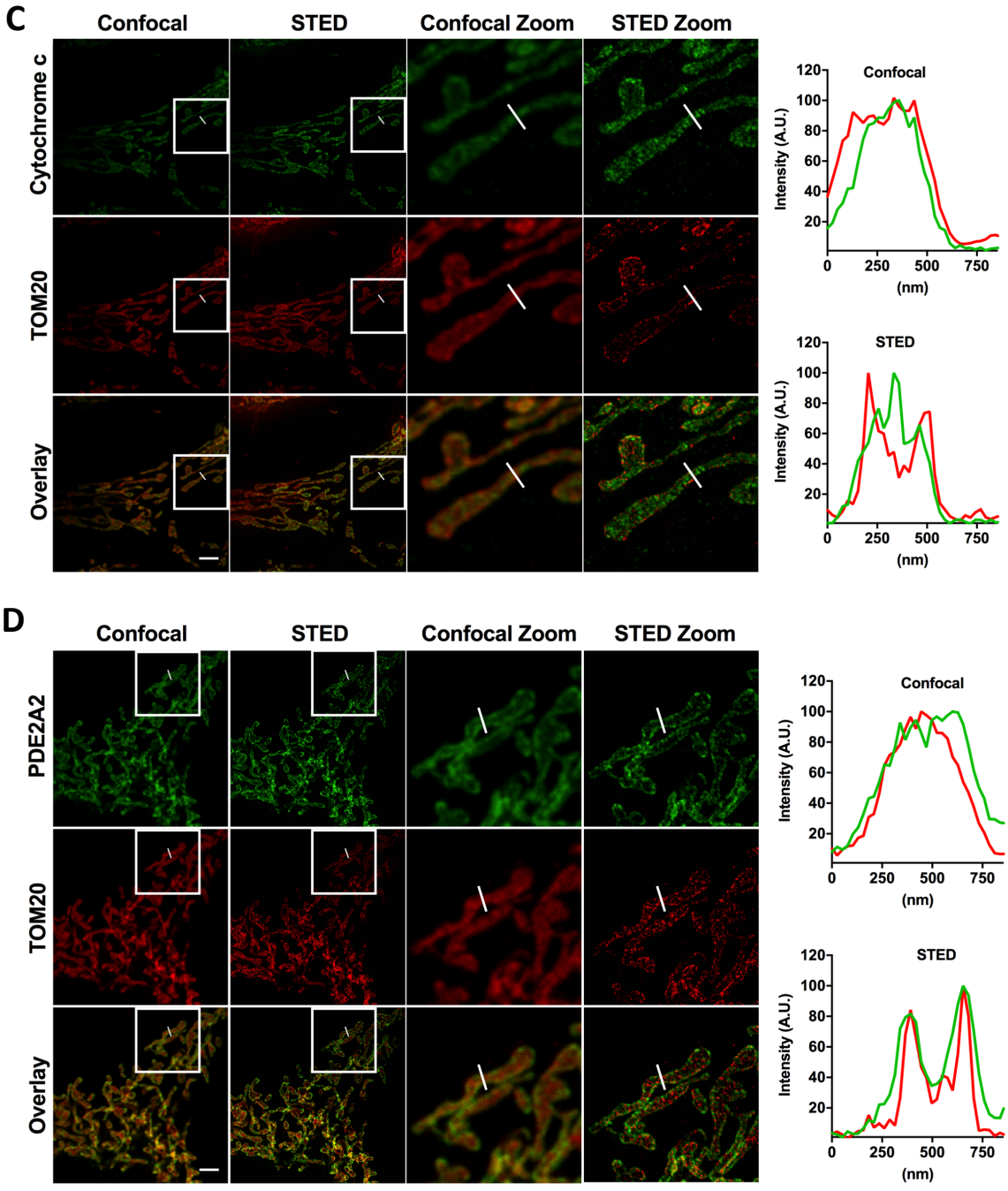
To further investigate the submitochondrial localization of PDE2A2, super-resolution stimulated emission depletion (STED) microscopy of HeLa cells was performed. Cells expressing PDE2A2-GFP were double labelled with anti-GFP antibodies and antibodies to cytochrome C as a marker for the intermembrane space (IMS). As shown in Figure 3.2B, PDE2A2 appears to be predominantly located at the periphery of mitochondria and to be excluded from the matrix and from the intra-cristae space (where cytochrome c is mostly found). My analysis shows that the PDE2A2 signal shows a profile that is substantially similar to that of the outer mitochondrial membrane (OMM) marker TOM20 (component of the Translocase of Outer Membrane complex) (*Fig. 3.2C and D*).

To further assess PDE2A2 localization, western blot analysis of subcellular fractions from HeLa cells and NRVM was performed. Overexpressed PDE2A2-GFP predominantly segregates with the mitochondrial fraction and treatment with proteinase K (PK, 10 μM), which hydrolyses proteins exposed to the cytosolic side of the OMM, significantly reduced the PDE2A2-GFP signal, although it did not completely ablate it (*Fig. 3.2E*). As expected, PK treatment completely depleted the mitochondrial fraction of TOM20, a protein exclusively found at the OMM. Cell fractionation and disruption of the OMM by osmotic shock allowed us to dissect

further the localization of endogenous PDE2A at the mitochondria. As shown in Figure 3.2F, endogenous PDE2A is clearly detected in the mitoplast fraction (mitochondria that have been stripped of their outer membrane leaving the inner membrane intact) obtained from NRVM but is completely depleted on treatment of mitoplasts with PK. The same treatment does not affect the matrix marker COX2, confirming the quality of the mitoplast preparation. These observations are in agreement with the previous results using overexpression models.

Overall, the above data support localization of PDE2A2 at the OMM and IMM/IMS, whereas the enzyme appears to be largely excluded from the intra-cristae space and from the mitochondrial matrix.


A
Mito-RFP
Overlay
PDE2A1-GFP
PDE2A2-GFP
PDE2A3-GFP
PDE2A4-GFP
B
Confocal
STED
Confocal Zoom
STED Zoom
Cytochrome c
PDE2A2
Overlay
Intensity (A.U.)
(nm)
120
100
80
60
40
20
0
250
500
750


C
Confocal
STED
Confocal Zoom
STED Zoom
Cytochrome c
TOM20
Overlay
Confocal
Intensity (A.U.)
120
100
80
60
40
20
0
250
500
750
(nm)
STED
D
PDE2A2

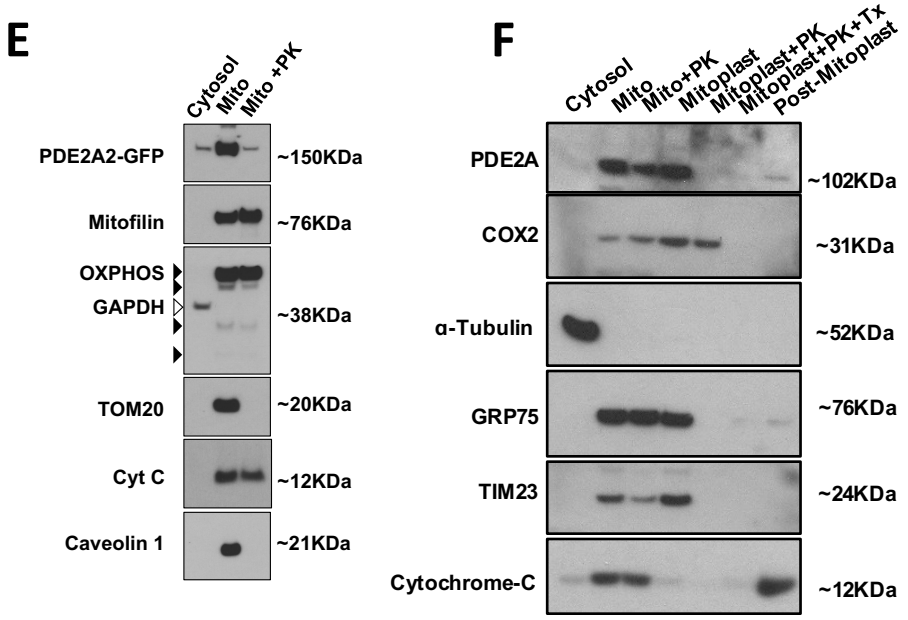


Figure 3.2 | **PDE2A2 localizes to the OMM and IMS of mitochondria.**
(A) Localization of PDE2A1-GFP, PDE2A2-GFP and PDE2A3-GFP in neonatal rat ventricular myocytes (NRVM) labelled with mitotracker red. Images are representative of two independent experiments. Scale bar: 10 μm.
(B) Confocal and STED image (first and second column, respectively) of a HeLa cell expressing PDE2A2-GFP and labelled with antibodies to cytochrome c and GFP. Third and fourth column show magnification of the boxed areas. Plots on the right show average intensity profiles across the indicated mitochondrial tubule section. Cytochrome c profile is in green and PDE2A2 profile is in red. Images are representative of four independent experiments. Scale bar: 2 μm.
(C) Representative confocal and STED images of a HeLa cell labelled with antibodies specific to cytochrome c and TOM20. Images are representative of four independent experiments. Scale bar: 2 μm.
(D) Representative confocal and STED images of HeLa cell expressing PDE2A2-GFP and labelled with antibodies specific to TOM20 and GFP. Images are representative of four independent experiments. Scale bar: 2 μm.
(E) Representative western blot analysis of cytosolic and mitochondrial sub-fractions obtained from Hela cells expressing PDE2A2-GFP. The mitochondrial fraction was either non treated or treated with Proteinase K (10 μM). PDE2A2 was assessed with a GFP-specific antibody. To assess fraction purity, antibody for OXPHOS subunits (black arrowheads), TOM20, Cytochrome C and Mitofilin were used. GAPDH was used to assess contamination of cytosol in the mitochondrial fraction. Blot is representative of two independent experiments.
(F) Representative western blot analysis of cytosolic, mitochondrial, mitoplasts and post-mitoplast sub-fractions obtained from NRVM lysates not treated, treated with Proteinase K (PK; 10 μM) or Triton-X plus PK. Mitoplast fraction contains mitochondria that have been stripped of their outer membrane leaving the inner membrane intact. Post-mitoplast fraction contains proteins from the intermembrane space. Endogenous PDE2A was probed with a PDE2A specific antibody. COX2, marker for mitochondrial matrix; α-Tubulin, marker for cytosol; GRP75 and TIM23, marker for IMM; cytochrome-c, marker for IMS. Blot representative of three independent experiments. Blot is representative of three independent experiments.

3.4 PDE2A2 domains responsible for its targeting to the mitochondria

While it has been reported that the N-terminus of PDE2A plays an important role in its subcellular localization (Acin-Perez et al., 2011a), it remains to be established whether other PDE2A domains may also be involved in targeting this enzyme to a specific location. For this purpose, multiple deletion mutants of PDE2A2-RFP domains (illustrated in *Fig. 3.3A)* were generated by PCR amplification to establish which region is important in determining its subcellular targeting. The N-terminus was considered to be the region before the GAF-A domain (1-201 aa). Figure 3.3B shows successful expression of all deletion mutants. To investigate the contribution of each domain to PDE2A2 localization, confocal microscopy of HeLa cells transiently expressing each PDE2A2-RFP fragment was performed (*Fig.3.3C*). Only fragments including the N-terminal region localized to the mitochondria, as shown by the overlap with cytochrome C staining. Additionally, western blot analysis of subcellular fractions from HEK293T expressing different PDE2A2-RFP constructs confirmed these results (*Fig.3.3D*).

Thus, the N-terminus of PDE2A2 is required for targeting the protein to the mitochondria while other domains are not sufficient to target PDE2A2 to this organelle.

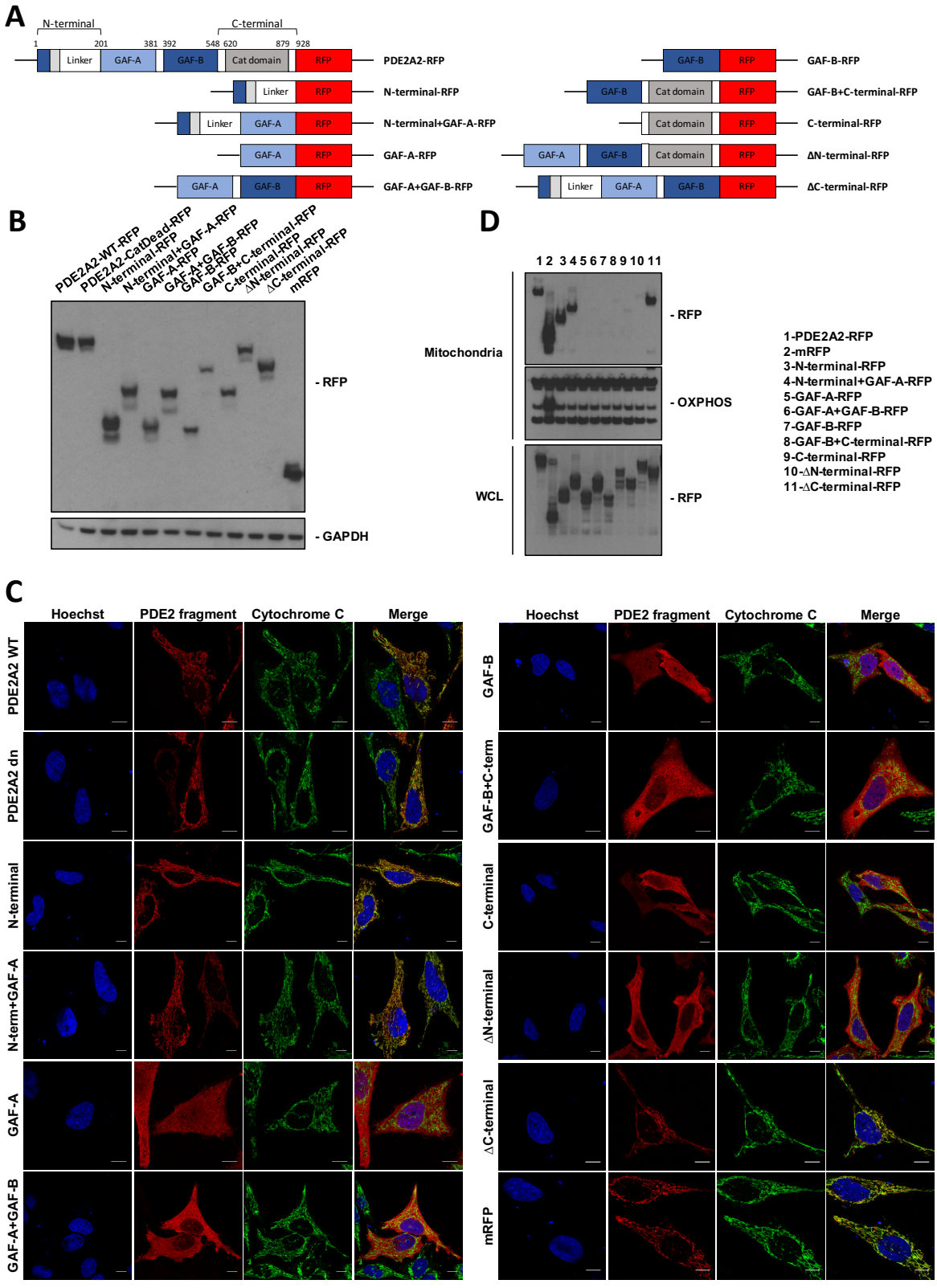

A
N-terminal
C-terminal
1
201
381
392
548
620
879
928
Linker
GAF-A
GAF-B
Cat domain
RFP
PDE2A2-RFP
N-terminal-RFP
N-terminal+GAF-A-RFP
GAF-A-RFP
GAF-A+GAF-B-RFP
GAF-B-RFP
GAF-B+C-terminal-RFP
C-terminal-RFP
ΔN-terminal-RFP
ΔC-terminal-RFP
B
PDE2A2-WT-RFP
PDE2A2-CatDead-RFP
N-terminal-RFP
N-terminal+GAF-A-RFP
GAF-A-RFP
GAF-A+GAF-B-RFP
GAF-B-RFP
GAF-B+C-terminal-RFP
C-terminal-RFP
ΔN-terminal-RFP
ΔC-terminal-RFP
mRFP
- RFP
- GAPDH
D
1 2 3 4 5 6 7 8 9 10 11
Mitochondria
WCL
- RFP
- OXPHOS
- RFP
1-PDE2A2-RFP
2-mRFP
3-N-terminal-RFP
4-N-terminal+GAF-A-RFP
5-GAF-A-RFP
6-GAF-A+GAF-B-RFP
7-GAF-B-RFP
8-GAF-B+C-terminal-RFP
9-C-terminal-RFP
10-ΔN-terminal-RFP
11-ΔC-terminal-RFP
C
Hoechst
PDE2 fragment
Cytochrome C
Merge
PDE2A2 WT
PDE2A2 dn
N-terminal
N-term+GAF-A
GAF-A
GAF-A+GAF-B
GAF-B
GAF-B+C-term
C-terminal
ΔN-terminal
ΔC-terminal
mRFP

Figure 3.3 | **The N-terminal region of PDE2A2 is necessary and sufficient to target the protein to the mitochondria.**
(A) PDE2A2-RFP constructs generated and (B) respective molecular weight upon expression in HEK293T cells. PDE2A2 dn stands for dominant negative. mRFP, mitochondrial RFP. Blot is representative of two independent experiments.
(C) Confocal images of HeLa cells over-expressing several PDE2A2-RFP constructs. Cells were fixed for immunofluorescence staining with RFP (red), cytochrome C (green) and respective secondary antibodies. The nuclei were stained with Hoechst (blue). Images are representative of two independent experiments. Scale bar: 10 μm.
(D) Representative western blot analysis of cytosolic and mitochondrial sub-fractions obtained from HEK293T cells expressing the PDE2A2-RFP constructs generated. To assess fraction purity, antibody for OXPHOS subunits was used. Blot is representative of two independent experiments.

Three different regions can be identified in the N-terminus of each PDE2A (*Fig. 3.4A*): a region unique and specific to each isoform (highlighted with different colors); a region common to all isoforms (gray box; not present in PDE2A1); and a linker region to the GAF-A domain (white box). To further investigate the role of these regions, shorter deletion mutants of the N-terminal domain for all PDE2A isoforms were generated (*Fig. 3.4A)* and expression validated *(Fig. 3.4B*). When expressing full length construct of each PDE2A isoform in HeLa cells I observed that PDE2A1 and PDE2A4 localize to the cytosol, PDE2A2 localizes to the mitochondria while PDE2A3 localizes to the plasma membrane (PM) (*Fig. 3.4C*), similarly to what was found in NRVM (*Fig. 3.2A*). Interestingly, PDE2A1 1-27-GFP and PDE2A4 1-39-GFP lost their subcellular localization since both fragments showed nuclear signal, while the respective full version was exclusively cytosolic. However, both PDE2A3 1-48-GFP and PDE2A3 1-24-GFP fragments still localized to the PM. On the other hand, PDE2A2 1-41-GFP showed partial mitochondria localization while PDE2A2 1-17-GFP localized completely to the cytosol. In agreement with these results, PDE2A2- 7-934-GFP localized to the cytosol while PDE2A2 1-137-GFP also showed partial mitochondria localization (*Fig. 3.4D*), similarly to PDE2A2 1-41-GFP and in comparison with PDE2A2 1-201-RFP (*Fig. 3.4E*). This suggests that for different isoforms, different regions of the N-terminus are required for efficient targeting to their sub-cellular localization.

Specifically, PDE2A2 unique region (1-17; blue box; MVLVLHHILIAVVQFLR) does not appear to be the only region involved in targeting the protein to the mitochondria, as it is required but not sufficient for optimal targeting, whereas PDE2A3 unique region (1-24 aa; orange box) is required and sufficient for targeting this isoform to the PM.

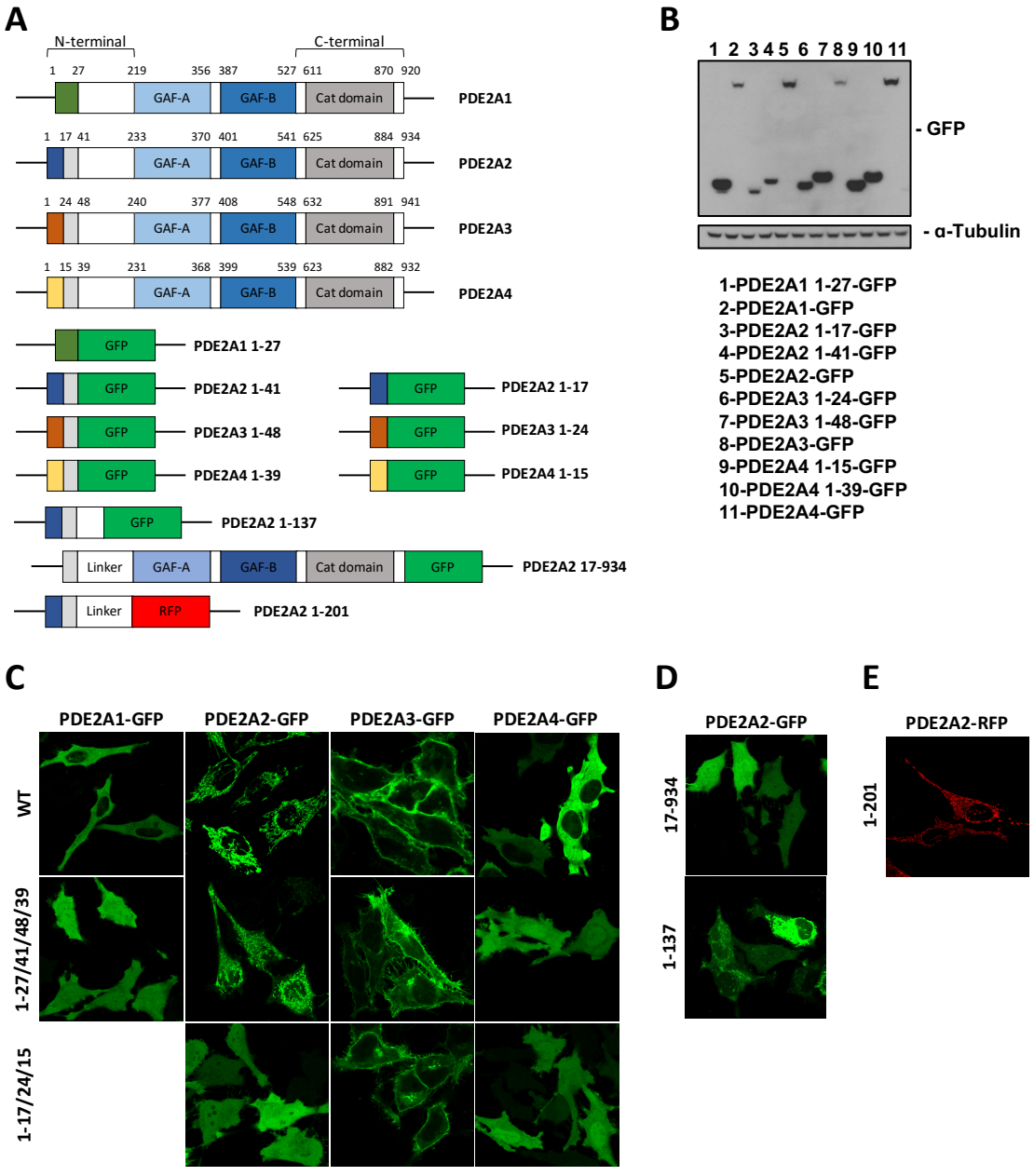


Figure 3.4 | **Unique domain of PDE2A2 is not sufficient to target the protein to the mitochondria.**
(A) PDE2A constructs generated and (B) respective molecular weight upon expression in HEK293T cells. Blot is representative of two independent experiments.
(C), (D) and (E) Live confocal imaging of HeLa cells over-expressing several PDE2A constructs tagged with either GFP or RFP.

3.5 Conclusion

In conclusion, PDE2A1 and PDE2A2 are expressed across all different cells and tissues tested while PDE2A3 was mostly found in neuronal cells. This underpins the importance of, prior to designing and undertaking large and expensive research studies, to rigorously demonstrate that the enzyme is expressed in a certain tissue. For instance, *Vettel et al.* has developed a transgenic mice overexpressing PDE2A3 specifically in cardiomyocytes, showing that PDE2A protects against arrhythmias and improves contraction force after severe ischemic insult (Vettel et al., 2017). On the basis of their results, the authors propose to develop PDE2A activators. However, their findings rely on overexpression of an isoform that normally is not present in myocytes, as I have shown. Therefore, if a PDE2A activator would be administered in patients to treat arrhythmia, these patients would not express in their myocytes the relevant isoform. Activation of other isoforms with different localization (non plasmalemma) may on the other hand have deleterious effects as a result of reduction of cAMP levels.

Additionally, STED microscopy and mitochondria fractionation showed that the sub-mitochondrial compartment where most PDE2A2 localizes to is not the matrix but the OMM and IMS. My analysis also reveals that the distribution of PDE2A2 at the OMM is not uniform but is dotted, suggesting that this enzyme may be part of a protein complex and may regulate cyclic nucleotide signaling at multiple sub-mitochondrial nano-domains. A previous study reported that PDE2A2 localizes to the mitochondrial matrix where it hydrolyses cAMP generated locally by sAC (Acin-Perez et al., 2011a). In this study using primary cells (NRVM) and cell lines (HeLa), I found that the majority of PDE2A2 localizes to mitochondrial membranes. My findings are in agreement with an earlier report of cGMP-activated mitochondrial PDE, 20 % of which was found to be associated with the OMM and 80 % with

the IMM (Cercek and Houslay, 1982). Additionally, *Monterisi et al.* failed to detect significant PDE2A activity in the mitochondrial matrix using FRET imaging (Monterisi et al., 2017).

By using multiple deletion mutants of PDE2A2, I confirmed that the full N-terminus of PDE2A2 (1-201 aa) is required for targeting the protein to the mitochondria (Acin-Perez et al., 2011a) and that other domains are not sufficient to target PDE2A2 to this organelle. On the other hand, PDE2A3 unique region (1-24 aa) is sufficient to target the protein to the PM, which is in agreement with myristoylation of the enzyme at a Glycine residue at position 2 (Russwurm et al., 2009).

Most of the localization studies were performed in overexpression models which have some limitations. For example, if a certain PDE2A isoform binds to a specific interactor, at some point the stoichiometric ratios will be exceeded and excess protein may mislocalize. To avoid wrong conclusions, localization images were taken from cells with lower expression levels and different tags were used to study the localization of the different PDE2A isoforms, namely GFP, RFP and FLAG. Taken together, specifically for PDE2A2, the data from fluorescence imaging, electron microscopy, mitochondria fractionation and FRET imaging (Monterisi et al., 2017) clearly suggests that PDE2A2 localizes to both OMM and IMS.

Chapter 4 - PDE2A2 interactors

4.1 Background

Although PDE2A has been suggested as a potential drug target for several diseases, including heart failure and cognitive disorders (Gomez and Breitenbucher, 2013; Zoccarato et al., 2015), no information is currently available on which proteins and complexes PDE2A binds to. Since PDE2A isoforms target to different subcellular localizations, one would expect that each isoform has different binding partners which may contribute to determine different functions of individual isoforms. The identification of PDE2A interacting proteins may provide an avenue for selective displacement, and therefore specific ablation, of PDE2A activity at a specific site – something that cannot be achieved by inhibiting PDE2A, since all PDE2A isoforms will be affected by pharmacological inhibitors.

In order to investigate the interactome of PDE2A2, three independent mass spectrometry (MS) experiments had been previously performed in our group using samples where PDE2A2-RFP was overexpressed in adult rat cardiomyocytes and after RFP pull-down, samples were analyzed by label-free quantitative mass spectrometry. RFP targeted to the mitochondria (mRFP) was used as a control. In agreement with my overexpression and localization data, a large number of potential interactors found are proteins located in the mitochondria. The most significant interactors were selected for further validation (*Table 4.1*). These include Caveolins, components of the MINOS (mitochondrial inner membrane organizing system) complex and β-Taxilin, among others. Interestingly, most of these proteins localize to the mitochondria or endoplasmic reticulum (ER). In this chapter, the most significant potential interactors resulting from the MS analysis were validated by confirming PDE2A2 interaction through co-immunoprecipitation experiments.

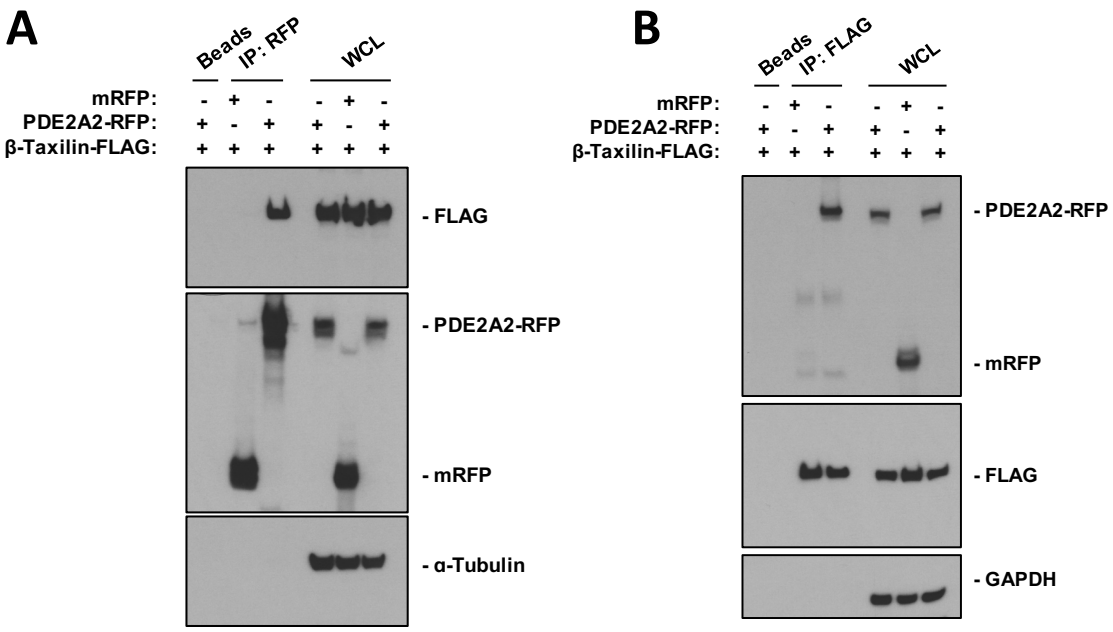
Table 4.1 | **PDE2A2 putative interactors identified through PDE2A2-RFP pull down and MS analysis and selected for further analysis.** MS data for the indicated proteins from the PDE2A2 IP. Statistical Significance (the higher the more significant), Fold Change (compared to mRFP IP), number of unique peptides identified by MS, % of sequence coverage and molecular weight are shown.

Protein Names	Statistical Significance	Fold Change	No. of unique peptides	Sequence coverage [%]	Mol. Weight [kDa]
Mitoflin	5.171	4.387	17	32.8	67.18
Metaxin 2	5.140	8.840	2	8.7	29.72
Beta-Taxilin	4.919	8.379	28	44.3	77.54
PDE2A (Phosphodiesterase 2A)	4.727	10.259	66	64.2	104.66
ChChD3 (Coiled-Coil-Helix-Coiled-Coil-Helix Domain-Containing Protein 3)	4.074	5.388	6	21.1	26.43
Caveolin 1	4.030	8.441	4	36.0	20.55
Caveolin 2	3.737	10.629	2	18.5	18.27
SAMM50 (Sorting and assembly machinery component 50)	3.485	4.498	10	24.3	51.96
Alpha-Taxilin	3.296	3.878	6	10.1	62.57
VDAC2 (Voltage-dependent anion-selective channel protein 2)	2.900	3.289	5	17.6	31.75
Gamma-Taxilin	2.143	7.580	5	16.5	35.47
ALDH3A2 (Fatty aldehyde dehydrogenase)	1.911	9.472	13	25.8	54.08
Erlin2 (Endoplasmic reticulum lipid raft-associated protein 2)	1.806	7.039	6	19.5	37.71
Caveolin 3	1.663	7.584	1	14.6	17.40
VDAC1 (Voltage-dependent anion-selective channel protein 1)	1.620	2.728	7	29.7	30.76

4.2 β-Taxilin

One of the proteins showing a very high score in the MS analysis was β-Taxilin. However, almost nothing is known about this protein. Taxilin has been identified as a Syntaxin-binding protein, a family implicated in intracellular vesicle trafficking (Nogami et al., 2003; Sakane et al., 2014), and is characterized by a long coiled-coil region at its C-terminal domain (Nogami et al., 2004). A database search has revealed the presence of two other molecules having a long coiled-coil region homologous to that of Taxilin in mammals. Original Taxilin was renamed α-Taxilin and the two other proteins were named β- and γ-Taxilins. All Taxilins have been shown to interact with members of the Syntaxin family, although, at this time, the precise function of Taxilins in intracellular vesicle trafficking is not known. β-Taxilin has been suggested to be a cytosolic protein predominantly expressed in skeletal muscle and heart tissues (Fujimori et al., 2002) that may be involved in cell differentiation from myoblasts into myotubes (Sakane et al., 2016).

To assess whether PDE2A2 interacts with β-Taxilin, co-immunoprecipitation experiments were performed in HEK293T cells overexpressing PDE2A2-RFP and β-Taxilin-FLAG (*Fig. 4.1A and B*). Regardless of which protein was being pulled-down, a consistent strong interaction was found between these two proteins. Additionally, since β-Taxilin is mostly expressed in muscle tissue, I assessed its sub-cellular localization in NRVM. Due to lack of commercially available antibodies, I used a custom-made antibody that has been previously developed (Nogami et al., 2004). As seen in Figure 4.1C, β-Taxilin shows a punctated pattern with a distribution that appears to coincide with cytoskeletal/sarcomeric elements.



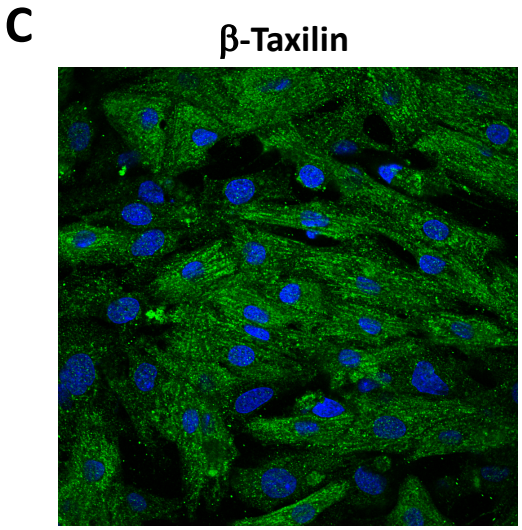


Figure 4.1 | **PDE2A2 interacts with β-Taxilin.**
(A) Detection of β-Taxilin-FLAG after PDE2A2-RFP or mRFP immunoprecipitation in HEK293T cells transiently transfected with β-Taxilin-FLAG and either PDE2A2-RFP or mRFP. Blot is representative of two independent experiments.
(B) Detection of PDE2A2-RFP and mRFP after β-Taxilin-FLAG immunoprecipitation in HEK293T cells transiently transfected with β-Taxilin-FLAG and either PDE2A2-RFP or mRFP. Blot is representative of two independent experiments.
(C) Live confocal imaging of NRVM stained for β-Taxilin (green). The nuclei were stained with Hoechst (blue). Image is representative of two independent experiments.

To investigate the functional role of the interaction between PDE2A2 and β-Taxilin, I aimed at developing a strategy to disrupt this interaction. To this end, I first assessed which PDE2A2 domain binds directly to β-Taxilin. By using the PDE2A2 fragments that had been generated in Chapter 3, co-immunoprecipitation experiments were performed in HEK293T cells overexpressing each PDE2A2-RFP fragment and β-Taxilin-FLAG. As shown in Figure 4.2A, only fragments that contain both GAF-A and GAF-B domains bind to β-Taxilin-FLAG. Thus, I propose that both GAF domains constitute the binding site for β-Taxilin (*Fig. 4.2B*).

Since β-Taxilin sub-cellular localization does not resemble mitochondrial pattern, I tested whether β-Taxilin is an exclusive interactor of PDE2A2 isoform. To address this question, I performed co-immunoprecipitation experiments in HEK293T cell overexpressing each PDE2A-GFP isoform and β-Taxilin-FLAG (*Fig. 4.2C*). Results show that β-Taxilin-FLAG can bind to all PDE2A-GFP isoforms, at least when both proteins are being over-expressed. By performing gel electrophoresis in native conditions to preserve endogenous protein-protein interactions, I also observed that all four isoforms form a ~1000kDa macromolecular complex with β-Taxilin-FLAG (*Fig. 4.2D*). However, when testing this interaction by probing for endogenous β-Taxilin in NRVM, I observed that the interaction is stronger with PDE2A1-GFP (*Fig. 4.2E*), in contrast with results obtained when over-expressing β-Taxilin (*Fig. 4.2C*). This was not surprising since both proteins have a cytosolic localization and shows that over-expressing models can lead to artifacts. Analysis of putative PKA phosphorylation sites on β-Taxilin using GPS3.0 software revealed the presence of two high score RRxS/T motifs, S15 and T16, respectively. To better understand if cAMP/PKA signaling could regulate β-Taxilin function, I assessed β-Taxilin-FLAG phosphorylation status after incubating cells for 2h with forskolin (Fsk) and IBMX (Fsk/IBMX) and Fsk/IBMX/H89 (*Fig. 4.2F*). Forskolin is an adenylyl cyclase agonist, IBMX is a phosphodiesterase inhibitor while H89 is a PKA inhibitor. As seen, Fsk/IBMX treatment induced PKA-mediated phosphorylation of β-Taxilin-FLAG that was abolished by H89 treatment. To

further validate these results and confirm the PKA phosphorylation site, point-mutations of S15 and T16 of β-Taxilin could have been performed. However, it remains to be studied how or if PKA-mediated phosphorylation of β-Taxilin can regulate its function.

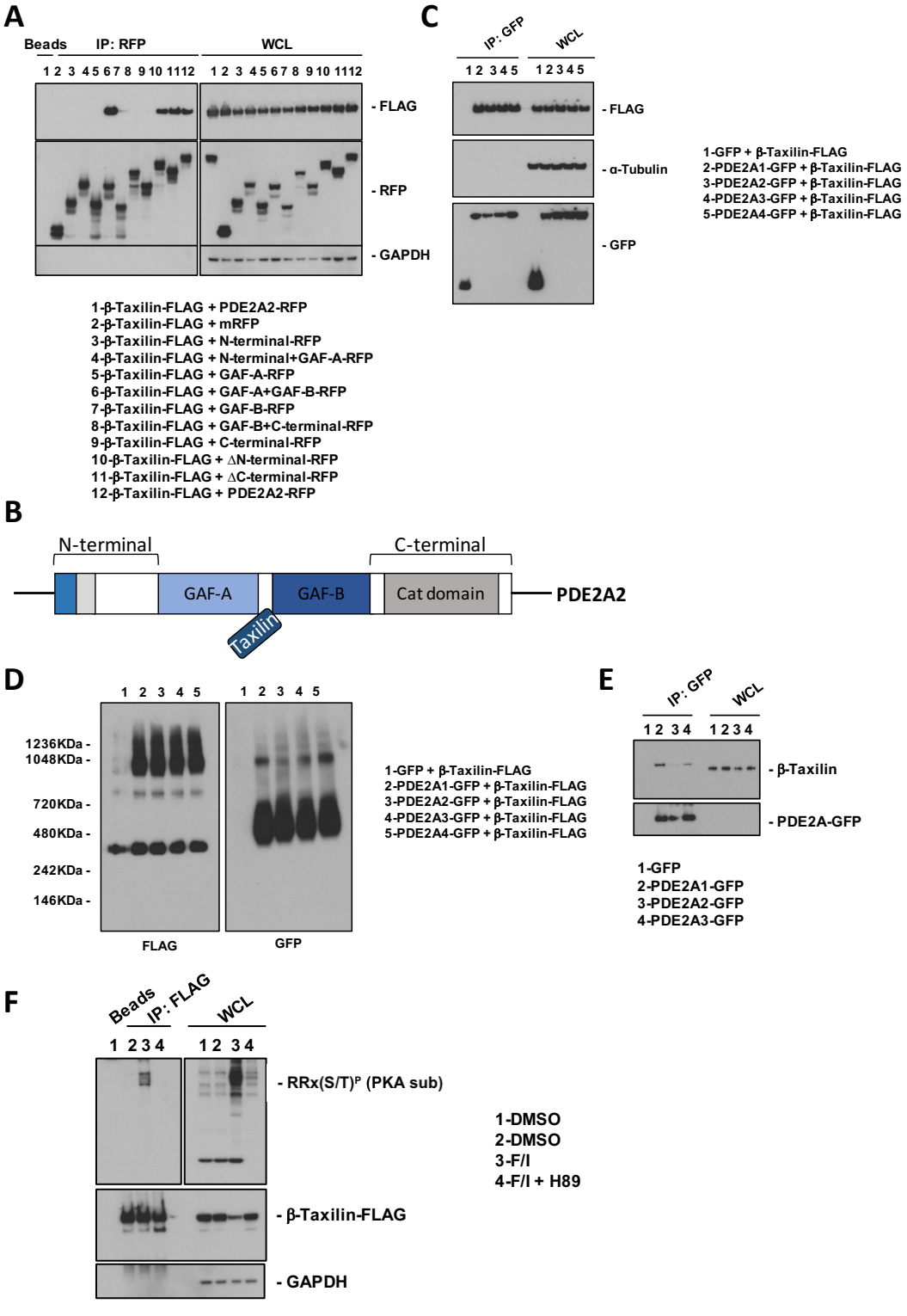

A
Beads
IP: RFP
WCL
1 2 3 4 5 6 7 8 9 10 11 12
1 2 3 4 5 6 7 8 9 10 11 12
- FLAG
- RFP
- GAPDH
1-β-Taxilin-FLAG + PDE2A2-RFP
2-β-Taxilin-FLAG + mRFP
3-β-Taxilin-FLAG + N-terminal-RFP
4-β-Taxilin-FLAG + N-terminal+GAF-A-RFP
5-β-Taxilin-FLAG + GAF-A-RFP
6-β-Taxilin-FLAG + GAF-A+GAF-B-RFP
7-β-Taxilin-FLAG + GAF-B-RFP
8-β-Taxilin-FLAG + GAF-B+C-terminal-RFP
9-β-Taxilin-FLAG + C-terminal-RFP
10-β-Taxilin-FLAG + ΔN-terminal-RFP
11-β-Taxilin-FLAG + ΔC-terminal-RFP
12-β-Taxilin-FLAG + PDE2A2-RFP
C
IP: GFP
WCL
1 2 3 4 5
1 2 3 4 5
- FLAG
- α-Tubulin
- GFP
1-GFP + β-Taxilin-FLAG
2-PDE2A1-GFP + β-Taxilin-FLAG
3-PDE2A2-GFP + β-Taxilin-FLAG
4-PDE2A3-GFP + β-Taxilin-FLAG
5-PDE2A4-GFP + β-Taxilin-FLAG
B
N-terminal
C-terminal
GAF-A
GAF-B
Cat domain
PDE2A2
Taxilin
D
1 2 3 4 5
1 2 3 4 5
1236KDa -
1048KDa -
720KDa -
480KDa -
242KDa -
146KDa -
FLAG
GFP
1-GFP + β-Taxilin-FLAG
2-PDE2A1-GFP + β-Taxilin-FLAG
3-PDE2A2-GFP + β-Taxilin-FLAG
4-PDE2A3-GFP + β-Taxilin-FLAG
5-PDE2A4-GFP + β-Taxilin-FLAG
E
IP: GFP
WCL
1 2 3 4
1 2 3 4
- β-Taxilin
- PDE2A-GFP
1-GFP
2-PDE2A1-GFP
3-PDE2A2-GFP
4-PDE2A3-GFP
F
Beads
IP: FLAG
WCL
1 2 3 4
1 2 3 4
- RRx(S/T)P (PKA sub)
- β-Taxilin-FLAG
- GAPDH
1-DMSO
2-DMSO
3-F/I
4-F/I + H89

Figure 4.2 | **Interaction of PDE2A2 domains with β-Taxilin.**
(A) Detection of β-Taxilin-FLAG after PDE2A2-RFP fragments immunoprecipitation in HEK293T cells transiently transfected with PDE2A2-RFP constructs and β-Taxilin-FLAG. Pull-down of mRFP was used as a negative control. Blot is representative of three independent experiments.
(B) Summary of PDE2A2 domains involved in β-Taxilin interaction.
(C) Detection of β-Taxilin-FLAG after immunoprecipitation of each PDE2A isoform in HEK293T cells transiently transfected with PDE2A isoforms and β-Taxilin-FLAG. Blot is representative of two independent experiments.
(D) Blue-Native PAGE of cell extracts from HEK293T co-expressing β-Taxilin-FLAG and PDE2A-GFP. Blot is representative of two independent experiments.
(E) Detection of endogenous β-Taxilin after immunoprecipitation of each PDE2A isoform in HEK293T cells transiently transfected with either PDE2A isoforms or GFP. Blot is representative of three independent experiments.
(F) Phosphorylation status of β-Taxilin in HEK293T cells overexpressing β-Taxilin-FLAG and treated with cAMP-generating agonists for 2 h. A phospho-(Ser/Thr) PKA substrate antibody was used both on whole cell lysate (WCL) and after pulling-down β-Taxilin-FLAG (IP). Blot is representative of two independent experiments.

Since it has been reported that β-Taxilin interacts with Dysbindin, a protein constituent of the dystrophin-associated protein complex in muscle cells, I hypothesized that PDE2A could also be part of this protein complex. To test this hypothesis, I assessed the interaction between PDE2A1 and endogenous Dysbindin in HEK293T cells overexpressing PDE2A1-GFP. As seen in Figure 4.3A, Dysbindin does not interact with PDE2A1-GFP, not even when β-Taxilin-FLAG is co-expressed.

To further characterize the role of the interaction between PDE2A1 and β-Taxilin, I attempted to selectively disrupt this interaction. Since I had defined the GAF-A-GAF-B-RFP fragment as the sequence involved in the interaction of PDE2A with β-Taxilin, I overexpressed the GAF-A-GAF-B-RFP fragment in HEK293T cells expressing PDE2A2-GFP and β-Taxilin-FLAG. The expectation was that the GAF-A-GAF-B-RFP fragment would compete with full length PDE2A2-GFP for β-Taxilin-FLAG binding site and disrupt the interaction between full length PDE2A2 and β-Taxilin. Unfortunately, this strategy did not work since β-Taxilin-FLAG was still detected after pulling-down PDE2A2-GFP (*Fig. 4.3B*).

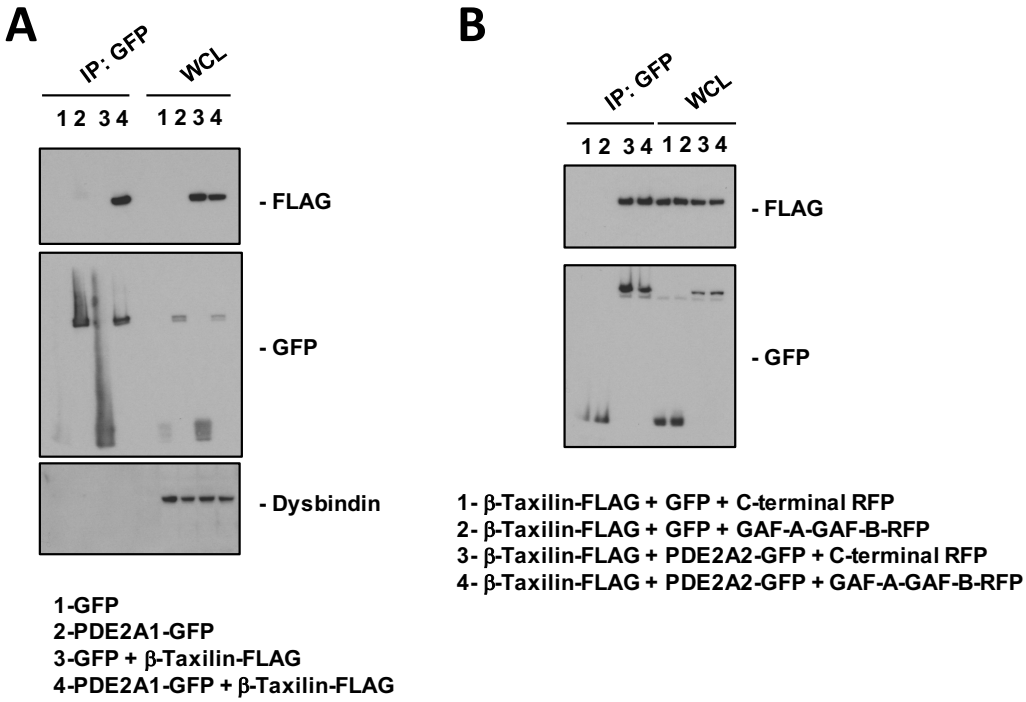


Figure 4.3 | **Attempt to disrupt PDE2A and β-Taxilin interaction.**
(A) Detection of Dysbindin after PDE2A1-GFP or GFP immunoprecipitation in HEK293T cells transiently transfected with β-Taxilin-FLAG and either PDE2A1-GFP or GFP. Blot is representative of two independent experiments.
(B) Detection of β-Taxilin after PDE2A2-GFP or GFP immunoprecipitation in HEK293T cells transiently transfected with β-Taxilin-FLAG, either PDE2A2-GFP or GFP and C-terminal-RFP or GAF-A-GAF-B-RFP. Blot is representative of two independent experiments.

4.3 Caveolins

Caveolins are well known scaffolding proteins that are the main component of caveolae, 50 to 100 nm omega-shaped invaginations of the plasma membrane rich in cholesterol and sphingolipids (Drab et al., 2001). In contrast to classical membrane coats such as clathrin, coat protein (COP)I and COPII, the caveolar coat represents a stable structure that, once assembled, does not undergo cycles of assembly and disassembly (Tagawa et al., 2005). All three Caveolin family members (Caveolin 1, 2 and 3) are caveolar coat proteins, but only Caveolin 1 and the muscle-specific Caveolin 3 have the capacity to induce caveolae formation (Capozza et al., 2005; Fra et al., 1995). The major Caveolin in non-muscle cells, Caveolin 1, is a 21 kDa integral membrane protein with a central hydrophobic domain inserted as a loop inside the membrane. With both N and C termini facing the cytoplasm, Caveolin assumes a hairpin topology (Dupree et al., 1993; Monier et al., 1995). Caveolin 1 binds cholesterol and serves in cholesterol-associated form as a key component in the assembly of the caveolar coat (Murata et al., 1995). Although not essential for caveolae formation, Caveolin 2 is coexpressed with Caveolin 1 in many cell types, and is part of Caveolin assemblies in a ratio of less than half that of Caveolin 1 (Scheiffele et al., 1998; Scherer et al., 1996). Caveolin 1 is synthesized in the ER and assembles along the membranes of the secretory pathway into large caveolar domains that subsequently travel between the plasma membrane and ER/endosomes (Ritz et al., 2011).

Caveolins function as plasma membrane microdomains by bringing together key components of Ca^{2+} signaling and other signaling pathways. Caveolins are found in many different cell types, but most prominently in endothelial cells as well as in adipocytes, where caveolae can comprise up to 20-30 % of total plasma membrane area (Fan et al., 1983; Pani and Singh, 2009). In addition to signaling, Caveolin 1 also plays an important role in intracellular

cholesterol and sphingolipid transport (Liu et al., 2002; Sonnino and Prinetti, 2009). Mice lacking Caveolin 1 display a variety of phenotypes such as reduced whole-body fat mass, elevated triglyceride levels, elevated free fatty acid levels and a blunted response to β3-adrenergic receptor stimulation (Cohen et al., 2004; Razani et al., 2002). Interestingly, Caveolin 1/3 double KO (knockout) mice are viable but develop a severe cardiomyopathic phenotype (Park et al., 2002).

Recently, Caveolins have also been shown to localize to other cellular compartments, such as mitochondria-associated membranes (MAM), a special ER domain that interacts with mitochondria (Fridolfsson et al., 2012; Sala-Vila et al., 2016). MAMs were primarily proposed to constitute areas gating the interchange of inorganic ions and complex lipids between these two organelles - indeed, these physical contacts determine Ca^{2+} fluxes and allow for specific lipid transactions such as the conversion of ER-derived phosphatidylserine into phosphatidylethanolamine and other phospholipid species on the mitochondrial surface (Vance, 2014; van Vliet et al., 2014). There have been several studies reporting Caveolins at the MAM and their involvement in regulation of lipid transfer and mitochondrial health (Asterholm et al., 2012; Bosch et al., 2011; Fridolfsson et al., 2012; Sala-Vila et al., 2016; Schilling and Patel, 2016; Volonte et al., 2016). MAMs have subsequently been shown to accrue multiple specific activities and are currently conceived as intracellular hubs, integrating numerous signaling pathways and coordinating the metabolic status of the cell with other cellular processes. Among these processes, the regulated tracking of cholesterol and its use as a precursor for steroid derivatives is highly represented. Accordingly, increasing evidence links MAM dysfunction with complex diseases such as neurodegenerative disorders, aberrant lysosomal storage syndromes, obesity-related pathologies and diabetes (Marchi et al., 2014; Vance, 2014).

To validate the potential interaction between PDE2A2 and Caveolins, co-immunoprecipitation experiments in HEK293T cell overexpressing either Caveolin 1-FLAG or Caveolin 2-RFP and PDE2A2-RFP or PDE2A2-GFP, respectively, were performed (*Fig. 4.4A-C*). Results show that both Caveolins interact with PDE2A2. The immunoprecipitation experiment was also performed in HEK293T cells overexpressing PDE2A2-RFP only, therefore probing interaction with endogenous Caveolin 1 and 2 (*Fig. 4.4D*), and confirmed that Caveolins co-immunoprecipitate with PDE2A2. To address the cellular localization where this interaction occurs, confocal microscopy of HeLa cells and NRVM overexpressing PDE2A2-RFP and endogenous Caveolins was performed (*Fig. 4.4E and F*). As shown, Caveolins do not seem to co-localize with PDE2A2 at the PM of HeLa cells or NRVM. Further experiments described in Chapter 6 were done to further characterize the PDE2A2-Caveolin interaction and to tackle the apparent paradox between co-localization and co-immunoprecipitation data.

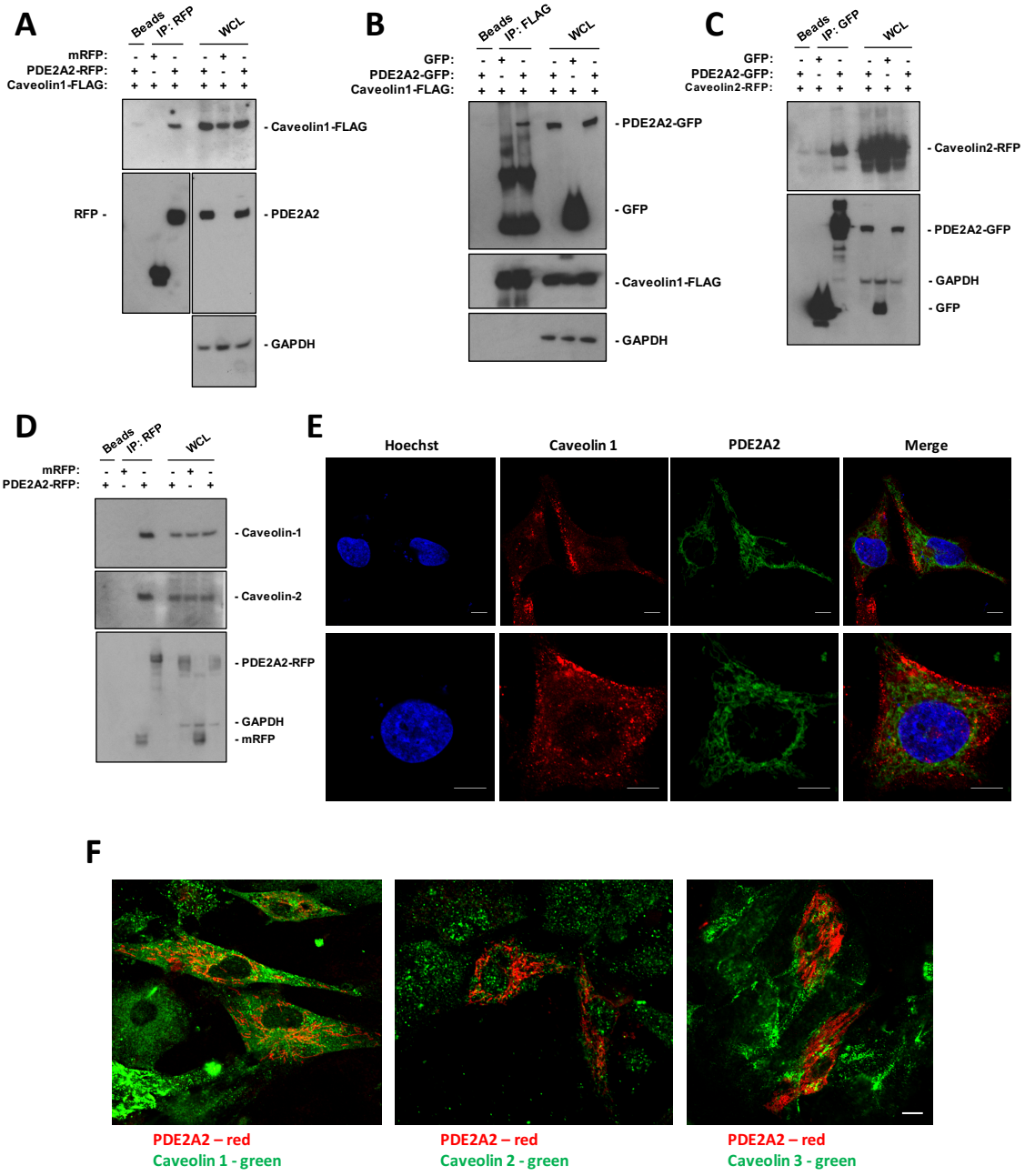

A
Beads
IP: RFP
WCL
mRFP:
PDE2A2-RFP:
Caveolin1-FLAG:
- Caveolin1-FLAG
RFP -
- PDE2A2
- GAPDH
B
Beads
IP: FLAG
WCL
GFP:
PDE2A2-GFP:
Caveolin1-FLAG:
- PDE2A2-GFP
- GFP
- Caveolin1-FLAG
- GAPDH
C
Beads
IP: GFP
WCL
GFP:
PDE2A2-GFP:
Caveolin2-RFP:
- Caveolin2-RFP
- PDE2A2-GFP
- GAPDH
- GFP
D
Beads
IP: RFP
WCL
mRFP:
PDE2A2-RFP:
- Caveolin-1
- Caveolin-2
- PDE2A2-RFP
- GAPDH
- mRFP
E
Hoechst
Caveolin 1
PDE2A2
Merge
F
PDE2A2 – red
Caveolin 1 - green
PDE2A2 – red
Caveolin 2 - green
PDE2A2 – red
Caveolin 3 - green

Figure 4.4 | **PDE2A2 interacts with Caveolins.**
(A) Detection of Caveolin 1-FLAG after PDE2A2-RFP or mRFP immunoprecipitation in HEK293T cells transiently transfected with Caveolin 1-FLAG and either PDE2A2-RFP or mRFP. Pull-down of mRFP and pull-down with beads only (without conjugated antibody) were used as a negative control. Blot is representative of three independent experiments.
(B) Detection of PDE2A2-GFP and GFP after Caveolin 1-FLAG immunoprecipitation in HEK293T cells transiently transfected with Caveolin 1-FLAG and either PDE2A2-GFP or GFP. Blot is representative of two independent experiments.
(C) Detection of Caveolin2-RFP after PDE2A2-GFP or GFP immunoprecipitation in HEK293T cells transiently transfected with Caveolin2-RFP and either PDE2A2-GFP or GFP. Blot is representative of two independent experiments.
(D) Detection of endogenous Caveolin 1 and Caveolin 2 after PDE2A2-RFP or mRFP immunoprecipitation in HEK293T cells transiently transfected with either PDE2A2-RFP or mRFP. Blot is representative of two independent experiments.
(E) Confocal images of HeLa cells over-expressing PDE2A2-RFP. Cells were fixed for immunofluorescence staining with RFP (green), Caveolin 1 (red) and respective secondary antibodies. The nuclei were stained with Hoechst (blue). Images are representative of two independent experiments. Scale bars: 10 μm.
(F) Confocal imaging of PDE2A2-RFP and endogenous Caveolins in NRVM. Images are representative of two independent experiments. Scale bar: 10 μm.

4.4 Other Endoplasmic Reticulum hits

ALDH3A2 is a fatty aldehyde dehydrogenase localized at the ER membrane that catalyses the oxidation of long-chain aliphatic aldehydes to fatty acids. Erlin2 is known to be involved in the ER-associated degradation (ERAD) of inositol trisphosphate (IP3) receptor (IP3R), a ER Ca^{2+} channel activated by IP3 (Pearce et al., 2009). To assess the interaction between these two proteins and PDE2A2, co-immunoprecipitation experiments were performed in HEK293T cells over-expressing PDE2A2-RFP or PDE2A2-GFP and either ALDH3A2-FLAG or Erlin2-FLAG (*Fig. 4.5 A-C*). The results show that ALDH3A2 and Erlin2 interact with PDE2A2.

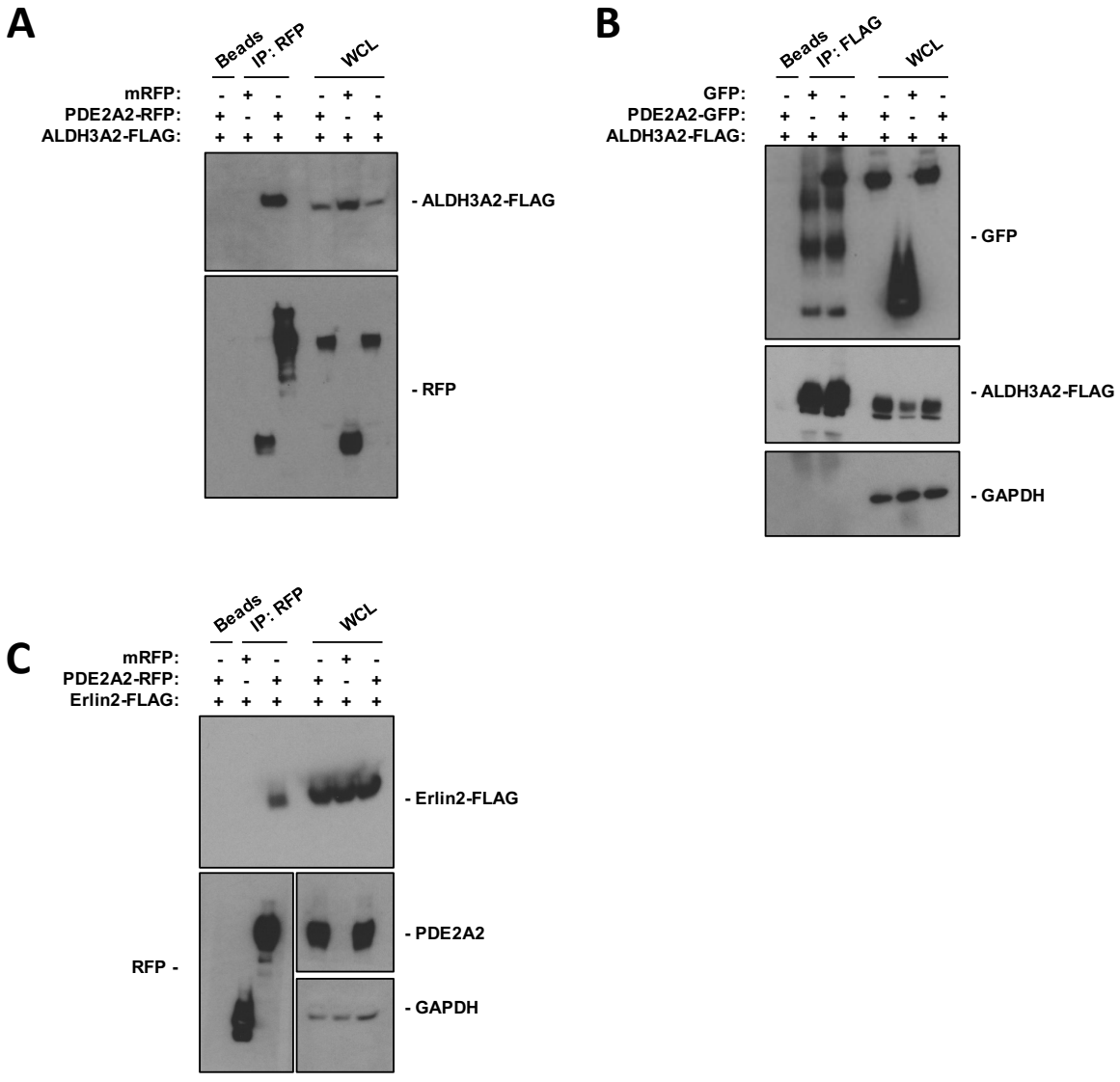


Figure 4.5 | **PDE2A2 interacts with ALDH3A2 and Erlin2.**
(A) Detection of ALDH3A2-FLAG after PDE2A2-RFP or mRFP immunoprecipitation in HEK293T cells transiently transfected with ALDH3A2-FLAG and either PDE2A2-RFP or mRFP. Pull-down of mRFP and pull-down with beads only (without conjugated antibody) were used as a negative control. Blot is representative of two independent experiments.
(B) Detection of PDE2A2-GFP and GFP after ALDH3A2-FLAG immunoprecipitation in HEK293T cells transiently transfected with ALDH3A2-FLAG and either PDE2A2-GFP or GFP. Blot is representative of two independent experiments.
(C) Detection of Erlin2-FLAG after PDE2A2-RFP or mRFP immunoprecipitation in HEK293T cells transiently transfected with Erlin2-FLAG and either PDE2A2-RFP or mRFP. Blot is representative of two independent experiments.

4.5 MINOS complex

The mitochondrial inner membrane organizing system (MINOS) was discovered as a large protein complex essential for mitochondrial membrane architecture and has a crucial role in the formation of cristae junctions and contact sites between the outer and inner membranes as well as in mitochondrial dynamics (Darshi et al., 2011; von der Malsburg et al., 2011; Pfanner et al., 2014; Zerbes et al., 2012). The MINOS complex is highly conserved from yeast to humans and comprises several components in mammals, including Mitofilin, ChChD3, ChChD6, MINOS1, QIL1, APOOL and APOO (Guarani et al., 2015; Pfanner et al., 2014). Mitofilin is an inner membrane protein that consists of an N-terminal transmembrane domain and a large C-terminal domain facing the intermembrane space (Harner et al., 2011; Hoppins et al., 2011; von der Malsburg et al., 2011). It is thought to be a central component of the MINOS complex and interacts with several outer membrane proteins, including SAMM50, a protein involved in sorting and assembly of mitochondrial complexes and structure of mitochondrial cristae (Ding et al., 2015; Friedman et al., 2015).

To assess whether PDE2A2 interacts with components of the MINOS complex, co-immunoprecipitation experiments were performed in HEK293T cells overexpressing PDE2A2-RFP and Mitofilin-FLAG (*Fig. 4.6A*). Results show that PDE2A2-RFP binds to Mitofilin-FLAG. Additionally, co-immunoprecipitation experiments were performed in HEK293T cells overexpressing PDE2A2-RFP and endogenous Mitofilin (*Fig. 4.6B*), ChChD3 (*Fig. 4.6C*) and SAMM50 (*Fig. 4.6D*). Results confirmed the interaction between PDE2A2 and the MINOS complex, more specifically, Mitofilin, ChChD3 and SAMM50. Co-immunoprecipitation experiments where Mitofilin-FLAG (*Fig. 4.7A*) and SAMM50-FLAG (*Fig. 4.7B*) were pulled-down followed by detection of PDE2A2-GFP were also performed and the results confirmed the previous observations. Additionally, ChChD6 was also detected after pulling down PDE2A2 in HEK293T cells overexpressing both proteins, although the interaction was not as strong as

found for other MINOS complex components (*Fig. 4.7C*). To further confirm the interaction between Mitofilin and PDE2A2 I also performed pulldown experiments of endogenous Mitofilin and probed for endogenous PDE2A in immunoprecipitates from rat brain homogenate (*Fig. 4.6E*). Overall, the above data support the interaction of PDE2A2 with the MINOS complex. To further investigate the co-localization between PDE2A2 and Mitofilin, SH-SY5Y cells were transfected with PDE2A2-GFP and double labelled with anti-GFP and anti-Mitofilin antibodies. As shown in Figure 4.6F, PDE2A2 largely overlaps with Mitofilin, which was expected since both proteins localize to the mitochondria. Based on these results, I propose that Mitofilin, at the IMM, interacts with the local pool of PDE2A2 in the IMS. The role of PDE2A2-MINOS complex interaction is further studied in Chapter 5.

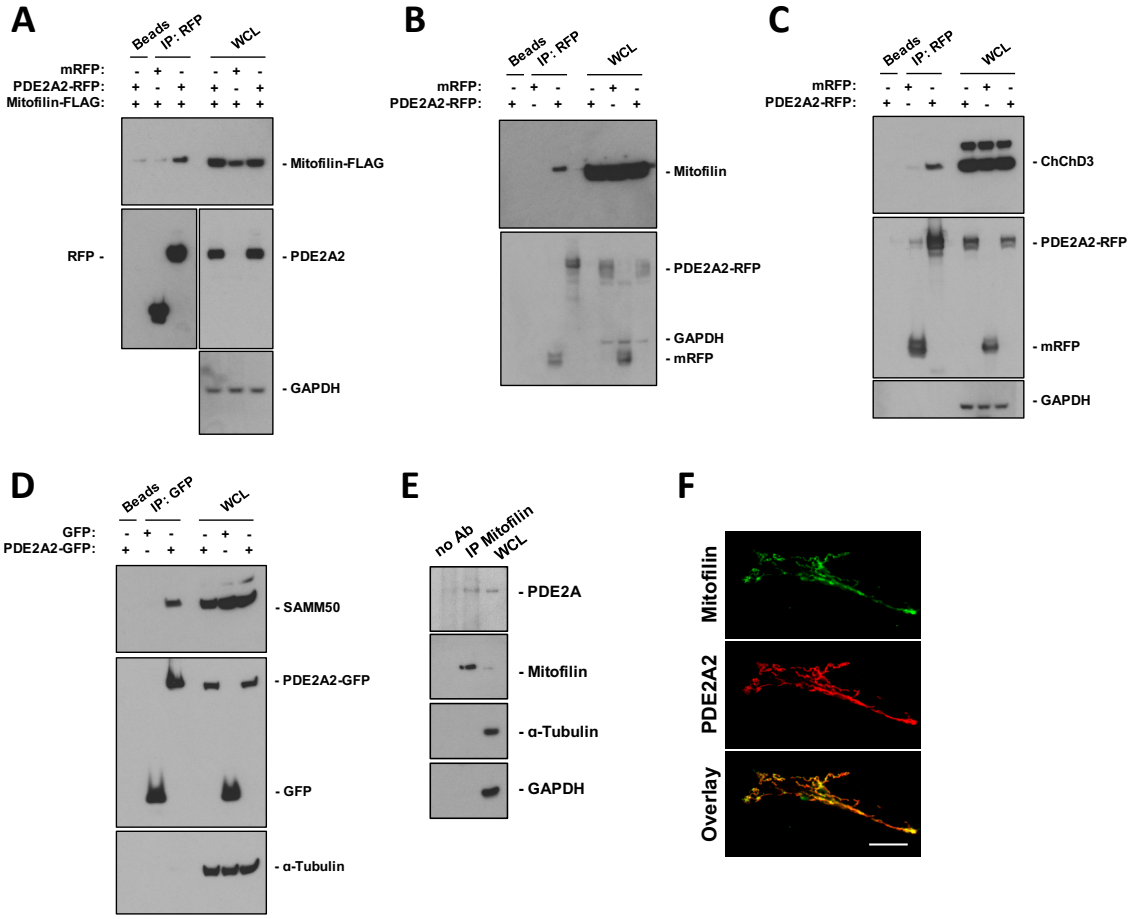


Figure 4.6 | **PDE2A2 interacts with proteins of the MINOS complex.**
(A) Detection of Mitofilin-FLAG after PDE2A2-RFP or mRFP immunoprecipitation in HEK293T cells transiently transfected with Mitofilin-FLAG and either PDE2A2-RFP or mRFP. Pull-down of mRFP and pull-down with beads only (without conjugated antibody) were used as a negative control. Blot is representative of three independent experiments.
(B) Detection of endogenous Mitofilin after PDE2A2-RFP or mRFP immunoprecipitation in HEK293T cells transiently transfected with either PDE2A2-RFP or mRFP. Blot is representative of three independent experiments.
(C) Detection of endogenous ChChD3 after PDE2A2-RFP or mRFP immunoprecipitation in HEK293T cells transiently transfected with either PDE2A2-RFP or mRFP. Blot is representative of tthree independent experiments.
(D) Detection of endogenous SAMM50 after PDE2A2-GFP or GFP immunoprecipitation in HEK293T cells transiently transfected with either PDE2A2-GFP or GFP. Blot is representative of three independent experiments.
(E) Detection of endogenous PDE2A after Mitofilin immunoprecipitation in cell lysate from rat brain. Blot is representative of two independent experiments.
(F) Confocal images of SH-SY5Y cells over-expressing PDE2A2-GFP. Cells were fixed for immunofluorescence staining with GFP (red), Mitofilin (green) and respective secondary antibodies. Images are representative of two independent experiments. Scale bar: 10 μm.

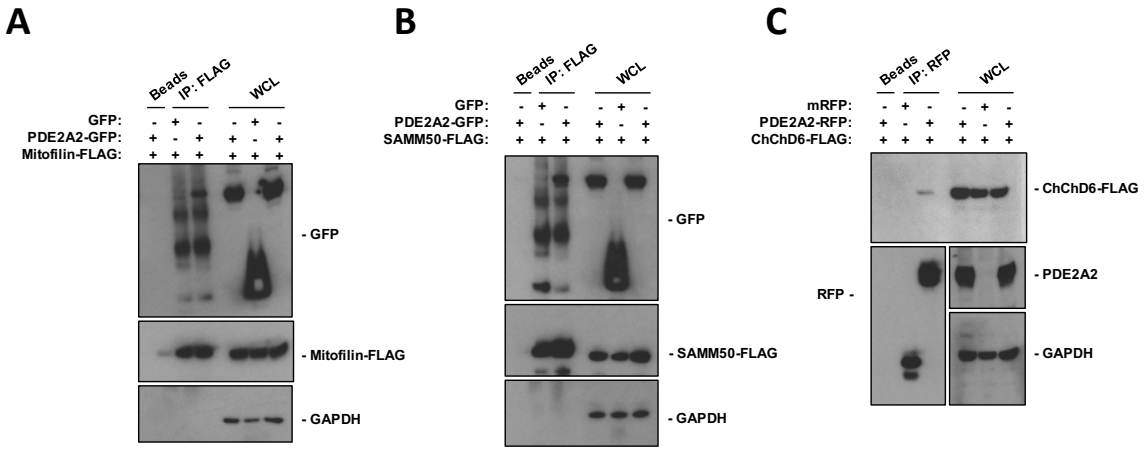


Figure 4.7 | **Proteins of the MINOS complex interact with PDE2A2.**
(A) Detection of PDE2A2-GFP and GFP after Mitofilin-FLAG immunoprecipitation in HEK293T cells transiently transfected with Mitofilin-FLAG and either PDE2A2-GFP or GFP. Blot is representative of two independent experiments.
(B) Detection of PDE2A2-GFP and GFP after SAMM50-FLAG immunoprecipitation in HEK293T cells transiently transfected with SAMM50-FLAG and either PDE2A2-GFP or GFP. Blot is representative of two independent experiments.
(C) Detection of ChChD6-FLAG after PDE2A2-RFP or mRFP immunoprecipitation in HEK293T cells transiently transfected with ChChD6-FLAG and either PDE2A2-RFP or mRFP. Blot is representative of two independent experiments.

4.6 Other Mitochondrial hits

Other mitochondrial proteins were identified as potential interactors by the MS analysis. These include Metaxin 2, involved in the transport of proteins into the mitochondria, and Mitofusin 2, a GTPase embedded in the OMM and ER and essential for mitochondrial fusion and ER-mitochondria tethering (Armstrong et al., 1999; de Brito and Scorrano, 2008). Using the same co-immunoprecipitation approach described above, results suggest that Mitofusin 1 and 2 and Metaxin 2 may also be PDE2A2 binding partners, although the IPs are not clean or strong enough to consider them as one of the main interactors (*Fig. 4.8A-E and G*).

Additionally, it has been suggested that Mitofusin 2 is a PKA target and that this specific phosphorylation site plays a key role in muscle cells proliferation (Zhou et al., 2010). As shown in Figure 4.8F, Mitofusin 2 seems to be slightly phosphorylated after treatment with Fsk (25μM) and IBMX (100μM). H89 completely abolished the phosphorylation pattern of Mitofusin 2, confirming this phosphorylation is PKA-mediated. However, it is not clear whether treatment with the PDE2A inhibitor BAY-60 (1μM) also induces PKA-mediated phosphorylation of Mitofusin 2.

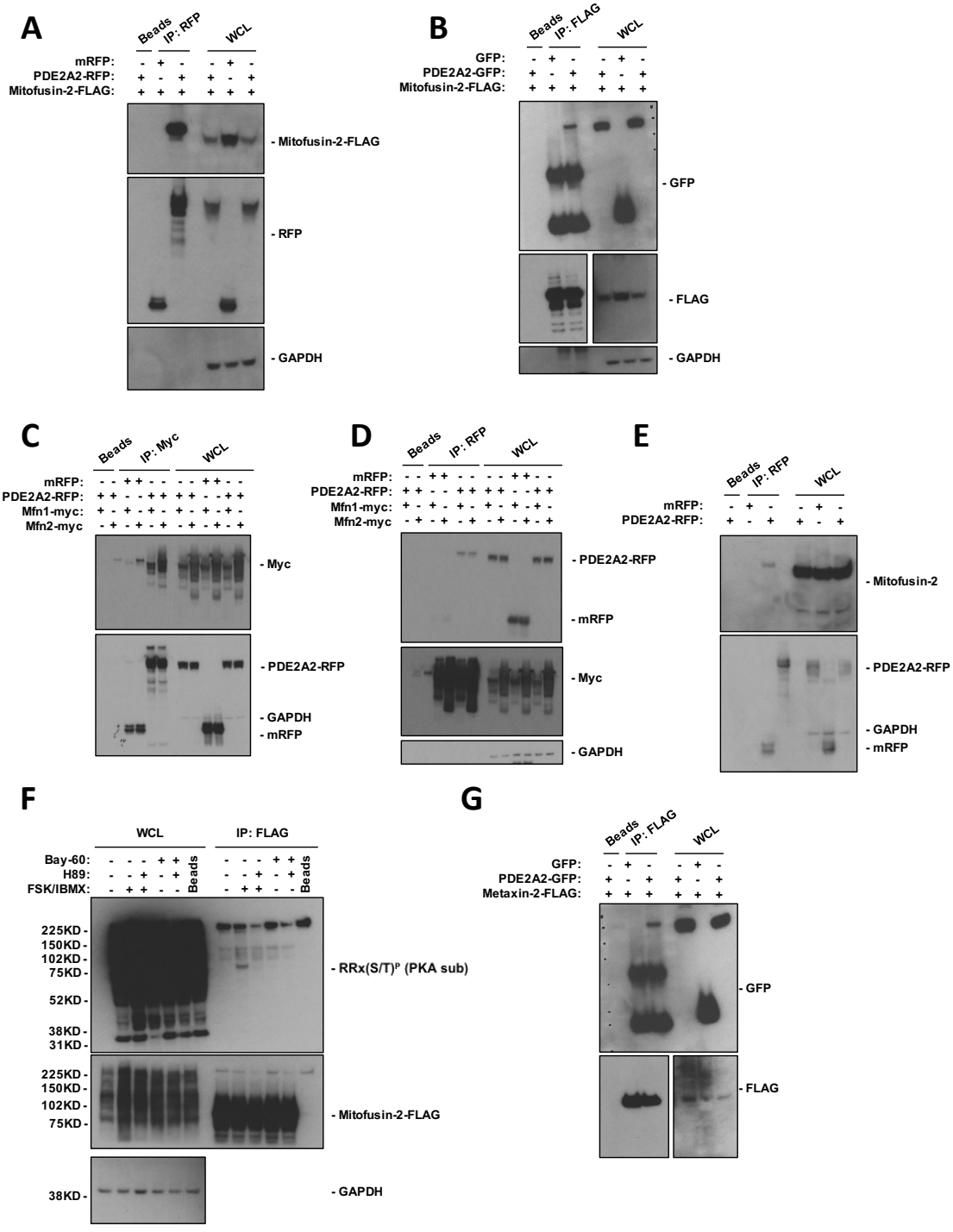

A
Beads
IP: RFP
WCL
mRFP:
PDE2A2-RFP:
Mitofusin-2-FLAG:
- Mitofusin-2-FLAG
- RFP
- GAPDH
B
Beads
IP: FLAG
WCL
GFP:
PDE2A2-GFP:
Mitofusin-2-FLAG:
- GFP
- FLAG
- GAPDH
C
Beads
IP: Myc
WCL
mRFP:
PDE2A2-RFP:
Mfn1-myc:
Mfn2-myc
- Myc
- PDE2A2-RFP
- GAPDH
- mRFP
D
Beads
IP: RFP
WCL
mRFP:
PDE2A2-RFP:
Mfn1-myc:
Mfn2-myc
- PDE2A2-RFP
- mRFP
- Myc
- GAPDH
E
Beads
IP: RFP
WCL
mRFP:
PDE2A2-RFP:
- Mitofusin-2
- PDE2A2-RFP
- GAPDH
- mRFP
F
WCL
IP: FLAG
Bay-60:
H89:
FSK/IBMX:
Beads
225KD
150KD
102KD
75KD
52KD
38KD
31KD
- RRx(S/T)P (PKA sub)
- Mitofusin-2-FLAG
- GAPDH
G
Beads
IP: FLAG
WCL
GFP:
PDE2A2-GFP:
Metaxin-2-FLAG:
- GFP
- FLAG

Figure 4.8 | **PDE2A2 interacts with other mitochondrial protein, such as Metaxin 2 and Mitofusins.**
(A) Detection of Mitofusin 2-FLAG after PDE2A2-RFP or mRFP immunoprecipitation in HEK293T cells transiently transfected with Mitofusin 2-FLAG and either PDE2A2-RFP or mRFP. Pull-down of mRFP and pull-down with beads only (without conjugated antibody) were used as a negative control. Blot is representative of two independent experiments.
(B) Detection of PDE2A2-GFP and GFP after Mitofusin 2-FLAG immunoprecipitation in HEK293T cells transiently transfected with Mitofusin 2-FLAG and either PDE2A2-GFP or GFP. Blot is representative of two independent experiments.
(C) Detection of Mitofusin 1-Myc (Mfn1) or Mitofusin 2-Myc (Mfn2) after PDE2A2-RFP or mRFP immunoprecipitation in HEK293T cells transiently transfected with either Mitofusin 1-Myc or Mitofusin 2-Myc and either PDE2A2-RFP or mRFP.
(D) Detection of PDE2A2-RFP and mRFP after Mitofusin 1-Myc or Mitofusin 2-Myc immunoprecipitation in HEK293T cells transiently transfected with either Mitofusin 1-Myc or Mitofusin 2-Myc and either PDE2A2-RFP or mRFP.
(E) Detection of endogenous Mitofusin 2 after PDE2A2-RFP or mRFP immunoprecipitation in HEK293T cells transiently transfected with either PDE2A2-RFP or mRFP. Blot is representative of two independent experiments.
(F) Phosphorylation status of Mitofusin 2 in HEK293T cells overexpressing Mitofusin 2-FLAG and treated with cAMP-generating agonists. A phosphor-(Ser/Thr) PKA substrate antibody was used both on whole cell lysate (WCL) and after pulling-down Mitofusin 2-FLAG (upper panel). Blot is representative of two independent experiments.
(G) Detection of PDE2A2-GFP and GFP after Metaxin 2-FLAG immunoprecipitation in HEK293T cells transiently transfected with Metaxin 2-FLAG and either PDE2A2-GFP or GFP. Blot is representative of two independent experiments.

4.7 Conclusion

Until now, only one protein had been shown to interact with PDE2A – AIP (AhR-interacting protein), a component of the aryl hydrocarbon receptor (AhR) complex (de Oliveira and Smolenski, 2009; de Oliveira et al., 2007). Binding of PDE2A to AIP inhibits the nuclear translocation of AhR in hepatocytes. Thus, PDE2A has a role in AhR trafficking through binding to AIP, and may regulate AhR mobility in the cytosol. However, which PDE2A isoforms interact with AIP remains to be established.

Here, my colleagues and I tackled the lack of information regarding PDE2A2 interactors by performing MS in adult rat cardiomyocytes overexpressing PDE2A2-RFP. Several novel interactors have been confirmed whereas for others, although they had scored highly in the MS analysis, it was not possible to confirm the interaction using the more direct co-immunoprecipitation approach. A summary of all the interactors that have been tested is shown in Table 4.2. Among these, the main subsets of PDE2A binding partners are:

a) β-Taxilin;
b) Caveolins;
c) MINOS complex, including Mitofilin, ChChD3 and SAMM-50.

From this subset of confirmed interactors, MINOS complex and Caveolins were further studied, on Chapter 5 and 6, respectively. However, it is worth to point out that in this study we have not tested if these interactors bind directly, or not, to PDE2A. Further studies, for instance using purified recombinant protein produced in bacteria, would be required to tackle this question and validate the interaction. Additionally, many of these interactions were only tested in overexpressing models, which may saturate a certain binding site and induce unspecific binding with other proteins, as seen between β-Taxilin and PDE2A2. To avoid this, antibody

against endogenous PDE2A could have been used, as it was done for PDE2A-Mitofilin interaction. However, a drawback of this strategy is that the commercially available antibodies are not isoform-specific. On a different note, the basis of the interaction studies was a set of MS experiments performed by different colleagues. As mentioned above, the basis of the MS experiment was overexpression of PDE2A2 by viral infection, which can lead to unspecific interactions. Additionally, other controls could have been included, such as quantification of the amount of a specific interactor inside the cell, to better understand the proportion/percentage of that protein that is binding PDE2A2. Overall, these interactors should be carefully considered since some interactions may result from false positives produced by co-immunoprecipitation experiments.

Table 4.2 | **Summary of PDE2A2 co-immunoprecipitations.** '?' means that data obtained is not clear enough to conclude if both proteins interact or not.

Protein	Co-immunoprecipitation with PDE2A2
ALDH3A2	Yes/?
β-Taxilin	Yes
Caveolin 1	Yes
Caveolin 2	Yes
Caveolin 3	Yes
ChChD3	Yes
Erlin2	Yes/?
Mitofilin	Yes
SAMM50	Yes
ChChD6	?
Metaxin 2	?
Mitofusin 1	?
Mitofusin 2	?
DNAJC11	No
RTN4	No
TMEM38-A	No
VDAC1	No
VDAC2	No
VDAC3	No

Chapter 5 - PDE2A2 regulates PKA-mediated phosphorylation of Mitofilin and Parkin-dependent mitophagy

5.1 Background

Compartmentalization of cAMP prompts the idea that with a detailed understanding of the organization, regulation and function of individual cAMP compartments it may be possible to target individual cAMP pools, rather than global intracellular cAMP levels, in order to achieve greater therapeutic efficacy and specificity (Maurice et al., 2014a). Several components of the cAMP/PKA cascade have been located to different mitochondrial sub-compartments, suggesting the presence of multiple cAMP/PKA signaling domains within the organelle (Lefkimmiatis and Zaccolo, 2014). Indeed, every mitochondrial compartment, including the OMM, IMS and the mitochondrial matrix, potentially harbour a spatially and functionally distinct cAMP signalosome (Monterisi and Zaccolo, 2017). cAMP/PKA signaling is involved in multiple mitochondrial processes, including ATP production (García-Bermúdez et al., 2015), apoptosis (Nunnari and Suomalainen, 2012) and regulation of mitochondrial membrane potential and mitochondrial morphology (Monterisi et al., 2017). In addition Akabane *et al*. have recently reported that PKA-mediated phosphorylation of Mitofilin is involved in the regulation of Parkin recruitment to the mitochondria and in mitophagy – mitochondria degradation by autophagy (Akabane et al., 2016).

The proteins Parkin and PTEN-induced kinase 1 (PINK1) are key players in the mitophagic process (Pickrell and Youle, 2015). Parkin is an E3 ubiquitin ligase which catalyzes the transfer of ubiquitin from an E2 ubiquitin-conjugating enzyme to a protein substrate in a process called ubiquitination (Winklhofer, 2014). PINK1 is a mitochondrially targeted serine/threonine kinase (Mukherjee et al., 2015). In healthy mitochondria with normal membrane potential and under basal conditions, Parkin is located mainly in the cytosol, where its ubiquitin ligase activity is inhibited while PINK1 is imported into the mitochondria and becomes degraded by proteolysis. Following cellular stress, the depolarization of the mitochondrial membrane potential leads to

stabilization of PINK1 at the OMM, where it phosphorylates ubiquitin. This induces activation of Parkin and its translocation to damaged mitochondria in a PINK1-dependent manner. Parkin then ubiquitinates a number of mitochondrial substrates mediating mitochondrial fragmentation, degradation and mitophagy (Matsuda et al., 2010). In other words, PINK1 detects mitochondrial dysfunction and then signals Parkin to ubiquitinate specifically the damaged mitochondria to instigate their removal by mitophagy.

Recent advances revealed that Parkin recruitment to depolarized mitochondria is severely inhibited by treatment with cAMP raising agents. cAMP-dependent activation of PKA was shown to reduce PINK1 protein levels at the OMM through phosphorylation of Mitofilin and ChChD3, components of the MINOS complex (*Fig. 5.1*). Based on their findings, Akabane et al. proposed a model whereby phosphorylation of the MINOS complex by PKA reduces the interaction between PINK1 and the MINOS complex, leading to PINK1 destabilization and degradation. Consequently, recruitment of Parkin to damaged mitochondria is prevented. Thus, mitochondrial clearance initiated by PINK1 and Parkin is negatively regulated by PKA-mediated phosphorylation of MINOS (Akabane et al., 2016). Modulation of the mitochondrial cAMP pool and of the local PKA activity would therefore offer a route to regulate PINK1 sensing of mitochondrial damage and activation of Parkin.

We have recently shown that in cardiac myocytes and other cell types PDE2A2 is part of a distinct cAMP/PKA signaling domain located at the mitochondria (Monterisi et al., 2017). This PDE2A2 subset localizes to mitochondrial membranes where it controls a pool of cAMP generated at the plasma membrane by the hormone-responsive adenylyl cyclase (TmAC), and regulates PKA-dependent phosphorylation of Drp1, a mitochondrial fission protein. Inhibition of this subset of PDE2A2 results in elongated mitochondria and protection from mitochondrial-dependent cell death (Monterisi et al., 2017). Evidence suggests that mitochondria morphology determines the cellular response to autophagy and that elongated mitochondria are spared

from mitophagic degradation (Gomes et al., 2011). In addition (Chapter 4.5), I have demonstrated that PDE2A2 interacts with components of the MINOS complex, including Mitofilin and ChChD3. Thus, I hypothesized that PDE2A2 regulates a local cAMP pool in the intermembrane space (IMS) that controls PKA-dependent phosphorylation of Mitofilin and Parkin recruitment to damaged mitochondria.

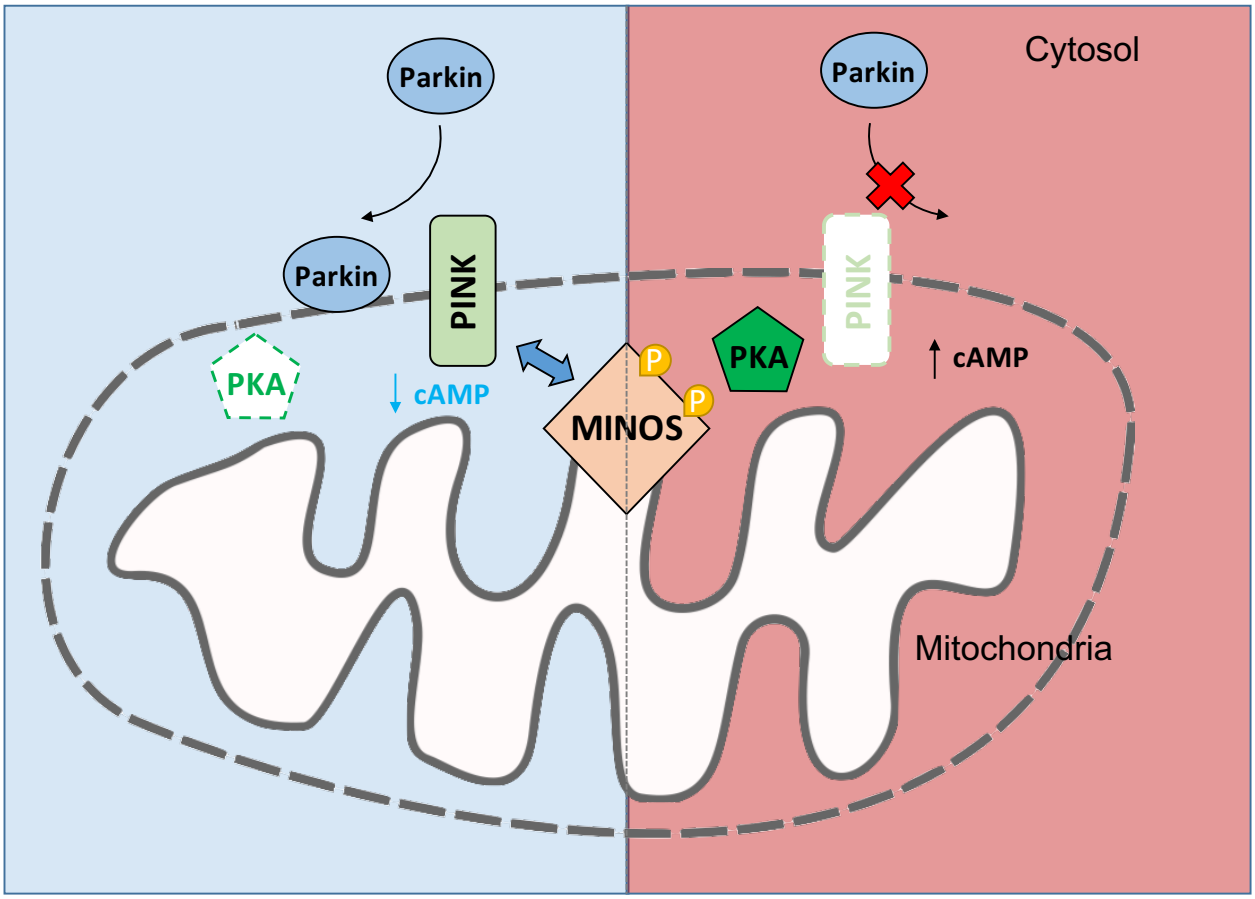
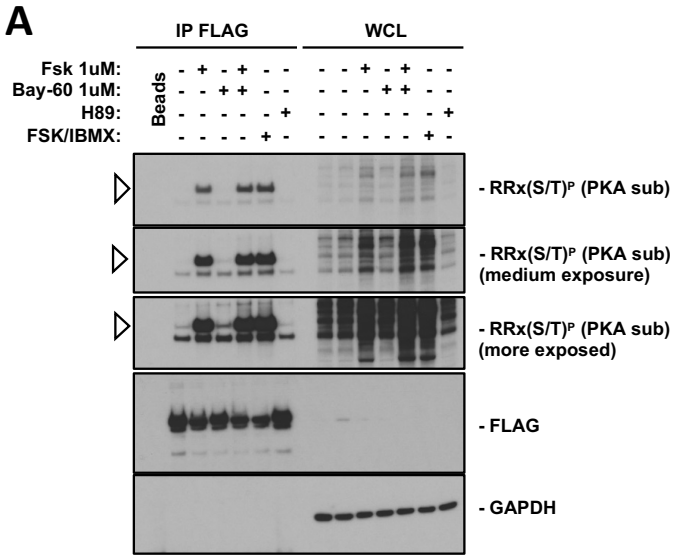
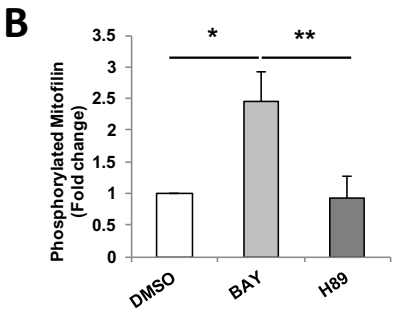


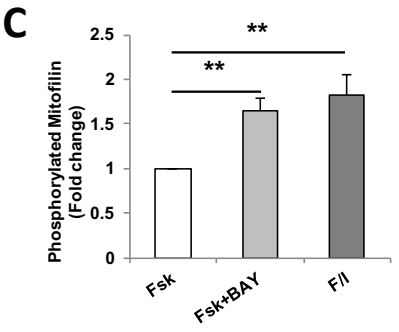
Figure 5.1 | **Model of cAMP-regulation of Parkin recruitment to the mitochondria.**
PKA activation reduces PINK1 protein levels through phosphorylation of Mitofilin/ChChD3 and consequently prevents recruitment of Parkin to damaged mitochondria.

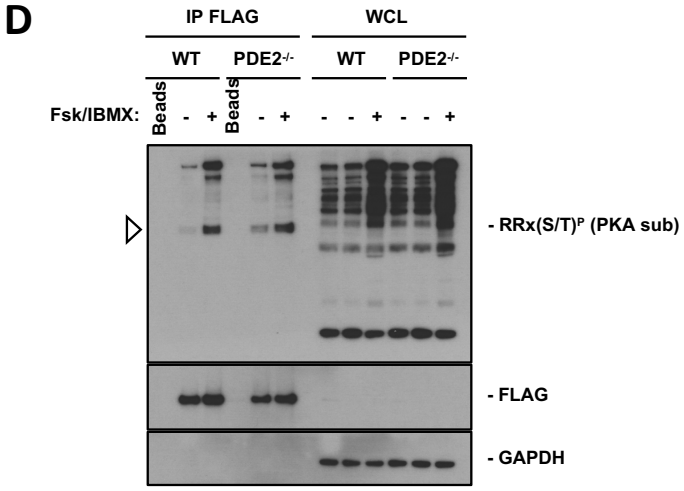
5.2 PDE2A regulates Mitofilin phosphorylation status

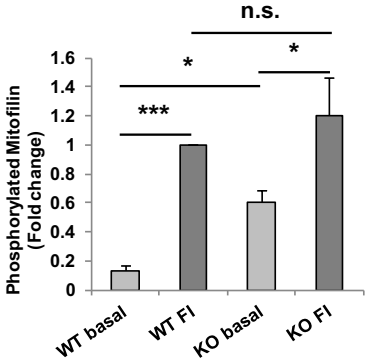
To test the hypothesis that PDE2A2 is involved in PKA-mediated phosphorylation of Mitofilin, I expressed Mitofilin-FLAG in HEK293T cells and probed for its PKA-mediated phosphorylation on application of the AC activator forskolin. I observed that treatment for 2 h with 1 μM forskolin substantially increased Mitofilin phosphorylation compared to DMSO-treated cells (*Fig. 5.2A*), confirming the previously published results (Akabane et al., 2016). Interestingly, 2 h incubation with the PDE2A selective inhibitor, BAY-60, was sufficient to significantly increase Mitofilin phosphorylation compared to DMSO-treated cells (*Fig. 5.2A and B*). Treatment with the PKA inhibitor H89 completely abolished the phosphorylation pattern of Mitofilin, confirming that the phosphorylation of Mitofilin is mediated by PKA (*Fig. 5.2A and B*). Additionally, combination of BAY-60 and forskolin had a cumulative effect, promoting Mitofilin phosphorylation compared with treatment with forskolin alone, but not significantly different from treatment with forskolin and the non-selective PDE inhibitor IBMX (*Fig. 5.2A and C*). This observation further strengthens the hypothesis that PDE2A is involved in the regulation of PKA-mediated phosphorylation of Mitofilin. Furthermore, my data shows that in mouse embryonic fibroblasts whose PDE2A gene had been deleted $(MEF)^{PDE2A-/-}$, the amount of phosphorylated Mitofilin under basal conditions is higher when compared to MEFs wt (*Fig. 5.2D and E*). This difference was abolished upon treatment with forskolin and IBMX since both wt and PDE2A-/- MEFs showed similar, increased levels of Mitofilin phosphorylation. Lastly, I also observed a positive effect of PDE2A inhibition on Mitofilin phosphorylation status in SH-SY5Y cells, a neuroblastoma cell line and therefore a more relevant cell model for neurodegenerative diseases (*Fig. 5.2F and G*). Taken together, the above data support a role of PDE2A on PKA-mediated phosphorylation of Mitofilin.

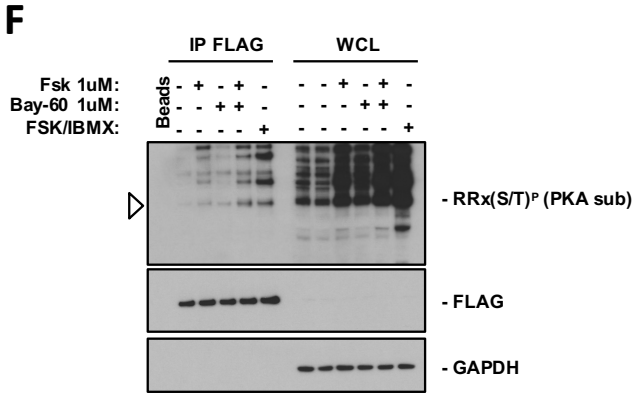

A
IP FLAG
WCL
Fsk 1uM:
Bay-60 1uM:
H89:
FSK/IBMX:
Beads
- RRx(S/T)P (PKA sub)
- RRx(S/T)P (PKA sub) (medium exposure)
- RRx(S/T)P (PKA sub) (more exposed)
- FLAG
- GAPDH


B
Phosphorylated Mitofilin (Fold change)
DMSO
BAY
H89


C
Phosphorylated Mitofilin (Fold change)
Fsk
Fsk+BAY
F/I


D
IP FLAG
WCL
WT
PDE2-/-
Fsk/IBMX:
Beads
- RRx(S/T)P (PKA sub)
- FLAG
- GAPDH


E
n.s.
Phosphorylated Mitofilin (Fold change)
WT basal
WT FI
KO basal
KO FI


F
IP FLAG
WCL
Fsk 1uM:
Bay-60 1uM:
FSK/IBMX:
Beads
- RRx(S/T)P (PKA sub)
- FLAG
- GAPDH

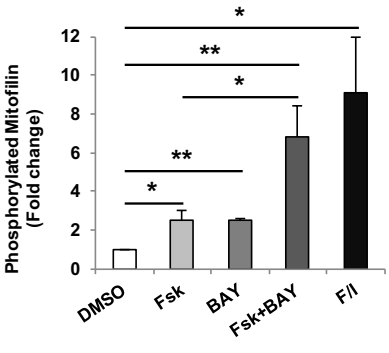

G
Phosphorylated Mitofilin (Fold change)
DMSO
Fsk
BAY
Fsk+BAY
F/I

Figure 5.2 | **PDE2A inhibition and knockout affect the phosphorylation status of Mitofilin.**
(A) Phosphorylation status of Mitofilin in HEK293T cells overexpressing Mitofilin-FLAG and treated with cAMP-generating agonists for 2 h. A phospho-(Ser/Thr) PKA substrate antibody was used both on whole cell lysate (WCL) and after pulling-down Mitofilin-FLAG (IP).
(B) The amount of phosphorylated Mitofilin was normalized to the amount of precipitated Mitofilin and shown as the fold change relative to levels in DMSO-treated cells. n=4.
(C) The amount of phosphorylated Mitofilin was normalized to the amount of precipitated Mitofilin and shown as the fold change relative to levels in Fsk-treated cells. n=4.
(D) Phosphorylation status of Mitofilin in wt or PDE2A$^{-/-}$ MEF cells overexpressing Mitofilin-FLAG and treated or not with Fsk/IBMX for 2 h. A phospho-(Ser/Thr) PKA substrate antibody was used both on whole cell lysate (WCL) and after pulling-down Mitofilin-FLAG (IP).
(E) The amount of phosphorylated Mitofilin was normalized to the amount of precipitated Mitofilin and shown as the fold change relative to levels in wt FI-treated cells. n=5.
(F) Phosphorylation status of Mitofilin in ShSy5y cells overexpressing Mitofilin-FLAG and treated with cAMP-generating agonists for 2 h. A phospho-(Ser/Thr) PKA substrate antibody was used both on whole cell lysate (WCL) and after pulling-down Mitofilin-FLAG (IP).
(G) The amount of phosphorylated Mitofilin was normalized to the amount of precipitated Mitofilin and shown as the fold change relative to levels in DMSO-treated cells. n=3.
All data represent mean±s.e.m. One-way ANOVA and Tukey's multiple comparison tests were performed. *P<0.05; **P<0.01; ***P<0.005; ns=not significant.

It has been reported that retinoic acid (RA), which induces differentiation of SH-SY5Y cells to dopaminergic neuron-like cells (Cuende et al., 2008; Lopes et al., 2010), promotes PKA-mediated phosphorylation of Mitofilin (Akabane et al., 2016). I not only confirmed these results but also observed that combination of BAY-60 with RA increases the level of Mitofilin phosphorylation compared to treatment with RA alone (*Fig. 5.3A and B*). Since RA promotes Mitofilin phosphorylation and induces differentiation, I hypothesized that BAY-60 could also induce the same effect. I therefore analyzed SH-SY5Y proliferation and their differentiation into neuron-like cells by performing live cell imaging over more than 9 days. As shown in Figure 5.3C, RA treatment reduces cell proliferation while combination with BAY-60 partially, but significantly, restored cell proliferation, although no observable difference was found regarding cell differentiation (*data not shown*). Assuming differentiation is somehow linked to Mitofilin phosphorylation, BAY-60 seems to affect other pathways that are involved in proliferation. There are other possible interpretations of these data as we do not know what is the link between RA and its effect on Mitofilin phosphorylation and differentiation.

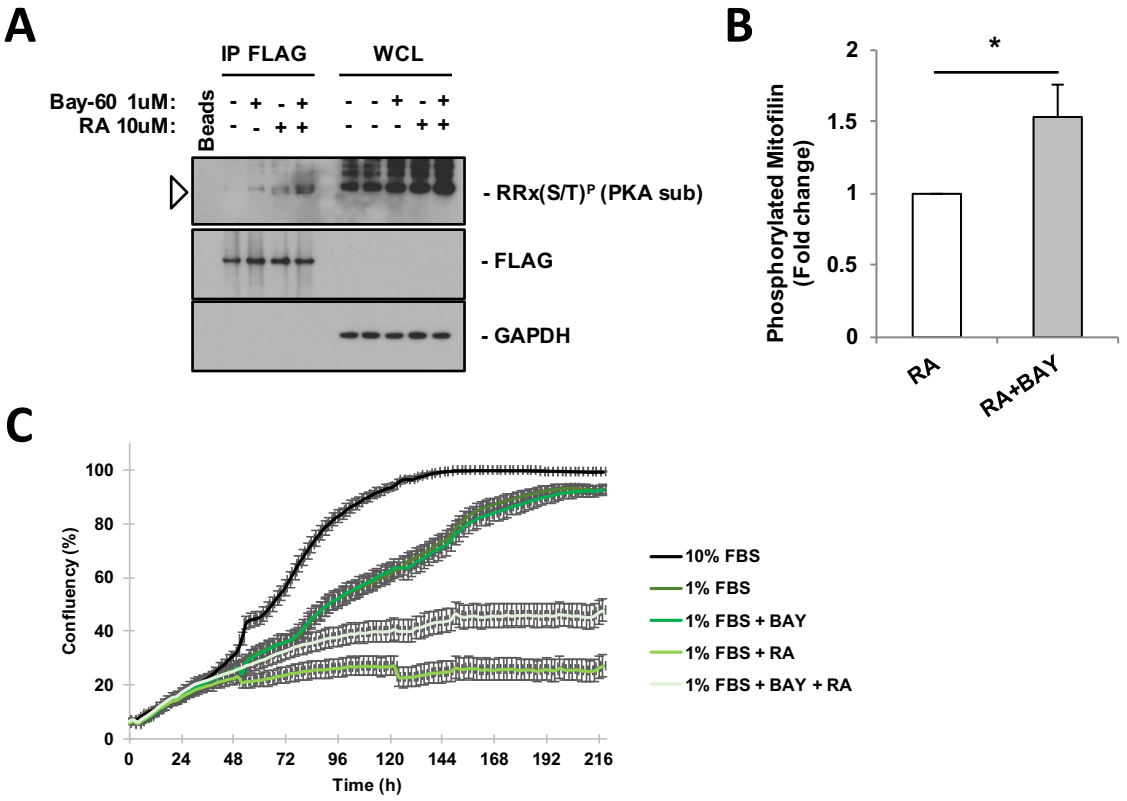


Figure 5.3 | **PDE2A inhibition induces Mitofilin phosphorylation in combination with Retinoic Acid.**
(A) Phosphorylation status of Mitofilin in ShSy5y cells overexpressing Mitofilin-FLAG and treated with either BAY-60 or Retinoic Acid (RA) for 24 h. A phospho-(Ser/Thr) PKA substrate antibody was used both on whole cell lysate (WCL) and after pulling-down Mitofilin-FLAG (IP).
(B) The amount of phosphorylated Mitofilin was normalized to the amount of precipitated Mitofilin and shown as the fold change relative to levels in RA-treated cells. Data represent mean±s.e.m. n=5. *P<0.05 (t-test).
(C) Cell proliferation shown as confluency (%) of SH-SY5Y cells in culture medium with 10 % or 1 % FBS, combined with 1 μM BAY-60 or 10 μM RA. Media was replaced at 0 h, 48 h and 120 h. Data represent mean±s.e.m. n=4, each n corresponds to an average of 9 image acquisitions over time.

Since MINOS-deficient cells show disrupted cristae structures (Darshi et al., 2011), I tested whether PDE2A$^{-/-}$ MEFs would have a similar phenotype. As assessed by transmission electron microscopy (TEM), mitochondrial cristae morphology does not seem to be affected by PDE2A knockout (*Fig. 5.4A*). This is in agreement with the data reported by Akabane et al. where increased phosphorylation of Mitofilin does not affect cristae morphology (Akabane et al., 2016). Next, I compared the levels of expression of Mitofilin, Parkin and PINK1 in MEFs wt and

PDE2A$^{-/-}$ and I observed no differences due to PDE2A ablation (*Fig. 5.4B*). These results confirmed that PDE2A deletion only affects Mitofilin phosphorylation status rather than total protein levels.

Overall, these findings indicate that PDE2A regulates PKA-mediated phosphorylation of Mitofilin without impacting mitochondrial cristae organization.

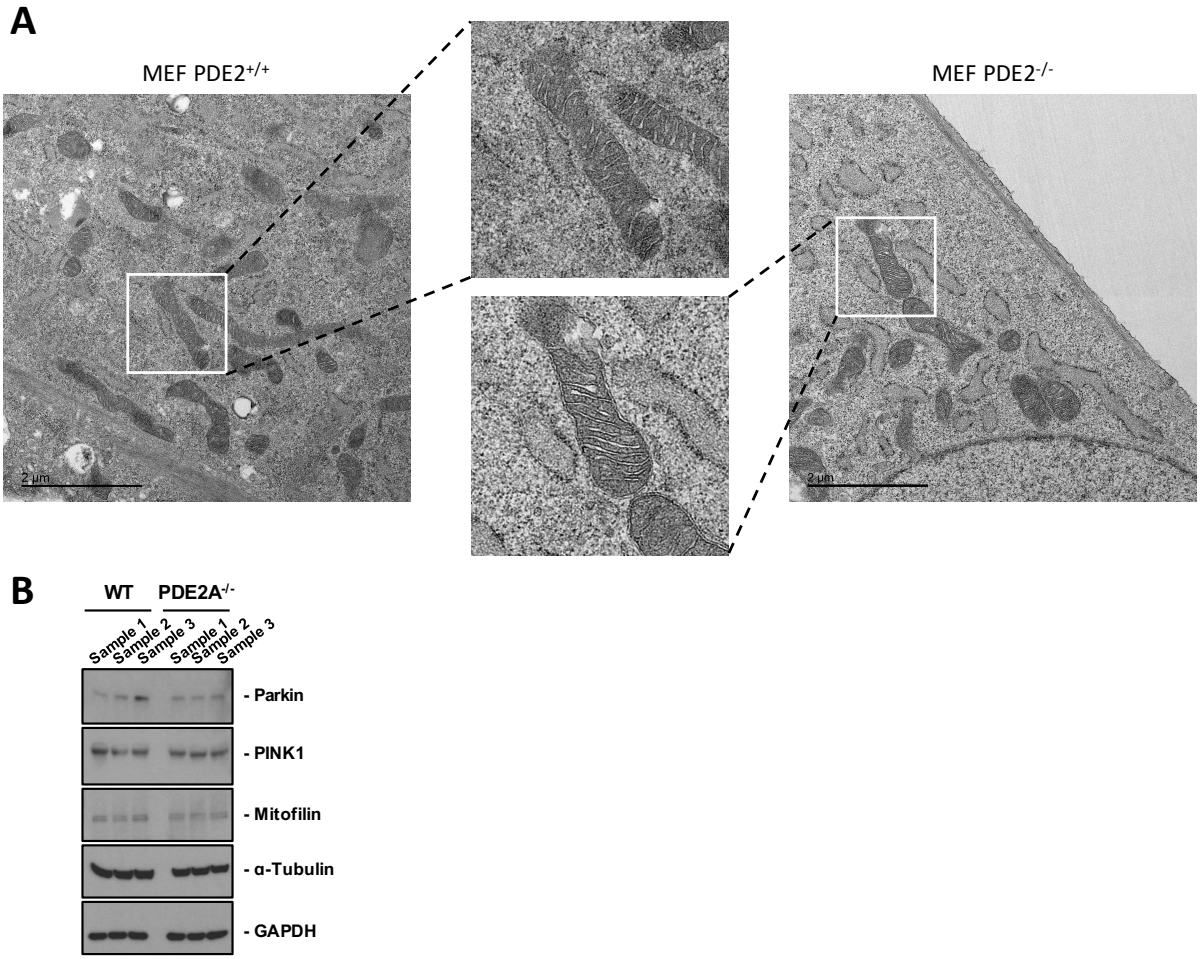


Figure 5.4 | **PDE2A2 knock-out does not alter cristae morphology.**
(A) Transmission electron microscopy of mitochondria in control MEF wt (PDE2$^{+/+}$) and PDE2A-knockout (PDE2$^{-/-}$) cells. Images are representative of two independent experiments. Scale bar: 2 µm.
(B) Protein levels of Parkin, PINK1 and Mitofilin in wt and PDE2A$^{-/-}$ MEF cells.

5.3 PDE2A2 interacts with Mitofilin through GAF-B domain

To characterize the interaction between Mitofilin and PDE2A2, I first assessed which PDE2A2 domain binds to Mitofilin. Co-immunoprecipitation experiments were performed in HEK293T cells overexpressing each PDE2A2-RFP fragment generated previously (*Fig. 3.3A*) and Mitofilin-FLAG. As shown in Figure 5.5A, only fragments that contain GAF-B domain bind to Mitofilin. Thus, I propose that GAF-B domain constitute the binding site for Mitofilin, although the N-terminus is still required to target GAF-B domain to the mitochondria (*Fig. 5.5B*).

Another important question is whether Mitofilin is an exclusive interactor of PDE2A2 isoform. To address this question, I performed co-immunoprecipitation experiments in HEK293T cell overexpressing each PDE2A-GFP isoform and Mitofilin-FLAG (*Fig. 5.5C*). Results show that Mitofilin binds specifically to PDE2A2. This was expected since PDE2A2 is the only PDE2A isoform that localizes to the mitochondria. Since all isoforms have the GAF-B domain, this result confirms that only GAF-B domain that is targeted to the mitochondria (via PDE2A2) is able to interact with Mitofilin.

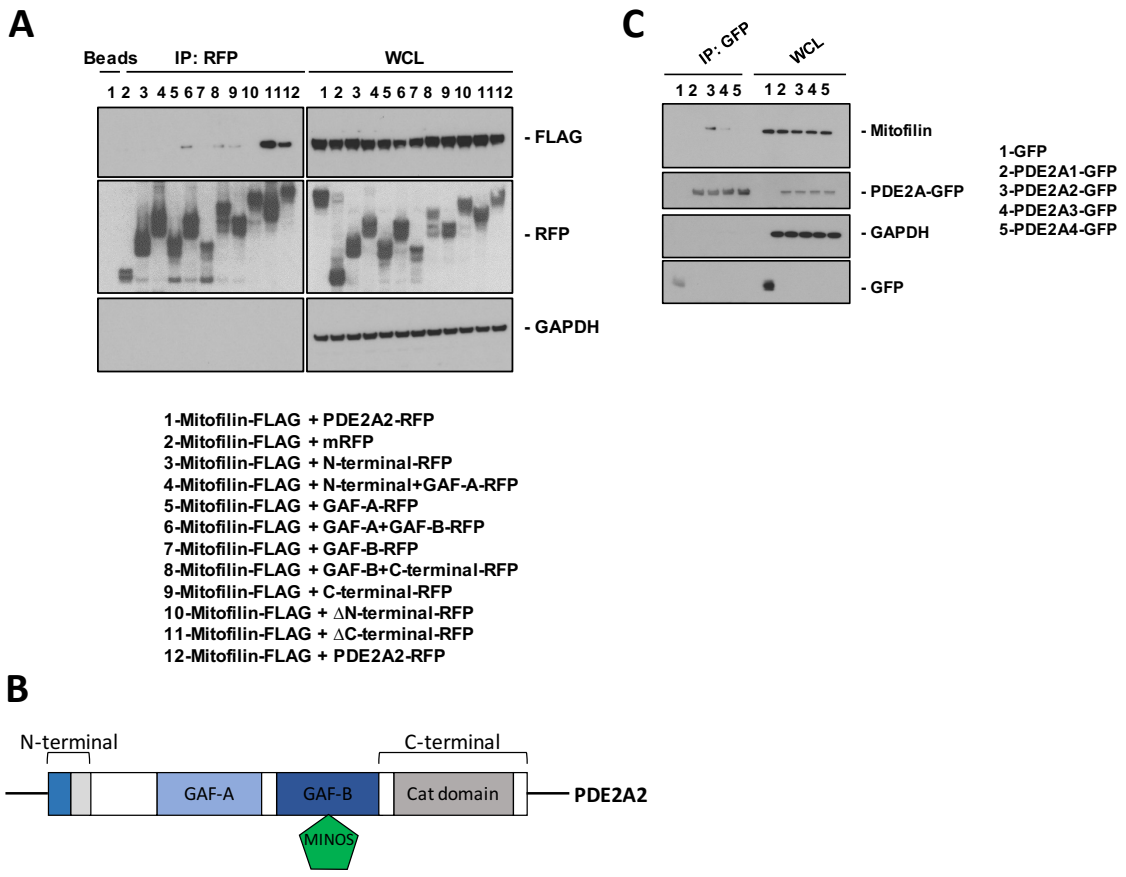


Figure 5.5 | **The GAF-B region of PDE2A2 is necessary to bind to Mitofilin.**
(A) Detection of Mitofilin-FLAG after PDE2A2-RFP fragments immunoprecipitation in HEK293T cells transiently transfected with PDE2A2-RFP constructs and Mitofilin-FLAG. Pull-down of mRFP was used as a negative control. Blot is representative of three independent experiments.
(B) Summary of PDE2A2 domains involved in the interaction with Mitofilin.
(C) Detection of endogenous Mitofilin after immunoprecipitation of each PDE2A isoform in HEK293T cells transiently transfected with PDE2A isoforms. Blot is representative of three independent experiments.

I have shown that PDE2A2 binds to Mitofilin through its GAF-B domain. However, the full N-terminal region of PDE2A2 is sufficient to target the enzyme to the mitochondria while other domains, including GAF-B, are not required for PDE2A2 targeting. Thus, a plausible hypothesis is that binding of PDE2A2 to Mitofilin is not involved in retaining the enzyme to this organelle. I wondered what keeps PDE2A2 in the mitochondria and I hypothesized that PDE2A2 is able to stay in the mitochondria due to lipid interaction. To test this hypothesis, I enriched for each PDE2A-FLAG isoform by overexpressing each isoform in HEK293T cells followed by immunoprecipitation and elution from the beads by using FLAG peptide. Each eluate was probed for FLAG to confirm the presence of each PDE2A isoform (*Fig. 5.6A*). Then, I performed a protein:lipid dot-blot by overlaying nitrocellulose membranes spotted with different lipids with PDE2A-FLAG isoforms (*Fig. 5.6B*). As observed, all PDE2A isoforms strongly bind directly to Cardiolipin. One possible interpretation of these results is that in cells PDE2A2 is the only isoform that interacts with Cardiolipin due to its mitochondrial localization. Cardiolipin is almost exclusively present in the IMM (Claypool and Koehler, 2012). Additionally, it has been reported that Cardiolipin externalization to the OMM acts as an elimination signal for mitophagy in neuronal cells (Chu et al., 2013). Given the clear interaction of the mitochondrial PDE2A2 with Cardiolipin and the role of PDE2A2 in the regulation of mitophagy (see below), the functional role of PDE2A-Cardiolipin interaction warrants further investigations.

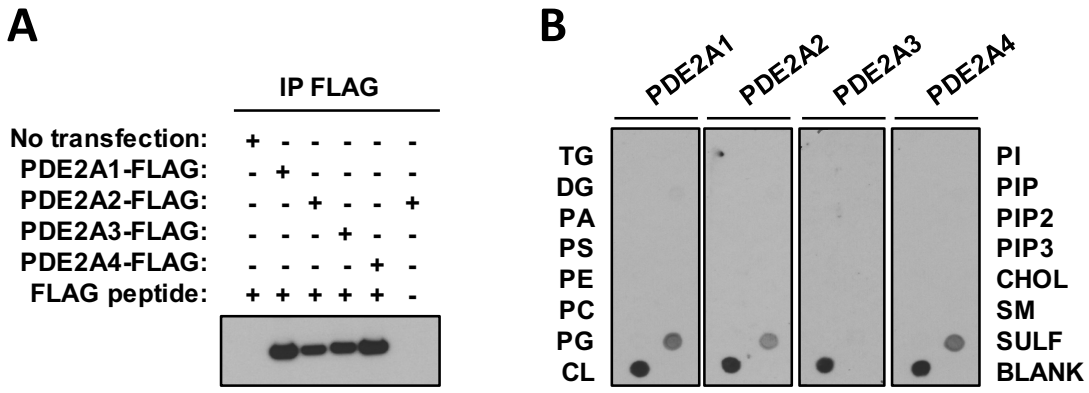


Figure 5.6 | **PDE2A binds directly to Cardiolipin.**
(A) Efficiency of PDE2A-FLAG pull-down followed by protein elution through the addition of FLAG peptide. HEK293T cells were transfected with each of the PDE2A-FLAG isoforms.
(B) PDE2A isoforms immunoreactivity is shown on a protein:lipid dot-blot experiment in which each PDE2A-FLAG isoform was overlaid onto nitrocellulose membranes spotted with some of the most common glycerolipids and sphingolipids present in mammalian cells. TG, triacylglycerol; DG, diacylglycerol; PA, phosphatidic acid; PS, phosphatidylserine; PE, phosphatidylethanolamine; PC, phosphatidylcholine; PG, phosphatidylglycerol; CL, cardiolipin; PI, phosphatidylinositol; PIP, phosphatidylinositol phosphate; PIP2, phosphatidylinositol biphosphate; PIP3, PIP2, phosphatidylinositol triphosphate; CHOL, cholesterol, SM, sphingomyelin; SULF, 3-sulfogalactosylceramide (sulfatide); BLANK, no lipid.

5.4 PDE2A2 regulates Parkin-dependent Mitophagy

To assess the involvement of PDE2A in the selective clearance of damaged mitochondria, I examined the effect of PDE2A ablation and inhibition on the mitochondrial recruitment of Parkin in MEF cells expressing mCherry-Parkin. MEFs PDE2A$^{-/-}$ show significantly less Parkin recruitment to the mitochondria under basal conditions compared to MEFs wt (*Fig. 5.7A*). PDE2A inhibition by BAY-60 in MEFs wt also significantly decreased Parkin recruitment to the mitochondria compared to MEFs wt. However, treatment with cilostamide, a selective PDE3 inhibitor which leads to an overall increase in cytosolic cAMP as PDE2A inhibition with BAY-60 (Monterisi et al., 2017), had no significant effect on Parkin recruitment (*Fig. 5.7A*). Next, to confirm the involvement of PDE2A2 in Parkin recruitment, I transiently co-transfected MEFs PDE2A$^{-/-}$ with either PDE2A1 or PDE2A2-GFP and mCherry-Parkin (*Fig. 5.7B*). In agreement with the previous results, PDE2A2 overexpression, but not PDE2A1, induced a two-fold increase in Parkin recruitment to the mitochondria compared to untreated cells, suggesting that with higher PDE2A2 activity one can promote Parkin recruitment.

Incubation with the protonophore carbonyl cyanide m-chlorophenylhydrazone (CCCP), which induces mitochondria depolarization, it is a very well established protocol in the field used to substantially promote Parkin translocation to the mitochondria, as previously reported (Narendra et al., 2008). This CCCP-induced accumulation of Parkin on mitochondria is independent of the ATP consumption by mitochondrial uncouplers since incubation with ATP synthase inhibitor oligomycin did not affect CCCP-induced Parkin recruitment to the mitochondria (Narendra et al., 2008). In contrast, Parkin recruitment to the mitochondria is severely inhibited by pretreatment with forskolin (Akabane et al., 2016). I observed that MEFs PDE2A$^{-/-}$ show significantly reduced mitochondrial recruitment of mCherry-Parkin compared with MEFs wt upon CCCP treatment for 3h (*Fig. 5.7C*), which is consistent with the role of

PDE2A in regulating local PKA-dependent phosphorylation of Mitofilin. Treatment with forskolin increases intracellular cAMP levels, reducing the differences between MEF wt and PDE2A$^{-/-}$ cells (*Fig. 5.7C*).

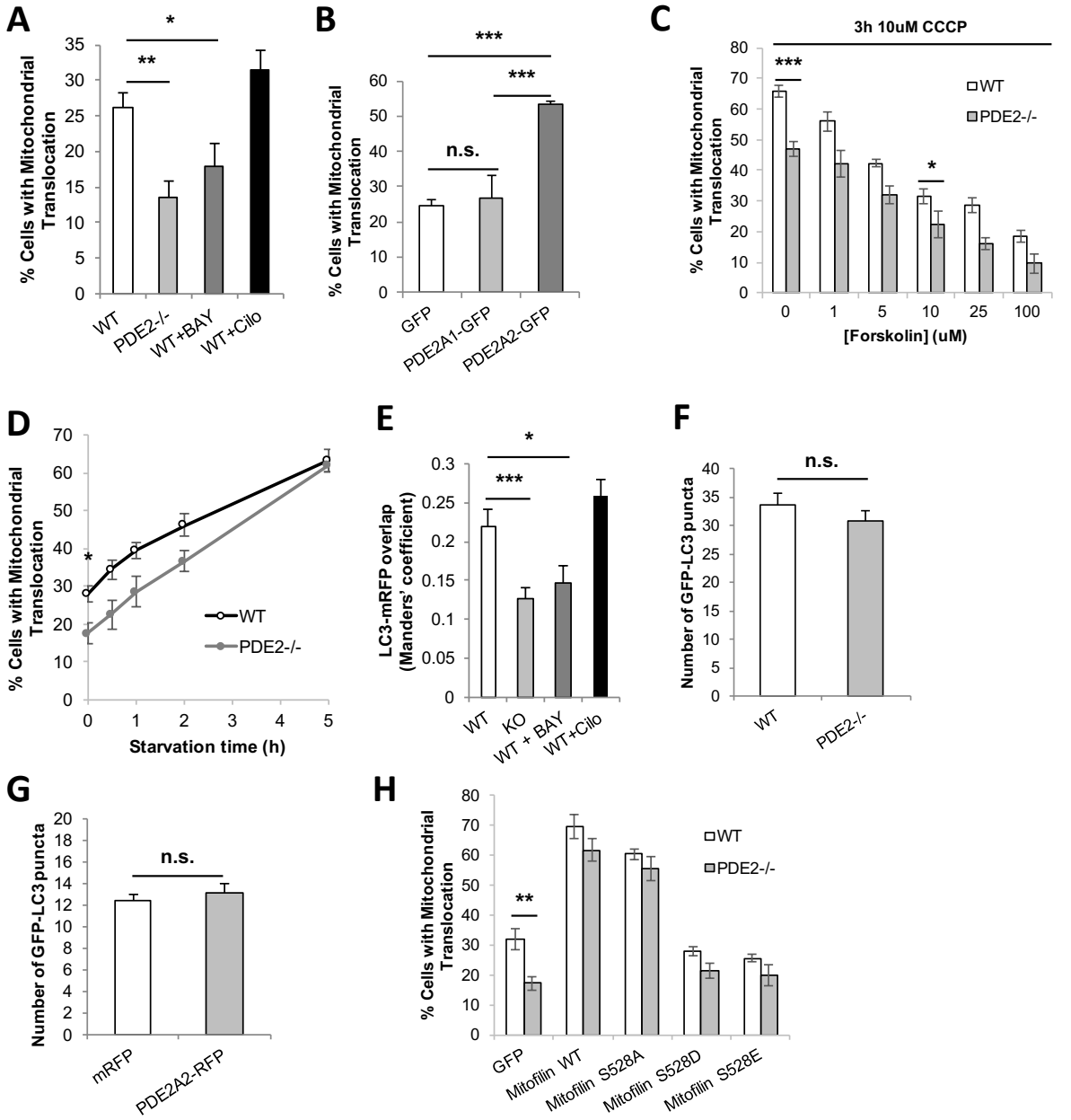


Figure 5.7 | **Effect of PDE2A on autophagy and Parkin-mediated mitophagy.**
(A) % wt or PDE2A$^{-/-}$ MEF cells with mitochondrial Parkin, after transfection with mCherry-Parkin, under basal conditions, 1 μM BAY-60 (BAY) or 10 μM Cilostamide (Cilo) treatment for 2 h. n=33-171 cells (3-10 independent experiments).
(B) % wt MEF cells with mitochondrial Parkin, after co-transfection with mCherry-Parkin and either GFP, PDE2A1-GFP or PDE2A2-GFP. n=48-115 cells (5 independent experiments).
(C) % wt or PDE2A$^{-/-}$ MEF cells with mitochondrial Parkin, after transfection with mCherry-Parkin, upon forskolin treatment for 1 h followed by 10 μM CCCP treatment for 3 h. n=46-142 cells (4-10 independent experiments).
(D) % wt or PDE2A$^{-/-}$ MEF cells with mitochondrial Parkin, after transfection with mCherry-Parkin, under different starvation periods. n=49-114 cells (4-7 independent experiments).
(E) % of GFP-LC3 puncta that overlaps with mitochondria in wt or PDE2A$^{-/-}$ MEF cells transfected with GFP-LC3 and mRFP under basal conditions, 1 μM BAY-60 (BAY) or 10 μM Cilostamide (Cilo) treatment for 2 h. n=15-19 cells.
(F) Number of GFP-LC3 puncta (marker of autophagy) in wt and PDE2A$^{-/-}$ MEF cells transfected with GFP-LC3 under basal conditions. n=71-74 wt/PDE2A$^{-/-}$ cells (5 independent experiments).
(G) Number of GFP-LC3 puncta in HeLa cells co-transfected with GFP-LC3 and either mRFP or PDE2A2-RFP under basal conditions. n=100-123 cells (4 independent experiments).
(H) % wt or PDE2A$^{-/-}$ MEF cells with mitochondrial Parkin, after co-transfection with mCherry-Parkin and either GFP, Mitofilin wt, S528A, S528D or S528E. n=50-64 cells (4 independent experiments).
All data represent mean±s.e.m. One-way ANOVA and Tukey's multiple comparison tests were performed for A, B and E. t-test statistical analysis was performed for F and G. Two-way ANOVA and Sidak's multiple comparison tests were performed for C and H. *P<0.05; **P<0.01; ***P<0.005; ns=not significant.

Another way of inducing autophagy is starvation (Gomes et al., 2011) which can be achieved by incubating cells in media without nutrients. Parkin translocation to the mitochondria can be observed as soon as 1h after nutrient deprivation (*Fig. 5.7D*). In agreement with the previous results, cells with PDE2A ablation showed less Parkin recruitment compared with MEFs wt, for up to 2h of starvation (*Fig. 5.7D*). No difference was observed for 5h of starvation – this could suggest that 5h of nutrient deprivation is too severe for cells and therefore PDE2A ablation does not induce a protective effect.

LC3 (Microtubule-associated proteins 1A/1B light chain 3B) is a protein involved in autophagy and commonly used as a marker of autophagosomes. To specifically assess mitochondrial autophagy, co-localization of mitochondria and LC3 is a widely used method to measure mitophagy (Narendra et al., 2008). To test whether PDE2A may regulate this process, I used MEF cells expressing LC3-GFP and mRFP (RFP targeted to the mitochondria). MEFs wt

showed higher degree of co-localization between mitochondria and autophagosomes compared to MEFs PDE2A$^{-/-}$ under basal conditions (*Fig. 5.7E*). MEFs wt treated with BAY-60 showed similar co-localization as MEFs PDE2A$^{-/-}$ while incubation with cilostamide had no significant effect on LC3-mRFP co-localization (*Fig. 5.7E*). In terms of absolute values, although the LC3-mRFP overlap, according to Mander's coefficient, was relatively low regardless of which condition was being applied, I could still observe a ~2-fold difference between wt and PDE2A KO cells. This is similar to what others have observed under different treatments (Khalil et al., 2015). It is worth to point out that a value of 0.25 in wt MEFs means that 25% of the LC3 punctae co-localize with mitochondria. In other words, 25% of the autophagosomes are involved in mitophagy. In PDE2A KO MEFs this value drops to 12%. For a process that is highly regulated and involves movement and changes in the dynamics of organelles, a decrease from ~25% to ~12% can be considered biologically relevant. Interestingly, PDE2A knockout (*Fig. 5.7F*) or overexpression (*Fig. 5.7G*) did not affect the total number of LC3 puncta, which are a measure of global autophagy (Klionsky et al., 2016). In conclusion, I propose that PDE2A2 specifically regulates mitochondrial autophagy – mitophagy.

To confirm the involvement of Mitofilin phosphorylation in Parkin recruitment, I used phosphorylation-deficient (S528A) and phosphorylation-mimetic (S528D and S528E) Mitofilin mutants (Akabane et al., 2016). Expression of wt and S528A mutant significantly increased the mitochondrial recruitment of mCherry-Parkin in both MEFs wt and PDE2A$^{-/-}$ (*Fig. 5.7H*). In contrast, Mitofilin mutants S528D and S528E had no effect on the intracellular localization of mCherry-Parkin, confirming that unphosphorylated, but not phosphorylated, form of Mitofilin is responsible for Parkin recruitment to mitochondria. These results confirm that PDE2A2 regulates Parkin recruitment to the mitochondria through PKA-mediated phosphorylation of Mitofilin. Additionally, I observed that Isoproterenol treatment prevents Parkin translocation to

the mitochondria upon CCCP treatment, confirming that β-adrenergic stimulation regulates this mechanism (*Fig. 5.8A and B*).

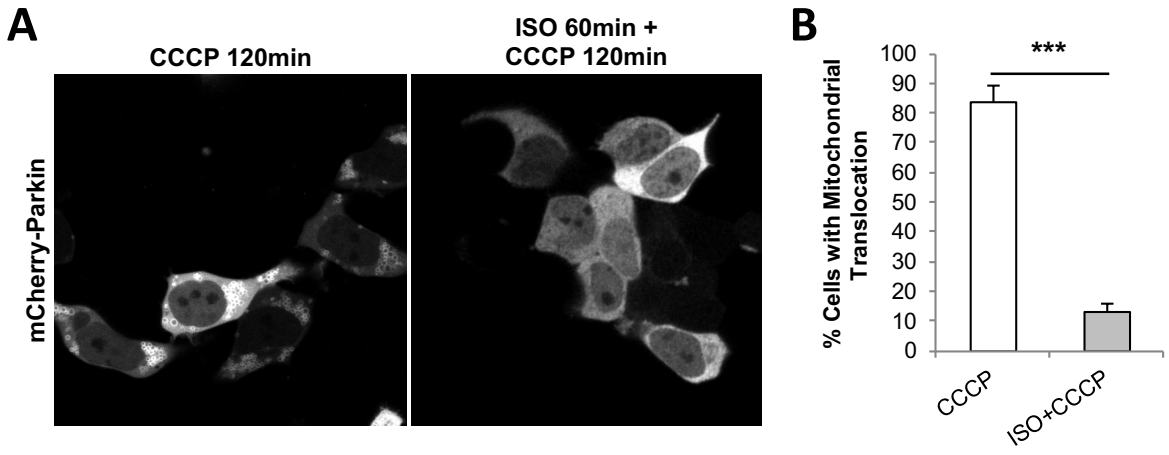


Figure 5.8 | **Effect of Isoproterenol on Parkin translocation to the mitochondria.**
(A) Live cell imaging of HEK293T cells transfected with mCherry-Parkin upon 120 min incubation with 10 μM CCCP or 60 min with 10 nM Isoproterenol (ISO) followed 120 min incubation with 10 μM CCCP. (B) % HEK293T cells with mitochondrial Parkin. Data represents mean+s.e.m. n=62-161 cells (3 independent experiments). ***P<0.005 (t-test).

5.5 Activation of PKG promotes Parkin recruitment to damaged mitochondria independently of PDE2A

My findings suggest the novel and exciting possibility that modulation of PDE2A activity may provide a new avenue to control Parkin-dependent mitophagy. I have already shown that PDE2A inhibition reduces Parkin-dependent mitophagy (Fig. 5.7A) and that increased activity of PDE2A2 by overexpression of the enzyme promotes Parkin-dependent mitophagy (Fig. 5.7B). Since PDE2A2 cAMP-hydrolytic activity can be increased upon allosteric binding of cGMP to the GAFB domain, I proposed that PDE2A activation by cGMP may also promote Parkin recruitment to the mitochondria. Indeed, MEFs wt treated with increasing concentrations of cGMP showed higher percentage of cells with mitochondrial Parkin (Fig. 5.9A). To confirm that this effect is mediated by PDE2A, I repeated the same experiments in MEFs PDE2A$^{-/-}$. Surprisingly, as shown in Figure 5.9A, the effect of cGMP on Parkin mitochondrial translocation is independent of PDE2A. This suggests that cGMP may exert an effect that is independent of PDE2A activation and that is opposite of the cAMP effect. To assess the involvement of the cGMP effector, Protein Kinase G (PKG), in the selective clearance of damaged mitochondria, MEFs wt were either transfected with wt or catalytically dead mutant PKG (*Fig. 5.9B*). Results show that active PKG induces mitochondrial localization of Parkin while mutant PKG had no effect compared to MEFs wt. Thus, I conclude that cyclic nucleotides can either promote or inhibit Parkin recruitment to the mitochondria through PKG or PKA, respectively.

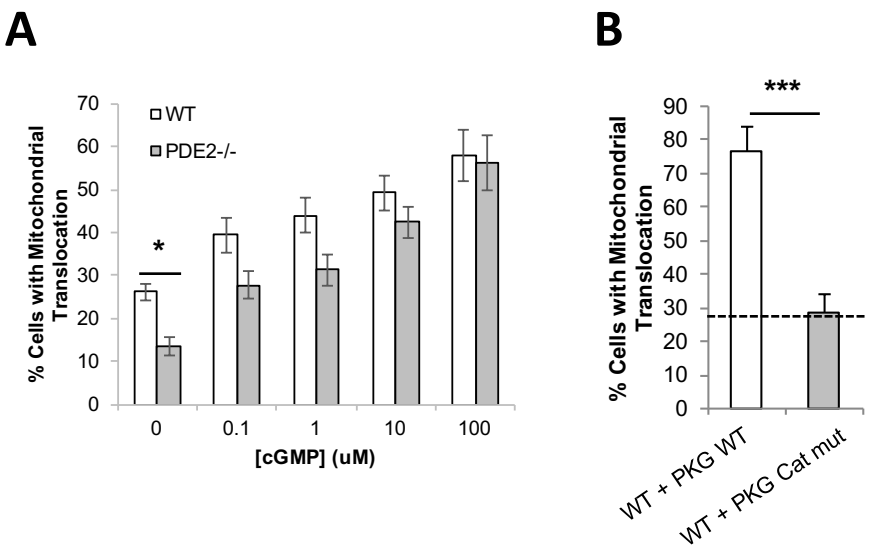


Figure 5.9 | **cGMP promotes Parkin-mediated mitophagy through PKG and independently of PDE2A.**
(A) % wt or PDE2A$^{-/-}$ MEF cells with mitochondrial Parkin, after transfection with mCherry-Parkin, upon cGMP treatment for 2 h. n=48-171 cells (4-10 independent experiments).
(B) % wt MEF cells with mitochondrial Parkin, after co-transfection with mCherry-Parkin and either PKG wt or PKG Catalytic Mutant. Dashed line represents MEFs wt under basal conditions. n=33-40 cells (3 independent experiments).
All data represent mean±s.e.m. t-test statistical analysis was performed for B. Two-way ANOVA and Sidak's multiple comparison tests were performed for A. *P<0.05; ***P<0.005.

5.6 CCCP promotes transient Mitofilin phosphorylation

I have shown that CCCP treatment promotes Parkin recruitment to mitochondria (*Fig. 5.7C*) and that Mitofilin is phosphorylated even under basal conditions (*Fig. 5.2D*). Since phosphorylation of Mitofilin inhibits Parkin recruitment to the mitochondria, I hypothesized that CCCP treatment could affect and/or reduce basal Mitofilin phosphorylation status. In other words, I evaluated the effect of CCCP on Mitofilin phosphorylation. Unexpectedly, CCCP treatment stimulated a transient phosphorylation of Mitofilin between 5 and 15 minutes after treatment (*Fig. 5.10A and B*). This effect was abolished by combining PKA inhibitor H89 with CCCP. After 30 min of incubation with CCCP, no significant difference was found compared with untreated cells. However, 30 min with CCCP did not induce Parkin translocation to the mitochondria (*Fig. 5.10C*). To observe Parkin recruitment to the mitochondria, 2 h treatment with CCCP was necessary, although at this point in time no effect of CCCP on Mitofilin's phosphorylation was visible any longer. This suggests that Mitofilin phosphorylation may act as an initial trigger to promote CCCP-induced Parkin recruitment. Interestingly, incubation with CCCP induces PDE2A2-Mitofilin interaction, although total Mitofilin protein levels decreased upon treatment (*Fig. 5.10D-F*), which could be a consequence of increased damaged mitochondria upon CCCP.

Taken together, these results suggest that interaction of PDE2A2 with the MINOS complex inhibits PKA-mediated phosphorylation of Mitofilin.

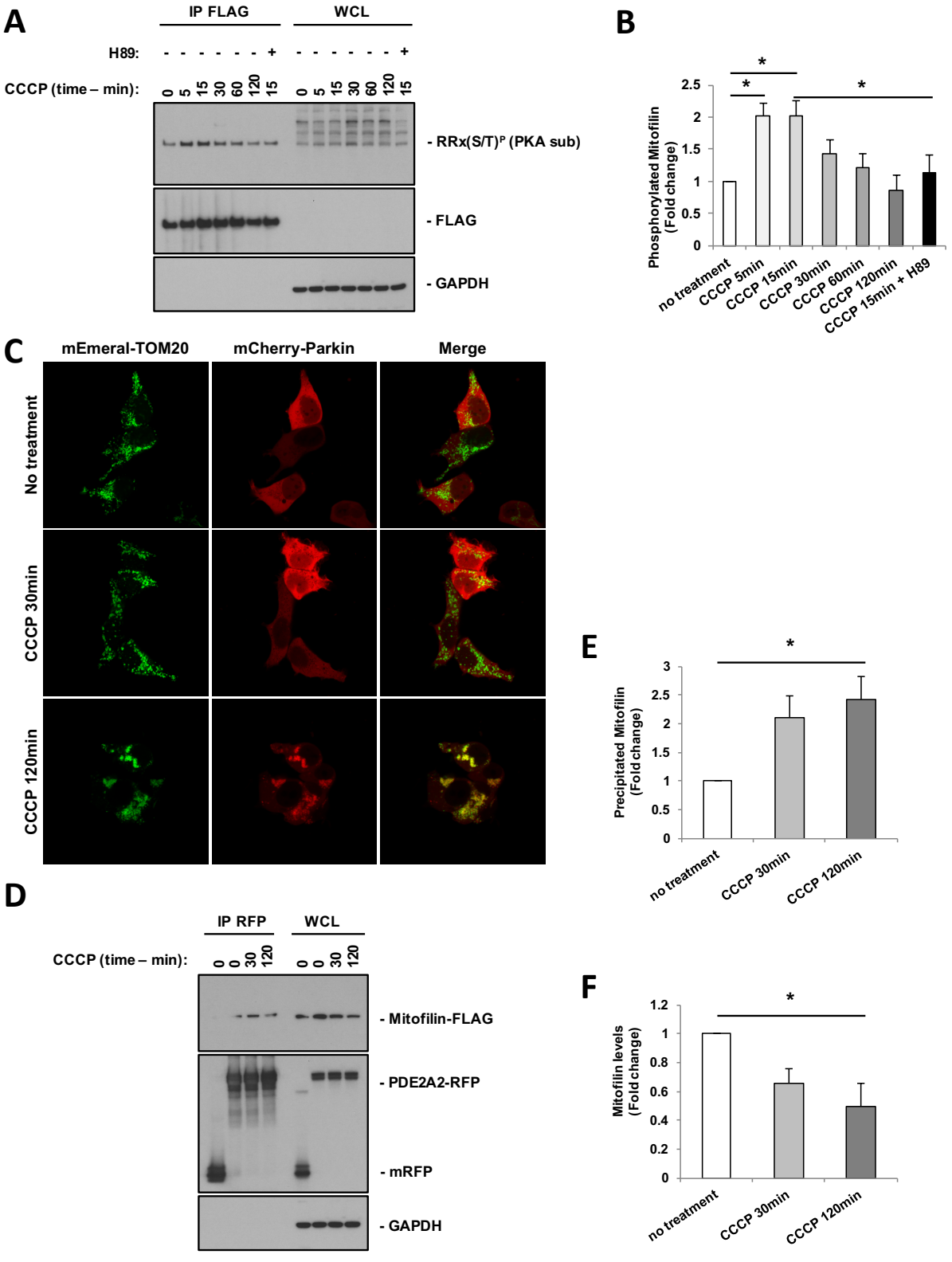

A
IP FLAG
WCL
H89:
CCCP (time – min):
- RRx(S/T)P (PKA sub)
- FLAG
- GAPDH
B
Phosphorylated Mitofilin (Fold change)
no treatment
CCCP 5min
CCCP 15min
CCCP 30min
CCCP 60min
CCCP 120min
CCCP 15min + H89
C
mEmeral-TOM20
mCherry-Parkin
Merge
No treatment
CCCP 30min
CCCP 120min
D
IP RFP
WCL
CCCP (time – min):
- Mitofilin-FLAG
- PDE2A2-RFP
- mRFP
- GAPDH
E
Precipitated Mitofilin (Fold change)
no treatment
CCCP 30min
CCCP 120min
F
Mitofilin levels (Fold change)
no treatment
CCCP 30min
CCCP 120min

Figure 5.10 | **Effect of CCCP on Mitofilin phosphorylation.**
(A) Phosphorylation status of Mitofilin in HEK293T cells overexpressing Mitofilin-FLAG and treated with 10 µM CCCP for different incubation times. A phospho-(Ser/Thr) PKA substrate antibody was used both on whole cell lysate (WCL) and after pulling-down Mitofilin-FLAG (IP).
(B) The amount of phosphorylated Mitofilin was normalized to the amount of precipitated Mitofilin and shown as the fold change relative to levels in non-treated cells. n=3.
(C) Live cell imaging of HEK293T cells transfected with mCherry-Parkin and mEmerald-TOM20 (marker for mitochondria) under basal conditions, 30 min or 120 min incubation with 10 µM CCCP.
(D) Detection of Mitofilin-FLAG after PDE2A2-RFP immunoprecipitation in HEK293T cells transiently transfected with Mitofilin-FLAG and either mRFP or PDE2A2-RFP after treatment with 10 µM CCCP.
(E) The amount of precipitated Mitofilin was normalized to the amount of total Mitofilin and shown as the fold change relative to levels in non-treated cells. n=4.
(F) The amount of total Mitofilin was normalized to the amount of total GAPDH and shown as the fold change relative to levels in non-treated cells. n=4.
All data represent mean±s.e.m. One-way ANOVA and Tukey's multiple comparison tests were performed. *P<0.05.

5.7 Conclusion

The cAMP/PKA signaling pathway is involved in a wide variety of subcellular processes, including PINK1 protein levels at the OMM and consequently regulation of Parkin translocation to depolarized mitochondria (Akabane et al., 2016). Here, I demonstrated that PDE2A2 regulates PKA-mediated phosphorylation of Mitofilin and Parkin-dependent mitophagy (*Fig. 5.11*). PDE2A2 interacts with components of the MINOS complex, such as Mitofilin and ChChD3, and PDE2A inhibition promotes Mitofilin PKA-mediated phosphorylation. I also showed that PDE2A ablation does not affect mitochondria cristae morphology and total protein levels of Parkin, PINK1 or Mitofilin, suggesting selective effect on Mitofilin phosphorylation status that does not interfere with role of the MINOS complex on cristae organization. Moreover, PDE2A inhibition results in reduced recruitment of Parkin to the mitochondria and reduced mitophagy. Conversely, PDE2A2 overexpression promotes Parkin translocation to damaged mitochondria and enhances mitophagy. PDE2A2 is a potentially 'druggable' enzyme and, unlike the highly promiscuous PKA, it specifically localizes to the mitochondria where it interacts with the MINOS complex to regulate a local pool of cAMP (Monterisi et al., 2017). Additionally, mitochondrial recruitment of Parkin was stimulated by both cGMP treatment and PKG overexpression. This suggests that both cyclic nucleotides regulate Parkin recruitment to the mitochondria although in opposite ways. One hypothesis is that PKG can phosphorylate Mitofilin at a site distinct from the PKA phosphorylation site and promote Parkin recruitment. Alternatively, PKG activation triggers another pathway that induces mitochondria damage, activating Parkin/PINK1-dependent clearance via an alternative mechanism that does not involve Mitofilin. A dual-controlled mechanism involving cAMP and cGMP would allow a fine tuning of Parkin recruitment to the mitochondria.

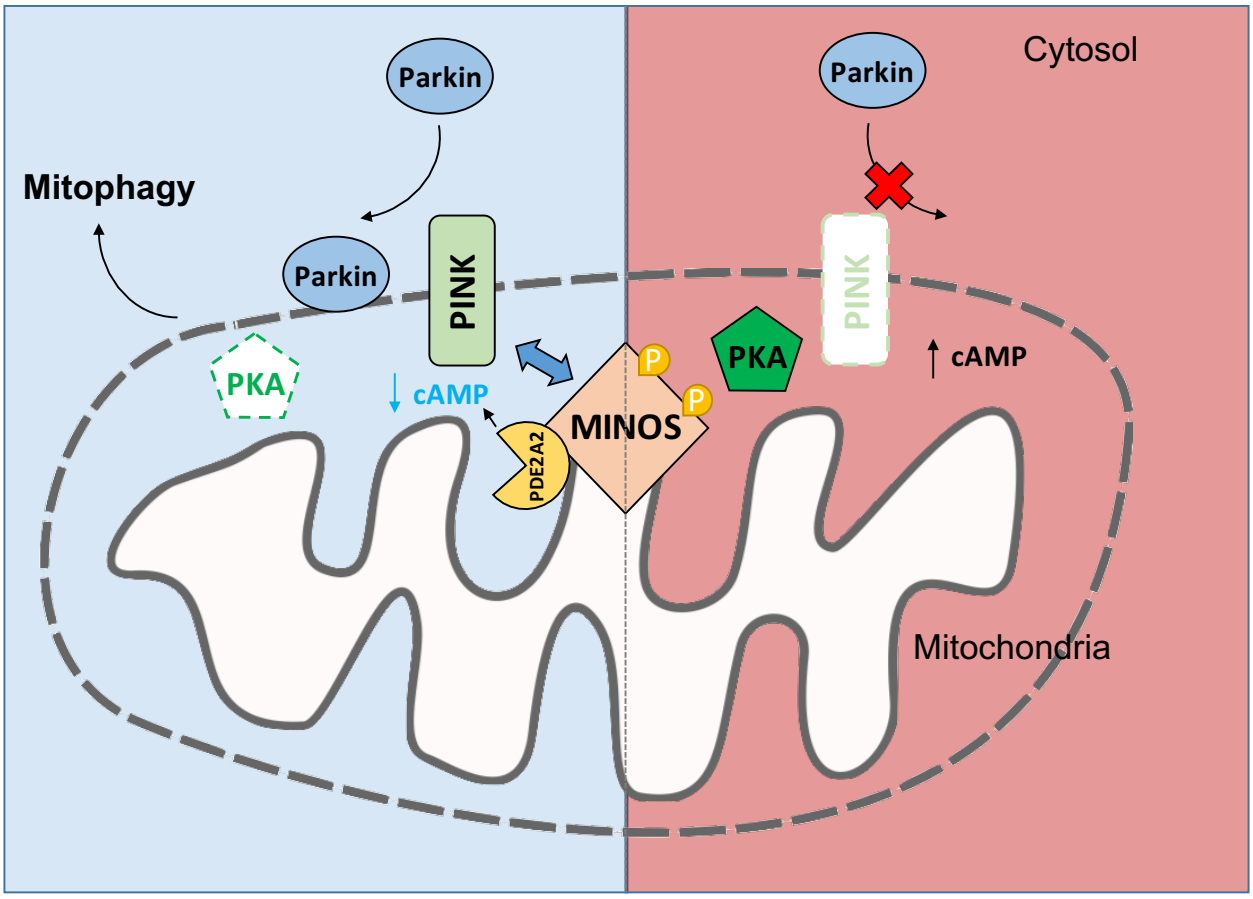


Figure 5.11 | **Model for role of PDE2A2/cAMP/PKA axis on Parkin dependent mitophagy.** PDE2A2 interacts with the MINOS complex, regulating a local pool of cAMP and, subsequently, PKA-dependent phosphorylation of Mitofilin and Parkin recruitment to damaged mitochondria.

Disrupted mitochondrial quality control is a hallmark of Parkinson's disease (PD). Activation of Parkin and its translocation to damaged mitochondria promotes mitophagy and maintenance of mitochondrial homeostasis. Thus, augmenting mitophagy by activating the PINK1/Parkin pathway is an attractive target for therapeutic intervention (Mukherjee et al., 2015). PD affects 1-2 % of the population and is the second most common neurodegenerative disease. Clinically, it is characterized by rigidity, bradykinesia, resting tremor and postural instability, that stem from the progressive loss of dopaminergic neurons (Mukherjee et al., 2015). There is no cure, and the best treatment options only provide symptomatic relief with no abatement or reversal

of disease progression. Although a large majority of diagnosed PD cases are idiopathic, autosomal dominant and recessive familial forms have been identified and represent 5-10 % of PD cases. Understanding how monogenic forms of PD lead to cell dysfunction and neuron death may identify causes of parkinsonism and new avenues for treatment (Pickrell and Youle, 2015). Increasing evidence suggests that compromised mitochondrial function is a key factor in PD. In stress conditions mitochondria can be damaged and this can trigger apoptosis. Through mitophagy, a highly specialized quality control process that removes dysfunctional or superfluous mitochondria through the autophagic pathway, the cell protects itself from the damage of disordered mitochondrial metabolism and apoptosis induction. Further supporting the model that mitochondrial quality control is the essential function of PINK1 and Parkin contributing to the prevention of parkinsonism, disease-associated mutations in both PINK1 and Parkin prevent PINK1-mediated recruitment of Parkin to mitochondria and have been associated with autosomal recessive PD. Thus, augmenting mitophagy by activation of the PINK1/Parkin pathway has been proposed to be an attractive strategy for treatment of PD (Pickrell and Youle, 2015). My findings suggest the novel and exciting possibility that modulation of PDE2A activity may provide a new avenue to control Parkin-dependent mitophagy in the context of PD.

Chapter 6 - PDE2A localizes to mitochondria-associated membranes (MAM) and regulates IP3-dependent Ca^{2+} release

6.1 Background

I have shown in Chapter 4 that PDE2A2 interacts with Caveolins, which are generally considered to be localized at the PM and ER (Han et al., 2016). The localization of PDE2A at the PM has been hypothesized on the basis of experimental evidence linking PDE2A effects with NO signaling and the localization of endothelial nitric oxide synthase (eNOS) at the PM (Mongillo et al., 2006). However, as seen in Figure 4.4E and F, none of the Caveolin isoforms seems to co-localize with PDE2A2 at the PM, both in HeLa cells and NRVM, respectively.

Recently, it has been reported that Caveolin 1 is an integral component of mitochondrial associated membranes (MAMs), a specialized subdomain of the ER that makes contact with the OMM and acts as an intracellular signaling hub (Sala-Vila et al., 2016). The formation of these membrane contact sites is important not only for Ca^{2+} homeostasis but also for lipid metabolism (de Brito and Scorrano, 2010). Since it has been reported that Caveolins may localize at the MAM and they can be involved in regulation of lipid transfer and Ca^{2+} signaling (Sala-Vila et al., 2016; Sundivakkam et al., 2009), I hypothesized that PDE2A, via its interaction with Caveolins, could localize to the MAM and be involved in the regulation of these processes.

6.2 PDE2A2 interacts with Caveolins through its N-terminus

To investigate the functional role of the interaction between PDE2A2 and Caveolins 1 and 2, I aimed at developing a strategy to disrupt this interaction. To this end, I first assessed which PDE2A2 domain binds to endogenous Caveolins by using PDE2A2 fragments generated previously (*Fig. 3.3A*). Co-immunoprecipitation experiments were performed in HEK293T cells overexpressing each PDE2A2-RFP fragment. As shown in Figure 6.1A, only fragments that contain N-terminal domain bind to Caveolin 1 and 2. Next, I used shorter fragments of the PDE2A2 N-terminal (characterized in *Fig. 3.4*) and showed that amino acid residues 1-41 are required for isoform 2 of PDE2A to form a complex with Caveolin 1 in cells (*Fig. 6.1B and C*). Additionally, I investigated which Caveolin 1 domain binds to PDE2A2. The domains considered are shown in Fig 6.1D. Co-immunoprecipitation experiments were done in HEK293T cells overexpressing each Caveolin 1-GFP fragment and PDE2A2-RFP (*Fig. 6.1E*). I observed that both the Signature domain and the Scaffolding domain are required for interaction with PDE2A2 since only fragments with these domains were able to interact with PDE2A2. The Scaffolding domain has been shown to interact with a broad range of signal transducing molecules, including tyrosine kinase receptors, eNOS and heterodimeric G proteins, while the Signature domain is the only region shared by all Caveolin isoforms (Machleidt et al., 2000). Since PDE2A2 binds to the Signature domain, I hypothesized that this enzyme also binds to Caveolin 3, since I had already shown the interaction with Caveolin 1 and 2. As observed in *Fig. 6.2A*, overexpressed PDE2A2 also binds to overexpressed Caveolin 3, indicating that all Caveolins bind to PDE2A2.

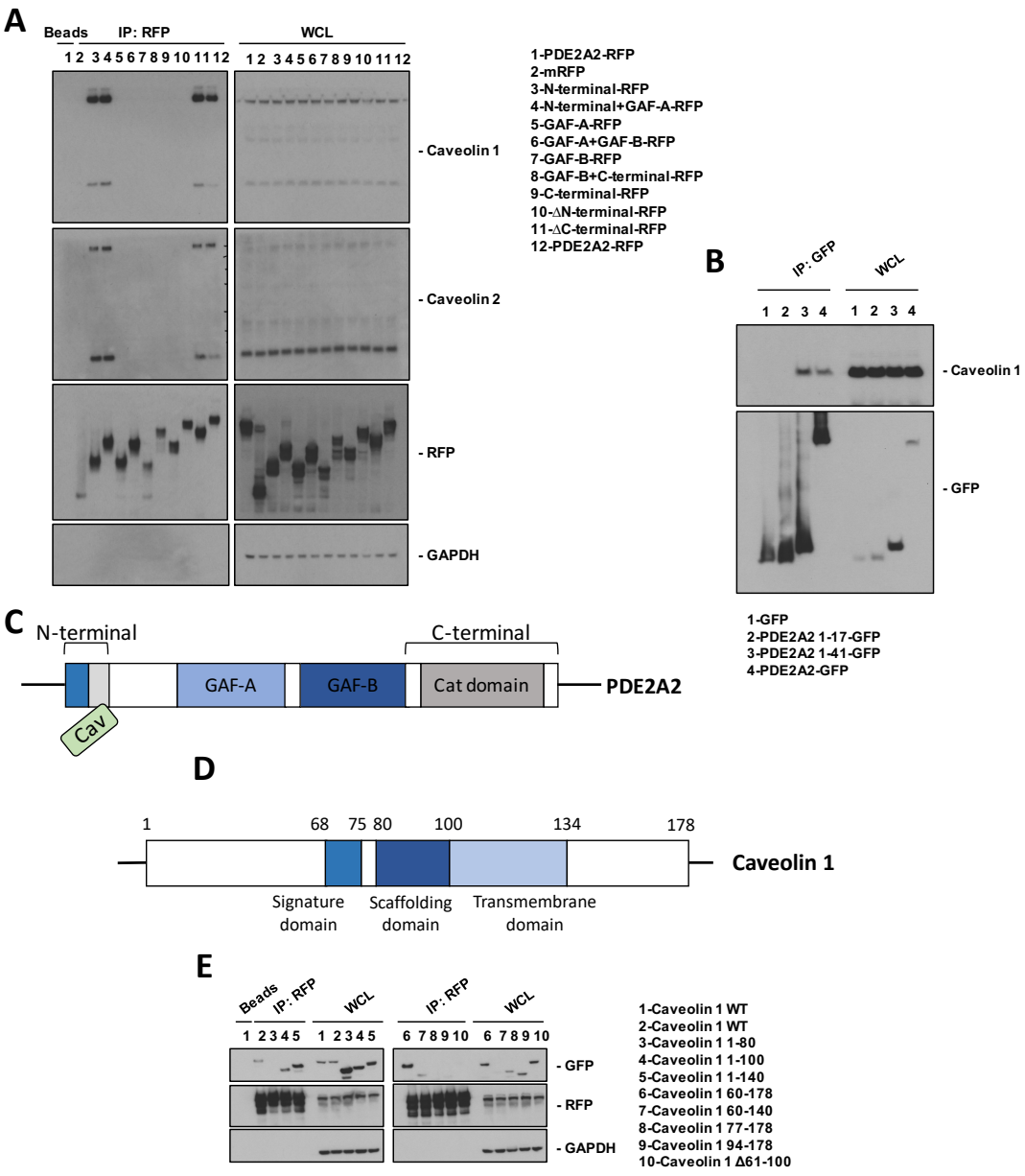


Figure 6.1 | **Interaction between N-terminal of PDE2A2 and Caveolins' signature and scaffolding domains.**
(A) Detection of endogenous Caveolin 1 and Caveolin 2 after PDE2A2-RFP fragments immunoprecipitation in HEK293T cells transiently transfected with PDE2A2-RFP constructs. Pull-down of mRFP was used as a negative control. Blot is representative of three independent experiments.
(B) Detection of endogenous Caveolin 1 after immunoprecipitation of PDE2A2 fragments in HEK293T cells transiently transfected with PDE2A2 constructs. Blot is representative of two independent experiments.
(C) Summary of PDE2A2 domains involved in the interaction with Caveolin.
(D) Schematic of Caveolin 1 domains.
(E) Detection of Caveolin 1 fragments (GFP tagged) after PDE2A2-RFP immunoprecipitation in HEK293T cells transiently transfected with Caveolin 1 fragments and PDE2A2-RFP. Blot is representative of three independent experiments.

Another important question is whether Caveolin is an exclusive interactor of the PDE2A2 isoform. To address this question, I performed co-immunoprecipitation experiments in HEK293T cell overexpressing each PDE2A isoform (*Fig. 6.2B*). Results show that Caveolins only bind to PDE2A2 and not other isoforms. This was unexpected since PDE2A3 localizes to the PM and contains the predicted binding site for Caveolin. Selective interaction of Caveolins with the mitochondrially-targeted PDE2A2 and lack of interaction with the membrane-targeted PDE2A3 further strengthened the hypothesis that only PDE2A that is targeted to the mitochondria is able to interact with Caveolin.

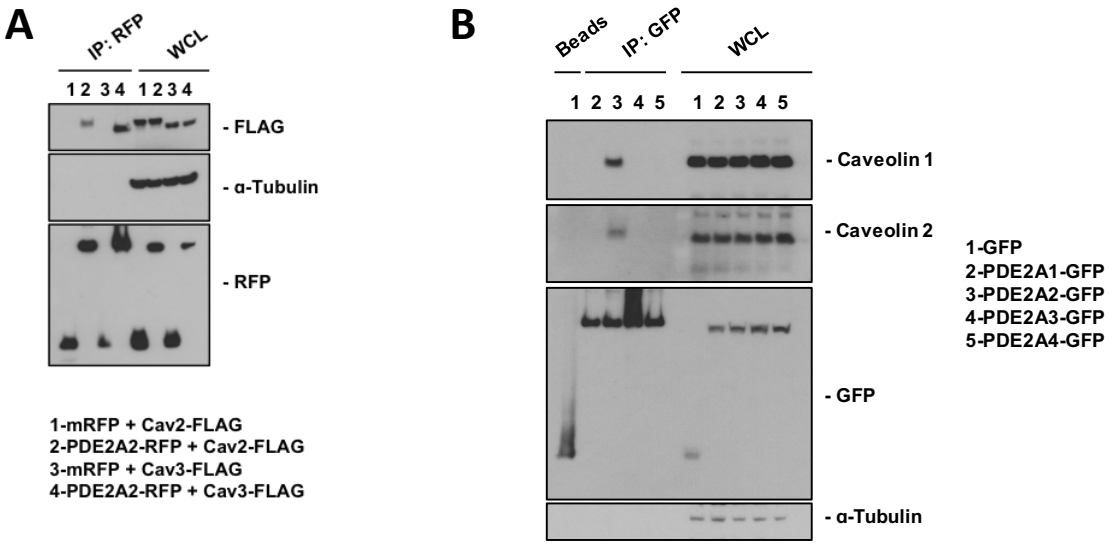


Figure 6.2 | **All Caveolins interact with PDE2A2.**
(A) Detection of Caveolin 2-FLAG or Caveolin 3-FLAG after PDE2A2-RFP immunoprecipitation in HEK293T cells transiently transfected with Caveolin-FLAG constructs and PDE2A2-RFP. Blot is representative of two independent experiments.
(B) Detection of endogenous Caveolin 1 and Caveolin 2 after immunoprecipitation of each PDE2A isoform in HEK293T cells transiently transfected with PDE2A isoforms. Blot is representative of two independent experiments.

As Caveolin and MINOS complex are known to localize to two distinct sites in the mitochondria and given the data showing interaction of PDE2A2 with both Caveolin and MINOS, the expectation would be that PDE2A2 forms independent mitochondrial complexes with these two proteins. To confirm this, co-immunoprecipitation experiments were performed in HEK293T cells where either Mitofilin or Caveolin 1 were pulled-down (*Fig. 6.3A and B, respectively*). The results show that the MINOS complex and Caveolins belong to two different protein complexes. This was expected since the MINOS complex localizes to the IMM while Caveolins were identified at the interface between OMM and ER.

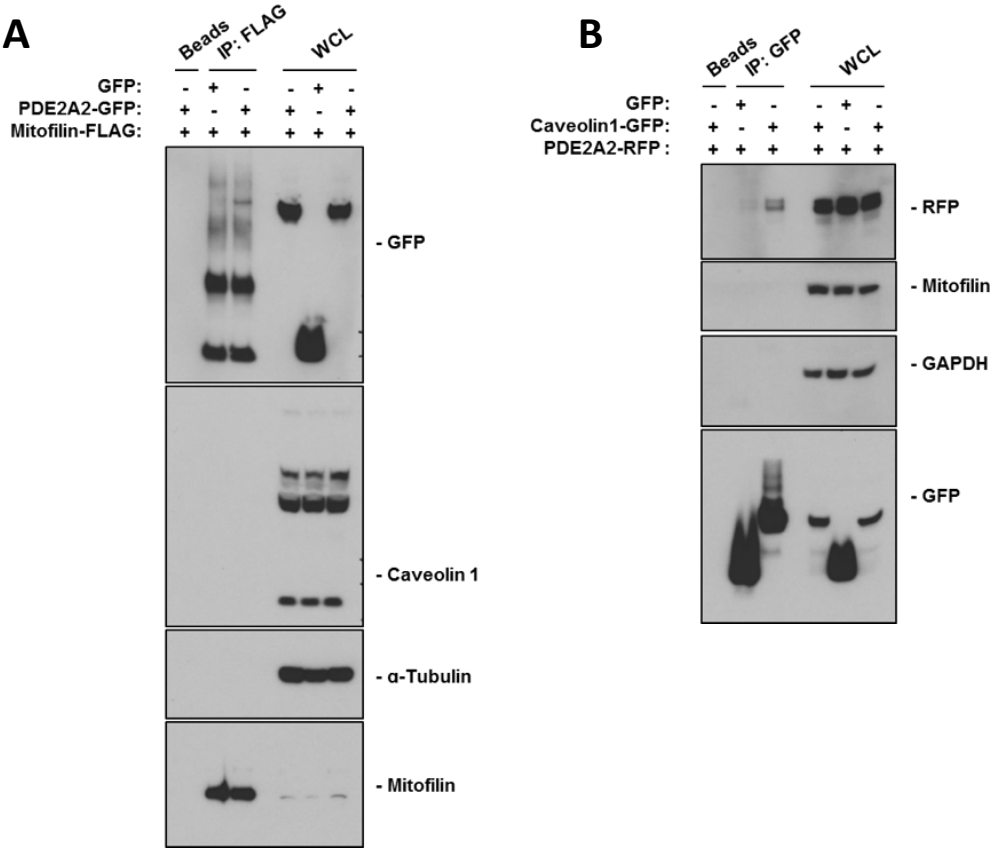


Figure 6.3 | **PDE2A2 interaction with Caveolins and Mitofilin occurs at two distinct protein complexes.**
(A) Detection of PDE2A2-GFP and endogenous Caveolin 1 after Mitofilin-FLAG immunoprecipitation in HEK293T cells transiently transfected with PDE2A2-GFP and Mitofilin-FLAG constructs. Blot is representative of two independent experiments.
(B) Detection of PDE2A2-RFP and endogenous Mitofilin after Caveolin 1-GFP immunoprecipitation in HEK293T cells transiently transfected with PDE2A2-RFP and Caveolin 1-GFP constructs. Blot is representative of two independent experiments.

6.3 PDE2A2 interacts with Caveolin 1 at the MAM

To test the hypothesis that PDE2A2 interacts with Caveolin 1 at the MAM, I first performed protein fractionation of HEK293T and HeLa cells to obtain purified MAM fractions, as previously described (Wieckowski et al., 2009). I first assessed the purity of the subcellular fractions by western blot analysis (*Fig. 6.4A*). In agreement with published data (Sala-Vila et al., 2016; Wieckowski et al., 2009), MAMs were highly enriched in acyl-CoA synthetase long chain 4 (FACL4), a well-established MAM marker, as well as Caveolins. ER-resident proteins, such as IP3R, Calnexin and Calreticulin were mostly present in the ER fraction. MAM-containing fractions displayed trace amounts of mitochondrial proteins such as TOM20 (OMM) and cytochrome C (IMS and cytosol), although mitochondrial inner membrane proteins such as TIM23 and Mitofilin were not detectable, supporting a high purity of the MAM membrane fractions. The cytosolic protein α-Tubulin was only detected in the cytosolic fraction. As shown in Fig 6.4A, overexpressed PDE2A2-GFP was also found to be enriched in MAMs, both in HEK293T and HeLa, as well as Caveolin 1.

Having previously shown that PDE2A2 binds to Caveolins, I proposed that this interaction takes place at the MAM. To assess this, I performed protein fractionation followed by co-immunoprecipitation of PDE2A2-GFP. As seen in Figure 6.4B, Caveolin 1 binds to PDE2A2 specifically in the MAM fraction. These results confirm that the interaction between PDE2A2 and Caveolin 1 occurs at the ER-mitochondria interface.

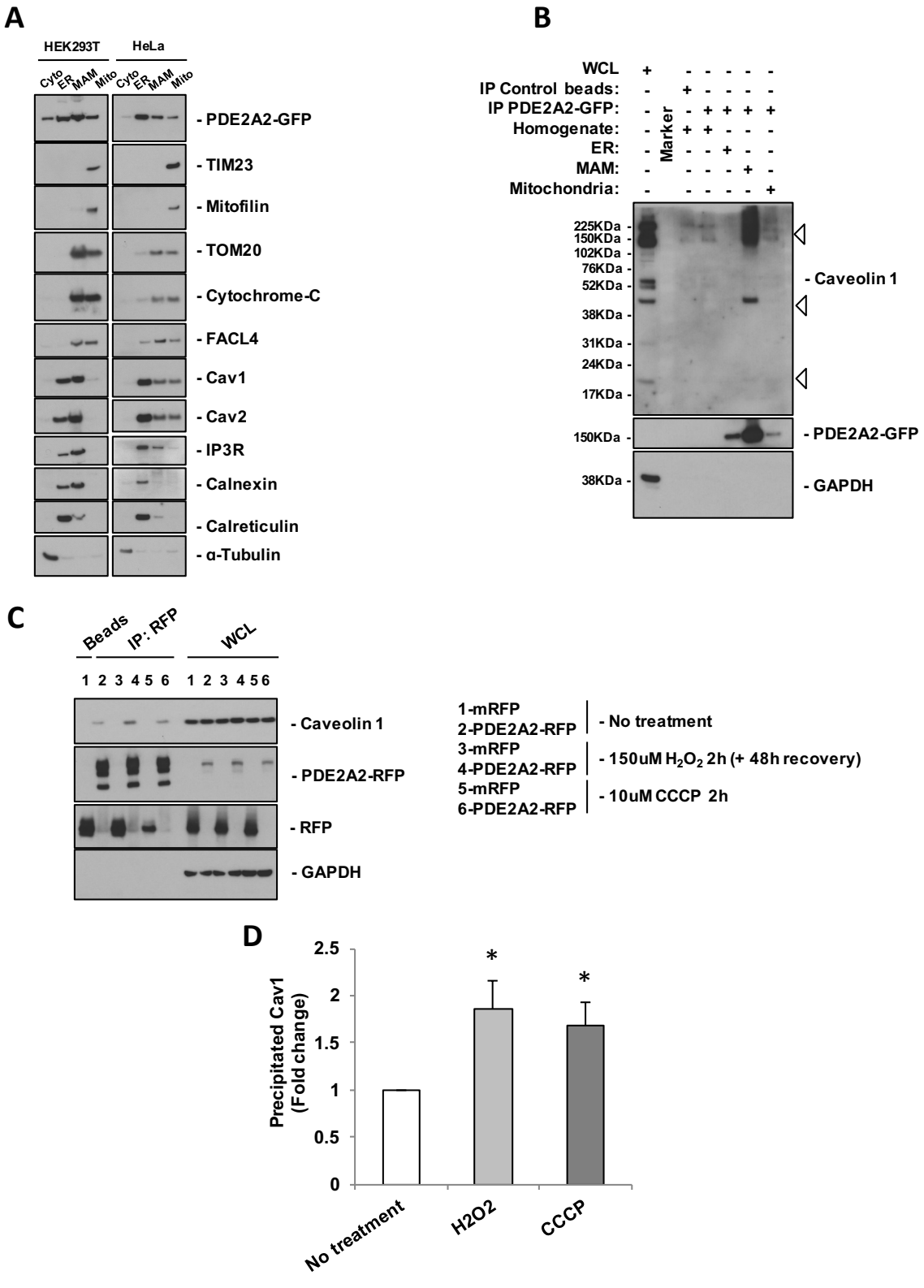

A
HEK293T
HeLa
Cyto
ER
MAM
Mito
- PDE2A2-GFP
- TIM23
- Mitofilin
- TOM20
- Cytochrome-C
- FACL4
- Cav1
- Cav2
- IP3R
- Calnexin
- Calreticulin
- α-Tubulin
B
WCL
IP Control beads:
IP PDE2A2-GFP:
Homogenate:
ER:
MAM:
Mitochondria:
Marker
225KDa
150KDa
102KDa
76KDa
52KDa
38KDa
31KDa
24KDa
17KDa
- Caveolin 1
150KDa
- PDE2A2-GFP
38KDa
- GAPDH
C
Beads
IP: RFP
WCL
1 2 3 4 5 6 1 2 3 4 5 6
- Caveolin 1
- PDE2A2-RFP
- RFP
- GAPDH
1-mRFP
2-PDE2A2-RFP
- No treatment
3-mRFP
4-PDE2A2-RFP
- 150uM H2O2 2h (+ 48h recovery)
5-mRFP
6-PDE2A2-RFP
- 10uM CCCP 2h
D
Precipitated Cav1
(Fold change)
2.5
2
1.5
1
0.5
0
*
*
No treatment
H2O2
CCCP

Figure 6.4 | **PDE2A2 localizes to the MAM and interacts with Caveolin 1 at this site.**
(A) Cytosolic, endoplasmic reticulum (ER), mitochondria-associated membranes (MAM) and mitochondria (Mito) fractions of HEK293T or HeLa cells transiently transfected with PDE2A2-GFP. Mitochondrial markers: TIM23, Mitofilin, TOM20 and Cytochrome-C; MAM markers: FACL4 and Caveolins; ER markers: IP3R, Calnexin and Calreticulin. Cytosol marker: α-Tubulin. Blot is representative of three independent experiments.
(B) Detection of endogenous Caveolin 1 after PDE2A2-GFP immunoprecipitation in HEK293T cells transiently transfected with PDE2A2-GFP after ER, MAM and mitochondria fractionation.
(C) Detection of endogenous Caveolin 1 after PDE2A2-RFP immunoprecipitation in HEK293T cells transiently transfected with PDE2A2-RFP after treatment with either H_2O_2 or CCCP.
(D) The amount of precipitated Caveolin 1 was normalized to the amount of total Caveolin 1 and shown as the fold change relative to levels in non-treated cells. Data represent mean±s.e.m. n=3. One-way ANOVA and Tukey's multiple comparison tests were performed. *P<0.05.

It has been previously shown that sub-cytotoxic levels of oxidants up-regulate Caveolin 1 protein expression (Dasari et al., 2006; Volonte et al., 2002), activate Caveolin 1-mediated signaling (Volonte et al., 2013, 2015) and promote its translocation to the mitochondria (Volonte et al., 2016). Since Caveolin 1-mediated signaling is activated under conditions of oxidative stress to maintain mitochondrial function, I asked whether sub-toxic levels of oxidants promote the interaction of Caveolin 1 with PDE2A2. Indeed, I found that the interaction between Caveolin 1 and PDE2A2 was enhanced by oxidative stress (*Fig. 6.4C and D)*. Interestingly, the same was observed when cells were treated with CCCP, a mitochondrial decoupling agent, suggesting that Caveolin 1-PDE2A2 interaction is promoted upon mitochondrial stress.

6.4 PDE2A regulates IP3-dependent Ca^{2+} release from ER

After characterizing the binding site between PDE2A2 and Caveolins, I attempted to gain some insight into the role of this interaction by disrupting it using fragments of PDE2A2 involved in the interaction with Caveolin as disrupting peptides. To assess whether this approach was viable, I overexpressed PDE2A2 N-terminus (fragments characterized in *Fig. 3.3 and 3.4*) to compete with full length PDE2A2-GFP for Caveolin binding site. The results showed that unfortunately this strategy would not work, as I could still detect full length Caveolin after pulling-down PDE2A2-GFP (*Fig. 6.5A and B*). Fragments and peptides corresponding to the Scaffolding and Signature domain of Caveolins were also used to disrupt PDE2A2-Caveolin interaction but again no disruption of the interaction was observed (*data not shown*).

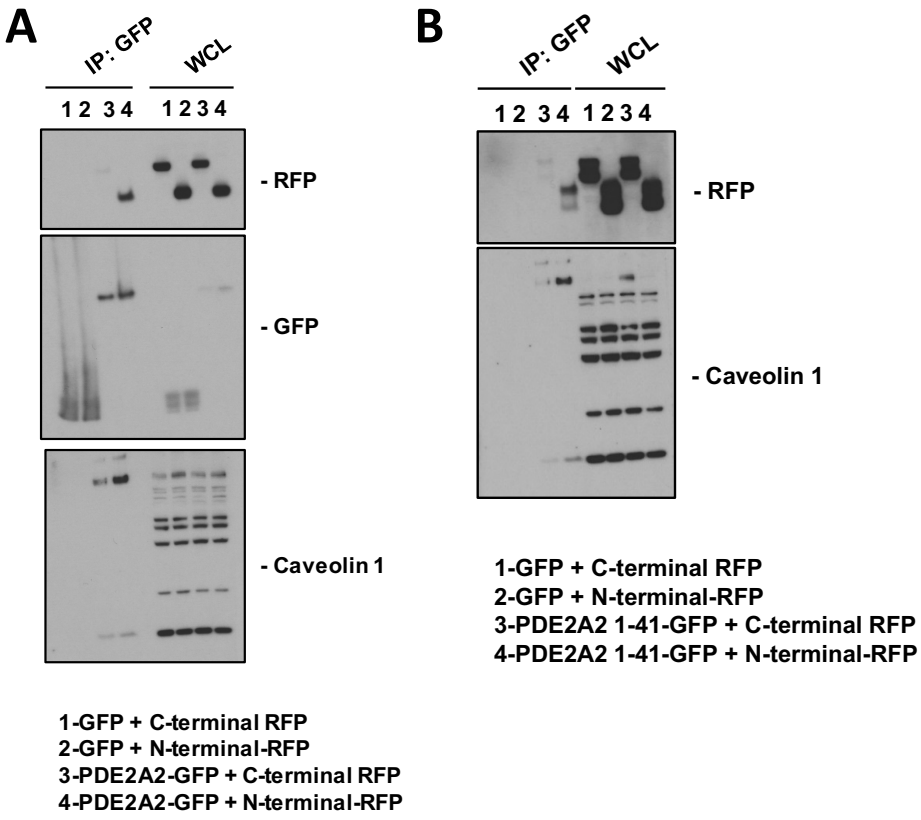


Figure 6.5 | **Attempt to disrupt PDE2A2 and Caveolin 1 interaction.**
(A) Detection of endogenous Caveolin 1 after PDE2A2-GFP or GFP immunoprecipitation in HEK293T cells transiently transfected with either PDE2A2-GFP or GFP and C-terminal-RFP or N-terminal-RFP. Blot is representative of two independent experiments.
(B) Detection of endogenous Caveolin 1 after PDE2A2 1-41-GFP or GFP immunoprecipitation in HEK293T cells transiently transfected with either PDE2A2 1-41-GFP or GFP and C-terminal-RFP or N-terminal-RFP. Blot is representative of two independent experiments.

The interface between mitochondria and ER is emerging as a crucial hub for Ca^{2+} signaling, lipid biosynthesis/transport and mitochondrial morphology (de Brito and Scorrano, 2010; Naon and Scorrano, 2014). We have recently shown that PDE2A2 regulates a local cAMP domain at the OMM affecting mitochondria morphology and apoptotic cell death (Monterisi et al., 2017). To further explore the possible role of PDE2A2 at the ER, I tested the contribution of PDE2A on ER Ca^{2+} handling since one of the major roles of the ER is to function as a Ca^{2+} store. Rapid Ca^{2+} release from ER through inositol trisphosphate (IP3) receptor (IP3R), followed by Ca^{2+}

entry through SERCA (sarcoplasmic-endoplasmic reticulum Ca^{2+} ATPase) is an essential signaling mechanism which participates in the regulation of neurotransmitter release and mitochondrial bioenergetics (Denton, 2009; DeSouza et al., 2002). Indeed, IP3R has also been found to localized at the MAM (Raturi and Simmen, 2013). Thus, I proposed to study the involvement of PDE2A on both ER Ca^{2+} loading and release. To monitor ER Ca^{2+} handling, I used a cytosolic Ca^{2+} FRET sensor dc3pv, dc3pv targeted to the mitochondria and the Ca^{2+} sensor D1ER to measure Ca^{2+} inside the ER (Miyawaki et al., 1997; Palmer et al., 2004) and compared the Ca^{2+} signals detected by these reporters in wt and PDE2A KO (knockout) MEFs. First, to test ER Ca^{2+} loading, cells were treated with the sarcoplasmic reticulum Ca^{2+} ATPase inhibitor Thapsigargin (TG) and Ca^{2+} levels were monitored both in the cytosol and ER (*Fig. 6.6*). All wt and PDE2A KO cells showed ER Ca^{2+} release upon TG addition. Moreover, by depleting the ER Ca^{2+} content by using ionomycin (an ionophore), I observed that wt and PDE2A KO cells have similar remaining levels of Ca^{2+} in the ER upon addition of TG. These results suggest that ER Ca^{2+} loading is not impaired in PDE2A KO cells.

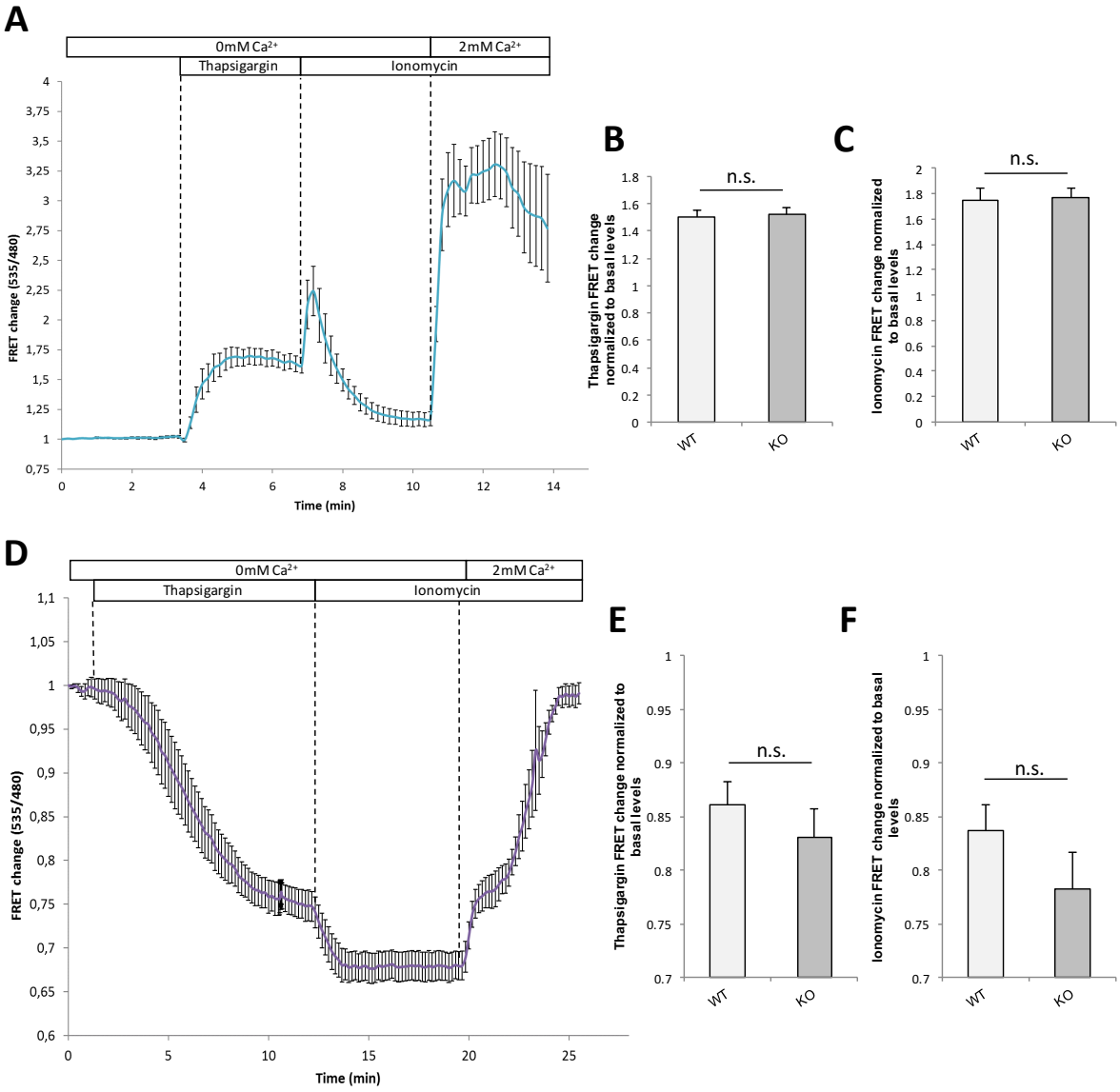


Figure 6.6 | **PDE2A knockout does not affect ER Ca^{2+} levels.**
(A) Representative kinetics of FRET change in MEF wt cells expressing the cytosolic D3cpv Ca^{2+} sensor and treated with Thapsigargin followed by ionomycin. Similar kinetics were found in MEF PDE2A KO cells.
Quantification of the % of FRET change induced by Thapsigargin (B) and ionomycin (C) treatment. n=18/22 MEF wt/MEF PDE2A KO cells (4/4 independent experiments).
(D) Representative kinetics of FRET change in MEF wt cells expressing the ER D1ER Ca^{2+} sensor and treated with Thapsigargin followed by ionomycin. Similar kinetics were found in MEF PDE2A KO cells.
Quantification of the % of FRET change induced by Thapsigargin (E) and ionomycin (F) treatment. n=13/10 MEF wt/MEF PDE2A KO cells (9/4 independent experiments).
All data represent mean±s.e.m. t-test statistical analysis was performed. ns=not significant.

Next, to assess whether PDE2A is involved in IP3R-dependent Ca^{2+} release, cells were perfused in Ca^{2+}-free solution and Ca^{2+} release from the ER was triggered by stimulation of purinergic receptors with 1 mM ATP (Valsecchi et al., 2017). The bath solution was then replaced with 1 mM Ca^{2+}. At the end of the experiment, a solution containing ionomycin was applied to control for sensor activity. After ATP stimulation, a significantly smaller number of PDE2A KO cells showed a cytosolic or mitochondrial Ca^{2+} response in comparison to wt (*Fig. 6.7A-D and G*). Treatment with ionomycin rapidly increases Ca^{2+} both in the cytosol and in the mitochondria. The same experiments were repeated in the presence of EGTA, a Ca^{2+} chelating agent, although similar results were observed (*Fig. 6.7E and F*). Overall, IP3R-dependent Ca^{2+} release was impaired in PDE2A KO cells, while ER Ca^{2+} loading/content was unaffected. It is worth to note that addition of ionomycin induced a transient response in some cells while tonic in others. This observation was independent of which cell type was being used (wt vs PDE2A KO cells) and possibly results from the fact that ionomycin induces cell death – dying cells start to shrink which may cause FRET artifacts.

Treatment of wt cells with BAY-60 decreased the number of cells responding to ATP stimulation with a Ca^{2+} transient (*Fig. 6.7G*). These results suggest that the probability of ER releasing Ca^{2+} upon ATP stimulation was decreased in cells with reduced or absent PDE2A activity. Additionally, PDE2A1 overexpression, but not PDE2A2, partially restored the number of cells that respond to ATP (*Fig. 6.7H*). This finding suggests that the effect of PDE2A on ER Ca^{2+} release is mediated by PDE2A1 rather than PDE2A2, as previously hypothesized, and it is likely independent of PDE2A-Caveolin interaction. Further experiments are required to test the involvement of PDE2A-Caveolin interaction in ER Ca^{2+} handling. Additionally, in this thesis I have not addressed whether lack of PDE2A affects Ca^{2+} uptake in the mitochondria – future studies would be required to address this hypothesis.

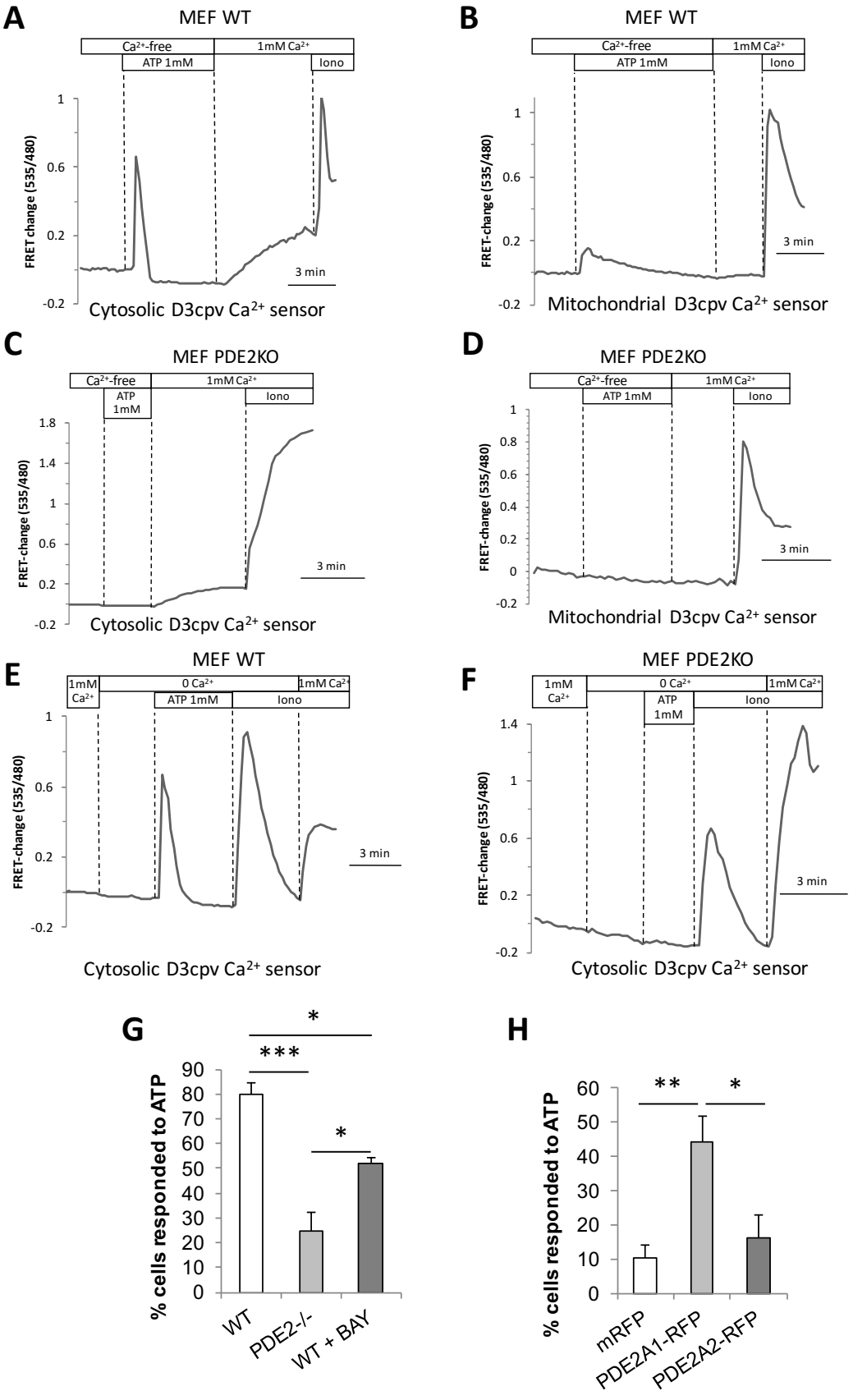

A
MEF WT
Ca2+-free
1mM Ca2+
ATP 1mM
Iono
FRET change (535/480)
3 min
Cytosolic D3cpv Ca2+ sensor
B
MEF WT
Mitochondrial D3cpv Ca2+ sensor
C
MEF PDE2KO
Cytosolic D3cpv Ca2+ sensor
D
MEF PDE2KO
Mitochondrial D3cpv Ca2+ sensor
E
MEF WT
1mM Ca2+
0 Ca2+
Cytosolic D3cpv Ca2+ sensor
F
MEF PDE2KO
Cytosolic D3cpv Ca2+ sensor
G
% cells responded to ATP
WT
PDE2-/-
WT + BAY
H
mRFP
PDE2A1-RFP
PDE2A2-RFP

Figure 6.7 | **PDE2A knockout disrupts ATP-induced Ca^{2+} release from the ER.**
(A/E) Representative kinetics of FRET change in MEF wt cells expressing the cytosolic D3cpv Ca^{2+} sensor and treated with ATP (1 mM).
(B) Representative kinetics of FRET change in MEF wt cells expressing the mitochondrial D3cpv Ca^{2+} sensor and treated with ATP (1 mM).
(C/F) Representative kinetics of FRET change in MEF PDE2A KO cells expressing the cytosolic D3cpv Ca^{2+} sensor and treated with ATP (1 mM).
(D) Representative kinetics of FRET change in MEF PDE2A KO cells expressing the mitochondrial D3cpv Ca^{2+} sensor and treated with ATP (1 mM).
(G) Quantification of the % of MEF cells that responded to ATP (36/37 MEF wt/MEF PDE2A$^{-/-}$ cells). MEF wt cells were treated with BAY-60 1 μM for 24 h. n=3-4.
(H) Quantification of the % of cells that responded to ATP upon mRFP, PDE2A1-RFP or PDE2A2-RFP over-expression in MEF cells (25-33 MEF cells). n=4. *P<0.05.
All data represent mean±s.e.m. One-way ANOVA and Tukey's multiple comparison tests were performed. *P<0.05; **P<0.01; ***P<0.005.

I next-tested whether the lower probability of ER Ca^{2+} release in PDE2A KO cells was due to lower number of IP3R. Surprisingly, PDE2A KO cells showed higher IP3R protein levels compared to wt cells (*Fig. 6.8A and B*). This suggests a possible compensatory mechanism in PDE2A KO cells that aims to compensate for deficient ER Ca^{2+} release upon IP3 simulation by increasing the number of IP3R.

IP3R phosphorylation is involved in the regulation of Ca^{2+} release by IP3R (Vanderheyden et al., 2009). PKA phosphorylates IP3R, which is abundantly expressed in MEFs (Oakes et al., 2005), at two sites, S1588 and S1756 (Ferris et al., 1991), leading to an increase in the channel activity of the receptor (Nakade et al., 1994; Tang et al., 2003; Wagner et al., 2004). Additionally, decreased probability of ER Ca^{2+} release has been reported in sAC KO cells, similarly to what I have observed in PDE2A KO cells (Valsecchi et al., 2017). The authors propose that this phenotype is associated with diminished phosphorylation of the IP3R. Thus, I hypothesized whether PKA-mediated phosphorylation of IP3R could be affected in PDE2A KO cells. By performing western blot analysis, I observed that the levels of phospho-S1756 IP3R, relative to total IP3R, were not different between wt and PDE2A KO cells (*Fig. 6.8C*).

Based on these results, since both wt and PDE2A KO cells have similar ER Ca^{2+} and IP3R protein levels, it is more likely that PDE2A KO disrupts some component upstream of the IP3R and of the ER. Further studies are required to address this hypothesis.

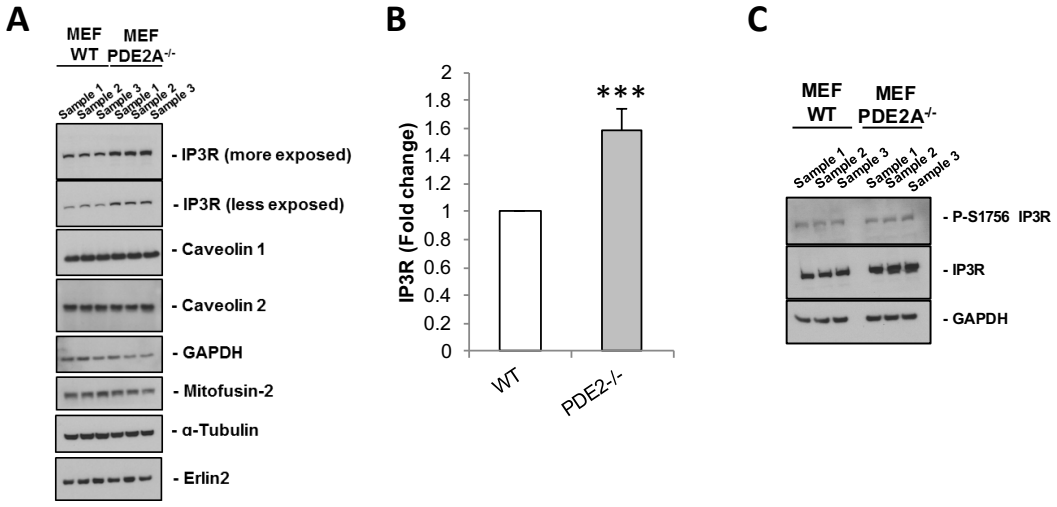


Figure 6.8 | **PDE2A knockout does not regulate PKA-mediated phosphorylation of IP3R.**
(A) Protein levels of IP3R in wt and PDE2A$^{-/-}$ MEF cells.
(B) Quantification of total protein levels of IP3R, normalized to the amount of α-Tubulin. Data represents mean+s.e.m. n=15. ***P<0.005 (t-test).
(C) Protein levels of P-S1756 IP3R and total IP3R in wt and PDE2A$^{-/-}$ MEF cells.

6.5 Conclusion

In this chapter I described a novel interaction between PDE2A2 and Caveolin 1 at the MAM. The finding that this interaction is specific for PDE2A2 and not PDE2A1 reinforces the notion that besides the critical role in mitochondrial morphology (Monterisi et al., 2017), PDE2A2 plays additional intracellular functions, particularly at the MAM. However, when I assessed the role of PDE2A on IP3R-mediated ER Ca^{2+} handling, I found that this was mediated by PDE2A1, rather than PDE2A2.

Similar phenotype has been found in soluble AC (sAC) KO cells (Valsecchi et al., 2017). ATP stimulation induced a Ca^{2} transient in the majority of MEF wt cells, while this was observed in a significantly smaller proportion of sAC KO. The authors determined that this was not due to lower levels of Ca^{2+} in the ER, but to decreased IP3R phosphorylation. Their interpretation of the results is that lack of sAC-generated cAMP leads to decreased PKA-mediated phosphorylation of IP3R in the ER and desensitization of the receptor, resulting in lower probability of its open state.

I have shown that the lower proportion of PDE2A KO cells responsive to ATP is not due to lower levels of ER Ca^{2+} or to reduced IP3R PKA-mediated phosphorylation at S1756. Phosphorylation of S1588 remains to be studied. Additional experiments will be required to establish the mechanism by which PDE2A ablation disrupts ER Ca^{2+} release upon ATP stimulation.

In humans, mutations in the Caveolin 1 gene result in lipodystrophies (rare disorders characterized by loss of adipose tissue) and Caveolin 1 KO in the liver results in intracellular lipid imbalance, decreased formation of lipid droplets and a cholesterol-promoted mitochondrial dysfunction (Sala-Vila et al., 2016). In fact, the interface between mitochondria and ER is emerging as a crucial site for lipid biosynthesis and transport between organelles (de Brito and

Scorrano, 2010; Naon and Scorrano, 2014). However, the role of cAMP signaling in modulation of lipid metabolism at the MAM is unknown. Considering that PDE2A2 localizes to the MAM where it interacts with Caveolin 1, it is possible that PDE2A is involved in the cAMP/PKA-dependent regulation of lipid metabolism at the MAM. To test this hypothesis, I have established a collaboration with Prof. Benedikt Kessler's laboratory at the Nuffield Department of Medicine to apply a lipidomics approach to investigate, in an unbiased fashion, the involvement of PDE2A in the regulation of mitochondrial lipid metabolism. Lipidomics analysis will be performed using purified mitochondria in order to compare the mitochondrial lipid composition between wt and PDE2A KO MEFs. The results of these investigations are expected to further elucidate the role of PDE2A at the MAM.

Chapter 7 – Cytosol and ER are distinct cAMP/PKA signaling domains as a consequence of compartmentalized Phosphatase activity

7.1 Background

Elements of the cAMP signaling cascade are organized into distinct signaling components called microdomains. Spatial confinement of the signaling pathway components allows for the formation of cAMP signaling hubs at discrete subcellular sites that are the effectors of specific responses to different stimuli (Lefkimmiatis and Zaccolo, 2014). The subcellular localization of microdomains is determined by several components of the cAMP/PKA signaling cascade:

- AKAPs, a family of proteins that tether PKA and regulatory elements of the cAMP cascade to specific cellular sites in proximity of PKA targets (Kritzer et al., 2012);
- PDEs control the availability of cAMP in a microdomain (Lomas and Zaccolo, 2014);
- Phosphatases terminate the signaling cascade by dephosphorylation of PKA targets (Haj Slimane et al., 2014; Heijman et al., 2013; Hinke et al., 2012).

PKA tetramers containing RI-type are activated at lower concentrations of cAMP compared to ones including RIIs (Dostmann et al., 1990). AKAPs, which bind to R subunits, preferentially bind to RII (Kritzer et al., 2012). Thus, the more sensitive RI subunits are found predominantly in the soluble fractions of the cells, whereas the RII-based enzymes, which require higher cAMP levels for activation, are found in the particulate fractions (Taylor et al., 2012). Since the most sensitive PKA is in the cytosol, this may favour inappropriate activation of cytosolic PKA before activation of localized AKAP-targeted PKA, which would abrogate the advantage of compartmentalization.

cAMP-dependent phosphorylation has been reported to exert biological effect at the ER, as mentioned before on Chapter 1.3.2, including regulation of Ca^{2+} handling at the ER (Ikeda et al., 2008; Konieczny et al., 2017; Lefkimmiatis and Zaccolo, 2014). However, the kinetics, regulators and effectors of the cAMP cascade at this organelle remain unknown. Since I have

previously shown that PDE2A localizes to the MAM and is involved in ER Ca^{2+} handling (*Chapter 6*), I next explored if PDE2A could also be involved in cAMP/PKA signaling compartmentalization at the ER.

7.2 PKA signaling is not promptly terminated at the ER compared to cytosol

To study cAMP/PKA signaling at the ER, I generated ER-targeted FRET sensors based either on the cAMP reporter H90 (van der Krogt et al., 2008) or on the PKA-activity reporter AKAR4 (Depry et al., 2011). Using Cytochrome P450 2C1 N-terminal sequence, both H90 and AKAR4 were targeted to the ER facing the cytosolic side (ER-cyto-H90 and ER-cyto-AKAR4). On the other hand, Calreticulin N-terminal and KDEL motif were used to target both H90 and AKAR4 to the lumen of the ER (ER-lumen-H90 and ER-lumen-AKAR4) (*Fig. 7.1A*). As shown in Figure 7.1B-D, by live cell imaging and ER fractionation, all sensors are correctly targeted to the ER. The maximum FRET change for all sensors was measured in HeLa cells expressing each reporter upon addition of Fsk 25 μM + IBMX 100 μM (Fsk/IBMX) (*Fig. 7.1E and F*) and was found to be similar between H90 and ER-cyto-H90 as well as between AKAR4 and ER-cyto-AKAR4. Since both pairs of sensors have similar maximum FRET ratios, this allows direct comparison between the signals they generate. ER-lumen-sensors were designed to be used as a negative control. When I assessed the response of these sensors to cAMP analogues, no signal was detected. Therefore, I could not use them as negative controls.

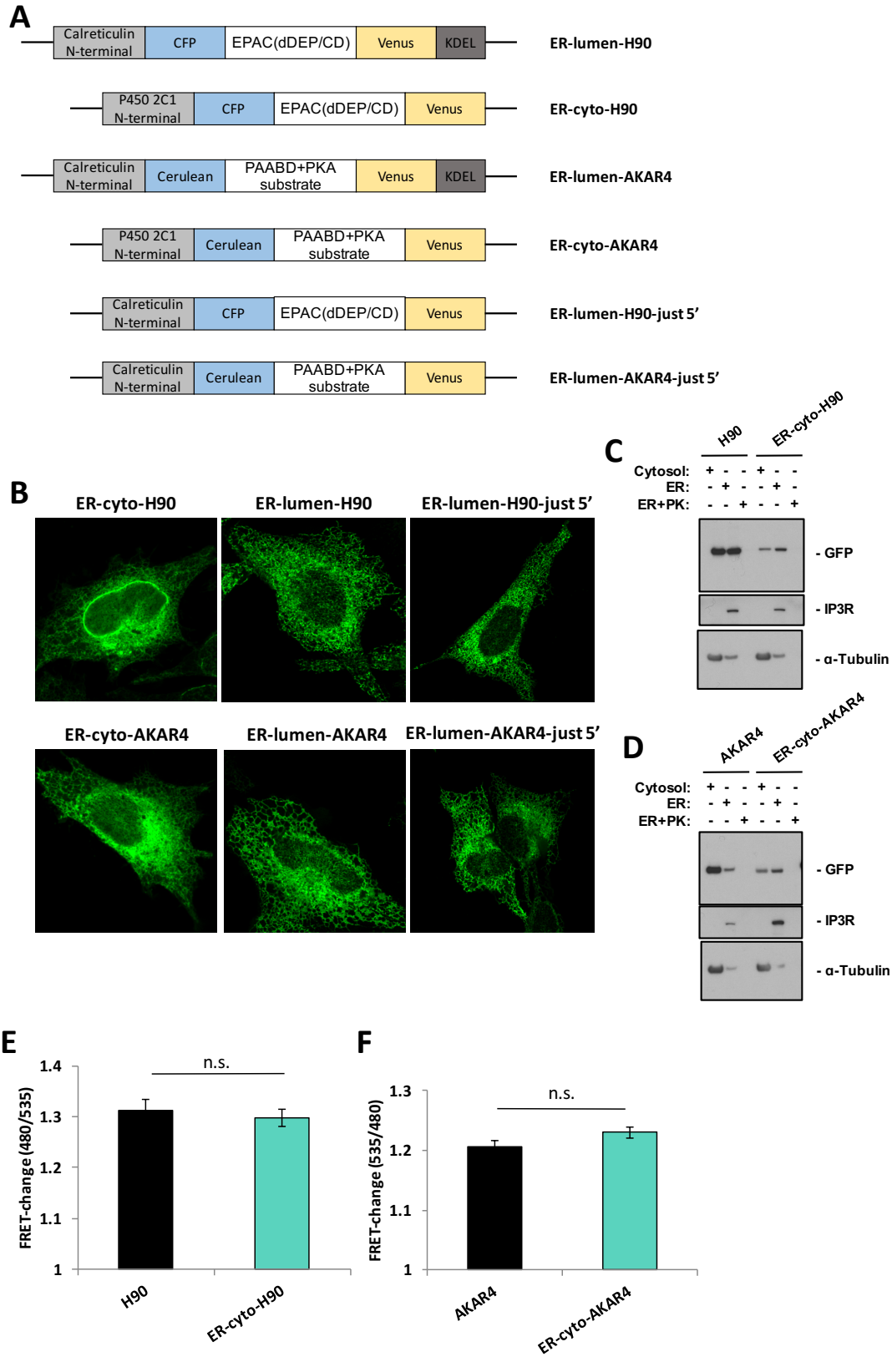

A
Calreticulin N-terminal
CFP
EPAC(dDEP/CD)
Venus
KDEL
ER-lumen-H90
P450 2C1 N-terminal
ER-cyto-H90
Cerulean
PAABD+PKA substrate
ER-lumen-AKAR4
ER-cyto-AKAR4
ER-lumen-H90-just 5'
ER-lumen-AKAR4-just 5'
B
ER-cyto-H90
ER-lumen-H90
ER-lumen-H90-just 5'
ER-cyto-AKAR4
ER-lumen-AKAR4
ER-lumen-AKAR4-just 5'
C
H90
ER-cyto-H90
Cytosol:
ER:
ER+PK:
- GFP
- IP3R
- α-Tubulin
D
AKAR4
ER-cyto-AKAR4
E
n.s.
FRET-change (480/535)
1.4
1.3
1.2
1.1
1
H90
ER-cyto-H90
F
n.s.
FRET-change (535/480)
1.3
1.2
1.1
1
AKAR4
ER-cyto-AKAR4

Figure 7.1 | **H90 and AKAR4 sensors targeted to the ER.**
(A) Schematic representation showing all ER-FRET-sensors generated.
(B) Live confocal imaging of HeLa cells over-expressing each sensors. Images are representative of two independent experiments.
(C) Representative western blot analysis of H90 and ER-cyto-H90 sensors in cytosolic and endoplasmic reticulum sub-fractions obtained from HeLa lysates non treated and treated with Proteinase K (10 µM). Blot is representative of two independent experiments.
(D) Representative western blot analysis of AKAR4 and ER-cyto-AKAR4 sensors in cytosolic and endoplasmic reticulum sub-fractions obtained from HeLa lysates non treated and treated with Proteinase K (10 µM). Blot is representative of two independent experiments.
(E) Maximum FRET change comparison between H90 and ER-cyto-H90 sensors expressed in HeLa cells. Fsk 25 µM + IBMX 100 µM was applied to achieve saturation of the sensors. n=38/50 H90/ER-cyto-H90 cells (8/9 independent experiments).
(F) Maximum FRET change comparison between AKAR4 and ER-cyto-AKAR4 sensors expressed in HeLa cells. Fsk 25 µM + IBMX 100 µM was applied to achieve saturation of the sensors. n=70/49 H90/ER-cyto-H90 cells (12/13 independent experiments).
All data represent mean±s.e.m. t-test statistical analysis was performed. ns=not significant.

In HeLa cells expressing either ER-cyto-H90 or H90, treatment with a low dose of Fsk (2 µM) remained undetected both in cytosol and ER because of the strong PDE activity in this cell type (Lefkimmiatis et al., 2013). However, both domains responded equally upon treatment with IBMX, unveiling the underlying cAMP production, and upon removal of Fsk/IBMX, suggesting that the cAMP production rates are similar in the cytosol and at the ER (*Fig. 7.2A*). Using AKAR4 sensors, I consistently observed that in HeLa cells challenged with Fsk/IBMX, ER-cyto-AKAR4 responses were significantly larger compared to the cytosol (*Fig. 7.2B*), confirming a previous observation by *Liu et al.* using AKAR3 targeted to the Sarcoplasmic Reticulum via a different targeting strategy (Liu et al., 2011). In addition, upon application of the PKA inhibitor H89, ER-cyto-AKAR4 exhibited slower dephosphorylation kinetics. Similar results were found on HEK293T cells, challenged with cAMP-generating agonist isoproterenol (ISO; 10 nM): the cAMP signal detected by ER-cyto-H90 or H90 was very similar in the two compartments (*Fig. 7.2C*) whereas cells expressing ER-cyto-AKAR4 and AKAR4 showed that the termination of the PKA-dependent phosphorylation signal at the ER upon ISO removal was again dramatically slower than in the cytosol (*Fig. 7.2D*). Moreover, cells expressing ER-cyto-H90 or H90 showed similar degradation rates of cAMP upon removal of ISO, suggesting similar PDE activity in the cytosol and at the ER (*Fig. 7.2C*).

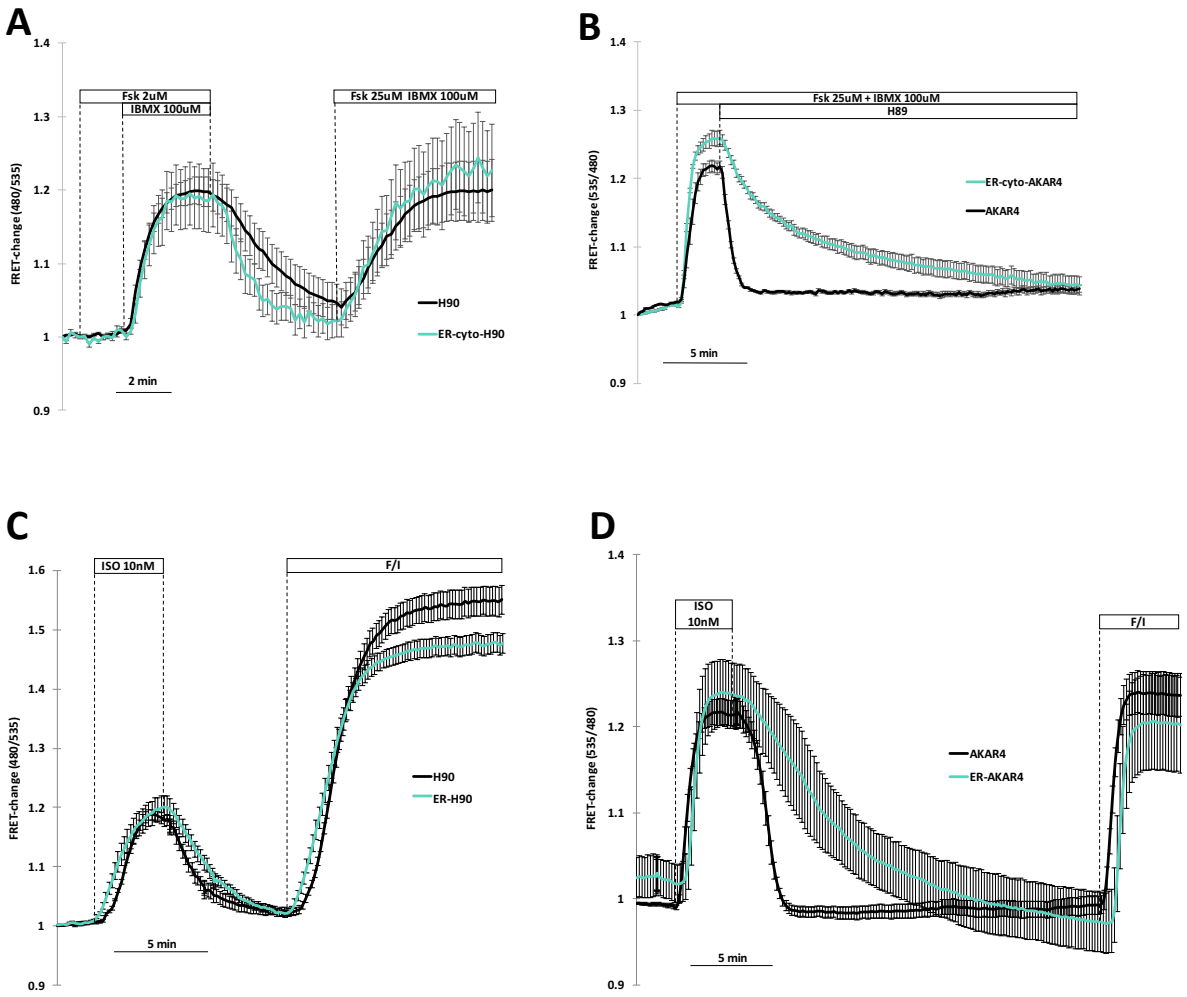


Figure 7.2 | **Comparison of cAMP and PKA signals at the ER and cytosol.**
(A) Comparison of H90 (black trace; mean of six cells) and ER-cyto-H90 (blue trace; mean of six cells) FRET responses, in HeLa cells, upon addition of Fsk 2 μM + IBMX 100 μM. Fsk 25 μM + IBMX 100 μM was applied to achieve saturation of the sensors (n= 5 experiments).
(B) Comparison of AKAR4 (black trace; mean of six cells) and ER-cyto-AKAR4 (blue trace; mean of five cells) FRET responses, in HeLa cells, upon addition of Fsk 25 μM + IBMX 100 μM, followed by H89 (n= 5 experiments).
(C) Comparison of H90 (black trace; mean of eleven cells) and ER-cyto-H90 (blue trace; mean of ten cells) FRET responses, in HEK293T cells, upon addition of ISO 10 nM. Fsk 25 μM + IBMX 100 μM (F/I) was applied to achieve saturation of the sensors (n= 3 experiments).
(D) Comparison of AKAR4 (black trace; mean of five cells) and ER-cyto-AKAR4 (blue trace; mean of five cells) FRET responses, in HEK293T cells, upon addition of ISO 10 nM. Fsk 25 μM + IBMX 100 μM (F/I) was applied to achieve saturation of the sensors (n= 3 experiments).

As shown in Fig. 7.3A and B, when HeLa cells were treated with Fsk (20 μM), a concentration that generates a small but similar increase in intracellular cAMP in the cytosol and ER (17,37 % and 19,47 %, respectively), there was hardly any detectable PKA activity at the cytosol (2,26 %) whereas the PKA activity at the ER was robust (42,25 %, *Fig. 7.3C and D*).

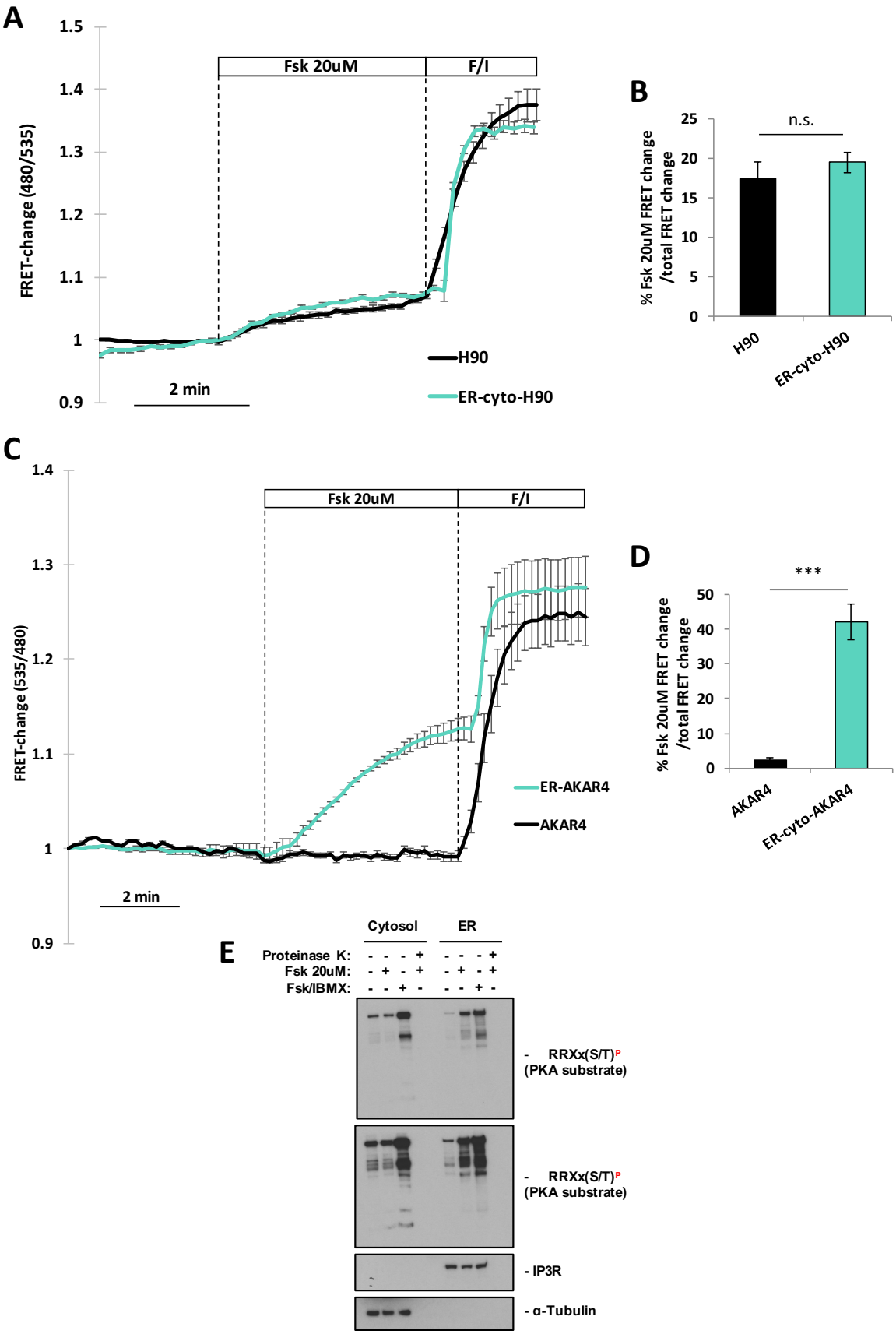

A
FRET-change (480/535)
1.5
1.4
1.3
1.2
1.1
1
0.9
Fsk 20uM
F/I
2 min
H90
ER-cyto-H90
B
% Fsk 20uM FRET change /total FRET change
25
20
15
10
5
0
n.s.
H90
ER-cyto-H90
C
FRET-change (535/480)
1.4
1.3
1.2
1.1
1
0.9
Fsk 20uM
F/I
2 min
ER-AKAR4
AKAR4
D
% Fsk 20uM FRET change /total FRET change
50
40
30
20
10
0
***
AKAR4
ER-cyto-AKAR4
E
Cytosol
ER
Proteinase K:
Fsk 20uM:
Fsk/IBMX:
- RRXx(S/T)P (PKA substrate)
- RRXx(S/T)P (PKA substrate)
- IP3R
- α-Tubulin

Figure 7.3 | **Forskolin induces differential PKA activity between cytosol and ER.**
(A/B) Comparison of H90 (black trace; mean of six cells) and ER-cyto-H90 (blue trace; mean of eleven cells) FRET responses, in HeLa cells, upon addition of Fsk 20 µM. Fsk 25 µM + IBMX 100 µM (F/I) was applied to achieve saturation of the sensors (n= 5 experiments).
(C/D) Comparison of AKAR4 (black trace; mean of six cells) and ER-cyto-AKAR4 (blue trace; mean of four cells) FRET responses, in HeLa cells, upon addition of Fsk 20 µM. Fsk 25 µM + IBMX 100 µM (F/I) was applied to achieve saturation of the sensors (n= 5 experiments).
(E) Cytosolic and endoplasmic reticulum (ER) fractions of HeLa cells treated with 20 µM Fsk or Fsk combined with IBMX for 1 h. Phosphorylation status was assessed by a phosphor-PKA substrate antibody (RRX(S/T)^{P}). Antibodies against IP3R and α-Tubulin were used to assess purity of ER and cytosol, respectively. Blot is representative of two independent experiments.
All data represent mean±s.e.m. t-test statistical analysis was performed. ***P<0.005; ns=not significant.

AKAR4 sensors are based on a specific PKA consensus (Depry et al., 2011), which may not represent the diversity of endogenous PKA consensus sites. To test whether the different PKA activity observed by FRET is mirrored by the phosphorylation of native PKA targets, HeLa cells were treated with Fsk (20 µM) or Fsk/IBMX. After treatment, ER and soluble fractions were isolated followed by western blot analysis for PKA-dependent phosphorylation (*Fig. 7.3E*). Fsk (20 µM) induced a strong phosphorylation pattern in ER compared to untreated cells, whereas proteins in the cytosolic fraction were unaffected, while Fsk/IBMX treatment induced strong phosphorylation in both fractions. Additionally, to determine which compartment has relevant PKA-dependent phosphorylation, Fsk-treated fractions were incubated with Proteinase K, which cleaves proteins in the ER exposed to the cytosol. I observed that Proteinase K treatment abolished the phosphorylation pattern as well as the ER marker IP3R, suggesting that the majority of PKA targets are at the ER and not in its lumen. Taken together, ER and cytosol appear to define distinct PKA activity domains. As these differences cannot be ascribed to different cAMP levels, it seems likely that they may be explained by different phosphatase activity at these two sites.

7.3 Phosphatases limit PKA activity in the cytosol

Since the difference observed in PKA activity between cytosol and ER did not depend on cAMP levels, I tested the possibility that other cAMP/PKA signaling regulatory elements may be involved in this phenomenon. To assess this, I analyzed the protein levels of several cAMP signaling components between the cytosol and ER of HEK293T and HeLa cells by western blot. Both cytosol and ER contained the main PKA catalytic type (PKA Cα) as well as PKA Cβ, PKA Cγ and type RII regulatory subunits (*Fig. 7.4A*). As expected, the majority of PKA RI subunits, which are more sensitive to cAMP, were found in the cytosol. This finding confirms that the higher PKA activity detected by FRET at the ER cannot be explained by an enrichment of the more sensitive PKA isoform at this site. Interestingly, I found that the three main phosphatases, PP2A, PP1 and Calcineurin, which are responsible for >90 % of protein phosphatase activity in cardiac myocytes (Heijman et al., 2013), were mostly present in the cytosolic fraction.

To test whether phosphatases are responsible for the low cytosolic PKA activity compared to the SR, I challenged NRVM expressing AKAR4 (*Fig. 7.4B*) or ER-cyto-AKAR4 (*Fig. 7.4C*) with low (20 nM) levels of Fsk, or in combination with calyculin A (CalA; inhibitor of PP2A and PP1) and cyclosporine A (CsA; inhibitor of Calcineurin). NRVM were used since in other cell types, including HEK293T and HeLa cells, phosphatase inhibitors result in cell death precluding the possibility to perform the experiment (*data not shown*). I observed that 20 nM Fsk induced a significant increase in ER-cyto-AKAR4, while cytosolic AKAR4 remained negligible (*Fig. 7.4D*). Upon addition of CalA and CsA, I observed a strong PKA response both in the cytosol and at the SR. In NRVM expressing either ER-cyto-H90 or H90, treatment with a low dose of Fsk (20 nM) remained under the detection limit of H90 sensors (*Fig. 7.4E*).

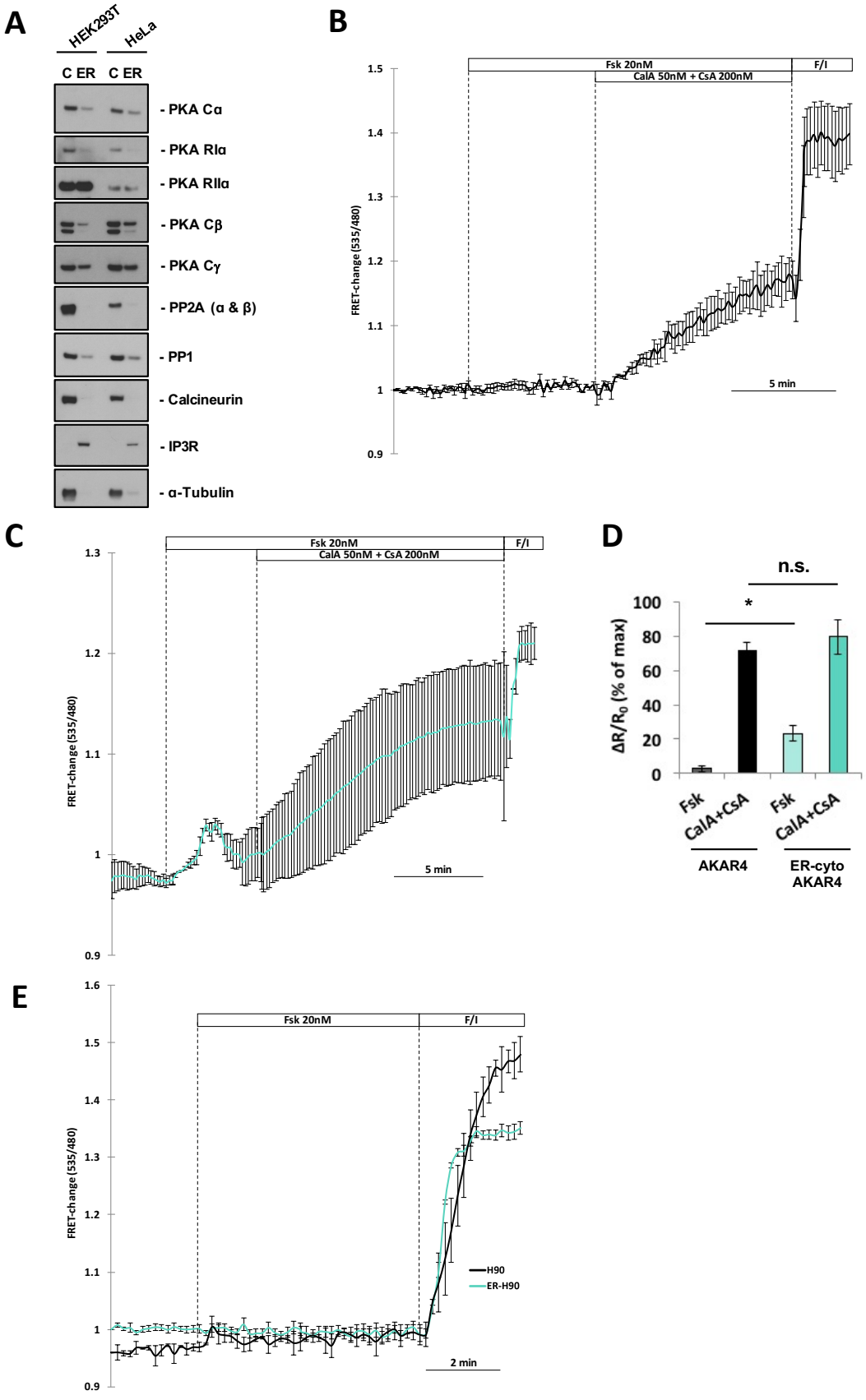

A
HEK293T
HeLa
C ER C ER
- PKA Cα
- PKA RIα
- PKA RIIα
- PKA Cβ
- PKA Cγ
- PP2A (α & β)
- PP1
- Calcineurin
- IP3R
- α-Tubulin
B
Fsk 20nM
CalA 50nM + CsA 200nM
F/I
FRET-change (535/480)
5 min
C
Fsk 20nM
CalA 50nM + CsA 200nM
F/I
FRET-change (535/480)
5 min
D
n.s.
*
ΔR/R0 (% of max)
Fsk
CalA+CsA
Fsk
CalA+CsA
AKAR4
ER-cyto AKAR4
E
Fsk 20nM
F/I
FRET-change (535/480)
H90
ER-H90
2 min

Figure 7.4 | **Phosphatases are responsible for the differential PKA activity between cytosol and SR.**
(A) Cytosolic and endoplasmic reticulum (ER) fractions of HEK293T and HeLa cells. Antibodies against IP3R and α-Tubulin were used to assess purity of ER and cytosol, respectively. Blot is representative of two independent experiments.
(B) NRVM expressing AKAR4 challenged with Fsk 20 nM followed by Calyculin A (CalA) 50 nM plus Cyclosporine A (CsA) 200 nM to inhibit phosphatases. Fsk 25 μM + IBMX 100 μM (F/I) was applied to achieve saturation of the sensor (black trace; mean of three cells; n= 8 experiments).
(C) NRVM expressing ER-cyto-AKAR4 challenged with Fsk 20 nM followed by Calyculin A (CalA) 50 nM plus Cyclosporine A (CsA) 200 nM to inhibit phosphatases. Fsk 25 μM + IBMX 100 μM (F/I) was applied to achieve saturation of the sensor (blue trace; mean of two cells; n= 3 experiments).
(D) FRET change comparison between AKAR4 and ER-cyto-AKAR4 upon addition of Fsk 20 nM followed by Calyculin A (CalA) 50 nM plus Cyclosporine A (CsA) 200 nM. n=38/50 H90/ER-cyto-H90 cells (8/9 independent experiments). Data represent mean±s.e.m. One-way ANOVA and Tukey's multiple comparison tests were performed. *P<0.05; n.s. non-significant.
(E) Comparison of H90 (black trace; mean of three cells) and ER-cyto-H90 (blue trace; mean of three cells) FRET responses in NRVM challenged with Fsk 20 nM. Fsk 25 μM + IBMX 100 μM (F/I) was applied to achieve saturation of the sensors (n= 5 experiments).

PP2A and PP1 are the main regulators of cytosolic PKA in NRVM (Haj Slimane et al., 2014). Indeed, CalA alone was sufficient to significantly raise PKA activity, while the effect of CsA alone remained undetected, as measured by AKAR4 (*Fig. 7.5*). These results suggest that phosphatases, more specifically PP2A and PP1, obliterate cytosolic PKA activity when a stimulus that is able to trigger a robust PKA response at the SR is applied.

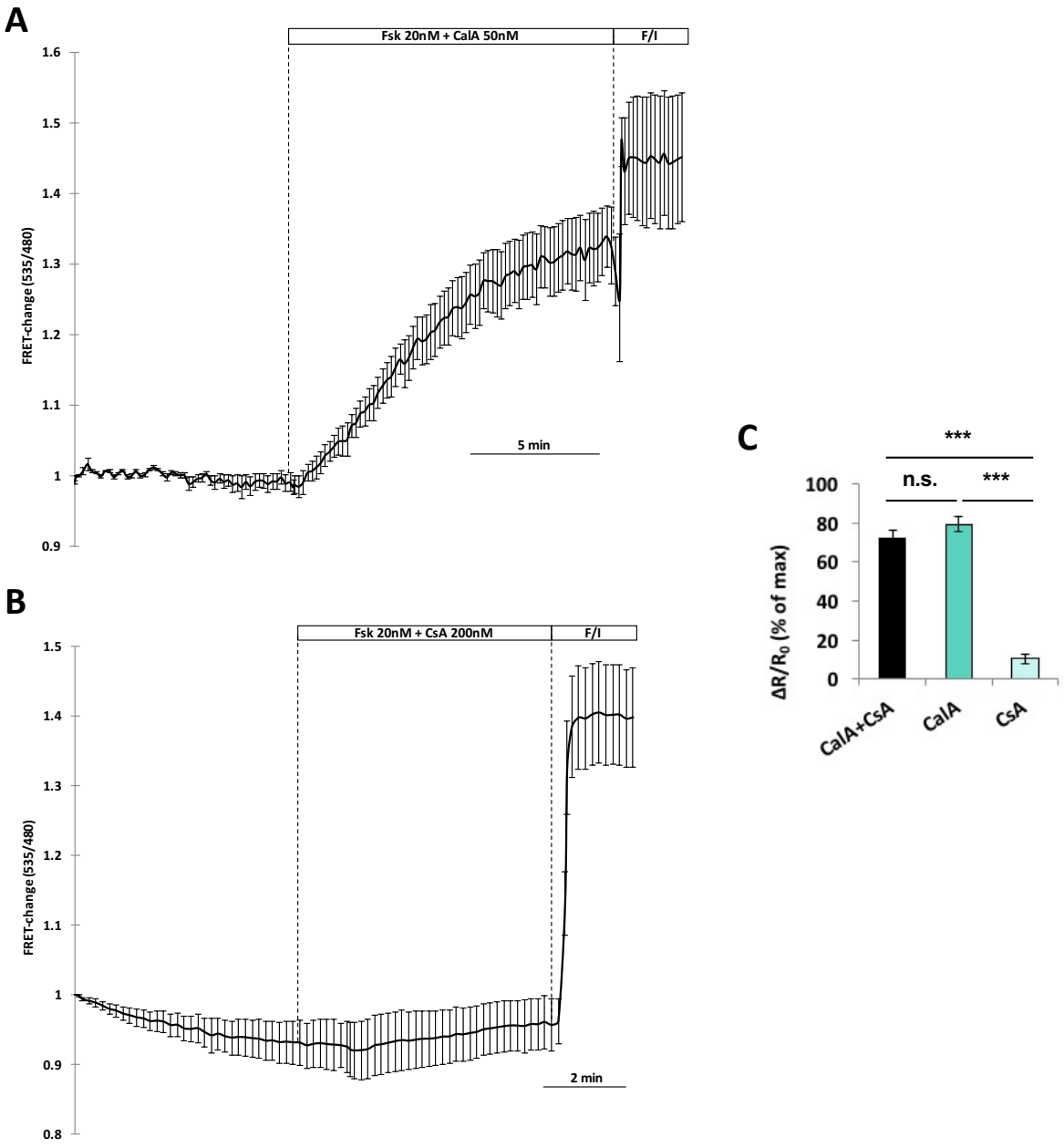


Figure 7.5 | **PP1 and PP2A are responsible for the differential PKA activity between cytosol and SR.**
(A) NRVM expressing AKAR4 challenged with Fsk 20 nM plus Calyculin A (CalA) 50 nM. Fsk 25 μM + IBMX 100 μM (F/I) was applied to achieve saturation of the sensor (black trace; mean of three cells; n= 3 experiments).
(B) NRVM expressing AKAR4 challenged with Fsk 20 nM plus Cyclosporine A (CsA) 200 nM. Fsk 25 μM + IBMX 100 μM (F/I) was applied to achieve saturation of the sensor (black trace; mean of three cells; n= 3 experiments).
(C) AKAR4 FRET change comparison between cells treated with Calyculin A (CalA) 50 nM, Cyclosporine A (CsA) 200 nM, or both. Data represent mean±s.e.m. One-way ANOVA and Tukey's multiple comparison tests were performed. ***P<0.005; n.s. non-significant.

7.4 Conclusion

cAMP/PKA signaling compartmentalization is based on the idea that different PKA subsets can be activated independently by different stimuli. However, how cAMP signals can selectively activate specific PKA hubs while avoiding non-specific activation of PKA that is free in the cytosol, has remained an open question. A well tested hypothesis for this mechanism is that during cAMP elevation, PDEs maintain cytosolic cAMP low resulting in inactive PKA, while higher levels of the messenger are attained at AKAP-bound PKA (Houslay, 2010; Sprenger et al., 2015; Zaccolo and Pozzan, 2002). However, this model does not predict how higher concentration of cAMP can be attained at these hubs, except for those that are at the plasma membrane in proximity of ACs, while bulk cAMP is kept at lower levels. Here, I have shown that a rise in cAMP that activates PKA at the ER subdomains fails to induce comparable PKA activity in the cytosol of HEK293T, HeLa and NRVM cells. I further demonstrated that the difference in PKA activity between cytosol and ER is due to differences in phosphatase activity between these two compartments rather than differences in the cAMP levels. Interestingly, similar results were previously described for cytosol and OMM, where the authors concluded that the OMM is a privileged cAMP signaling microdomain with high PKA activity (Lefkimmiatis et al., 2013). My results suggest instead that rather than the mitochondria being a compartment with more persistent PKA activity, the bulk cytosol is a site where inappropriate PKA activity is suppressed by strong phosphatase activity. This feature of bulk cytosolic PKA-regulation may be an important contributing factor to specificity of response. In NRVM, the identification of phosphatases, PP2A and PP1, as key players in PKA signaling compartmentalization, adds another layer to this complex mechanism. Collectively, I propose that phosphatases and PDEs act in parallel to shape distinct cAMP/PKA signaling microdomains.

Chapter 8 - Discussion

The cAMP/PKA signaling pathway is central to cell physiology and pathophysiology, being involved in several cellular functions such as hormone secretion, gene expression, cell metabolism, cell survival and cell death. Several disorders have been linked to dysregulation of cAMP signaling, including cancer, hormonal disorders, pulmonary hypertension and cardiovascular, neurological and psychiatric conditions (Maurice et al., 2014a). In recent years it has become apparent that cAMP signaling is compartmentalized within the cell, with tight spatial and temporal control of signal propagation underpinning specificity of response (Zaccolo, 2009). Compartmentalization of cAMP offers the opportunity to target therapeutically individual cAMP pools, rather than global intracellular cAMP levels, in order to achieve greater therapeutic efficacy and specificity (Maurice et al., 2014a). The cAMP-degrading enzymes, phosphodiesterases (PDEs), are key regulators of this process. They are situated in specific subcellular domains within which they control local cAMP levels, dictating which PKA subsets are activated and therefore the downstream targets that are phosphorylated (Surdo et al., 2017). Among these, PDE2A, a cyclic GMP-stimulated phosphodiesterase that hydrolyzes both cAMP and cGMP, has been shown to be involved in shaping cAMP compartments, including at the mitochondria (Monterisi et al., 2017; Zoccarato et al., 2015). Numerous studies have linked PDE2A to pathological conditions, including psychiatric, neurological (Salpietro et al., 2018; Xu et al., 2015), cardiovascular (Assenza et al., 2018; Li et al., 2015; Mehel et al., 2013; Zoccarato et al., 2015) and respiratory (Zhang et al., 2015) disorders. Indeed, genetic ablation of PDE2A results in high embryonic lethality past E17.5–E18.5 dpc (Stephenson et al., 2009), indicating a key role in embryonic development. In addition, pharmacological inhibition of PDE2A in animal models has been shown to have beneficial effects in a number of pathological conditions, namely pulmonary hypertension (Bubb et al., 2014), cardiac hypertrophy (Zoccarato et al., 2015) and neurological conditions such as anxiety, depression and cognition deficits in Alzheimer's disease (Zhang et al., 2015). Despite extensive evidence linking PDE2A to disease and a growing interest of pharmaceutical companies in PDE2A as a

potential therapeutic target (a phase I clinical trial examining a PDE2A inhibitor for the treatment of schizophrenia (Trabanco et al., 2016) is currently ongoing), the role of PDE2A in the regulation of cellular function and the mechanisms underlying PDE2A involvement in disease remain largely to be clarified. The aim of this thesis was to further our understanding of the molecular role of PDE2A in cAMP/PKA signaling compartmentalization and its biological function.

8.1 Summary of Results and Discussion

8.1.1 Expression and sub-cellular localization of PDE2A

A single PDE2A gene gives rise to four PDE2A variants due to alternative splicing and alternative initiation codons. Firstly, it was attempted to determine the expression of PDE2A across different tissues and cell types by RT-PCR (*Fig. 3.1*). I observed that PDE2A1 and PDE2A2 are expressed across all different cells and tissues tested, including HEK293T, HeLa, SH-SY5Y, MEFs, Stellate Ganglia Neurons, mouse and rat cardiomyocytes and human heart tissue. PDE2A3 expression seems to be largely confined to neuronal cell types, which is in agreement with a previous report where the authors observed protein level PDE2A3 expression selectively in mouse brain by performing western blot analysis (Russwurm et al., 2009). This finding underpins the importance of identifying which isoforms are expressed in a certain tissue/cell type before starting characterizing PDE2A subcellular role.

Next, I assessed PDE2A isoforms localization in NRVM and HeLa cells. I observed that PDE2A1, PDE2A2 and PDE2A3 predominantly localize to the cytosol, mitochondria and plasma membrane, respectively, as previously shown in other cell types (Acin-Perez et al.,

2011a). The sequence for another PDE2A isoform, PDE2A4, has been deposited (NCBI Reference Sequence: NM_001146209.2), although no further characterization of this isoform is available. For the first time I showed that overexpressed PDE2A4 localizes to the cytosol, although expression of endogenous PDE2A4 could not be detected by RT-PCR in any of the samples tested. This may suggest that isoform 4 of PDE2A is not expressed as a protein or it may be expressed in other cell types/tissues not analyzed in this study.

Using super-resolution microscopy and mitochondria fractionation, I found that most of PDE2A2 localizes to OMM and IMS, and not to the mitochondrial matrix (*Fig. 3.2*) (Monterisi et al., 2017). My analysis also revealed a dotted distribution of PDE2A2 at the mitochondrial membranes, suggesting that this enzyme may be part of a larger protein complexes and may be involved in regulation of cyclic nucleotide signaling at multiple sub-mitochondrial nano-domains. This dotted distribution supports the interaction between PDE2A2 and MINOS complex, since the latter is also organized in clusters at the crista junctions (Jans et al., 2013; Sastri et al., 2017). These results are in contrast with a previous study where PDE2A2 was found to localize to the mitochondrial matrix where it was suggested to control cAMP levels generated by a local sAC (Acin-Perez et al., 2011a). It should be noted that Acin-Perez et al. clearly show by confocal microscopy that PDE2A2 localizes to the edges of mitochondria. Additionally, in Monterisi et al. we showed by EM that the majority of PDE2A2 localizes to mitochondrial membranes, which is in agreement with the observations presented in this thesis. Although we have failed to detect significant PDE2A activity in the mitochondrial matrix using FRET imaging, the possibility remains that a minor fraction of the enzyme localizes to this compartment (Monterisi et al., 2017). However, if that is the case, the PDE2A2 pool localized to the matrix would be completely isolated from cytosolic signaling events due to IMM impermeability to cAMP (Lefkimmiatis et al., 2013).

Overall, my findings indicate that PDE2A2 localizes predominantly to two different mitochondrial sub-compartments, OMM and IMS, respectively, potentially regulating distinct cAMP-dependent functions at these two sites. Since OMM is permeable to cAMP, PDE2A2 localized at the IMS can be reached by cAMP generated at the plasma membrane. However, further research is needed to test this hypothesis.

All PDE2A isoforms share the same sequence for the GAF-A, GAF-B and catalytic domains but they differ in the N-terminal domain, which is responsible for targeting the enzyme to different subcellular compartments (Acin-Perez et al., 2011a; Azevedo et al., 2014). It has been reported that PDE2A2 possesses a mitochondria targeting sequence within its 17 amino acids N-terminal sequence (Acin-Perez et al., 2011a). Generation of multiple PDE2A deletion mutants revealed that a longer N-terminal polypeptide (1-233 residues in the human sequence or residues 1-201 in the mouse sequence) is required for optimal PDE2A2 targeting to the mitochondria (*Fig. 3.3 and 3.4*). As for PDE2A2, deletion of the N-terminus of PDE2A1 and PDE2A4, both of which normally show nuclear exclusion, affects their localization resulting in their ability to also localize to the nucleus. In agreement with previous results, I observed that residues 1-17 of PDE2A2 are required to target the enzyme to the mitochondria since deletion of this region (fragment 17-934) completely abolishes the mitochondria localization. On the other hand, residues 1-17 of PDE2A2 are not sufficient to target the protein to the mitochondria, as shown by fragment 1-17. Moreover, PDE2A3 unique region (residues 1-24) is sufficient to target the protein to the PM. This is in agreement with previous results showing that myristoylation at Glycine 2 underlies membrane targeting of PDE2A3 (Russwurm et al., 2009). I also concluded that GAF and catalytic domains are not required to localize PDE2A isoforms to their respective subcellular location.

8.1.2 PDE2A2 interactors

It has been shown that the biological function of PDE2A depends on its subcellular localization, however, the exact definition of the cAMP subcellular pools under the control of PDE2A is lacking (Monterisi et al., 2017; Zoccarato et al., 2015). Therefore, identification of PDE2A2 binding partners would provide a lead to the identification of these domains and of the cellular functions that are under the selective control of PDE2A2. Additionally, it may provide an avenue for selective displacement, and therefore specific ablation, of PDE2A2 activity at those sites – something that cannot be achieved by pharmacological inhibition, since current inhibitors bind the catalytic site and all PDE2A isoforms share the same catalytic domain. To address this, three independent mass spectrometry experiments were conducted in the laboratory using adult rat cardiomyocytes overexpressing PDE2A2-RFP. I undertook the validation of a number of the most interesting potential interactors and I subsequently focused on the characterization of the interaction with Caveolins, components of the MINOS complex and β-Taxilin.

β-Taxilin is a fairly uncharacterized protein. Data available in the literature suggest that it is a cytosolic protein selectively expressed in skeletal muscle and heart tissues (Fujimori et al., 2002; Uyeda et al., 2000) that may be involved in cell differentiation from myoblasts into myotubes (Sakane et al., 2016). All Taxilins (α, β and γ-Taxilin) have been shown to interact with members of the Syntaxin family, which has been implicated in intracellular vesicle trafficking although, at this time, the precise function of Taxilins in this mechanism is not known. When overexpressed with PDE2A isoforms, I found interaction of β-Taxilin with PDE2A1, PDE2A2 and PDE2A3 in HEK293T cells. The interaction between β-Taxilin and PDE2A involves the GAF domains (*Fig 4.2*). Although the GAF domains would not traditionally be thought to be responsible for interaction with other proteins, as the interaction may interfere

with the cGMP allosteric regulation and dimerization of the PDE2A holoenzyme, co-immunoprecipitation results were clear and reproducible. Surprisingly, only overexpressed PDE2A1, but not the other isoforms, showed interaction with endogenous β-Taxilin in NRVM. This was unexpected because the interaction is mediated by a region (GAF domains) common to all isoforms (*Fig.4.1 and 4.2*). In addition, the original mass spectrometry experiment was performed in adult cardiomyocytes overexpressing PDE2A2, suggesting that isoform 2 would be a strong binding pattern of β-Taxilin. My results also showed that β-Taxilin localization is punctated with a distribution that appears to coincide with cytoskeletal/sarcomeric elements. In order to gain some insight into the role of PDE2A-β-Taxilin interaction, I attempted to disrupt the protein interaction. Unfortunately this was not successful. Further experiments are required to assess the molecular role of β-Taxilin.

8.1.3 PDE2A2 interaction with MINOS complex: role in the regulation of mitochondrial autophagy

The MINOS complex is involved in the maintenance of mitochondria cristae morphology (Hessenberger et al., 2017) and comprises multiple components including Mitofilin, ChChD3 and ChChD6. The complex also directly binds SAMM50, a protein involved in sorting and assembly of mitochondrial complexes and in maintaining the structure of mitochondrial cristae (Ding et al., 2015). The experiments performed here identified PDE2A2 as an interactor of the MINOS complex, via binding to Mitofilin, ChChD3 and SAMM50 (*Fig. 4.6* and 4.7). However, it remains to be established whether PDE2A2 interacts with these three proteins directly or if there is a direct interaction with one of these components only . My data also suggest that the interaction between PDE2A2 and Mitofilin is mediated by the GAF-B domain (*Fig. 5.5*). Interestingly, a loss-of-function homozygous point mutation in the GAF-B domain of PDE2A

has been recently associated with early-onset chorea, a neurological disorder characterized by abnormal involuntary movement (Salpietro et al., 2018). It would be interesting to test if this point mutation could disrupt the interaction between PDE2A2 and Mitofilin and further assess the involvement of this interaction in the context of chorea.

Identifying PDE2A2 as part of the MINOS complex led to the possibility of PDE2A2 playing a significant role in maintaining cristae architecture as disruption of a number of proteins within the MINOS complex significantly altered IMM morphology (Zerbes et al., 2012; Darshi et al., 2012; Rabl et al., 2009). However, EM analysis of MEF PDE2A KO cells showed no changes on the fine mitochondrial structure (*Fig. 5.4*). Thus, PDE2A does not appear to play a role in the regulation of cristae architecture.

Recently, Parkin recruitment to depolarized mitochondria has been shown to be dependent on PKA-mediated phosphorylation of both Mitofilin and ChChD3 (Akabane et al., 2016), leading to reduced PINK-dependent recruitment of Parkin at the mitochondria. Here, for the first time, I demonstrate that PDE2A2 regulates Parkin-dependent mitophagy via PKA-mediated phosphorylation of Mitofilin in the MINOS complex (*Fig. 5.2 and 5.7*). I observed that PDE2A inhibition results in reduced recruitment of Parkin to the mitochondria and reduced mitophagy. Conversely, PDE2A2 overexpression promotes Parkin translocation to damaged mitochondria and enhances mitophagy. When cGMP was used to allosterically activate endogenous PDE2A2, I observed that cGMP treatment induced Parkin recruitment to the mitochondria. Surprisingly however, this effect was maintained in PDE2A KO cells, pointing to a cGMP-dependent but a PDE2A2-independent mechanism (*Fig. 5.9)*. This was confirmed by overexpression of PKG resulting in increased Parkin recruitment to the mitochondria. Thus, while activation of PKA by cAMP prevents Parkin-dependent mitophagy, a process that is inhibited by PDE2A2-dependent degradation of cAMP, activation of PKG by cGMP seems to induce the opposite effect, suggesting that the two cyclic nucleotides regulate Parkin-

dependent mitophagy through separate mechanisms with opposite effects. I propose that a dual-controlled mechanism would allow a fine tuning of Parkin recruitment to the mitochondria. Since PDE2A2 is a potentially 'druggable' enzyme (Maurice et al., 2014a), my findings suggest the novel and exciting possibility that modulation of PDE2A activity may provide a new avenue to control Parkin-dependent mitophagy, a process that is altered in several pathological conditions.

PKA has been shown to phosphorylate ChChd3 and Mitofilin, components of the MINOS complex. In addition, Sphingosine kinase interacting protein (SKIP) has been shown to be an AKAP that anchors exclusively type I PKA holoenzyme in the IMS (Means et al., 2011; Schauble et al., 2007b). Taken together, the results presented here are compatible with a model where PDE2A2 regulates SKIP-tethered PKA activity by modulation of a local pool of cAMP.

We have previously published that PDE2A inhibition affects mitochondria morphology and protects from apoptotic cell death by regulating OMM cAMP levels and PKA-dependent phosphorylation of Dynamin-related protein 1 (Drp1), a GTPase involved in mitochondria fission (Monterisi et al., 2017). Based on the data presented in this thesis, I suggest that OMM PDE2A2 regulates mitochondria morphology while IMS PDE2A2 controls mitochondria degradation through mitophagy. In fact, mitochondria morphology and mitophagy are two interconnected processes. During starvation, cellular cAMP levels increase, leading to Drp1 PKA-mediated phosphorylation and mitochondrial elongation (Gomes et al., 2011). Elongated mitochondria are spared from autophagic degradation, maintaining ATP production (Gomes et al., 2011). Thus, changes in mitochondrial morphology determine the fate of the cell during autophagy. Thus, the cAMP/PDE2A2/PKA axis appears to promote mitochondrial survival by enhancing elongation through the phosphorylation of Drp1 and by inhibiting autophagy through the phosphorylation of the MINOS complex.

8.1.4 PDE2A localization at the ER: regulation of Ca^{2+} handling

The last PDE2A2 protein interactors that I have studied are Caveolins, scaffolding proteins that are the main component of the caveolae (invaginations of the plasma membrane), hubs of Ca^{2+} signaling (Pani and Singh, 2009). Caveolins have also been shown to localize to mitochondria-associated membrane (MAM), domains of intense Ca^{2+} signaling and lipid metabolism (Asterholm et al., 2012; Bosch et al., 2011; Fridolfsson et al., 2012; Sala-Vila et al., 2016; Schilling and Patel, 2016; Volonte et al., 2016). Here I have shown that isoform 2 of PDE2A selectively interacts with Caveolins at the ER-mitochondrial interface (*Fig. 4.4, 6.2 and 6.4*). I have established that this interaction is mediated by an N-terminal region of PDE2A2 (1-41 residues) and the Caveolin signature and scaffolding domains (*Fig. 6.1*). It has been reported that Caveolins act as mitochondrial stress sensor (Volonte et al., 2016). Interestingly, I found that mitochondrial damage induced by oxidative stress or CCCP, a mitochondrial decoupling agent, promotes Caveolin 1-PDE2A2 interaction (*Fig. 6.4*).

In the attempt to establish whether PDE2A2 localization at the MAM may have any role in regulating ER Ca^{2+} handling, I compared ATP-induced Ca^{2+} release from the ER in MEFs PDE2A KO and WT counterparts (*Fig. 6.7*). I found that a smaller proportion of PDE2A KO cells respond with a transient cytosolic Ca^{2+} increase in response to ATP application compared to WT cells. This effect is not due to lower Ca^{2+} stores or reduced IP3R expression level or IP3R PKA-mediated phosphorylation at S1756, suggesting a defect upstream of the ER (*Fig. 6.6 and 6.8*). Interestingly, I found that the reduced response to ATP stimulation in MEF PDE2A KO cells could be rescued by overexpression of PDE2A1 and not by overexpression of PDE2A2 (*Fig. 6.7*). Further experiments will be required to establish the mechanism by which PDE2A1 ablation disrupts ER Ca^{2+} release upon ATP stimulation. Additionally, since I have shown that β-Taxilin selectively interacts with PDE2A1, it would be interesting to study the role of this interaction on ER Ca^{2+} handling.

8.1.5 Phosphatases play a role in cAMP/PKA signaling compartmentalization

cAMP/PKA signaling compartmentalization is based on the idea that different PKA subsets can be activated independently by different stimuli. However, how cAMP signals can selectively activate specific PKA hubs while avoiding non-specific activation of PKA that is free in the cytosol, has remained an open question. One proposed mechanism is that during cAMP elevation, PDEs maintain cytosolic cAMP low resulting in inactive PKA, while higher levels of the messenger are attained at AKAP-bound PKA (Houslay, 2010; Sprenger et al., 2015; Zaccolo and Pozzan, 2002). However, one problem with this model is that it is difficult to explain how higher concentration of cAMP can be attained at these hubs while bulk cAMP is kept at lower levels, except for those locations that are at the plasma membrane in proximity of ACs. In addition, cAMP fast diffusion (around 40μm/s, an order of magnitude lower than in water) would contradict the notion of cAMP microdomains since it would result in simultaneous and homogeneous distribution of cAMP across the cell (Kokkonen and Kass, 2017; Lefkimmiatis and Zaccolo, 2014; Terrin et al., 2006). The fast diffusion of cAMP coupled with low activation threshold of PKA suggests that PKA should be fully activated even under resting conditions since PDE activity would not be enough to maintain the concentration of cAMP below the activation threshold of PKA. However, Koschinski et al. have recently shown that the sensitivity of PKA to cAMP is lower in the cell than previously observed in vitro (Koschinski and Zaccolo, 2017). The authors report a PKA apparent activation constant of 5.2 μM, five times higher than the estimated basal concentration of cAMP, 1 μM. This would suggest that PDEs may play a role in modulation of subcellular cAMP microdomains, since the activation threshold of PKA would be in the same magnitude as the one of PDEs. Furthermore, other factors come into play inside a living cell to slow down cAMP diffusion at specific subcellular locations, including cAMP buffering (Chen et al., 1999; Lefkimmiatis et al., 2009), cytosol viscosity (Feinstein et al.,

2012) and physical barriers (Richards et al., 2016).

Another aspect that appears to contradict the model of cAMP/PKA compartmentalized signaling is the PKA activation modality, in which PKA C subunits are released from anchored R-subunits on cAMP binding, potentially obliterating any advantage of PKA anchoring to AKAPs. Recent studies have provided some possible alternatives to this model. Walker-Gray et al. have recently shown that R subunits are always in large molar excess compared with C subunits (average ~17-fold). This suggests that the range over which the C subunit can phosphorylate substrates will depend on its rate of diffusion and the rate of recapture by R subunits (Walker-Gray et al., 2017). Another possibility has been proposed by Smith et al. They suggest that for the C subunit to phosphorylate its targets, dissociation from R subunit is not necessary. Thus, catalytically active PKA holoenzymes remain intact, which would generate a highly compartmentalized signal (Smith et al., 2013, 2017). However, other studies have shown that on cAMP elevation the C subunit can diffuse and translocate into the nucleus to phosphorylate transcription factors (Harootunian et al., 1993). Future experiments may shed some light into this open and highly controversial question.

Phosphatases are another important component of the cAMP/PKA signaling cascade to consider as, by dephosphorylating PKA targets, they are the last layer of control that can terminate the signal. Here, I have shown that a rise in cAMP that activates PKA at the ER fails to induce comparable PKA activity in the cytosol of HEK293T, HeLa and NRVM cells. This is due to differences in phosphatase activity between cytosol and ER rather than differences in the cAMP levels or PDE activity. According to the PKA activation model, my results suggest that even if C subunits are released from a certain domain into the bulk cytosol, strong phosphatase activity could counteract their effect. Interestingly, a previous study comparing the activity of PKA at the OMM and in the cytosol also found relatively enhanced phosphorylation at the OMM in the face of equal increase in cAMP in the two compartments (Lefkimmiatis et al., 2013). Lefkimmiatis et al. concluded that the OMM is a privileged cAMP

signaling microdomain with high PKA activity compared to the bulk cytosol. My results considered in combination with the previous study suggest a different interpretation: rather than the mitochondria being a compartment with more persistent PKA activity, the bulk cytosol appears to be a site with high phosphatase activity. This arrangement would provide a level of control over inappropriate activation of cytosolic, non-anchored PKA as well as over target phosphorylation by C subunits that may diffuse away from localized signalosomes upon activation. This feature of phosphatase-dependent regulation of bulk cytosolic PKA activity may be an important contributing factor to the achievement of response specificity.

8.2 Concluding remarks

All second messengers, including cAMP, cGMP, IP3 and Ca^{2+}, have been shown to be highly regulated and interconnected (Brescia and Zaccolo, 2016; Connor, 1993; Konieczny et al., 2017; Shapira et al., 1990). Here, although the focus was on cAMP/PKA signaling, I was unexpectedly diverged into considering the interaction of cAMP with other second messengers. The results of my studies show that PDE2A plays an important role on the interconnectivity of multiple signaling systems by being able to regulate both cyclic nucleotides and by affecting IP3 and Ca^{2+} signaling at the ER, a feature that had not been appreciated so far. Specifically, I have shown that PDE2A2 regulates a cAMP pool at the mitochondria involved in regulation of mitochondria degradation by mitophagy, while the cGMP signaling pathway also seems to be involved in the regulation of this process. In addition, I observed that PDE2A ablation disrupts IP3-dependent ER Ca^{2+} release, although the exact mechanism remains to be established. Overall, PDE2A emerges as an integrator of multiple signaling systems promoting robustness and plasticity of cellular functions.

Chapter 9 - Appendices

9.1 Timing and Venue of Research

The research presented in this thesis was performed from October 2015 to January 2018 in the Departments of Physiology, Anatomy and Genetics (DPAG) in the University of Oxford, United Kingdom, and May 2016 in The European Molecular Biology Laboratory (EMBL), Heidelberg, Germany. The research supervisor was Professor Manuela Zaccolo (DPAG).

9.2 Research Funding

The D.Phil. project was funded by a Medical Research Council (MRC) studentship and funds from the British Heart Foundation to Manuela Zaccolo. Additional grants were awarded to sponsor this project:

- 2018: St John's College Special Grant to sponsor attendance of a conference (Japan) – 900£
- 2017: British Heart Foundation (BHF) Centre of Research Excellence (CRE) pump priming project – 11.000£
- 2017: MRC Supplementary Funding to sponsor D.Phil. research projects – 5.000£
- 2017: DPAG Travel grant to sponsor attendance of a conference (USA) – 500£
- 2017: St John's College Special Grant to sponsor attendance of a conference (USA) – 800£
- 2016: MRC Supplementary Funding to sponsor my D.Phil. research projects – 2.400£
- 2016: St John's College Special Grant to sponsor my D.Phil. research projects – 700£
- 2015: Santander Travel Award to sponsor training in super resolution imaging – 600£
- 2015: MRC Supplementary Funding to sponsor my D.Phil. research projects – 1.200£

9.3 Publications arising from this work

- Lobo, M.J., *et al.* PDE2A2 regulates PKA-mediated phosphorylation of Mitofilin and Parkin-dependent mitophagy, manuscript in preparation

- Lobo, M.J., and Zaccolo, M. Compartmentalization of cAMP signaling, manuscript in preparation. *Pharmacological Reviews*

- Lobo, M.J., and Zaccolo, M. (2018). PDE2A. in Encyclopedia of Signaling Molecules, Vol. 2 (ed. Choi, S.). *Springer International Publishing*

- Monterisi, S., Lobo, M.J., Livie, C., Castle, J.C., Weinberger, M., Baillie, G.S., Surdo, N.C., Musheshe, N., Stangherlin, A., Gottlieb, E., et al. (2017). PDE2A2 regulates mitochondria morphology and apoptotic cell death via local modulation of cAMP/PKA signaling. *ELife 6*

Chapter 10 - References

Aaron, J.S., Taylor, A.B., and Chew, T.-L. (2018). Image co-localization – co-occurrence versus correlation. J. Cell Sci. *131*, jcs211847.

Abrenica, B., AlShaaban, M., and Czubryt, M.P. (2009). The A-kinase anchor protein AKAP121 is a negative regulator of cardiomyocyte hypertrophy. J. Mol. Cell. Cardiol. *46*, 674–681.

Acin-Perez, R., Salazar, E., Kamenetsky, M., Buck, J., Levin, L.R., and Manfredi, G. (2009a). Cyclic AMP produced inside mitochondria regulates oxidative phosphorylation. Cell Metab. *9*, 265–276.

Acin-Perez, R., Salazar, E., Brosel, S., Yang, H., Schon, E.A., and Manfredi, G. (2009b). Modulation of mitochondrial protein phosphorylation by soluble adenylyl cyclase ameliorates cytochrome oxidase defects. EMBO Mol. Med. *1*, 392–406.

Acin-Perez, R., Russwurm, M., Günnewig, K., Gertz, M., Zoidl, G., Ramos, L., Buck, J., Levin, L.R., Rassow, J., Manfredi, G., et al. (2011a). A phosphodiesterase 2A isoform localized to mitochondria regulates respiration. J. Biol. Chem. *286*, 30423–30432.

Acin-Perez, R., Gatti, D.L., Bai, Y., and Manfredi, G. (2011b). Protein phosphorylation and prevention of cytochrome oxidase inhibition by ATP: coupled mechanisms of energy metabolism regulation. Cell Metab. *13*, 712–719.

Affaitati, A., Cardone, L., de Cristofaro, T., Carlucci, A., Ginsberg, M.D., Varrone, S., Gottesman, M.E., Avvedimento, E.V., and Feliciello, A. (2003). Essential role of A-kinase anchor protein 121 for cAMP signaling to mitochondria. J. Biol. Chem. *278*, 4286–4294.

Ahmad, F., Shen, W., Vandeput, F., Szabo-Fresnais, N., Krall, J., Degerman, E., Goetz, F., Klussmann, E., Movsesian, M., and Manganiello, V. (2015). Regulation of sarcoplasmic reticulum Ca2+ ATPase 2 (SERCA2) activity by phosphodiesterase 3A (PDE3A) in human myocardium: phosphorylation-dependent interaction of PDE3A1 with SERCA2. J. Biol. Chem. *290*, 6763–6776.

Akabane, S., Uno, M., Tani, N., Shimazaki, S., Ebara, N., Kato, H., Kosako, H., and Oka, T. (2016). PKA Regulates PINK1 Stability and Parkin Recruitment to Damaged Mitochondria through Phosphorylation of MIC60. Mol. Cell *62*, 371–384.

Alcalay, Y., Hochhauser, E., Kliminski, V., Dick, J., Zahalka, M.A., Parnes, D., Schlesinger, H., Abassi, Z., Shainberg, A., Schindler, R.F.R., et al. (2013). Popeye Domain Containing 1 (Popdc1/Bves) Is a Caveolae-Associated Protein Involved in Ischemia Tolerance. PLOS ONE *8*, e71100.

Allen, M.D., and Zhang, J. (2006). Subcellular dynamics of protein kinase A activity visualized by FRET-based reporters. Biochem. Biophys. Res. Commun. *348*, 716–721.

Alto, N.M., Soderling, J., and Scott, J.D. (2002). Rab32 is an A-kinase anchoring protein and participates in mitochondrial dynamics. J. Cell Biol. *158*, 659–668.

Andrée, B., Hillemann, T., Kessler-Icekson, G., Schmitt-John, T., Jockusch, H., Arnold, H.-H., and Brand, T. (2000). Isolation and Characterization of the Novel Popeye Gene Family Expressed in Skeletal Muscle and Heart. Dev. Biol. *223*, 371–382.

Aoyama, H., Ikeda, Y., Miyazaki, Y., Yoshimura, K., Nishino, S., Yamamoto, T., Yano, M., Inui, M., Aoki, H., and Matsuzaki, M. (2011). Isoform-specific roles of protein phosphatase 1 catalytic subunits in sarcoplasmic reticulum-mediated Ca(2+) cycling. Cardiovasc. Res. *89*, 79–88.

Appukuttan, A., Kasseckert, S.A., Micoogullari, M., Flacke, J.-P., Kumar, S., Woste, A., Abdallah, Y., Pott, L., Reusch, H.P., and Ladilov, Y. (2012). Type 10 adenylyl cyclase mediates mitochondrial Bax translocation and apoptosis of adult rat cardiomyocytes under simulated ischaemia/reperfusion. Cardiovasc. Res. *93*, 340–349.

Armstrong, L.C., Saenz, A.J., and Bornstein, P. (1999). Metaxin 1 interacts with metaxin 2, a novel related protein associated with the mammalian mitochondrial outer membrane. J. Cell. Biochem. *74*, 11–22.

Asirvatham, A.L., Galligan, S.G., Schillace, R.V., Davey, M.P., Vasta, V., Beavo, J.A., and Carr, D.W. (2004). A-kinase anchoring proteins interact with phosphodiesterases in T lymphocyte cell lines. J. Immunol. Baltim. Md 1950 *173*, 4806–4814.

Assenza, M.R., Barbagallo, F., Barrios, F., Cornacchione, M., Campolo, F., Vivarelli, E., Gianfrilli, D., Auletta, L., Soricelli, A., Isidori, A.M., et al. (2018). Critical role of Phosphodiesterase 2A in mouse congenital heart defects. Cardiovasc. Res.

Asterholm, I.W., Mundy, D.I., Weng, J., Anderson, R.G.W., and Scherer, P.E. (2012). Altered mitochondrial function and metabolic inflexibility associated with loss of caveolin-1. Cell Metab. *15*, 171–185.

Aye, T.-T., Soni, S., van Veen, T.A.B., van der Heyden, M.A.G., Cappadona, S., Varro, A., de Weger, R.A., de Jonge, N., Vos, M.A., Heck, A.J.R., et al. (2012). Reorganized PKA-AKAP associations in the failing human heart. J. Mol. Cell. Cardiol. *52*, 511–518.

Azevedo, M.F., Faucz, F.R., Bimpaki, E., Horvath, A., Levy, I., de Alexandre, R.B., Ahmad, F., Manganiello, V., and Stratakis, C.A. (2014). Clinical and molecular genetics of the phosphodiesterases (PDEs). Endocr. Rev. *35*, 195–233.

Bachmann, V.A., Mayrhofer, J.E., Ilouz, R., Tschaikner, P., Raffeiner, P., Röck, R., Courcelles, M., Apelt, F., Lu, T.-W., Baillie, G.S., et al. (2016). Gpr161 anchoring of PKA consolidates GPCR and cAMP signaling. Proc. Natl. Acad. Sci. U. S. A. *113*, 7786–7791.

Baillie, G.S., and Houslay, M.D. (2005). Arrestin times for compartmentalised cAMP signalling and phosphodiesterase-4 enzymes. Curr. Opin. Cell Biol. *17*, 129–134.

Baillie, G.S., Sood, A., McPhee, I., Gall, I., Perry, S.J., Lefkowitz, R.J., and Houslay, M.D. (2003). β-Arrestin-mediated PDE4 cAMP phosphodiesterase recruitment regulates β-adrenoceptor switching from Gs to Gi. Proc. Natl. Acad. Sci. *100*, 940–945.

Banky, P., Huang, L.J.-S., and Taylor, S.S. (1998). Dimerization/Docking Domain of the Type Iα Regulatory Subunit of cAMP-dependent Protein Kinase REQUIREMENTS FOR DIMERIZATION AND DOCKING ARE DISTINCT BUT OVERLAPPING. J. Biol. Chem. *273*, 35048–35055.

Bauman, A.L., Soughayer, J., Nguyen, B.T., Willoughby, D., Carnegie, G.K., Wong, W., Hoshi, N., Langeberg, L.K., Cooper, D.M.F., Dessauer, C.W., et al. (2006). Dynamic Regulation of

cAMP Synthesis through Anchored PKA-Adenylyl Cyclase V/VI Complexes. Mol. Cell *23*, 925–931.

Beavo, J.A., and Brunton, L.L. (2002). Cyclic nucleotide research -- still expanding after half a century. Nat. Rev. Mol. Cell Biol. *3*, 710–718.

Beavo, J.A., Bechtel, P.J., and Krebs, E.G. (1974). Activation of protein kinase by physiological concentrations of cyclic AMP. Proc. Natl. Acad. Sci. U. S. A. *71*, 3580–3583.

Beca, S., Helli, P.B., Simpson, J.A., Zhao, D., Farman, G.P., Jones, P., Tian, X., Wilson, L.S., Ahmad, F., Chen, S.R.W., et al. (2011). Phosphodiesterase 4D regulates baseline sarcoplasmic reticulum Ca2+ release and cardiac contractility, independently of L-type Ca2+ current. Circ. Res. *109*, 1024–1030.

Beca, S., Ahmad, F., Shen, W., Liu, J., Makary, S., Polidovitch, N., Sun, J., Hockman, S., Chung, Y.W., Movsesian, M., et al. (2013). Phosphodiesterase type 3A regulates basal myocardial contractility through interacting with sarcoplasmic reticulum calcium ATPase type 2a signaling complexes in mouse heart. Circ. Res. *112*, 289–297.

Bender, A.T., and Beavo, J.A. (2006). Cyclic nucleotide phosphodiesterases: molecular regulation to clinical use. Pharmacol. Rev. *58*, 488–520.

Bers, D.M. (2006). Cardiac ryanodine receptor phosphorylation: target sites and functional consequences. Biochem. J. *396*, e1-3.

Berthouze-Duquesnes, M., Lucas, A., Saulière, A., Sin, Y.Y., Laurent, A.-C., Galés, C., Baillie, G., and Lezoualc'h, F. (2013). Specific interactions between Epac1, β-arrestin2 and PDE4D5 regulate β-adrenergic receptor subtype differential effects on cardiac hypertrophic signaling. Cell. Signal. *25*, 970–980.

Biel, M., and Michalakis, S. (2009). Cyclic Nucleotide-Gated Channels. In CGMP: Generators, Effectors and Therapeutic Implications, (Springer, Berlin, Heidelberg), pp. 111–136.

Bitterman, J.L., Ramos-Espiritu, L., Diaz, A., Levin, L.R., and Buck, J. (2013). Pharmacological distinction between soluble and transmembrane adenylyl cyclases. J. Pharmacol. Exp. Ther. *347*, 589–598.

Boess, F.G., Hendrix, M., van der Staay, F.-J., Erb, C., Schreiber, R., van Staveren, W., de Vente, J., Prickaerts, J., Blokland, A., and Koenig, G. (2004). Inhibition of phosphodiesterase 2 increases neuronal cGMP, synaptic plasticity and memory performance. Neuropharmacology *47*, 1081–1092.

Bogard, A.S., Xu, C., and Ostrom, R.S. (2011). Human bronchial smooth muscle cells express adenylyl cyclase isoforms 2, 4, and 6 in distinct membrane microdomains. J. Pharmacol. Exp. Ther. *337*, 209–217.

Bomar, J., Moreira, P., Balise, J.J., and Collas, P. (2002). Differential regulation of maternal and paternal chromosome condensation in mitotic zygotes. J. Cell Sci. *115*, 2931–2940.

Börner, S., Schwede, F., Schlipp, A., Berisha, F., Calebiro, D., Lohse, M.J., and Nikolaev, V.O. (2011). FRET measurements of intracellular cAMP concentrations and cAMP analog permeability in intact cells. Nat. Protoc. *6*, 427–438.

Bos, J.L. (2006). Epac proteins: multi-purpose cAMP targets. Trends Biochem. Sci. *31*, 680–686.

Bosch, M., Marí, M., Herms, A., Fernández, A., Fajardo, A., Kassan, A., Giralt, A., Colell, A., Balgoma, D., Barbero, E., et al. (2011). Caveolin-1 deficiency causes cholesterol-dependent mitochondrial dysfunction and apoptotic susceptibility. Curr. Biol. CB *21*, 681–686.

Brand, T., and Schindler, R. (2017). New kids on the block: The Popeye domain containing (POPDC) protein family acting as a novel class of cAMP effector proteins in striated muscle. Cell. Signal. *40*, 156–165.

Braun, T. (1975). The effect of divalent cations on bovine spermatozoal adenylate cyclase activity. J. Cyclic Nucleotide Res. *1*, 271–281.

Braun, T., and Dods, R.F. (1975). Development of a Mn-2+-sensitive, “soluble” adenylate cyclase in rat testis. Proc. Natl. Acad. Sci. U. S. A. *72*, 1097–1101.

Brescia, M., and Zaccolo, M. (2016). Modulation of Compartmentalised Cyclic Nucleotide Signalling via Local Inhibition of Phosphodiesterase Activity. Int. J. Mol. Sci. *17*.

Bridges, D., MacDonald, J.A., Wadzinski, B., and Moorhead, G.B.G. (2006). Identification and characterization of D-AKAP1 as a major adipocyte PKA and PP1 binding protein. Biochem. Biophys. Res. Commun. *346*, 351–357.

Brisson, G.R., Malaisse-Lagae, F., and Malaisse, W.J. (1972). The stimulus-secretion coupling of glucose-induced insulin release. VII. A proposed site of action for adenosine-3’,5’-cyclic monophosphate. J. Clin. Invest. *51*, 232–241.

de Brito, O.M., and Scorrano, L. (2008). Mitofusin 2 tethers endoplasmic reticulum to mitochondria. Nature *456*, 605–610.

de Brito, O.M., and Scorrano, L. (2010). An intimate liaison: spatial organization of the endoplasmic reticulum-mitochondria relationship. EMBO J. *29*, 2715–2723.

Brown, R.L., Strassmaier, T., Brady, J.D., and Karpen, J.W. (2006). The Pharmacology of Cyclic Nucleotide-Gated Channels: Emerging from the Darkness. Curr. Pharm. Des. *12*, 3597–3613.

Bubb, K.J., Trinder, S.L., Baliga, R.S., Patel, J., Clapp, L.H., MacAllister, R.J., and Hobbs, A.J. (2014). Inhibition of phosphodiesterase 2 augments cGMP and cAMP signaling to ameliorate pulmonary hypertension. Circulation *130*, 496–507.

Bui, M., Gilady, S.Y., Fitzsimmons, R.E.B., Benson, M.D., Lynes, E.M., Gesson, K., Alto, N.M., Strack, S., Scott, J.D., and Simmen, T. (2010). Rab32 modulates apoptosis onset and mitochondria-associated membrane (MAM) properties. J. Biol. Chem. *285*, 31590–31602.

Burgers, P.P., Ma, Y., Margarucci, L., Mackey, M., van der Heyden, M.A.G., Ellisman, M., Scholten, A., Taylor, S.S., and Heck, A.J.R. (2012). A small novel A-kinase anchoring protein (AKAP) that localizes specifically protein kinase A-regulatory subunit I (PKA-RI) to the plasma membrane. J. Biol. Chem. *287*, 43789–43797.

Burgers, P.P., Bruystens, J., Burnley, R.J., Nikolaev, V.O., Keshwani, M., Wu, J., Janssen, B.J.C., Taylor, S.S., Heck, A.J.R., and Scholten, A. (2016). Structure of smAKAP and its regulation by PKA-mediated phosphorylation. FEBS J. *283*, 2132–2148.

Calaghan, S., Kozera, L., and White, E. (2008). Compartmentalisation of cAMP-dependent signalling by caveolae in the adult cardiac myocyte. J. Mol. Cell. Cardiol. *45*, 88–92.

Calebiro, D., Nikolaev, V.O., Gagliani, M.C., de Filippis, T., Dees, C., Tacchetti, C., Persani, L., and Lohse, M.J. (2009). Persistent cAMP-signals triggered by internalized G-protein-coupled receptors. PLoS Biol. *7*, e1000172.

Calebiro, D., Nikolaev, V.O., and Lohse, M.J. (2010). Imaging of persistent cAMP signaling by internalized G protein-coupled receptors. J. Mol. Endocrinol. *45*, 1–8.

Capozza, F., Cohen, A.W., Cheung, M.W.-C., Sotgia, F., Schubert, W., Battista, M., Lee, H., Frank, P.G., and Lisanti, M.P. (2005). Muscle-specific interaction of caveolin isoforms: differential complex formation between caveolins in fibroblastic vs. muscle cells. Am. J. Physiol. Cell Physiol. *288*, C677-691.

Carlisle Michel, J.J., Dodge, K.L., Wong, W., Mayer, N.C., Langeberg, L.K., and Scott, J.D. (2004). PKA-phosphorylation of PDE4D3 facilitates recruitment of the mAKAP signalling complex. Biochem. J. *381*, 587–592.

Carlson, C.R., Lygren, B., Berge, T., Hoshi, N., Wong, W., Taskén, K., and Scott, J.D. (2006). Delineation of type I protein kinase A-selective signaling events using an RI anchoring disruptor. J. Biol. Chem. *281*, 21535–21545.

Carr, D.W., Hausken, Z.E., Fraser, I.D., Stofko-Hahn, R.E., and Scott, J.D. (1992). Association of the type II cAMP-dependent protein kinase with a human thyroid RII-anchoring protein. Cloning and characterization of the RII-binding domain. J. Biol. Chem. *267*, 13376–13382.

Cazorla, O., Lucas, A., Poirier, F., Lacampagne, A., and Lezoualc'h, F. (2009). The cAMP binding protein Epac regulates cardiac myofilament function. Proc. Natl. Acad. Sci. *106*, 14144–14149.

Cegielska, A., Shaffer, S., Derua, R., Goris, J., and Virshup, D.M. (1994). Different oligomeric forms of protein phosphatase 2A activate and inhibit simian virus 40 DNA replication. Mol. Cell. Biol. *14*, 4616–4623.

Cercek, B., and Houslay, M.D. (1982). Submitochondrial localization and asymmetric disposition of two peripheral cyclic nucleotide phosphodiesterases. Biochem. J. *207*, 123–132.

Chakrabarti, S., Chang, A., Liu, N.-J., and Gintzler, A.R. (2016). Chronic opioid treatment augments caveolin-1 scaffolding: relevance to stimulatory mu-opioid receptor adenylyl cyclase signaling. J. Neurochem. *139*, 737–747.

Chen, C., Nakamura, T., and Koutalos, Y. (1999). Cyclic AMP diffusion coefficient in frog olfactory cilia. Biophys. J. *76*, 2861–2867.

Chen, Y., Cann, M.J., Litvin, T.N., Iourgenko, V., Sinclair, M.L., Levin, L.R., and Buck, J. (2000). Soluble adenylyl cyclase as an evolutionarily conserved bicarbonate sensor. Science *289*, 625–628.

Christian, F., Szaszák, M., Friedl, S., Drewianka, S., Lorenz, D., Goncalves, A., Furkert, J., Vargas, C., Schmieder, P., Götz, F., et al. (2011). Small molecule AKAP-protein kinase A (PKA) interaction disruptors that activate PKA interfere with compartmentalized cAMP signaling in cardiac myocytes. J. Biol. Chem. *286*, 9079–9096.

Chu, C.T., Ji, J., Dagda, R.K., Jiang, J.F., Tyurina, Y.Y., Kapralov, A.A., Tyurin, V.A., Yanamala, N., Shrivastava, I.H., Mohammadyani, D., et al. (2013). Cardiolipin externalization to the outer mitochondrial membrane acts as an elimination signal for mitophagy in neuronal cells. Nat. Cell Biol. *15*, 1197–1205.

Claypool, S.M., and Koehler, C.M. (2012). The complexity of cardiolipin in health and disease. Trends Biochem. Sci. *37*, 32–41.

Coghlan, V.M., Langeberg, L.K., Fernandez, A., Lamb, N.J., and Scott, J.D. (1994). Cloning and characterization of AKAP 95, a nuclear protein that associates with the regulatory subunit of type II cAMP-dependent protein kinase. J. Biol. Chem. *269*, 7658–7665.

Cohen, A.W., Razani, B., Schubert, W., Williams, T.M., Wang, X.B., Iyengar, P., Brasaemle, D.L., Scherer, P.E., and Lisanti, M.P. (2004). Role of caveolin-1 in the modulation of lipolysis and lipid droplet formation. Diabetes *53*, 1261–1270.

Collas, P., Le Guellec, K., and Taskén, K. (1999). The A-kinase-anchoring protein AKAP95 is a multivalent protein with a key role in chromatin condensation at mitosis. J. Cell Biol. *147*, 1167–1180.

Connor, J.A. (1993). Intracellular calcium mobilization by inositol 1,4,5-trisphosphate: intracellular movements and compartmentalization. Cell Calcium *14*, 185–200.

Consonni, S.V., Gloerich, M., Spanjaard, E., and Bos, J.L. (2012). cAMP regulates DEP domain-mediated binding of the guanine nucleotide exchange factor Epac1 to phosphatidic acid at the plasma membrane. Proc. Natl. Acad. Sci. U. S. A. *109*, 3814–3819.

Cooper, D.M.F., and Crossthwaite, A.J. (2006). Higher-order organization and regulation of adenylyl cyclases. Trends Pharmacol. Sci. *27*, 426–431.

Covian, R., French, S., Kusnetz, H., and Balaban, R.S. (2014). Stimulation of oxidative phosphorylation by calcium in cardiac mitochondria is not influenced by cAMP and PKA activity. Biochim. Biophys. Acta *1837*, 1913–1921.

Crossthwaite, A.J., Ciruela, A., Rayner, T.F., and Cooper, D.M.F. (2006). A direct interaction between the N terminus of adenylyl cyclase AC8 and the catalytic subunit of protein phosphatase 2A. Mol. Pharmacol. *69*, 608–617.

Cuende, J., Moreno, S., Bolaños, J.P., and Almeida, A. (2008). Retinoic acid downregulates Rae1 leading to APC(Cdh1) activation and neuroblastoma SH-SY5Y differentiation. Oncogene *27*, 3339–3344.

Darshi, M., Mendiola, V.L., Mackey, M.R., Murphy, A.N., Koller, A., Perkins, G.A., Ellisman, M.H., and Taylor, S.S. (2011). ChChd3, an inner mitochondrial membrane protein, is essential for maintaining crista integrity and mitochondrial function. J. Biol. Chem. *286*, 2918–2932.

Darshi, M., Trinh, K.N., Murphy, A.N., and Taylor, S.S. (2012). Targeting and import mechanism of coiled-coil helix coiled-coil helix domain-containing protein 3 (ChChd3) into the mitochondrial intermembrane space. J. Biol. Chem. *287*, 39480–39491.

Das Banerjee, T., Dagda, R.Y., Dagda, M., Chu, C.T., Rice, M., Vazquez-Mayorga, E., and Dagda, R.K. (2017). PINK1 regulates mitochondrial trafficking in dendrites of cortical neurons through mitochondrial PKA. J. Neurochem. *142*, 545–559.

Dasari, A., Bartholomew, J.N., Volonte, D., and Galbiati, F. (2006). Oxidative stress induces premature senescence by stimulating caveolin-1 gene transcription through p38 mitogen-activated protein kinase/Sp1-mediated activation of two GC-rich promoter elements. Cancer Res. *66*, 10805–10814.

DeGrande, S.T., Little, S.C., Nixon, D.J., Wright, P., Snyder, J., Dun, W., Murphy, N., Kilic, A., Higgins, R., Binkley, P.F., et al. (2013). Molecular mechanisms underlying cardiac protein phosphatase 2A regulation in heart. J. Biol. Chem. *288*, 1032–1046.

Dema, A., Schröter, M.F., Perets, E., Skroblin, P., Moutty, M.C., Deàk, V.A., Birchmeier, W., and Klussmann, E. (2016). The A-Kinase Anchoring Protein (AKAP) Glycogen Synthase Kinase 3β Interaction Protein (GSKIP) Regulates β-Catenin through Its Interactions with Both Protein Kinase A (PKA) and GSK3β. J. Biol. Chem. *291*, 19618–19630.

Denton, R.M. (2009). Regulation of mitochondrial dehydrogenases by calcium ions. Biochim. Biophys. Acta *1787*, 1309–1316.

Depry, C., Allen, M.D., and Zhang, J. (2011). Visualization of PKA activity in plasma membrane microdomains. Mol. Biosyst. *7*, 52–58.

DeSouza, N., Reiken, S., Ondrias, K., Yang, Y.-M., Matkovich, S., and Marks, A.R. (2002). Protein kinase A and two phosphatases are components of the inositol 1,4,5-trisphosphate receptor macromolecular signaling complex. J. Biol. Chem. *277*, 39397–39400.

Dessauer, C.W. (2009). Adenylyl Cyclase–A-kinase Anchoring Protein Complexes: The Next Dimension in cAMP Signaling. Mol. Pharmacol. *76*, 935–941.

Di Benedetto, G., Zoccarato, A., Lissandron, V., Terrin, A., Li, X., Houslay, M.D., Baillie, G.S., and Zaccolo, M. (2008). Protein kinase A type I and type II define distinct intracellular signaling compartments. Circ. Res. *103*, 836–844.

Di Benedetto, G., Scalzotto, E., Mongillo, M., and Pozzan, T. (2013). Mitochondrial Ca^{2+} uptake induces cyclic AMP generation in the matrix and modulates organelle ATP levels. Cell Metab. *17*, 965–975.

Ding, C., Wu, Z., Huang, L., Wang, Y., Xue, J., Chen, S., Deng, Z., Wang, L., Song, Z., and Chen, S. (2015). Mitofilin and CHCHD6 physically interact with Sam50 to sustain cristae structure. Sci. Rep. *5*, 16064.

DiPilato, L.M., Cheng, X., and Zhang, J. (2004). Fluorescent indicators of cAMP and Epac activation reveal differential dynamics of cAMP signaling within discrete subcellular compartments. Proc. Natl. Acad. Sci. U. S. A. *101*, 16513–16518.

Dodge-Kafka, K.L., Bauman, A., Mayer, N., Henson, E., Heredia, L., Ahn, J., McAvoy, T., Nairn, A.C., and Kapiloff, M.S. (2010). cAMP-stimulated protein phosphatase 2A activity associated with muscle A kinase-anchoring protein (mAKAP) signaling complexes inhibits the phosphorylation and activity of the cAMP-specific phosphodiesterase PDE4D3. J. Biol. Chem. *285*, 11078–11086.

Dostmann, W.R., Taylor, S.S., Genieser, H.G., Jastorff, B., Døskeland, S.O., and Ogreid, D. (1990). Probing the cyclic nucleotide binding sites of cAMP-dependent protein kinases I and II with analogs of adenosine 3',5'-cyclic phosphorothioates. J. Biol. Chem. *265*, 10484–10491.

Drab, M., Verkade, P., Elger, M., Kasper, M., Lohn, M., Lauterbach, B., Menne, J., Lindschau, C., Mende, F., Luft, F.C., et al. (2001). Loss of caveolae, vascular dysfunction, and pulmonary defects in caveolin-1 gene-disrupted mice. Science *293*, 2449–2452.

Dupré, D.J., Baragli, A., Rebois, R.V., Ethier, N., and Hébert, T.E. (2007). Signalling complexes associated with adenylyl cyclase II are assembled during their biosynthesis. Cell. Signal. *19*, 481–489.

Dupree, P., Parton, R.G., Raposo, G., Kurzchalia, T.V., and Simons, K. (1993). Caveolae and sorting in the trans-Golgi network of epithelial cells. EMBO J. *12*, 1597–1605.

Eide, T., Coghlan, V., Orstavik, S., Holsve, C., Solberg, R., Skålhegg, B.S., Lamb, N.J., Langeberg, L., Fernandez, A., Scott, J.D., et al. (1998). Molecular cloning, chromosomal localization, and cell cycle-dependent subcellular distribution of the A-kinase anchoring protein, AKAP95. Exp. Cell Res. *238*, 305–316.

Eide, T., Taskén, K.A., Carlson, C., Williams, G., Jahnsen, T., Taskén, K., and Collas, P. (2003). Protein kinase A-anchoring protein AKAP95 interacts with MCM2, a regulator of DNA replication. J. Biol. Chem. *278*, 26750–26756.

Ellisdon, A.M., and Halls, M.L. (2016). Compartmentalization of GPCR signalling controls unique cellular responses. Biochem. Soc. Trans. *44*, 562–567.

Erneux, C., Couchie, D., and Dumont, J.E. (1980). Characterization of horse thyroid cyclic nucleotide phosphodiesterases. Eur. J. Biochem. FEBS *104*, 297–304.

Fan, J.Y., Carpentier, J.L., van Obberghen, E., Grunfeld, C., Gorden, P., and Orci, L. (1983). Morphological changes of the 3T3-L1 fibroblast plasma membrane upon differentiation to the adipocyte form. J. Cell Sci. *61*, 219–230.

Feinstein, W.P., Zhu, B., Leavesley, S.J., Sayner, S.L., and Rich, T.C. (2012). Assessment of cellular mechanisms contributing to cAMP compartmentalization in pulmonary microvascular endothelial cells. Am. J. Physiol. Cell Physiol. *302*, C839-852.

Ferguson, S.S. (2001). Evolving concepts in G protein-coupled receptor endocytosis: the role in receptor desensitization and signaling. Pharmacol. Rev. *53*, 1–24.

Ferrandon, S., Feinstein, T.N., Castro, M., Wang, B., Bouley, R., Potts, J.T., Gardella, T.J., and Vilardaga, J.-P. (2009). Sustained cyclic AMP production by parathyroid hormone receptor endocytosis. Nat. Chem. Biol. *5*, 734–742.

Ferris, C.D., Cameron, A.M., Bredt, D.S., Huganir, R.L., and Snyder, S.H. (1991). Inositol 1,4,5-trisphosphate receptor is phosphorylated by cyclic AMP-dependent protein kinase at serines 1755 and 1589. Biochem. Biophys. Res. Commun. *175*, 192–198.

Fesenko, E.E., Kolesnikov, S.S., and Lyubarsky, A.L. (1985). Induction by cyclic GMP of cationic conductance in plasma membrane of retinal rod outer segment. Nature *313*, 310.

Fra, A.M., Williamson, E., Simons, K., and Parton, R.G. (1995). De novo formation of caveolae in lymphocytes by expression of VIP21-caveolin. Proc. Natl. Acad. Sci. U. S. A. *92*, 8655–8659.

Francis, S.H., Corbin, J.D., and Bischoff, E. (2009). Cyclic GMP-hydrolyzing phosphodiesterases. Handb. Exp. Pharmacol. 367–408.

Francis, S.H., Houslay, M.D., and Conti, M. (2011). Phosphodiesterase inhibitors: factors that influence potency, selectivity, and action. Handb. Exp. Pharmacol. 47–84.

Fridolfsson, H.N., Kawaraguchi, Y., Ali, S.S., Panneerselvam, M., Niesman, I.R., Finley, J.C., Kellerhals, S.E., Migita, M.Y., Okada, H., Moreno, A.L., et al. (2012). Mitochondria-localized caveolin in adaptation to cellular stress and injury. FASEB J. Off. Publ. Fed. Am. Soc. Exp. Biol. *26*, 4637–4649.

Friedman, J.R., Mourier, A., Yamada, J., McCaffery, J.M., and Nunnari, J. (2015). MICOS coordinates with respiratory complexes and lipids to establish mitochondrial inner membrane architecture. ELife *4*.

Froese, A., Breher, S.S., Waldeyer, C., Schindler, R.F.R., Nikolaev, V.O., Rinné, S., Wischmeyer, E., Schlueter, J., Becher, J., Simrick, S., et al. (2012). Popeye domain containing proteins are essential for stress-mediated modulation of cardiac pacemaking in mice. J. Clin. Invest. *122*, 1119–1130.

Fujimori, K.E., Uyeda, A., and Taguchi, T. (2002). Regulatory expression of MDP77 protein in the skeletal and cardiac muscles. FEBS Lett. *529*, 303–308.

Fujita, T., Umemura, M., Yokoyama, U., Okumura, S., and Ishikawa, Y. (2017). The role of Epac in the heart. Cell. Mol. Life Sci. CMLS *74*, 591–606.

García-Bermúdez, J., Sánchez-Aragó, M., Soldevilla, B., Del Arco, A., Nuevo-Tapioles, C., and Cuezva, J.M. (2015). PKA Phosphorylates the ATPase Inhibitory Factor 1 and Inactivates Its Capacity to Bind and Inhibit the Mitochondrial H(+)-ATP Synthase. Cell Rep. *12*, 2143–2155.

Geelen, M.J., and Vaartjes, W.J. (1977). Levels of cyclic 3'-5' -adenosine monophosphate (cAMP) in maintenance cultures of rat hepatocytes in response to insulin and glucagon. Lipids *12*, 577–580.

Giansanti, P., Stokes, M.P., Silva, J.C., Scholten, A., and Heck, A.J.R. (2013). Interrogating cAMP-dependent Kinase Signaling in Jurkat T Cells via a Protein Kinase A Targeted Immune-precipitation Phosphoproteomics Approach. Mol. Cell. Proteomics MCP *12*, 3350–3359.

Gloerich, M., and Bos, J.L. (2010). Epac: defining a new mechanism for cAMP action. Annu. Rev. Pharmacol. Toxicol. *50*, 355–375.

Gloerich, M., Ponsioen, B., Vliem, M.J., Zhang, Z., Zhao, J., Kooistra, M.R., Price, L.S., Ritsma, L., Zwartkruis, F.J., Rehmann, H., et al. (2010). Spatial regulation of cyclic AMP-Epac1 signaling in cell adhesion by ERM proteins. Mol. Cell. Biol. *30*, 5421–5431.

Gold, M.G., Lygren, B., Dokurno, P., Hoshi, N., McConnachie, G., Taskén, K., Carlson, C.R., Scott, J.D., and Barford, D. (2006). Molecular basis of AKAP specificity for PKA regulatory subunits. Mol. Cell *24*, 383–395.

Gold, M.G., Fowler, D.M., Means, C.K., Pawson, C.T., Stephany, J.J., Langeberg, L.K., Fields, S., and Scott, J.D. (2013). Engineering A-kinase anchoring protein (AKAP)-selective regulatory subunits of protein kinase A (PKA) through structure-based phage selection. J. Biol. Chem. *288*, 17111–17121.

Gomes, L.C., Di Benedetto, G., and Scorrano, L. (2011). During autophagy mitochondria elongate, are spared from degradation and sustain cell viability. Nat. Cell Biol. *13*, 589–598.

Gomez, L., and Breitenbucher, J.G. (2013). PDE2 inhibition: potential for the treatment of cognitive disorders. Bioorg. Med. Chem. Lett. *23*, 6522–6527.

Gómez-Sánchez, R., Gegg, M.E., Bravo-San Pedro, J.M., Niso-Santano, M., Alvarez-Erviti, L., Pizarro-Estrella, E., Gutiérrez-Martín, Y., Alvarez-Barrientos, A., Fuentes, J.M., González-Polo, R.A., et al. (2014). Mitochondrial impairment increases FL-PINK1 levels by calcium-dependent gene expression. Neurobiol. Dis. *62*, 426–440.

Gorshkov, K., Mehta, S., Ramamurthy, S., Ronnett, G.V., Zhou, F.-Q., and Zhang, J. (2017). AKAP-mediated feedback control of cAMP gradients in developing hippocampal neurons. Nat. Chem. Biol. *13*, 425–431.

Götz, F., Roske, Y., Schulz, M.S., Autenrieth, K., Bertinetti, D., Faelber, K., Zühlke, K., Kreuchwig, A., Kennedy, E.J., Krause, G., et al. (2016). AKAP18:PKA-RIIα structure reveals crucial anchor points for recognition of regulatory subunits of PKA. Biochem. J. *473*, 1881–1894.

Greenwald, E.C., and Saucerman, J.J. (2011). Bigger, better, faster: principles and models of AKAP anchoring protein signaling. J. Cardiovasc. Pharmacol. *58*, 462–469.

Grimsrud, P.A., Carson, J.J., Hebert, A.S., Hubler, S.L., Niemi, N.M., Bailey, D.J., Jochem, A., Stapleton, D.S., Keller, M.P., Westphall, M.S., et al. (2012). A quantitative map of the liver mitochondrial phosphoproteome reveals posttranslational control of ketogenesis. Cell Metab. *16*, 672–683.

Guarani, V., McNeill, E.M., Paulo, J.A., Huttlin, E.L., Fröhlich, F., Gygi, S.P., Van Vactor, D., and Harper, J.W. (2015). QIL1 is a novel mitochondrial protein required for MICOS complex stability and cristae morphology. ELife *4*.

Haj Slimane, Z., Bedioune, I., Lechêne, P., Varin, A., Lefebvre, F., Mateo, P., Domergue-Dupont, V., Dewenter, M., Richter, W., Conti, M., et al. (2014). Control of cytoplasmic and nuclear protein kinase A by phosphodiesterases and phosphatases in cardiac myocytes. Cardiovasc. Res. *102*, 97–106.

Halls, M.L., and Cooper, D.M.F. (2017). Adenylyl cyclase signalling complexes - Pharmacological challenges and opportunities. Pharmacol. Ther. *172*, 171–180.

Han, B., Copeland, C.A., Tiwari, A., and Kenworthy, A.K. (2016). Assembly and Turnover of Caveolae: What Do We Really Know? Front. Cell Dev. Biol. *4*, 68.

Harada, H., Becknell, B., Wilm, M., Mann, M., Huang, L.J., Taylor, S.S., Scott, J.D., and Korsmeyer, S.J. (1999). Phosphorylation and inactivation of BAD by mitochondria-anchored protein kinase A. Mol. Cell *3*, 413–422.

Harner, M., Körner, C., Walther, D., Mokranjac, D., Kaesmacher, J., Welsch, U., Griffith, J., Mann, M., Reggiori, F., and Neupert, W. (2011). The mitochondrial contact site complex, a determinant of mitochondrial architecture. EMBO J. *30*, 4356–4370.

Harootunian, A.T., Adams, S.R., Wen, W., Meinkoth, J.L., Taylor, S.S., and Tsien, R.Y. (1993). Movement of the free catalytic subunit of cAMP-dependent protein kinase into and out of the nucleus can be explained by diffusion. Mol. Biol. Cell *4*, 993–1002.

Hayes, J.S., Brunton, L.L., and Mayer, S.E. (1980). Selective activation of particulate cAMP-dependent protein kinase by isoproterenol and prostaglandin E1. J. Biol. Chem. *255*, 5113–5119.

Heijman, J., Dewenter, M., El-Armouche, A., and Dobrev, D. (2013). Function and regulation of serine/threonine phosphatases in the healthy and diseased heart. J. Mol. Cell. Cardiol. *64*, 90–98.

Henderson, D.J.P., Byrne, A., Dulla, K., Jenster, G., Hoffmann, R., Baillie, G.S., and Houslay, M.D. (2014). The cAMP phosphodiesterase-4D7 (PDE4D7) is downregulated in androgen-independent prostate cancer cells and mediates proliferation by compartmentalising cAMP at the plasma membrane of VCaP prostate cancer cells. Br. J. Cancer *110*, 1278–1287.

Henn, V., Edemir, B., Stefan, E., Wiesner, B., Lorenz, D., Theilig, F., Schmitt, R., Vossebein, L., Tamma, G., Beyermann, M., et al. (2004). Identification of a novel A-kinase anchoring protein 18 isoform and evidence for its role in the vasopressin-induced aquaporin-2 shuttle in renal principal cells. J. Biol. Chem. *279*, 26654–26665.

Herberg, F.W., Maleszka, A., Eide, T., Vossebein, L., and Tasken, K. (2000). Analysis of A-kinase anchoring protein (AKAP) interaction with protein kinase A (PKA) regulatory subunits: PKA isoform specificity in AKAP binding. J. Mol. Biol. *298*, 329–339.

Heroes, E., Lesage, B., Görnemann, J., Beullens, M., Van Meervelt, L., and Bollen, M. (2013). The PP1 binding code: a molecular-lego strategy that governs specificity. FEBS J. *280*, 584–595.

Herzig, S., and Neumann, J. (2000). Effects of serine/threonine protein phosphatases on ion channels in excitable membranes. Physiol. Rev. *80*, 173–210.

Hessenberger, M., Zerbes, R.M., Rampelt, H., Kunz, S., Xavier, A.H., Purfürst, B., Lilie, H., Pfanner, N., van der Laan, M., and Daumke, O. (2017). Regulated membrane remodeling by Mic60 controls formation of mitochondrial crista junctions. Nat. Commun. *8*, 15258.

Hinke, S.A., Navedo, M.F., Ulman, A., Whiting, J.L., Nygren, P.J., Tian, G., Jimenez-Caliani, A.J., Langeberg, L.K., Cirulli, V., Tengholm, A., et al. (2012). Anchored phosphatases modulate glucose homeostasis. EMBO J. *31*, 3991–4004.

Hochbaum, D., Barila, G., Ribeiro-Neto, F., and Altschuler, D.L. (2011). Radixin assembles cAMP effectors Epac and PKA into a functional cAMP compartment: role in cAMP-dependent cell proliferation. J. Biol. Chem. *286*, 859–866.

Hohl, C.M., and Li, Q.A. (1991). Compartmentation of cAMP in adult canine ventricular myocytes. Relation to single-cell free Ca2+ transients. Circ. Res. *69*, 1369–1379.

Hoppins, S., Collins, S.R., Cassidy-Stone, A., Hummel, E., Devay, R.M., Lackner, L.L., Westermann, B., Schuldiner, M., Weissman, J.S., and Nunnari, J. (2011). A mitochondrial-focused genetic interaction map reveals a scaffold-like complex required for inner membrane organization in mitochondria. J. Cell Biol. *195*, 323–340.

Houslay, M.D. (2010). Underpinning compartmentalised cAMP signalling through targeted cAMP breakdown. Trends Biochem. Sci. *35*, 91–100.

Houslay, M.D., and Milligan, G. (1997). Tailoring cAMP-signalling responses through isoform multiplicity. Trends Biochem. Sci. *22*, 217–224.

Hu, J., Khodadadi-Jamayran, A., Mao, M., Shah, K., Yang, Z., Nasim, M.T., Wang, Z., and Jiang, H. (2016). AKAP95 regulates splicing through scaffolding RNAs and RNA processing factors. Nat. Commun. *7*, 13347.

Hulme, J.T., Lin, T.W.-C., Westenbroek, R.E., Scheuer, T., and Catterall, W.A. (2003). Beta-adrenergic regulation requires direct anchoring of PKA to cardiac CaV1.2 channels via a leucine zipper interaction with A kinase-anchoring protein 15. Proc. Natl. Acad. Sci. U. S. A. *100*, 13093–13098.

Ikeda, Y., Hoshijima, M., and Chien, K.R. (2008). Toward biologically targeted therapy of calcium cycling defects in heart failure. Physiol. Bethesda Md *23*, 6–16.

Irannejad, R., and von Zastrow, M. (2014). GPCR signaling along the endocytic pathway. Curr. Opin. Cell Biol. *27*, 109–116.

Irannejad, R., Tomshine, J.C., Tomshine, J.R., Chevalier, M., Mahoney, J.P., Steyaert, J., Rasmussen, S.G.F., Sunahara, R.K., El-Samad, H., Huang, B., et al. (2013). Conformational biosensors reveal GPCR signalling from endosomes. Nature *495*, 534–538.

Jans, D.C., Wurm, C.A., Riedel, D., Wenzel, D., Stagge, F., Deckers, M., Rehling, P., and Jakobs, S. (2013). STED super-resolution microscopy reveals an array of MINOS clusters along human mitochondria. Proc. Natl. Acad. Sci. U. S. A. *110*, 8936–8941.

Jiang, H., Lu, X., Shimada, M., Dou, Y., Tang, Z., and Roeder, R.G. (2013). Regulation of transcription by the MLL2 complex and MLL complex-associated AKAP95. Nat. Struct. Mol. Biol. *20*, 1156–1163.

Jones, B.W., Brunet, S., Gilbert, M.L., Nichols, C.B., Su, T., Westenbroek, R.E., Scott, J.D., Catterall, W.A., and McKnight, G.S. (2012). Cardiomyocytes from AKAP7 knockout mice respond normally to adrenergic stimulation. Proc. Natl. Acad. Sci. U. S. A. *109*, 17099–17104.

Jones, B.W., Deem, J., Younts, T.J., Weisenhaus, M., Sanford, C.A., Slack, M.C., Chin, J., Nachmanson, D., McKennon, A., Castillo, P.E., et al. (2016). Targeted deletion of AKAP7 in dentate granule cells impairs spatial discrimination. ELife *5*.

Kamal, F.A., Travers, J.G., and Blaxall, B.C. (2012). G protein-coupled receptor kinases in cardiovascular disease: why “where” matters. Trends Cardiovasc. Med. *22*, 213–219.

Kapiloff, M.S., Schillace, R.V., Westphal, A.M., and Scott, J.D. (1999). mAKAP: an A-kinase anchoring protein targeted to the nuclear membrane of differentiated myocytes. J. Cell Sci. *112 (Pt 16)*, 2725–2736.

Kerfant, B.-G., Zhao, D., Lorenzen-Schmidt, I., Wilson, L.S., Cai, S., Chen, S.R.W., Maurice, D.H., and Backx, P.H. (2007). PI3Kgamma is required for PDE4, not PDE3, activity in subcellular microdomains containing the sarcoplasmic reticular calcium ATPase in cardiomyocytes. Circ. Res. *101*, 400–408.

Khalil, B., Fissi, N.E., Aouane, A., Cabirol-Pol, M.-J., Rival, T., and Liévens, J.-C. (2015). PINK1-induced mitophagy promotes neuroprotection in Huntington’s disease. Cell Death Dis. *6*, e1617.

Klionsky, D.J., Abdelmohsen, K., Abe, A., Abedin, M.J., Abeliovich, H., Acevedo Arozena, A., Adachi, H., Adams, C.M., Adams, P.D., Adeli, K., et al. (2016). Guidelines for the use and interpretation of assays for monitoring autophagy (3rd edition). Autophagy *12*, 1–222.

Kokkonen, K., and Kass, D.A. (2017). Nanodomain Regulation of Cardiac Cyclic Nucleotide Signaling by Phosphodiesterases. Annu. Rev. Pharmacol. Toxicol. *57*, 455–479.

Konieczny, V., Tovey, S.C., Mataragka, S., Prole, D.L., and Taylor, C.W. (2017). Cyclic AMP Recruits a Discrete Intracellular Ca(2+) Store by Unmasking Hypersensitive IP3 Receptors. Cell Rep. *18*, 711–722.

Körner, H., Sofia, H.J., and Zumft, W.G. (2003). Phylogeny of the bacterial superfamily of Crp-Fnr transcription regulators: exploiting the metabolic spectrum by controlling alternative gene programs. FEMS Microbiol. Rev. *27*, 559–592.

Koschinski, A., and Zaccolo, M. (2017). Activation of PKA in cell requires higher concentration of cAMP than in vitro: implications for compartmentalization of cAMP signalling. Sci. Rep. *7*, 14090.

Kovanich, D., van der Heyden, M.A.G., Aye, T.T., van Veen, T.A.B., Heck, A.J.R., and Scholten, A. (2010). Sphingosine kinase interacting protein is an A-kinase anchoring protein specific for type I cAMP-dependent protein kinase. Chembiochem Eur. J. Chem. Biol. *11*, 963–971.

Kritzer, M.D., Li, J., Dodge-Kafka, K., and Kapiloff, M.S. (2012). AKAPs: The Architectural Underpinnings of Local cAMP signaling. J. Mol. Cell. Cardiol. *52*, 351–358.

van der Krogt, G.N.M., Ogink, J., Ponsioen, B., and Jalink, K. (2008). A comparison of donor-acceptor pairs for genetically encoded FRET sensors: application to the Epac cAMP sensor as an example. PloS One *3*, e1916.

Kubota, S., Morii, M., Yuki, R., Yamaguchi, N., Yamaguchi, H., Aoyama, K., Kuga, T., Tomonaga, T., and Yamaguchi, N. (2015). Role for Tyrosine Phosphorylation of A-kinase Anchoring Protein 8 (AKAP8) in Its Dissociation from Chromatin and the Nuclear Matrix. J. Biol. Chem. *290*, 10891–10904.

Kumar, N., Prasad, P., Jash, E., Saini, M., Husain, A., Goldman, A., and Sehrawat, S. (2018). Insights into exchange factor directly activated by cAMP (EPAC) as potential target for cancer treatment. Mol. Cell. Biochem. 1–16.

Kumar, S., Kostin, S., Flacke, J.-P., Reusch, H.P., and Ladilov, Y. (2009). Soluble Adenylyl Cyclase Controls Mitochondria-dependent Apoptosis in Coronary Endothelial Cells. J. Biol. Chem. *284*, 14760–14768.

Lagerström, M.C., and Schiöth, H.B. (2008). Structural diversity of G protein-coupled receptors and significance for drug discovery. Nat. Rev. Drug Discov. *7*, 339–357.

Lan, T.-H., Liu, Q., Li, C., Wu, G., and Lambert, N.A. (2012). Sensitive and high resolution localization and tracking of membrane proteins in live cells with BRET. Traffic Cph. Den. *13*, 1450–1456.

Langeberg, L.K., and Scott, J.D. (2015). Signalling scaffolds and local organization of cellular behaviour. Nat. Rev. Mol. Cell Biol. *16*, 232–244.

Lefkimmiatis, K., and Zaccolo, M. (2014). cAMP signaling in subcellular compartments. Pharmacol. Ther. *143*, 295–304.

Lefkimmiatis, K., Moyer, M.P., Curci, S., and Hofer, A.M. (2009). “cAMP sponge”: a buffer for cyclic adenosine 3’, 5’-monophosphate. PloS One *4*, e7649.

Lefkimmiatis, K., Leronni, D., and Hofer, A.M. (2013). The inner and outer compartments of mitochondria are sites of distinct cAMP/PKA signaling dynamics. J. Cell Biol. *202*, 453–462.

Lehnart, S.E., Wehrens, X.H.T., Reiken, S., Warrier, S., Belevych, A.E., Harvey, R.D., Richter, W., Jin, S.-L.C., Conti, M., and Marks, A.R. (2005). Phosphodiesterase 4D deficiency in the ryanodine-receptor complex promotes heart failure and arrhythmias. Cell *123*, 25–35.

Lei, M., Wang, X., Ke, Y., and Solaro, R.J. (2015). Regulation of Ca(2+) transient by PP2A in normal and failing heart. Front. Physiol. *6*, 13.

Li, D., Lu, C.-J., Hao, G., Wright, H., Woodward, L., Liu, K., Vergari, E., Surdo, N.C., Herring, N., Zaccolo, M., et al. (2015). Efficacy of B-Type Natriuretic Peptide Is Coupled to Phosphodiesterase 2A in Cardiac Sympathetic Neurons. Hypertens. Dallas Tex 1979 *66*, 190–198.

Li, L., Fang, C., Xu, D., Xu, Y., Fu, H., and Li, J. (2016). Cardiomyocyte specific deletion of PP2A causes cardiac hypertrophy. Am. J. Transl. Res. *8*, 1769–1779.

Li, X., Wang, C., Zhang, G., Liang, M., and Zhang, B. (2017). AKAP2 is upregulated in ovarian cancer, and promotes growth and migration of cancer cells. Mol. Med. Rep. *16*, 5151–5156.

Li, Y., Asuri, S., Rebhun, J.F., Castro, A.F., Paranavitana, N.C., and Quilliam, L.A. (2006a). The RAP1 guanine nucleotide exchange factor Epac2 couples cyclic AMP and Ras signals at the plasma membrane. J. Biol. Chem. *281*, 2506–2514.

Li, Y., Kao, G.D., Garcia, B.A., Shabanowitz, J., Hunt, D.F., Qin, J., Phelan, C., and Lazar, M.A. (2006b). A novel histone deacetylase pathway regulates mitosis by modulating Aurora B kinase activity. Genes Dev. *20*, 2566–2579.

Li, Y., Chen, L., Kass, R.S., and Dessauer, C.W. (2012). The A-kinase anchoring protein Yotiao facilitates complex formation between adenylyl cyclase type 9 and the IKs potassium channel in heart. J. Biol. Chem. *287*, 29815–29824.

Liu, P., Rudick, M., and Anderson, R.G.W. (2002). Multiple functions of caveolin-1. J. Biol. Chem. *277*, 41295–41298.

Liu, S., Zhang, J., and Xiang, Y.K. (2011). FRET-based direct detection of dynamic protein kinase A activity on the sarcoplasmic reticulum in cardiomyocytes. Biochem. Biophys. Res. Commun. *404*, 581–586.

Livigni, A., Scorziello, A., Agnese, S., Adornetto, A., Carlucci, A., Garbi, C., Castaldo, I., Annunziato, L., Avvedimento, E.V., and Feliciello, A. (2006). Mitochondrial AKAP121 links cAMP and src signaling to oxidative metabolism. Mol. Biol. Cell *17*, 263–271.

Lobo, M.J., and Zaccolo, M. (2018). PDE2A. in Encyclopedia of Signaling Molecules, Vol. 2 (ed. Choi, S.) (Springer International Publishing).

Lobo, M.J., Amaral, M.D., Zaccolo, M., and Farinha, C.M. (2016). EPAC1 activation by cAMP stabilizes CFTR at the membrane by promoting its interaction with NHERF1. J. Cell Sci. *129*, 2599–2612.

Lomas, O., and Zaccolo, M. (2014). Phosphodiesterases maintain signaling fidelity via compartmentalization of cyclic nucleotides. Physiol. Bethesda Md *29*, 141–149.

Lopes, F.M., Schröder, R., da Frota, M.L.C., Zanotto-Filho, A., Müller, C.B., Pires, A.S., Meurer, R.T., Colpo, G.D., Gelain, D.P., Kapczinski, F., et al. (2010). Comparison between proliferative and neuron-like SH-SY5Y cells as an in vitro model for Parkinson disease studies. Brain Res. *1337*, 85–94.

Lu, J., Wang, W., Mi, Y., Zhang, C., Ying, H., Wang, L., Wang, Y., Myatt, L., and Sun, K. (2017). AKAP95-mediated nuclear anchoring of PKA mediates cortisol-induced PTGS2 expression in human amnion fibroblasts. Sci Signal *10*, eaac6160.

Lygren, B., Carlson, C.R., Santamaria, K., Lissandron, V., McSorley, T., Litzenberg, J., Lorenz, D., Wiesner, B., Rosenthal, W., Zaccolo, M., et al. (2007). AKAP complex regulates Ca2+ re-uptake into heart sarcoplasmic reticulum. EMBO Rep. *8*, 1061–1067.

Lynch, M.J., Baillie, G.S., Mohamed, A., Li, X., Maisonneuve, C., Klussmann, E., Heeke, G. van, and Houslay, M.D. (2005). RNA Silencing Identifies PDE4D5 as the Functionally Relevant cAMP Phosphodiesterase Interacting with βArrestin to Control the Protein Kinase A/AKAP79-mediated Switching of the β2-Adrenergic Receptor to Activation of ERK in HEK293B2 Cells. J. Biol. Chem. *280*, 33178–33189.

Ma, Y., and Taylor, S. (2002). A 15-residue bifunctional element in D-AKAP1 is required for both endoplasmic reticulum and mitochondrial targeting. J. Biol. Chem. *277*, 27328–27336.

Machleidt, T., Li, W.P., Liu, P., and Anderson, R.G. (2000). Multiple domains in caveolin-1 control its intracellular traffic. J. Cell Biol. *148*, 17–28.

MacKenzie, S.J., Baillie, G.S., McPhee, I., MacKenzie, C., Seamons, R., McSorley, T., Millen, J., Beard, M.B., van Heeke, G., and Houslay, M.D. (2002). Long PDE4 cAMP specific phosphodiesterases are activated by protein kinase A-mediated phosphorylation of a single serine residue in Upstream Conserved Region 1 (UCR1). Br. J. Pharmacol. *136*, 421–433.

Malbon, C.C. (2007). A-kinase anchoring proteins: trafficking in G-protein-coupled receptors and the proteins that regulate receptor biology. Curr. Opin. Drug Discov. Devel. *10*, 573–579.

Malbon, C.C., Tao, J., and Wang, H. (2004). AKAPs (A-kinase anchoring proteins) and molecules that compose their G-protein-coupled receptor signalling complexes. Biochem. J. *379*, 1–9.

von der Malsburg, K., Müller, J.M., Bohnert, M., Oeljeklaus, S., Kwiatkowska, P., Becker, T., Loniewska-Lwowska, A., Wiese, S., Rao, S., Milenkovic, D., et al. (2011). Dual role of mitofilin in mitochondrial membrane organization and protein biogenesis. Dev. Cell *21*, 694–707.

Marchi, S., Patergnani, S., and Pinton, P. (2014). The endoplasmic reticulum-mitochondria connection: one touch, multiple functions. Biochim. Biophys. Acta *1837*, 461–469.

Martins, T.J., Mumby, M.C., and Beavo, J.A. (1982). Purification and characterization of a cyclic GMP-stimulated cyclic nucleotide phosphodiesterase from bovine tissues. J. Biol. Chem. *257*, 1973–1979.

Marx, S.O., Reiken, S., Hisamatsu, Y., Jayaraman, T., Burkhoff, D., Rosemblit, N., and Marks, A.R. (2000). PKA phosphorylation dissociates FKBP12.6 from the calcium release channel (ryanodine receptor): defective regulation in failing hearts. Cell *101*, 365–376.

Matsuda, N., Sato, S., Shiba, K., Okatsu, K., Saisho, K., Gautier, C.A., Sou, Y.-S., Saiki, S., Kawajiri, S., Sato, F., et al. (2010). PINK1 stabilized by mitochondrial depolarization recruits Parkin to damaged mitochondria and activates latent Parkin for mitophagy. J. Cell Biol. *189*, 211–221.

Maurice, D.H., Ke, H., Ahmad, F., Wang, Y., Chung, J., and Manganiello, V.C. (2014a). Advances in targeting cyclic nucleotide phosphodiesterases. Nat. Rev. Drug Discov. *13*, 290–314.

Maurice, D.H., Ke, H., Ahmad, F., Wang, Y., Chung, J., and Manganiello, V.C. (2014b). Advances in targeting cyclic nucleotide phosphodiesterases. Nat. Rev. Drug Discov. *13*, 290–314.

McCahill, A., McSorley, T., Huston, E., Hill, E.V., Lynch, M.J., Gall, I., Keryer, G., Lygren, B., Tasken, K., van Heeke, G., et al. (2005). In resting COS1 cells a dominant negative approach shows that specific, anchored PDE4 cAMP phosphodiesterase isoforms gate the activation, by basal cyclic AMP production, of AKAP-tethered protein kinase A type II located in the centrosomal region. Cell. Signal. *17*, 1158–1173.

Means, C.K., Lygren, B., Langeberg, L.K., Jain, A., Dixon, R.E., Vega, A.L., Gold, M.G., Petrosyan, S., Taylor, S.S., Murphy, A.N., et al. (2011). An entirely specific type I A-kinase anchoring protein that can sequester two molecules of protein kinase A at mitochondria. Proc. Natl. Acad. Sci. U. S. A. *108*, E1227-1235.

Mehel, H., Emons, J., Vettel, C., Wittköpper, K., Seppelt, D., Dewenter, M., Lutz, S., Sossalla, S., Maier, L.S., Lechêne, P., et al. (2013). Phosphodiesterase-2 is up-regulated in human failing hearts and blunts β-adrenergic responses in cardiomyocytes. J. Am. Coll. Cardiol. *62*, 1596–1606.

Merrill, R.A., and Strack, S. (2014). MITOCHONDRIA: A kinase anchoring protein 1, a signaling platform for mitochondrial form and function. Int. J. Biochem. Cell Biol. *48*, 92–96.

Merrill, R.A., Dagda, R.K., Dickey, A.S., Cribbs, J.T., Green, S.H., Usachev, Y.M., and Strack, S. (2011). Mechanism of neuroprotective mitochondrial remodeling by PKA/AKAP1. PLoS Biol. *9*, e1000612.

Métrich, M., Laurent, A.-C., Breckler, M., Duquesnes, N., Hmitou, I., Courillau, D., Blondeau, J.-P., Crozatier, B., Lezoualc'h, F., and Morel, E. (2010). Epac activation induces histone deacetylase nuclear export via a Ras-dependent signalling pathway. Cell. Signal. *22*, 1459–1468.

Mika, D., Leroy, J., Vandecasteele, G., and Fischmeister, R. (2012). PDEs create local domains of cAMP signaling. J. Mol. Cell. Cardiol. *52*, 323–329.

Miyawaki, A., Llopis, J., Heim, R., McCaffery, J.M., Adams, J.A., Ikura, M., and Tsien, R.Y. (1997). Fluorescent indicators for Ca2+ based on green fluorescent proteins and calmodulin. Nature *388*, 882–887.

Mongillo, M., McSorley, T., Evellin, S., Sood, A., Lissandron, V., Terrin, A., Huston, E., Hannawacker, A., Lohse, M.J., Pozzan, T., et al. (2004). Fluorescence resonance energy transfer-based analysis of cAMP dynamics in live neonatal rat cardiac myocytes reveals distinct functions of compartmentalized phosphodiesterases. Circ. Res. *95*, 67–75.

Mongillo, M., Tocchetti, C.G., Terrin, A., Lissandron, V., Cheung, Y.-F., Dostmann, W.R., Pozzan, T., Kass, D.A., Paolocci, N., Houslay, M.D., et al. (2006). Compartmentalized phosphodiesterase-2 activity blunts beta-adrenergic cardiac inotropy via an NO/cGMP-dependent pathway. Circ. Res. *98*, 226–234.

Monier, S., Parton, R.G., Vogel, F., Behlke, J., Henske, A., and Kurzchalia, T.V. (1995). VIP21-caveolin, a membrane protein constituent of the caveolar coat, oligomerizes in vivo and in vitro. Mol. Biol. Cell *6*, 911–927.

Monterisi, S., and Zaccolo, M. (2017). Components of the mitochondrial cAMP signalosome. Biochem. Soc. Trans. *45*, 269–274.

Monterisi, S., Lobo, M.J., Livie, C., Castle, J.C., Weinberger, M., Baillie, G.S., Surdo, N.C., Musheshe, N., Stangherlin, A., Gottlieb, E., et al. (2017). PDE2A2 regulates mitochondria morphology and apoptotic cell death via local modulation of cAMP/PKA signalling. ELife *6*.

Morita, H., Murata, T., Shimizu, K., Okumura, K., Inui, M., and Tagawa, T. (2013). Characterization of phosphodiesterase 2A in human malignant melanoma PMP cells. Oncol. Rep. *29*, 1275–1284.

Mukherjee, U.A., Ong, S.-B., Ong, S.-G., and Hausenloy, D.J. (2015). Parkinson's disease proteins: Novel mitochondrial targets for cardioprotection. Pharmacol. Ther. *156*, 34–43.

Murata, M., Peränen, J., Schreiner, R., Wieland, F., Kurzchalia, T.V., and Simons, K. (1995). VIP21/caveolin is a cholesterol-binding protein. Proc. Natl. Acad. Sci. U. S. A. *92*, 10339–10343.

Nakade, S., Rhee, S.K., Hamanaka, H., and Mikoshiba, K. (1994). Cyclic AMP-dependent phosphorylation of an immunoaffinity-purified homotetrameric inositol 1,4,5-trisphosphate receptor (type I) increases Ca2+ flux in reconstituted lipid vesicles. J. Biol. Chem. *269*, 6735–6742.

Namkung, Y., Le Gouill, C., Lukashova, V., Kobayashi, H., Hogue, M., Khoury, E., Song, M., Bouvier, M., and Laporte, S.A. (2016). Monitoring G protein-coupled receptor and β-arrestin trafficking in live cells using enhanced bystander BRET. Nat. Commun. *7*, 12178.

Naon, D., and Scorrano, L. (2014). At the right distance: ER-mitochondria juxtaposition in cell life and death. Biochim. Biophys. Acta *1843*, 2184–2194.

Narendra, D., Tanaka, A., Suen, D.-F., and Youle, R.J. (2008). Parkin is recruited selectively to impaired mitochondria and promotes their autophagy. J. Cell Biol. *183*, 795–803.

Nicolaou, P., Hajjar, R.J., and Kranias, E.G. (2009). Role of protein phosphatase-1 inhibitor-1 in cardiac physiology and pathophysiology. J. Mol. Cell. Cardiol. *47*, 365–371.

Nikolaev, V.O., Bünemann, M., Hein, L., Hannawacker, A., and Lohse, M.J. (2004). Novel single chain cAMP sensors for receptor-induced signal propagation. J. Biol. Chem. *279*, 37215–37218.

Nikolaev, V.O., Bünemann, M., Schmitteckert, E., Lohse, M.J., and Engelhardt, S. (2006). Cyclic AMP imaging in adult cardiac myocytes reveals far-reaching beta1-adrenergic but locally confined beta2-adrenergic receptor-mediated signaling. Circ. Res. *99*, 1084–1091.

Nogami, S., Satoh, S., Nakano, M., Shimizu, H., Fukushima, H., Maruyama, A., Terano, A., and Shirataki, H. (2003). Taxilin; a novel syntaxin-binding protein that is involved in Ca2+-dependent exocytosis in neuroendocrine cells. Genes Cells Devoted Mol. Cell. Mech. *8*, 17–28.

Nogami, S., Satoh, S., Tanaka-Nakadate, S., Yoshida, K., Nakano, M., Terano, A., and Shirataki, H. (2004). Identification and characterization of taxilin isoforms. Biochem. Biophys. Res. Commun. *319*, 936–943.

Nunnari, J., and Suomalainen, A. (2012). Mitochondria: in sickness and in health. Cell *148*, 1145–1159.

Oakes, S.A., Scorrano, L., Opferman, J.T., Bassik, M.C., Nishino, M., Pozzan, T., and Korsmeyer, S.J. (2005). Proapoptotic BAX and BAK regulate the type 1 inositol trisphosphate receptor and calcium leak from the endoplasmic reticulum. Proc. Natl. Acad. Sci. U. S. A. *102*, 105–110.

de Oliveira, S.K., and Smolenski, A. (2009). Phosphodiesterases link the aryl hydrocarbon receptor complex to cyclic nucleotide signaling. Biochem. Pharmacol. *77*, 723–733.

de Oliveira, S.K., Hoffmeister, M., Gambaryan, S., Müller-Esterl, W., Guimaraes, J.A., and Smolenski, A.P. (2007). Phosphodiesterase 2A forms a complex with the co-chaperone XAP2 and regulates nuclear translocation of the aryl hydrocarbon receptor. J. Biol. Chem. *282*, 13656–13663.

Palmer, A.E., Jin, C., Reed, J.C., and Tsien, R.Y. (2004). Bcl-2-mediated alterations in endoplasmic reticulum Ca2+ analyzed with an improved genetically encoded fluorescent sensor. Proc. Natl. Acad. Sci. U. S. A. *101*, 17404–17409.

Pandit, J., Forman, M.D., Fennell, K.F., Dillman, K.S., and Menniti, F.S. (2009). Mechanism for the allosteric regulation of phosphodiesterase 2A deduced from the X-ray structure of a near full-length construct. Proc. Natl. Acad. Sci. U. S. A. *106*, 18225–18230.

Pani, B., and Singh, B.B. (2009). Lipid rafts/caveolae as microdomains of calcium signaling. Cell Calcium *45*, 625–633.

Papa, S., Sardanelli, A.M., Scacco, S., and Technikova-Dobrova, Z. (1999). cAMP-dependent protein kinase and phosphoproteins in mammalian mitochondria. An extension of the cAMP-mediated intracellular signal transduction. FEBS Lett. *444*, 245–249.

Park, D.S., Woodman, S.E., Schubert, W., Cohen, A.W., Frank, P.G., Chandra, M., Shirani, J., Razani, B., Tang, B., Jelicks, L.A., et al. (2002). Caveolin-1/3 double-knockout mice are viable, but lack both muscle and non-muscle caveolae, and develop a severe cardiomyopathic phenotype. Am. J. Pathol. *160*, 2207–2217.

Passariello, C.L., Li, J., Dodge-Kafka, K., and Kapiloff, M.S. (2015). mAKAP-a master scaffold for cardiac remodeling. J. Cardiovasc. Pharmacol. *65*, 218–225.

Pavlos, N.J., and Friedman, P.A. (2017). GPCR Signaling and Trafficking: The Long and Short of It. Trends Endocrinol. Metab. TEM *28*, 213–226.

Pawson, C.T., and Scott, J.D. (2010). Signal integration through blending, bolstering and bifurcating of intracellular information. Nat. Struct. Mol. Biol. *17*, 653–658.

Pearce, M.M.P., Wormer, D.B., Wilkens, S., and Wojcikiewicz, R.J.H. (2009). An endoplasmic reticulum (ER) membrane complex composed of SPFH1 and SPFH2 mediates the ER-associated degradation of inositol 1,4,5-trisphosphate receptors. J. Biol. Chem. *284*, 10433–10445.

Pendin, D., Greotti, E., Lefkimmiatis, K., and Pozzan, T. (2017). Exploring cells with targeted biosensors. J. Gen. Physiol. *149*, 1–36.

Pereira, L., Ruiz-Hurtado, G., Morel, E., Laurent, A.-C., Métrich, M., Domínguez-Rodríguez, A., Lauton-Santos, S., Lucas, A., Benitah, J.-P., Bers, D.M., et al. (2012). Epac enhances excitation-transcription coupling in cardiac myocytes. J. Mol. Cell. Cardiol. *52*, 283–291.

Pereira, L., Cheng, H., Lao, D.H., Na, L., van Oort, R.J., Brown, J.H., Wehrens, X.H.T., Chen, J., and Bers, D.M. (2013). Epac2 mediates cardiac β1-adrenergic-dependent sarcoplasmic reticulum Ca2+ leak and arrhythmia. Circulation *127*, 913–922.

Pereira, L., Rehmann, H., Lao, D.H., Erickson, J.R., Bossuyt, J., Chen, J., and Bers, D.M. (2015). Novel Epac fluorescent ligand reveals distinct Epac1 vs. Epac2 distribution and function in cardiomyocytes. Proc. Natl. Acad. Sci. *112*, 3991–3996.

Pereira, L., Bare, D.J., Galice, S., Shannon, T.R., and Bers, D.M. (2017). β-Adrenergic induced SR Ca2+leak is mediated by an Epac-NOS pathway. J. Mol. Cell. Cardiol. *108*, 8–16.

Perkins, G.A., Wang, L., Huang, L.J., Humphries, K., Yao, V.J., Martone, M., Deerinck, T.J., Barraclough, D.M., Violin, J.D., Smith, D., et al. (2001). PKA, PKC, and AKAP localization in and around the neuromuscular junction. BMC Neurosci. *2*, 17.

Perrino, C., Feliciello, A., Schiattarella, G.G., Esposito, G., Guerriero, R., Zaccaro, L., Del Gatto, A., Saviano, M., Garbi, C., Carangi, R., et al. (2010). AKAP121 downregulation impairs protective cAMP signals, promotes mitochondrial dysfunction, and increases oxidative stress. Cardiovasc. Res. *88*, 101–110.

Perry, S.J., Baillie, G.S., Kohout, T.A., McPhee, I., Magiera, M.M., Ang, K.L., Miller, W.E., McLean, A.J., Conti, M., Houslay, M.D., et al. (2002). Targeting of cyclic AMP degradation to beta 2-adrenergic receptors by beta-arrestins. Science *298*, 834–836.

Peters, P.J., and Hunziker, W. (2001). Subcellular localization of Rab17 by cryo-immunogold electron microscopy in epithelial cells grown on polycarbonate filters. Methods Enzymol. *329*, 210–225.

Pfanner, N., van der Laan, M., Amati, P., Capaldi, R.A., Caudy, A.A., Chacinska, A., Darshi, M., Deckers, M., Hoppins, S., Icho, T., et al. (2014). Uniform nomenclature for the mitochondrial contact site and cristae organizing system. J. Cell Biol. *204*, 1083–1086.

Pickrell, A.M., and Youle, R.J. (2015). The roles of PINK1, parkin, and mitochondrial fidelity in Parkinson's disease. Neuron *85*, 257–273.

Piggott, L.A., Bauman, A.L., Scott, J.D., and Dessauer, C.W. (2008). The A-kinase anchoring protein Yotiao binds and regulates adenylyl cyclase in brain. Proc. Natl. Acad. Sci. U. S. A. *105*, 13835–13840.

Podda, M.V., and Grassi, C. (2014). New perspectives in cyclic nucleotide-mediated functions in the CNS: the emerging role of cyclic nucleotide-gated (CNG) channels. Pflüg. Arch. - Eur. J. Physiol. *466*, 1241–1257.

Ponsioen, B., Zhao, J., Riedl, J., Zwartkruis, F., van der Krogt, G., Zaccolo, M., Moolenaar, W.H., Bos, J.L., and Jalink, K. (2004). Detecting cAMP-induced Epac activation by fluorescence resonance energy transfer: Epac as a novel cAMP indicator. EMBO Rep. *5*, 1176–1180.

Ponsioen, B., Gloerich, M., Ritsma, L., Rehmann, H., Bos, J.L., and Jalink, K. (2009). Direct spatial control of Epac1 by cyclic AMP. Mol. Cell. Biol. *29*, 2521–2531.

Qian, J., Vafiadaki, E., Florea, S.M., Singh, V.P., Song, W., Lam, C.K., Wang, Y., Yuan, Q., Pritchard, T.J., Cai, W., et al. (2011). Small heat shock protein 20 interacts with protein phosphatase-1 and enhances sarcoplasmic reticulum calcium cycling. Circ. Res. *108*, 1429–1438.

Qiao, J., Mei, F.C., Popov, V.L., Vergara, L.A., and Cheng, X. (2002). Cell cycle-dependent subcellular localization of exchange factor directly activated by cAMP. J. Biol. Chem. *277*, 26581–26586.

Rabl, R., Soubannier, V., Scholz, R., Vogel, F., Mendl, N., Vasiljev-Neumeyer, A., Körner, C., Jagasia, R., Keil, T., Baumeister, W., et al. (2009). Formation of cristae and crista junctions in mitochondria depends on antagonism between Fcj1 and Su e/g. J. Cell Biol. *185*, 1047–1063.

Raturi, A., and Simmen, T. (2013). Where the endoplasmic reticulum and the mitochondrion tie the knot: The mitochondria-associated membrane (MAM). Biochim. Biophys. Acta BBA - Mol. Cell Res. *1833*, 213–224.

Razani, B., Combs, T.P., Wang, X.B., Frank, P.G., Park, D.S., Russell, R.G., Li, M., Tang, B., Jelicks, L.A., Scherer, P.E., et al. (2002). Caveolin-1-deficient mice are lean, resistant to diet-induced obesity, and show hypertriglyceridemia with adipocyte abnormalities. J. Biol. Chem. *277*, 8635–8647.

Reese, D.E., Zavaljevski, M., Streiff, N.L., and Bader, D. (1999). bves:A Novel Gene Expressed during Coronary Blood Vessel Development. Dev. Biol. *209*, 159–171.

Rehmann, H., Das, J., Knipscheer, P., Wittinghofer, A., and Bos, J.L. (2006). Structure of the cyclic-AMP-responsive exchange factor Epac2 in its auto-inhibited state. Nature *439*, 625–628.

Rehmann, H., Arias-Palomo, E., Hadders, M.A., Schwede, F., Llorca, O., and Bos, J.L. (2008). Structure of Epac2 in complex with a cyclic AMP analogue and RAP1B. Nature *455*, 124–127.

Reinton, N., Collas, P., Haugen, T.B., Skâlhegg, B.S., Hansson, V., Jahnsen, T., and Taskén, K. (2000). Localization of a novel human A-kinase-anchoring protein, hAKAP220, during spermatogenesis. Dev. Biol. *223*, 194–204.

Richards, M., Lomas, O., Jalink, K., Ford, K.L., Vaughan-Jones, R.D., Lefkimmiatis, K., and Swietach, P. (2016). Intracellular tortuosity underlies slow cAMP diffusion in adult ventricular myocytes. Cardiovasc. Res. *110*, 395–407.

Rigatti, M., Le, A.V., Gerber, C., Moraru, I.I., and Dodge-Kafka, K.L. (2015). Phosphorylation state-dependent interaction between AKAP7δ/γ and phospholamban increases phospholamban phosphorylation. Cell. Signal. *27*, 1807–1815.

Ritz, D., Vuk, M., Kirchner, P., Bug, M., Schütz, S., Hayer, A., Bremer, S., Lusk, C., Baloh, R.H., Lee, H., et al. (2011). Endolysosomal sorting of ubiquitylated caveolin-1 is regulated by VCP and UBXD1 and impaired by VCP disease mutations. Nat. Cell Biol. *13*, 1116–1123.

Rogne, M., Stokka, A.J., Taskén, K., Collas, P., and Küntziger, T. (2009). Mutually exclusive binding of PP1 and RNA to AKAP149 affects the mitochondrial network. Hum. Mol. Genet. *18*, 978–987.

de Rooij, J., Zwartkruis, F.J., Verheijen, M.H., Cool, R.H., Nijman, S.M., Wittinghofer, A., and Bos, J.L. (1998). Epac is a Rap1 guanine-nucleotide-exchange factor directly activated by cyclic AMP. Nature *396*, 474–477.

de Rooij, J., Rehmann, H., van Triest, M., Cool, R.H., Wittinghofer, A., and Bos, J.L. (2000). Mechanism of regulation of the Epac family of cAMP-dependent RapGEFs. J. Biol. Chem. *275*, 20829–20836.

Rous, S. (1970). Effect of dibutyryl cAMP on the enzymes of fatty acid synthesis and of glycogen metabolism. FEBS Lett. *12*, 45–48.

Ruiz-Hurtado, G., Morel, E., Domínguez-Rodríguez, A., Llach, A., Lezoualc'h, F., Benitah, J.-P., and Gomez, A.M. (2013). Epac in cardiac calcium signaling. J. Mol. Cell. Cardiol. *58*, 162–171.

Russwurm, C., Zoidl, G., Koesling, D., and Russwurm, M. (2009). Dual acylation of PDE2A splice variant 3: targeting to synaptic membranes. J. Biol. Chem. *284*, 25782–25790.

Sakane, H., Horii, Y., Nogami, S., Kawano, Y., Kaneko-Kawano, T., and Shirataki, H. (2014). α-Taxilin interacts with sorting nexin 4 and participates in the recycling pathway of transferrin receptor. PloS One *9*, e93509.

Sakane, H., Makiyama, T., Nogami, S., Horii, Y., Akasaki, K., and Shirataki, H. (2016). β-Taxilin participates in differentiation of C2C12 myoblasts into myotubes. Exp. Cell Res. *345*, 230–238.

Sala-Vila, A., Navarro-Lérida, I., Sánchez-Alvarez, M., Bosch, M., Calvo, C., López, J.A., Calvo, E., Ferguson, C., Giacomello, M., Serafini, A., et al. (2016). Interplay between hepatic mitochondria-associated membranes, lipid metabolism and caveolin-1 in mice. Sci. Rep. *6*, 27351.

Salpietro, V., Perez-Dueñas, B., Nakashima, K., San Antonio-Arce, V., Manole, A., Efthymiou, S., Vandrovcova, J., Bettencourt, C., Mencacci, N.E., Klein, C., et al. (2018). A homozygous loss-of-function mutation in PDE2A associated to early-onset hereditary chorea. Mov. Disord. Off. J. Mov. Disord. Soc.

Sardanelli, A.M., Signorile, A., Nuzzi, R., Rasmo, D.D., Technikova-Dobrova, Z., Drahota, Z., Occhiello, A., Pica, A., and Papa, S. (2006). Occurrence of A-kinase anchor protein and associated cAMP-dependent protein kinase in the inner compartment of mammalian mitochondria. FEBS Lett. *580*, 5690–5696.

Sarma, G.N., Moody, I.S., Ilouz, R., Phan, R.H., Sankaran, B., Hall, R.A., and Taylor, S.S. (2015). D-AKAP2:PKA RII:PDZK1 ternary complex structure: insights from the nucleation of a polyvalent scaffold. Protein Sci. Publ. Protein Soc. *24*, 105–116.

Sastri, M., Darshi, M., Mackey, M., Ramachandra, R., Ju, S., Phan, S., Adams, S., Stein, K., Douglas, C.R., Kim, J.J., et al. (2017). Sub-mitochondrial localization of the genetic-tagged mitochondrial intermembrane space-bridging components Mic19, Mic60 and Sam50. J. Cell Sci. *130*, 3248–3260.

Schägger, H. (2001). Blue-native gels to isolate protein complexes from mitochondria. Methods Cell Biol. *65*, 231–244.

Schauble, S., King, C.C., Darshi, M., Koller, A., Shah, K., and Taylor, S.S. (2007a). Identification of ChChd3 as a Novel Substrate of the cAMP-dependent Protein Kinase (PKA) Using an Analog-sensitive Catalytic Subunit. J. Biol. Chem. *282*, 14952–14959.

Schauble, S., King, C.C., Darshi, M., Koller, A., Shah, K., and Taylor, S.S. (2007b). Identification of ChChd3 as a novel substrate of the cAMP-dependent protein kinase (PKA) using an analog-sensitive catalytic subunit. J. Biol. Chem. *282*, 14952–14959.

Scheiffele, P., Verkade, P., Fra, A.M., Virta, H., Simons, K., and Ikonen, E. (1998). Caveolin-1 and -2 in the exocytic pathway of MDCK cells. J. Cell Biol. *140*, 795–806.

Scherer, P.E., Okamoto, T., Chun, M., Nishimoto, I., Lodish, H.F., and Lisanti, M.P. (1996). Identification, sequence, and expression of caveolin-2 defines a caveolin gene family. Proc. Natl. Acad. Sci. U. S. A. *93*, 131–135.

Schilling, J.M., and Patel, H.H. (2016). Non-canonical roles for caveolin in regulation of membrane repair and mitochondria: implications for stress adaptation with age. J. Physiol. *594*, 4581–4589.

Schindler, R.F.R., and Brand, T. (2016). The Popeye domain containing protein family--A novel class of cAMP effectors with important functions in multiple tissues. Prog. Biophys. Mol. Biol. *120*, 28–36.

Schwencke, C., Yamamoto, M., Okumura, S., Toya, Y., Kim, S.J., and Ishikawa, Y. (1999). Compartmentation of cyclic adenosine 3',5'-monophosphate signaling in caveolae. Mol. Endocrinol. Baltim. Md *13*, 1061–1070.

Schwoch, G., Trinczek, B., and Bode, C. (1990). Localization of catalytic and regulatory subunits of cyclic AMP-dependent protein kinases in mitochondria from various rat tissues. Biochem. J. *270*, 181–188.

Schwoerer, A.P., Neuber, C., Schmechel, A., Melnychenko, I., Mearini, G., Boknik, P., Kirchhefer, U., Schmitz, W., Ehmke, H., Eschenhagen, T., et al. (2008). Mechanical unloading of the rat heart involves marked changes in the protein kinase-phosphatase balance. J. Mol. Cell. Cardiol. *45*, 846–852.

Scott, J.D., Dessauer, C.W., and Tasken, K. (2013). Creating Order from Chaos: Cellular Regulation by Kinase Anchoring. Annu. Rev. Pharmacol. Toxicol. *53*, 187–210.

Seybold, J., Thomas, D., Witzenrath, M., Boral, S., Hocke, A.C., Bürger, A., Hatzelmann, A., Tenor, H., Schudt, C., Krüll, M., et al. (2005). Tumor necrosis factor-alpha-dependent expression of phosphodiesterase 2: role in endothelial hyperpermeability. Blood *105*, 3569–3576.

Shapira, H., Lupu-Meiri, M., Gershengorn, M.C., and Oron, Y. (1990). Activation of two different receptors mobilizes calcium from distinct stores in Xenopus oocytes. Biophys. J. *57*, 1281–1285.

Shepherd, M., McSorley, T., Olsen, A.E., Johnston, L.A., Thomson, N.C., Baillie, G.S., Houslay, M.D., and Bolger, G.B. (2003). Molecular cloning and subcellular distribution of the novel PDE4B4 cAMP-specific phosphodiesterase isoform. Biochem. J. *370*, 429–438.

Shi, Y. (2009). Serine/threonine phosphatases: mechanism through structure. Cell *139*, 468–484.

Shimizu-Albergine, M., Tsai, L.-C.L., Patrucco, E., and Beavo, J.A. (2012). cAMP-specific phosphodiesterases 8A and 8B, essential regulators of Leydig cell steroidogenesis. Mol. Pharmacol. *81*, 556–566.

Singh, A., Redden, J.M., Kapiloff, M.S., and Dodge-Kafka, K.L. (2011). The Large Isoforms of A-Kinase Anchoring Protein 18 Mediate the Phosphorylation of Inhibitor-1 by Protein Kinase A and the Inhibition of Protein Phosphatase 1 Activity. Mol. Pharmacol. *79*, 533–540.

Smith, F.D., Reichow, S.L., Esseltine, J.L., Shi, D., Langeberg, L.K., Scott, J.D., and Gonen, T. (2013). Intrinsic disorder within an AKAP-protein kinase A complex guides local substrate phosphorylation. ELife *2*, e01319.

Smith, F.D., Esseltine, J.L., Nygren, P.J., Veesler, D., Byrne, D.P., Vonderach, M., Strashnov, I., Eyers, C.E., Eyers, P.A., Langeberg, L.K., et al. (2017). Local protein kinase A action proceeds through intact holoenzymes. Science *356*, 1288–1293.

Smith, K.E., Gibson, E.S., and Dell'Acqua, M.L. (2006). cAMP-Dependent Protein Kinase Postsynaptic Localization Regulated by NMDA Receptor Activation through Translocation of an A-Kinase Anchoring Protein Scaffold Protein. J. Neurosci. *26*, 2391–2402.

Soni, S., Raaijmakers, A.J.A., Raaijmakers, L.M., Damen, J.M.A., Stuijvenberg, L. van, Vos, M.A., Heck, A.J.R., Veen, T.A.B. van, and Scholten, A. (2016). A Proteomics Approach to Identify New Putative Cardiac Intercalated Disk Proteins. PLOS ONE *11*, e0152231.

Sonnenburg, W.K., Mullaney, P.J., and Beavo, J.A. (1991). Molecular cloning of a cyclic GMP-stimulated cyclic nucleotide phosphodiesterase cDNA. Identification and distribution of isozyme variants. J. Biol. Chem. *266*, 17655–17661.

Sonnino, S., and Prinetti, A. (2009). Sphingolipids and membrane environments for caveolin. FEBS Lett. *583*, 597–606.

Sprenger, J.U., Perera, R.K., Steinbrecher, J.H., Lehnart, S.E., Maier, L.S., Hasenfuss, G., and Nikolaev, V.O. (2015). In vivo model with targeted cAMP biosensor reveals changes in receptor-microdomain communication in cardiac disease. Nat. Commun. *6*, 6965.

Stephenson, D.T., Coskran, T.M., Wilhelms, M.B., Adamowicz, W.O., O'Donnell, M.M., Muravnick, K.B., Menniti, F.S., Kleiman, R.J., and Morton, D. (2009). Immunohistochemical localization of phosphodiesterase 2A in multiple mammalian species. J. Histochem. Cytochem. Off. J. Histochem. Soc. *57*, 933–949.

Stoddart, L.A., Johnstone, E.K.M., Wheal, A.J., Goulding, J., Robers, M.B., Machleidt, T., Wood, K.V., Hill, S.J., and Pfleger, K.D.G. (2015). Application of BRET to monitor ligand binding to GPCRs. Nat. Methods *12*, 661–663.

Stork, P.J.S., and Schmitt, J.M. (2002). Crosstalk between cAMP and MAP kinase signaling in the regulation of cell proliferation. Trends Cell Biol. *12*, 258–266.

Strack, S., Zaucha, J.A., Ebner, F.F., Colbran, R.J., and Wadzinski, B.E. (1998). Brain protein phosphatase 2A: developmental regulation and distinct cellular and subcellular localization by B subunits. J. Comp. Neurol. *392*, 515–527.

Suen, D.-F., Norris, K.L., and Youle, R.J. (2008). Mitochondrial dynamics and apoptosis. Genes Dev. *22*, 1577–1590.

Sunahara, R.K., Dessauer, C.W., and Gilman, A.G. (1996). Complexity and diversity of mammalian adenylyl cyclases. Annu. Rev. Pharmacol. Toxicol. *36*, 461–480.

Sundivakkam, P.C., Kwiatek, A.M., Sharma, T.T., Minshall, R.D., Malik, A.B., and Tiruppathi, C. (2009). Caveolin-1 scaffold domain interacts with TRPC1 and IP3R3 to regulate Ca2+ store release-induced Ca2+ entry in endothelial cells. Am. J. Physiol. Cell Physiol. *296*, C403-413.

Surdo, N.C., Berrera, M., Koschinski, A., Brescia, M., Machado, M.R., Carr, C., Wright, P., Gorelik, J., Morotti, S., Grandi, E., et al. (2017). FRET biosensor uncovers cAMP nano-domains at β-adrenergic targets that dictate precise tuning of cardiac contractility. Nat. Commun. *8*, 15031.

Swaney, J.S., Patel, H.H., Yokoyama, U., Head, B.P., Roth, D.M., and Insel, P.A. (2006). Focal adhesions in (myo)fibroblasts scaffold adenylyl cyclase with phosphorylated caveolin. J. Biol. Chem. *281*, 17173–17179.

Tagawa, A., Mezzacasa, A., Hayer, A., Longatti, A., Pelkmans, L., and Helenius, A. (2005). Assembly and trafficking of caveolar domains in the cell: caveolae as stable, cargo-triggered, vesicular transporters. J. Cell Biol. *170*, 769–779.

Tang, T.-S., Tu, H., Wang, Z., and Bezprozvanny, I. (2003). Modulation of type 1 inositol (1,4,5)-trisphosphate receptor function by protein kinase a and protein phosphatase 1alpha. J. Neurosci. Off. J. Soc. Neurosci. *23*, 403–415.

Taylor, S.S., Buechler, J.A., and Yonemoto, W. (1990). cAMP-dependent protein kinase: framework for a diverse family of regulatory enzymes. Annu. Rev. Biochem. *59*, 971–1005.

Taylor, S.S., Kim, C., Vigil, D., Haste, N.M., Yang, J., Wu, J., and Anand, G.S. (2005). Dynamics of signaling by PKA. Biochim. Biophys. Acta *1754*, 25–37.

Taylor, S.S., Ilouz, R., Zhang, P., and Kornev, A.P. (2012). Assembly of allosteric macromolecular switches: lessons from PKA. Nat. Rev. Mol. Cell Biol. *13*, 646–658.

Taylor, S.S., Zhang, P., Steichen, J.M., Keshwani, M.M., and Kornev, A.P. (2013). PKA: lessons learned after twenty years. Biochim. Biophys. Acta *1834*, 1271–1278.

Terrin, A., Di Benedetto, G., Pertegato, V., Cheung, Y.-F., Baillie, G., Lynch, M.J., Elvassore, N., Prinz, A., Herberg, F.W., Houslay, M.D., et al. (2006). PGE(1) stimulation of HEK293 cells generates multiple contiguous domains with different [cAMP]: role of compartmentalized phosphodiesterases. J. Cell Biol. *175*, 441–451.

Thakkar, A., Aljameeli, A., Thomas, S., and Shah, G.V. (2016). A-kinase anchoring protein 2 is required for calcitonin-mediated invasion of cancer cells. Endocr. Relat. Cancer *23*, 1–14.

Timofeyev, V., Myers, R.E., Kim, H.J., Woltz, R.L., Sirish, P., Heiserman, J.P., Li, N., Singapuri, A., Tang, T., Yarov-Yarovoy, V., et al. (2013). Adenylyl Cyclase Subtype-Specific Compartmentalization: Differential Regulation of L-type Ca2+ Current in Ventricular Myocytes. Circ. Res. *112*, 1567–1576.

Torres-Quesada, O., Mayrhofer, J.E., and Stefan, E. (2017). The many faces of compartmentalized PKA signalosomes. Cell. Signal. *37*, 1–11.

Trabanco, A.A., Buijnsters, P., and Rombouts, F.J.R. (2016). Towards selective phosphodiesterase 2A (PDE2A) inhibitors: a patent review (2010 - present). Expert Opin. Ther. Pat. *26*, 933–946.

Tröger, J., Moutty, M.C., Skroblin, P., and Klussmann, E. (2012). A-kinase anchoring proteins as potential drug targets. Br. J. Pharmacol. *166*, 420–433.

Tsai, L.-C.L., Shimizu-Albergine, M., and Beavo, J.A. (2011). The High-Affinity cAMP-Specific Phosphodiesterase 8B Controls Steroidogenesis in the Mouse Adrenal Gland. Mol. Pharmacol. *79*, 639–648.

Uyeda, A., Fukui, I., Fujimori, K., Kiyosue, K., Nishimune, H., Kasai, M., and Taguchi, T. (2000). MDP77: A novel neurite-outgrowth-promoting protein predominantly expressed in chick muscles. Biochem. Biophys. Res. Commun. *269*, 564–569.

Valsecchi, F., Konrad, C., and Manfredi, G. (2014). Role of soluble adenylyl cyclase in mitochondria. Biochim. Biophys. Acta *1842*, 2555–2560.

Valsecchi, F., Konrad, C., D'Aurelio, M., Ramos-Espiritu, L.S., Stepanova, A., Burstein, S.R., Galkin, A., Magranè, J., Starkov, A., Buck, J., et al. (2017). Distinct intracellular sAC-cAMP domains regulate ER calcium signaling and OXPHOS function. J. Cell Sci.

Vance, J.E. (2014). MAM (mitochondria-associated membranes) in mammalian cells: Lipids and beyond. Biochim. Biophys. Acta BBA - Mol. Cell Biol. Lipids *1841*, 595–609.

Vanderheyden, V., Devogelaere, B., Missiaen, L., De Smedt, H., Bultynck, G., and Parys, J.B. (2009). Regulation of inositol 1,4,5-trisphosphate-induced Ca2+ release by reversible phosphorylation and dephosphorylation. Biochim. Biophys. Acta *1793*, 959–970.

Vettel, C., Lindner, M., Dewenter, M., Lorenz, K., Schanbacher, C., Riedel, M., Lämmle, S., Meinecke, S., Mason, F.E., Sossalla, S., et al. (2017). Phosphodiesterase 2 Protects Against Catecholamine-Induced Arrhythmia and Preserves Contractile Function After Myocardial Infarction. Circ. Res. *120*, 120–132.

Virshup, D.M., and Shenolikar, S. (2009). From promiscuity to precision: protein phosphatases get a makeover. Mol. Cell *33*, 537–545.

van Vliet, A.R., Verfaillie, T., and Agostinis, P. (2014). New functions of mitochondria associated membranes in cellular signaling. Biochim. Biophys. Acta *1843*, 2253–2262.

Volonte, D., Zhang, K., Lisanti, M.P., and Galbiati, F. (2002). Expression of caveolin-1 induces premature cellular senescence in primary cultures of murine fibroblasts. Mol. Biol. Cell *13*, 2502–2517.

Volonte, D., Liu, Z., Musille, P.M., Stoppani, E., Wakabayashi, N., Di, Y.-P., Lisanti, M.P., Kensler, T.W., and Galbiati, F. (2013). Inhibition of nuclear factor-erythroid 2-related factor (Nrf2) by caveolin-1 promotes stress-induced premature senescence. Mol. Biol. Cell *24*, 1852–1862.

Volonte, D., Zou, H., Bartholomew, J.N., Liu, Z., Morel, P.A., and Galbiati, F. (2015). Oxidative stress-induced inhibition of Sirt1 by caveolin-1 promotes p53-dependent premature senescence and stimulates the secretion of interleukin 6 (IL-6). J. Biol. Chem. *290*, 4202–4214.

Volonte, D., Liu, Z., Shiva, S., and Galbiati, F. (2016). Caveolin-1 controls mitochondrial function through regulation of m-AAA mitochondrial protease. Aging *8*, 2355–2369.

Wachten, S., Masada, N., Ayling, L.-J., Ciruela, A., Nikolaev, V.O., Lohse, M.J., and Cooper, D.M.F. (2010). Distinct pools of cAMP centre on different isoforms of adenylyl cyclase in pituitary-derived GH3B6 cells. J. Cell Sci. *123*, 95–106.

Wagner, L.E., Li, W.-H., Joseph, S.K., and Yule, D.I. (2004). Functional consequences of phosphomimetic mutations at key cAMP-dependent protein kinase phosphorylation sites in the type 1 inositol 1,4,5-trisphosphate receptor. J. Biol. Chem. *279*, 46242–46252.

Walker-Gray, R., Stengel, F., and Gold, M.G. (2017). Mechanisms for restraining cAMP-dependent protein kinase revealed by subunit quantitation and cross-linking approaches. Proc. Natl. Acad. Sci. *114*, 10414–10419.

Wang, L., Sunahara, R.K., Krumins, A., Perkins, G., Crochiere, M.L., Mackey, M., Bell, S., Ellisman, M.H., and Taylor, S.S. (2001). Cloning and mitochondrial localization of full-length D-AKAP2, a protein kinase A anchoring protein. Proc. Natl. Acad. Sci. U. S. A. *98*, 3220–3225.

Wang, P., Liu, Z., Chen, H., Ye, N., Cheng, X., and Zhou, J. (2017). Exchange proteins directly activated by cAMP (EPACs): Emerging therapeutic targets. Bioorg. Med. Chem. Lett. *27*, 1633–1639.

Wang, Z., Liu, D., Varin, A., Nicolas, V., Courilleau, D., Mateo, P., Caubere, C., Rouet, P., Gomez, A.-M., Vandecasteele, G., et al. (2016). A cardiac mitochondrial cAMP signaling pathway regulates calcium accumulation, permeability transition and cell death. Cell Death Dis. *7*, e2198.

Weissinger, E.M., Eissner, G., Grammer, C., Fackler, S., Haefner, B., Yoon, L.S., Lu, K.S., Bazarov, A., Sedivy, J.M., Mischak, H., et al. (1997). Inhibition of the Raf-1 kinase by cyclic AMP agonists causes apoptosis of v-abl-transformed cells. Mol. Cell. Biol. *17*, 3229–3241.

Wieckowski, M.R., Giorgi, C., Lebiedzinska, M., Duszynski, J., and Pinton, P. (2009). Isolation of mitochondria-associated membranes and mitochondria from animal tissues and cells. Nat. Protoc. *4*, 1582–1590.

Winklhofer, K.F. (2014). Parkin and mitochondrial quality control: toward assembling the puzzle. Trends Cell Biol. *24*, 332–341.

Wuttke, M.S., Buck, J., and Levin, L.R. (2001). Bicarbonate-regulated soluble adenylyl cyclase. JOP J. Pancreas *2*, 154–158.

Xiao, B., Zhong, G., Obayashi, M., Yang, D., Chen, K., Walsh, M.P., Shimoni, Y., Cheng, H., Ter Keurs, H., and Chen, S.R.W. (2006). Ser-2030, but not Ser-2808, is the major phosphorylation site in cardiac ryanodine receptors responding to protein kinase A activation upon beta-adrenergic stimulation in normal and failing hearts. Biochem. J. *396*, 7–16.

Xu, Y., Pan, J., Sun, J., Ding, L., Ruan, L., Reed, M., Yu, X., Klabnik, J., Lin, D., Li, J., et al. (2015). Inhibition of phosphodiesterase 2 reverses impaired cognition and neuronal remodeling caused by chronic stress. Neurobiol. Aging *36*, 955–970.

Yamamoto, K.K., Gonzalez, G.A., Biggs, W.H., and Montminy, M.R. (1988). Phosphorylation-induced binding and transcriptional efficacy of nuclear factor CREB. Nature *334*, 494–498.

Yau, K.W., and Nakatani, K. (1985). Light-induced reduction of cytoplasmic free calcium in retinal rod outer segment. Nature *313*, 579–582.

Yin, X., Cuello, F., Mayr, U., Hao, Z., Hornshaw, M., Ehler, E., Avkiran, M., and Mayr, M. (2010). Proteomics analysis of the cardiac myofilament subproteome reveals dynamic alterations in phosphatase subunit distribution. Mol. Cell. Proteomics MCP *9*, 497–509.

Zaccolo, M. (2009). cAMP signal transduction in the heart: understanding spatial control for the development of novel therapeutic strategies. Br. J. Pharmacol. *158*, 50–60.

Zaccolo, M., and Movsesian, M.A. (2007). cAMP and cGMP signaling cross-talk: role of phosphodiesterases and implications for cardiac pathophysiology. Circ. Res. *100*, 1569–1578.

Zaccolo, M., and Pozzan, T. (2002). Discrete microdomains with high concentration of cAMP in stimulated rat neonatal cardiac myocytes. Science *295*, 1711–1715.

Zaccolo, M., De Giorgi, F., Cho, C.Y., Feng, L., Knapp, T., Negulescu, P.A., Taylor, S.S., Tsien, R.Y., and Pozzan, T. (2000). A genetically encoded, fluorescent indicator for cyclic AMP in living cells. Nat. Cell Biol. *2*, 25–29.

Zaccolo, M., Di Benedetto, G., Lissandron, V., Mancuso, L., Terrin, A., and Zamparo, I. (2006). Restricted diffusion of a freely diffusible second messenger: mechanisms underlying compartmentalized cAMP signalling. Biochem. Soc. Trans. *34*, 495–497.

Zerbes, R.M., van der Klei, I.J., Veenhuis, M., Pfanner, N., van der Laan, M., and Bohnert, M. (2012). Mitofilin complexes: conserved organizers of mitochondrial membrane architecture. Biol. Chem. *393*, 1247–1261.

Zhang, X., and Eggert, U.S. (2013). Non-traditional roles of G protein-coupled receptors in basic cell biology. Mol. Biosyst. *9*, 586–595.

Zhang, C., Yu, Y., Ruan, L., Wang, C., Pan, J., Klabnik, J., Lueptow, L., Zhang, H.-T., O'Donnell, J.M., and Xu, Y. (2015). The roles of phosphodiesterase 2 in the central nervous and peripheral systems. Curr. Pharm. Des. *21*, 274–290.

Zhang, F., Zhang, L., Qi, Y., and Xu, H. (2016). Mitochondrial cAMP signaling. Cell. Mol. Life Sci. CMLS *73*, 4577–4590.

Zhang, K.Y.J., Card, G.L., Suzuki, Y., Artis, D.R., Fong, D., Gillette, S., Hsieh, D., Neiman, J., West, B.L., Zhang, C., et al. (2004). A glutamine switch mechanism for nucleotide selectivity by phosphodiesterases. Mol. Cell *15*, 279–286.

Zhou, W., Chen, K.-H., Cao, W., Zeng, J., Liao, H., Zhao, L., and Guo, X. (2010). Mutation of the protein kinase A phosphorylation site influences the anti-proliferative activity of mitofusin 2. Atherosclerosis *211*, 216–223.

Zhu, J., Yang, Q., Dai, D., and Huang, Q. (2013). X-ray crystal structure of phosphodiesterase 2 in complex with a highly selective, nanomolar inhibitor reveals a binding-induced pocket important for selectivity. J. Am. Chem. Soc. *135*, 11708–11711.

Zippin, J.H., Chen, Y., Nahirney, P., Kamenetsky, M., Wuttke, M.S., Fischman, D.A., Levin, L.R., and Buck, J. (2003). Compartmentalization of bicarbonate-sensitive adenylyl cyclase in distinct signaling microdomains. FASEB J. Off. Publ. Fed. Am. Soc. Exp. Biol. *17*, 82–84.

Zippin, J.H., Chen, Y., Straub, S.G., Hess, K.C., Diaz, A., Lee, D., Tso, P., Holz, G.G., Sharp, G.W.G., Levin, L.R., et al. (2013). CO2/HCO3−- and Calcium-regulated Soluble Adenylyl Cyclase as a Physiological ATP Sensor. J. Biol. Chem. *288*, 33283–33291.

Zoccarato, A., Surdo, N.C., Aronsen, J.M., Fields, L.A., Mancuso, L., Dodoni, G., Stangherlin, A., Livie, C., Jiang, H., Sin, Y.Y., et al. (2015). Cardiac Hypertrophy Is Inhibited by a Local Pool of cAMP Regulated by Phosphodiesterase 2. Circ. Res. *117*, 707–719.